CRANFIELD UNIVERSITY

JONATHAN D HORSNELL

The use of Raman Spectroscopy for the Intra-Operative Assessment of Axillary Lymph Nodes in Breast Cancer

CRANFIELD HEALTH

DM. THESIS

Academic Year 2011-2012

Supervisors: Prof N Stone and Mr HY Chan

May 2012

Cranfield University

Cranfield Health

DM Thesis

Academic Year 2011-2012

Jonathan D Horsnell

The use of Raman Spectroscopy for the Intra-Operative Assessment of Axillary Lymph Nodes in Breast Cancer

Supervisors: Prof N Stone and Mr HY Chan

May 2012

This thesis is submitted in partial fulfilment of the requirements for the Degree of DM.

Abstract

Breast cancer remains a significant cause of morbidity and mortality. Assessment of the axillary lymph nodes is part of the staging of the disease. Advances in surgical management of breast cancer have seen a move towards intra-operative lymph node assessment that facilitates an immediate axillary clearance if it is indicated. Raman spectroscopy, a technique based on the inelastic scattering of light, has previously been shown to be capable of differentiating between normal and malignant tissue. These results, based on the biochemical composition of the tissue, potentially allow for this technique to be utilised in this clinical context.

The aim of this study was to evaluate the facility of Raman spectroscopy to both assess axillary lymph node tissue within the theatre setting and to achieve results that were comparable to other intra-operative techniques within a clinically relevant time frame.

Initial experiments demonstrated that these aims were feasible within the context of both the theatre environment and current surgical techniques. A laboratory based feasibility study involving 17 patients and 38 lymph node samples achieved sensivities and specificities of >90% in unsupervised testing .

339 lymph node samples from 66 patients were subsequently assessed within the theatre environment. Chemometric analysis of this data demonstrated sensitivities of up to 94% and specificities of up to 99% in unsupervised testing. The best results were achieved when comparing negative nodes from N_0 patients and nodes containing

macrometastases. Spectral analysis revealed increased levels of lipid in the negative nodes and increased DNA and protein levels in the positive nodes. Further studies highlighted the reproducibility of these results using different equipment, users and time from excision.

This study uses Raman spectroscopy for the first time in an operating theatre and demonstrates that the results obtained, in real-time, are comparable, if not superior, to current intra-operative techniques of lymph nodes assessment.

Acknowledgements

The work behind, and the writing of this thesis has been made possible by a number of people to whim I am truly grateful. I must firstly thank my supervisors, Nick and Charlie. Nick has been a source of great advice and encouragement during the time I have spent within his research department. He has given me freedom to explore the topic as well as valuable guidance to ensure that this always remained productive and relevant. Charlie has always been a source of numerous ideas and suggestions. Without him the clinical part of this project would have been a great deal more difficult and great deal less fun. Within the breast department at Cheltenham General I am also indebted to the other consultant surgeons, James Bristol and Fiona Court who have been equally supportive of this work. Dave Ryder their breast nurse specialist has helped enormously by ensuring that I always knew when relevant operations were taking place.

The enthusiasm and belief in the potential role of Raman spectroscopy that Professor Barr showed right from the outset was the inspiration that encouraged me to take the time away from clinical medicine and complete this research. His visits to the department always left us with smiling faces and renewed vigour towards the task in hand. Within the research department itself the warmth and friendliness shown by all of the other members of the team has ensured that coming to work was always enjoyable and relaxing. In particular Jo and Marleen have put up with my persistent need to clean the office and my low “Matlab age”.

Finally and most importantly I am hugely indebted to my family. The love and encouragement of my parents have been a constant throughout my educational career.

My wife Claire is the driving force behind all that I do and without her love, support and organisational skills (!) finishing this work on time would not have been possible. The birth of our sons Joshua and Oliver during this period has been a huge blessing and they are very much the apples of our eyes! Whilst I have written a thesis they have learnt to move, talk, eat, walk, drive us crazy and fill us with so much love!

Contents

List of Figures

List of Tables

List of Abbreviations

ACOSOG	*American College of Surgeons Oncology group*
ADH	*Atypical ductal hyperplasia*
ALND	*Axillary lymph node dissection*
AMAROS	*After mapping of the axilla radiotherapy or surgery (trial)*
ANOVA	*Analysis of variance (between groups)*
AU	*Arbitrary units*
CCD	*Charge coupled device*
CK-19	*Cytokeratin 19*
DCIS	*Ductal carcinoma in situ*
DNA	*De-oxy ribonucleic acid*
DRC	*Dendritic reticular cells*
ER	*Oestrogen receptor*
ESS	*Elastic scattering spectroscopy*
FA	*Fatty acids*
FNA	*Fine needle aspiration*
FTIR	*Fourier-transform infra red (spectroscopy)*
H&E	*Haematoxylin and eosin*
HER-2	*Human epidermal growth factor receptor - 2*
HPF	*High powered field*
IDC	*Inter-digitating dendritic cells*
IHC	*Immuno-histochemistry*
IO	*Intra-operative*
IR	*Infra-red*
ITC	*Isolated tumour cells*
LCIS	*Lobular carcinoma in situ*
LDA	*Linear discriminant analysis*
mRNA	*Messenger ribonucleic acid*
MDT	*Multi-disciplinary team*
N_0	*No nodal metastases (from TNM classification)*
NCCN	*National comprehensive cancer network*
NEG	*Negative*
NHS	*National Health Service*
NICE	*National Institute of Health and Clinical Excellence*
NIR	*Near infra red (light)*
NPI	*Nottingham prognostic indicator*
NSABP	*National surgical adjuvant breast and bowel project*
NTAC	*NHS Technology Adoption Centre*
OSNA	*One step nucleic acid amplification*
PC	*Principal component*
PCA	*Principal component analysis*
PET	*Positive emission tomography*
POS	*Positive*

PTFE	*Polytetrafluoroethylene*
RT-LAMP	*Reverse transcriptase loop mediated isothermal amplification*
RT-PCR	*Reverse transcriptase polymerase chain reaction*
Rx	*Treatment*
SD	*Standard deviation*
SEM	*Standard error of the mean*
SERS	*Surface enhanced Raman spectroscopy*
SLN	*Sentinel lymph node*
SLNB	*Sentinel lymph node biopsy*
SORS	*Spatially offset Raman spectroscopy*
TDLU	*Terminal ductal lobular unit*
TH	*T helper cells*
TIC	*Touch imprint cytology*
TNM	*tumour, node, metastases*
UK	*United Kingdom*
USS	*Ultrasound scan*
VM	*Vibrational modes*

1. Breast Cancer – The clinical rationale of the project

Breast cancer remains a huge problem that affects thousands of women and their families each year. The introduction of breast cancer screening has resulted in an earlier diagnosis for many women and has meant that, thankfully, the disease is increasingly detected before metastatic spread from the breast has occurred. Improvements and advances in the treatment and care that patients receive are continually being sought.

In this opening chapter the clinical context in which this project is set will be discussed. A review of the epidemiology of breast cancer will allow an appreciation of the magnitude of the clinical problem. The nature of "breast cancer" will be defined before discussing the current treatment guidelines within the UK. This project aims to demonstrate a new and novel technique for the intra-operative assesment of axillary lymph nodes in breast cancer patients. Therefore the final section of the chapter will focus on the clinical relevance and importance of the axillary lymph nodes to emphasise the clinical setting in which this project is placed.

1.1. Introduction and Epidemiology of Breast Cancer

Breast cancer is one of the most significant causes of morbidity and mortality in the UK. It is the second most common cause of cancer related deaths and accounts for 1 in 6 of all cancer deaths amongst women. 1 in 8 women will be affected by the disease in their lifetime (Cancer Research UK 2011). In 2008 over 47,500 patients were diagnosed with the disease and there are over 170,000 women who have either received or are

currently receiving treatment for it (National Institute for Health and Clinical Excellence 2009; Cancer Research UK 2011). The incidence in men remains low, with less than 350 new cases diagnosed in 2008, and thus reference will be made to women throughout this chapter.

Breast cancer is the most commonly occurring cancer in women with an incidence of almost 150 per 100,000 persons. This rate increases with age and in those over 85 years old the incidence is greater than 400 per 100,000 persons (Figure 1) (National Institute for Health and Clinical Excellence 2009).

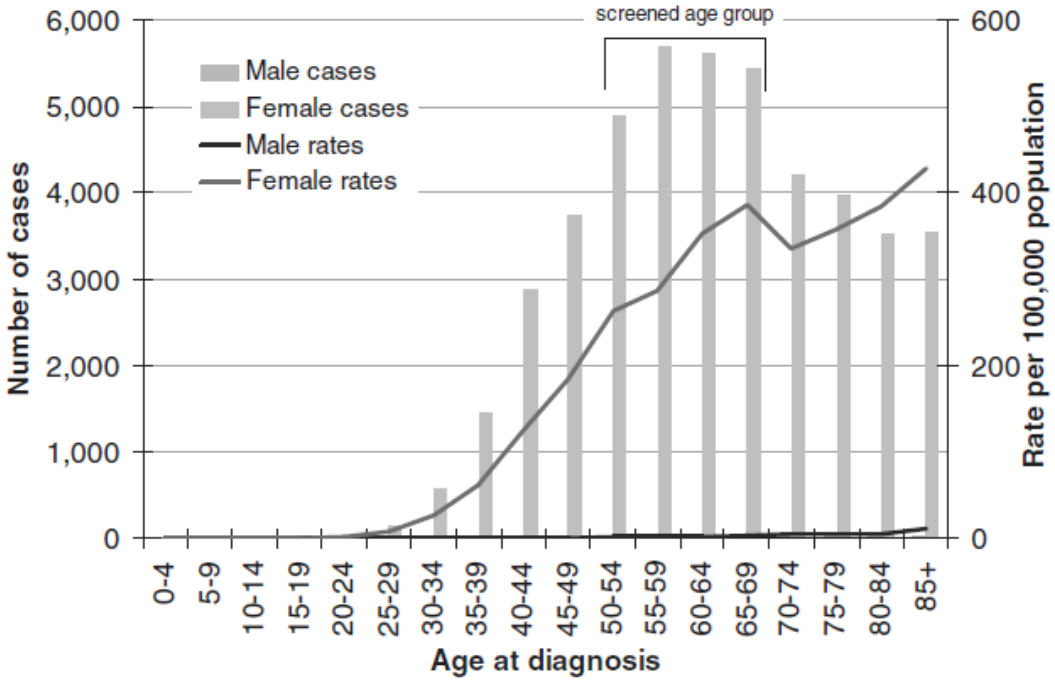

Figure 1- Age specific incidence and incidence rates of new cases of breast cancer in the UK, 2005 (National Institute for Health and Clinical Excellence 2009). The increase in incidence due to screening is clearly demonstrated.

The incidence of the disease has risen across all age groups in the UK over the past two decades (Figure 2). Evidence suggested that this rate of increase may be stabilising although figures released in 2011 reported that the incidence had risen by 3.8% in the last decade (Cancer Research UK 2011; National Institute for Health and Clinical Excellence 2009).

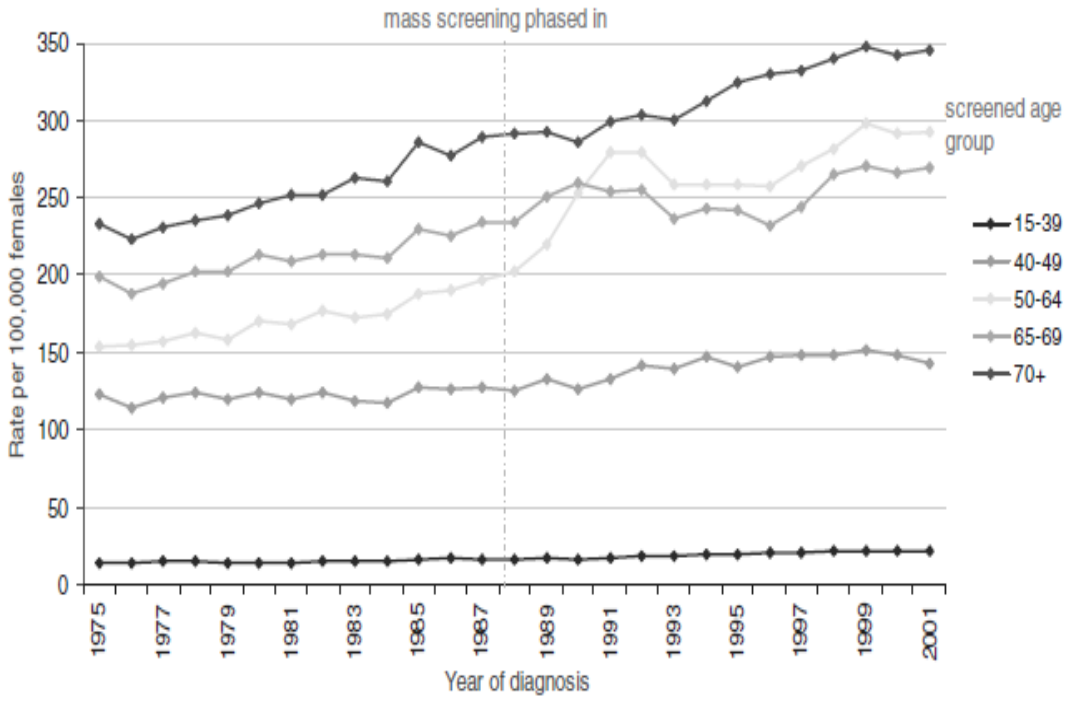

Figure 2- Trend in age specific incidence rates of breast cancer in the UK (National Institute for Health and Clinical Excellence 2009).

Whilst the incidence rate of breast cancer has been rising over the last 20 years the mortality rate has been consistently falling since the late 1980s (Figure 3). This may partly be explained by the UK national screening programme but also by increasingly effective treatment modalities (National Institute for Health and Clinical Excellence 2009).

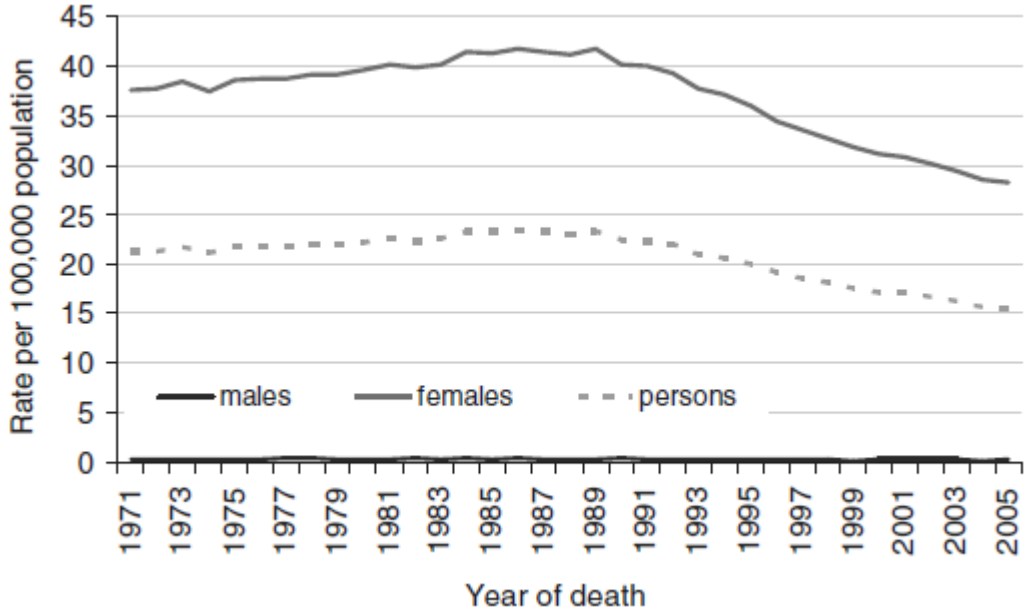

Figure 3- Age standardised rates of breast cancer mortality in the UK 1971-2005(National Institute for Health and Clinical Excellence 2009).

These improvements are reflected in the survival rates following diagnosis. Examination of the relative survival rate, defined as the proportion of patients with a particular condition who are alive at the end of a set period when compared to similar people of the same age that do not have the condition, confirms this. In the 1970s the relative survival rate of patients five years after diagnosis was less than 60%, this increased to just less than 70% by the 1990s and now stands at 80% for women diagnosed in the period between 2001-2003 (Early Breast Cancer Trialists' Collaborative Group (EBCTCG) 2005; NHS Cancer Screening Programmes and West Midlands Cancer Intelligence Unit 2009; West Midlands Cancer Intelligence Unit, 2009).

Closer examination of these survival figures, when categorised according to the stage of the disease at diagnosis, reveals wide variations. Five year survival for those with stage I disease (tumour less than 2 cm diameter and no evidence of metastases) is greater than 90%, but for those diagnosed with stage IV disease (evidence of distant metastases) the survival rate is less than 15% (Figure 4). The importance of early diagnosis can't be over emphasised and in relation to prognosis diagnosis of the disease before it has spread beyond the breast is particularly crucial.

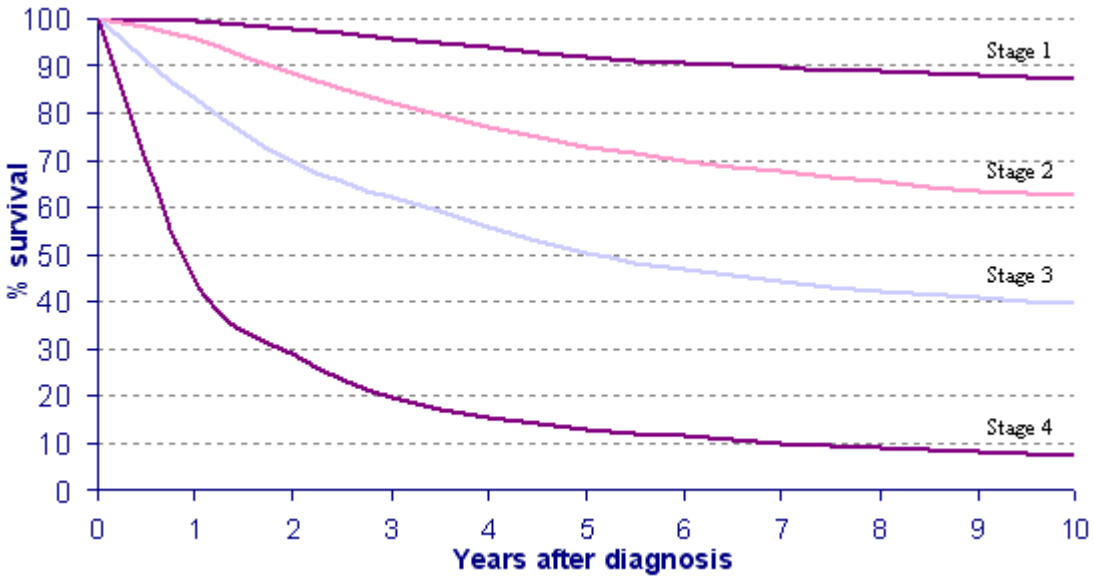

Figure 4- 0-10 year relative survival rates broken down by stage at diagnosis for patients diagnosed between 1990-4 in the West Midlands Cancer Screening Network (West Midlands Cancer Intelligence Unit 2009).

The appreciation of the importance of early diagnosis was one of the key influences that led to the introduction of the national breast screening programme in 1988 (Sant et al. 2006). Indeed it is thought that the recent improvements in survival and mortality rates

are partly due to advances in treatment for the disease but are largely as a result of the earlier diagnosis of many patients cancer.

The introduction of the national breast screening programme has meant that women in the UK with breast cancer present to medical services in one of three ways. This may be either with a symptomatic lesion, such as a breast lump, or with an asymptomatic change that was detected by either the screening programme or during an unrelated investigation. In 2006 just over 30,000 new cases presented with symptomatic changes and just under 16,000 patients presented via the screening programme (NHS Breast Screening Programme 2008).

As would be anticipated patients presenting via the screening programme, with an asymptomatic lesion, had a lower grade of disease than those who presented with a symptomatic lesion. 83% of patients presenting via screening have disease classified in the three most favourable prognostic index groups as opposed to 51% who present symptomatically (Rovera et al. 2008). By definition, this means that the percentage of patients who have spread of the disease from the breast will be lower in the group of patients presenting via screening.

This "contemporary" cohort of patients that present via the screening programme have, on average, a lower grade of disease, which is picked up at an earlier stage, with a reduction in the presence of disease beyond the breast. This has encouraged the adoption of new techniques in the surgical management of breast cancer that reduce both the invasiveness of treatment and the morbidity and psychological effects of

surgery. Breast conserving surgery , breast reconstruction and sentinel node biopsy are all examples of this change. It is hoped that Raman spectroscopy can further compliment this by allowing for the intra-operative assessment of axillary lymph nodes. As will be discussed later in the chapter this in turn would allow for an immediate axillary clearence, if indicated, rather than a delayed second procedure.

1.2. Anatomy, Histology and Pathology of the Human Breast and Lymph Nodes

The diagnosis and management of breast cancer is based on an appreciation of the anatomy and pathology of the breast. Therefore prior to discussing the treatment of breast cancer and reviewing in detail the management of the axilla, the key anatomical, pathological and histological features of normal and malignant breast tissue will be reviewed.

1.2.1. The human breast

The adult female breast sits on the anterior wall of the thorax and its base extends from the second to the sixth rib in the anatomical position. The medial aspect borders the lateral edge of the sternum and the lateral edge extends to the mid-axillary line. The axillary tail (of Spence) extends into the axilla along the inferior border of pectoralis major (Moore 2005) (Figure 5).

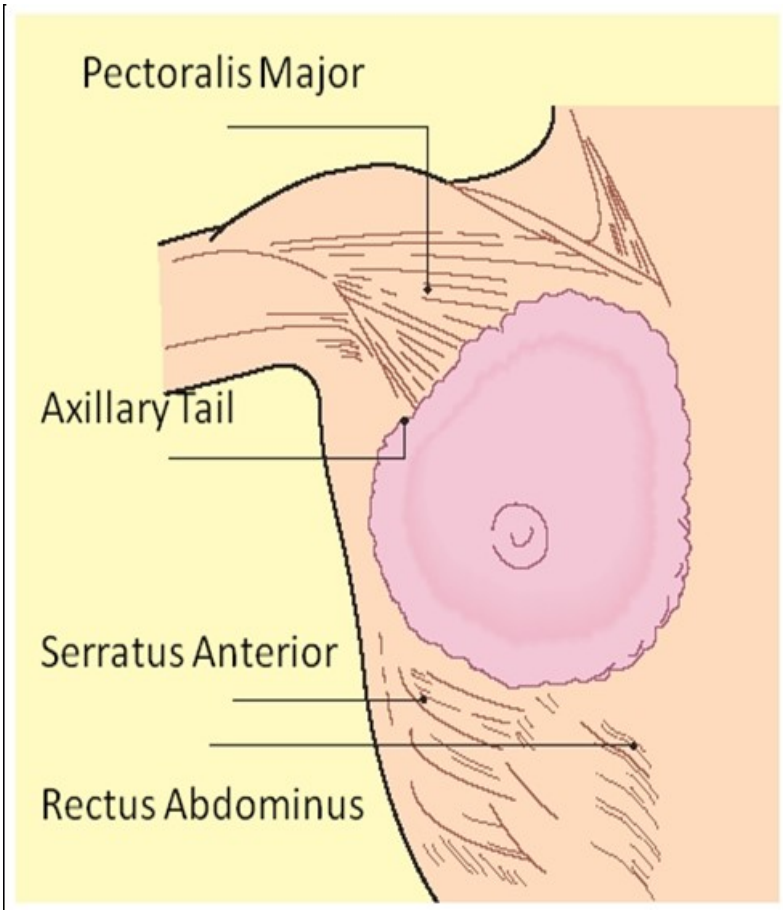

Figure 5- The anatomy of the female breast (adapted from Ellis 2003).

Histologically the breast can be viewed as a highly modified apocrine sweat gland which radiates towards the nipple. It is made up of 15-25 independent glandular units referred to as breast lobes (Wheater, Burkitt and Daniels 1995) (Figure 5, 6).

The lobes are surrounded by adipose tissue and are separated from each other by fibrous septa. Working from proximal to distal within a lobe there are a number of continuous structures. At the proximal end is a collection of secretory alveoli. The inner layer of each alveolus is lined with luminal epithelial cells and is surrounded by both a basal myoepithelial layer and a basement membrane.

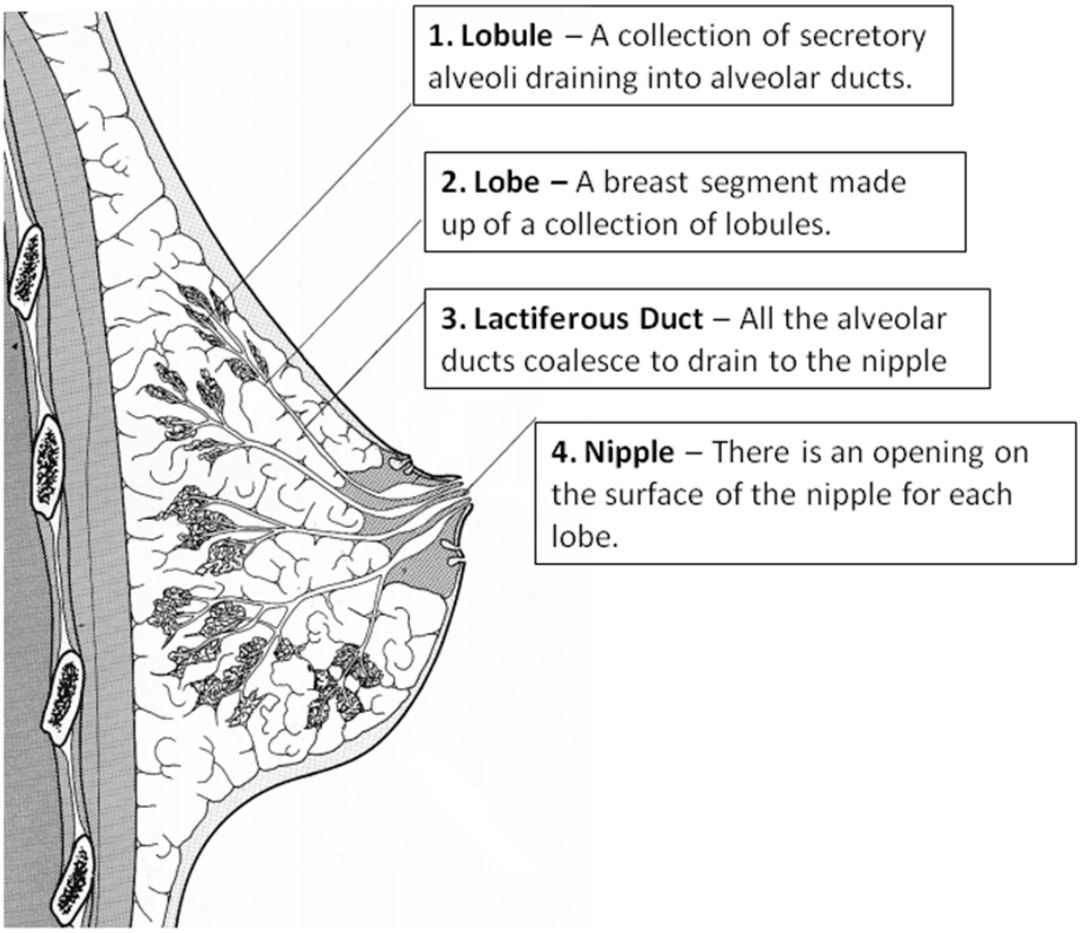

Figure 6- The components of the female breast (adapted from Wheater, Burkitt and Daniels 1995).

Between 10 and 100 alveoli make up a lobule and they drain into alveolar ducts that are lined with epithelial cells and surrounded by a basement membrane. Lobules and the proximal end of the alveolar ducts are referred to as terminal ductal lobular units (TDLU) and is the site where the majority of breast cancers originate (Ioachim and Ratech 2002). A variable number of lobules are found in each lobe of the breast and the ducts draining each lobule will eventually coalesce to form a lactiferous duct that is specific for each lobe. This duct opens on to a unique point on the nipple surface (Raftery 2000). The branching network of lobules and the ducts they drain into are surrounded by collagenous stroma within which is found blood and lymphatic vessels, fibroblasts and adipose tissue.

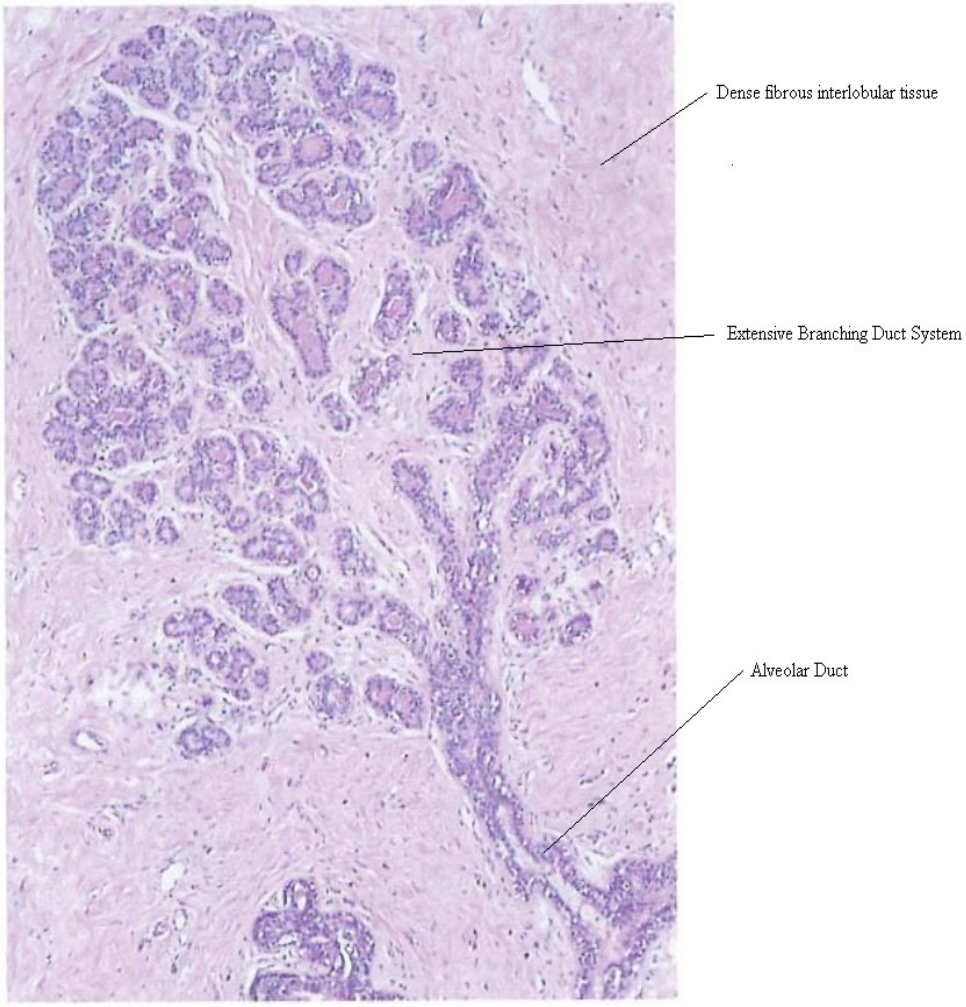

Figure 7- The branching network of the human breast as seen after H&E staining at 60x magnification (adapted from Wheater, Burkitt and Daniels 1995).

The fibroblasts are responsible for producing the supportive capacity of the stroma referred to as the extra cellular matrix. The stroma found within lobules, the intralobular stroma, and that found between lobules, the interlobular stroma has different characteristics. The intralobular stroma contains more fibroblasts and inflammatory cells yet the connective tissue is more loosely arranged whereas the interlobular stroma contains far less cells and has more closely packed collagen (Ioachim and Ratech 2002).

1.2.2. Histopathology of Breast Cancer

Cancer is defined as a disease in which a group of abnormal cells grow uncontrollably by disregarding the normal rules of cell division. Cancer may be classified according to the cells from which the uncontrolled growth originates (Hejmadi 2010).

Carcinoma, a cancer arising from epithelial cells, is the most common malignancy affecting the breast and can be further sub-classified into in situ or invasive carcinoma. Further division of the type of tumour is based on its anatomical site within the breast.

1.2.2.1. Carcinoma in situ

Carcinoma in situ (sometimes referred to as a "pre-malignant" condition) is predominantly detected as areas of micro-calcification on mammography or following the investigation of an invasive carcinoma. These changes can be defined as either ductal (DCIS) or the rarer lobular (LCIS) carcinoma in situ dependent on their position when viewed histologically. They are characterised by a neoplastic growth of the epithelium that is limited by the basement membrane. It is often associated with dystrophic calcification around the site and it is this that makes it visible on mammograms.

Historically this diagnosis was rare as it seldom resulted in overt symptoms. However since the introduction of screening programmes its incidence has risen and it now accounts for 22% of all screen detected breast cancers (NHS Cancer Screening

Programmes and West Midlands Cancer Intelligence Unit 2009). DCIS maybe classified as low, medium or high grade dependent on the atypia of the cancerous cells and this classification is an effective method of predicting the risk of reoccurrence following excision (National Institute for Health and Clinical Excellence 2009).

A varient of DCIS is atypical ductal hyperplasia (ADH). This is an intraductal epithelial proliferation that either shows some but not all of the features of DCIS or has features consistent with DCIS but is only present in a very small area. The presence of ADH is a risk factor for the development of either DCIS or invasive ductal carcinoma.

As will be discussed in later sections, the assessment of the axillary lymph nodes is not normally indicated in DCIS. It is therefore very unlikely that many of the patients recruited to this study will have this condition.

1.2.2.2. Invasive Carcinoma

Invasive carcinoma, in contrast to DCIS, invades into the breast stroma and spreads locally. It also has the potential to infiltrate the vascular and lymphatic systems and spread beyond the breast (Johnstone et al. 2002). Classification of invasive carcinoma may be according to anatomical cell origin (subtype) or histological grade. There are 16 subtypes of invasive breast cancer although some are very rarely encountered (Raftery 2000). These classifications are important as they help guide both initial investigations and subsequent treatment.

Invasive ductal carcinoma represents approximately 75% of all invasive carcinomas. Histologically it is characterised by malignant epithelial cells that originate in the alveolar ducts and spread within the fibrous stroma. Invasive lobular carcinoma accounts for between 10-15% of all cases of invasive breast cancer and arises from epithelium within the breast lobules. It has a tendency to multifocality with indolent and progressive characteristics that often result in a worse prognosis than ductal carcinoma (Rhakha, El-Sayed and Powe 2008). Unlike ductal carcinoma, cancer of lobular origin is less likely to be associated with calcification of the surrounding stroma and is therefore more difficult to detect on mammography (Raftery 2000).

There are a variety of other types of tumour. These include mucinous carcinomas which account for 5% of breast cancers, medullary carcinomas that account for less than 5% of tumours and tubular cancers that represent between 1 and 2% of all breast tumours. They each have particular characteristics which are beyond the scope of this review (Rosen 2001).

Each individual tumour can be classified histologically as well as anatomically. This helps predict how the tumour will progress based on the cytological and architectural features of the tumour cells. To maintain standardisation each tumour is categorised by a pathologist using a validated scoring systems such as the Nottingham Grading System (Elston and Ellis 1991). This grades the tumour according to the degree of tubular formation, the nuclear pleomorphism, and the mitotic activity into low (I), intermediate (II) and high (III) grade groups (Table 1).

Degree of Tubule formation within the tumour	Majority of tumour Moderate Degree Little or None	1 2 3
Mitotic Count	0-9 Mitoses/10 high power field (hpf) 10-19 Mitoses/10 hpf 20 or > Mitoses/10 hpf	1 2 3
Nuclear Pleomorphism	Small Regular Uniform Cells Moderate Nuclear Size and Variation Marked Nuclear Variation	1 2 3
Overall grade	Low Grade (I) Intermediate Grade (II) High Grade (III)	3-5 6-7 8-9

Table 1: The Nottingham grading scale for breast cancer (Elston and Ellis 1991).

1.2.2.3. Breast Cancer and Metastases

The presence of metastases, the migration of cells from the primary tumour to other sites around the body, is a key indicator of the prognosis of an individual's disease. The most common sites of metastasis in breast cancer are to the regional lymph nodes that drain the breast. If distant spread occurs then the three most common sites are to bone, the lungs and the liver. The pathological grading of the tumour and the assessment of both the local lymph nodes and common sites of distant metastasis is used to stage each individual patient's disease. It is a standardised way of documenting the extent of the disease spread at the time of presentation and is used to predict survival and guide treatment.

The most common staging index used across a range of malignancies is the TNM system. This categorises the disease based on the tumour itself (T), and the presence of nodal metastases (N) and distant metastases (M) (Johnson et al. 2004). Other staging indices which are particular to breast cancer include the widely used Nottingham Prognostic Index (NPI) (Tables 2, 3). There is a clear association between an increasing NPI score or TNM stage and worsening 5 year mortality (Figure 8).

Factor		Score
Lymph nodes	No Metastases 1-3 Positive Nodes >3 Positive Nodes	1 2 3
Grade	Stage I Stage II Stage III	1 2 3
Vascular Invasion	No Yes	0 1
Tumour Size	Size in cm	Multiplied by 0.2

Table 2: The Nottingham prognostic index (NPI). A score is then calculated for each patient by adding the lymph node score, the grade score and the vascular invasion score and multiplying them by 0.2 of the tumour size. (Sabel 2009).

Examination of the 5 years survival figures plotted against the stage of the disease highlight the prognostic importance of metastatic spread. Patients with a T1 tumour have a 10% reduced 5 year survival if there are lymph node metastases present and in the presence of distant metastases the 5 year survival is less than 20% (Figure 8).

Stage	Features
Primary Tumour (T) • Tx • T0 • Tis • T1 • T2 • T3 • T4	• Not assessed • No evidence of Primary Tumour • Carcinoma in Situ • Tumour < 2cm in diameter • (<0.1=T1mic, <0.5cm = T1a, <1cm=T1b , rest = T1c) • Tumour 2-5cm in diameter • Tumour >5cm in diameter • Any size with direct spread to chest wall or skin
Lymph Node Status (N) • Nx • N0 • N1 • N2 • N3	• Regional nodes cannot be assessed • No metastases • Metastases to mobile ipsilateral nodes • Metastases to fixed ipsilateral nodes • Metastases to ipsilateral internal mammary nodes
Metastases (M) • Mx • M0 • M1	• Presence of distant metastases cannot be assessed • No distant metastases • Distant metastases (including supraclavicular nodes)
Stage 0= **Tis**, N0, M0 Stage 1= **T1**, N0, M0 Stage 2a= T 0/1, **N1** or **T2**, N0 , M0 Stage 2b= T2, **N1** or **T3**, N0. M0	Stage 3a= T3, **N1** or T1-3, **N2** , M0 Stage 3b= **T4**, Any N, or Any T, **N3** , M0 Stage 4= Any T, Any N, **M1**

Table 3: The TNM index for staging breast cancer (Sabel, 2009)

Interrogation of the NPI also highlights the importance of the number of involved axillary lymph nodes. A women with a Grade II, 2 cm invasive tumour with no

lymphovascular invasion and no distant metastases (NPI = 3.4) has an anticipated 85% survival rate at 5 years. This is reduced to 50% if greater than 3 lymph nodes are positive (NPI = 5.4). As will be discussed later these factors also guide further treatment of the axilla after axillary surgery.

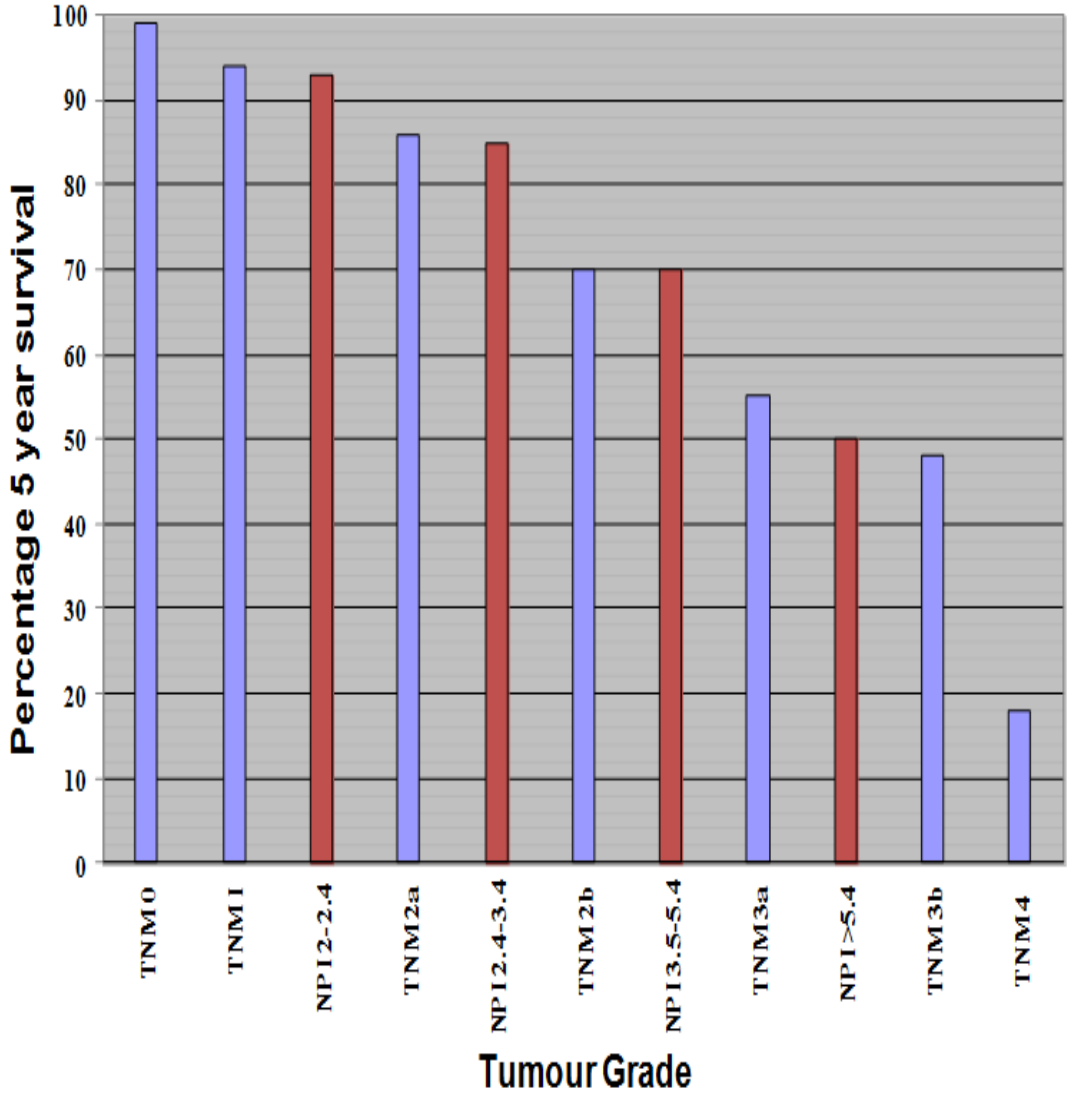

Figure 8- Percentage 5 year survival according to TNM stage or NPI score (Cancer Research UK 2009).

1.3. Lymph Nodes and the Lymphatic System

In the management of breast cancer lymph nodes are vital indicators of the spread of cancer beyond the breast. Metastasis of the cancer to the lymph nodes is an important factor in predicting the overall prognosis of an individual's disease. The status of the lymph nodes is used to help stage the disease and this helps guide treatment options and regimes (Rovera et al. 2008; Kurosumi and Takei 2007).

1.3.1. Anatomy of the Lymph Nodes

The lymph nodes are part of the lymphatic system which is divided into lymphoid tissues, such as the thymus, bone marrow or lymph nodes, and the circulating network that connects them. The circulatory network consists of permeable lymphatic vessels and capillaries which extend throughout the body.

Excess interstitial fluid within tissues drains into the lymphatic vessels and is eventually returned to the cardiovascular circulatory system. During this process the fluid is filtered through lymph nodes that are found at various positions throughout the body (Figure 9). Specific lymph nodes are responsible for filtering lymph from specific organs and regions. Within the lymph node the fluid drained from these specific areas is exposed to a large number of lymphocytes and other cells of the immune system. If an antigen is recognised it will trigger a cascade of events both within the lymph node and subsequently beyond it. Immune response mediators will drain from the lymph nodes to

enter the cardiovascular circulatory system along with the filtered interstitial fluid (Ioachim and Ratech 2002).

As a result of the topographical function of lymph nodes, examination of particular nodes enables one to gain information about disease within the organs that they drain. A familiar example of this is the easily palpable cervical lymph nodes which become enlarged when a patient has tonsillitis. In this scenario the infective process in the oropharynx causes antigens to be identified in the interstitial fluid draining from the region to the nodes. This causes an immune response in the lymph node as it mounts a response to the antigen and as a result the node enlarges.

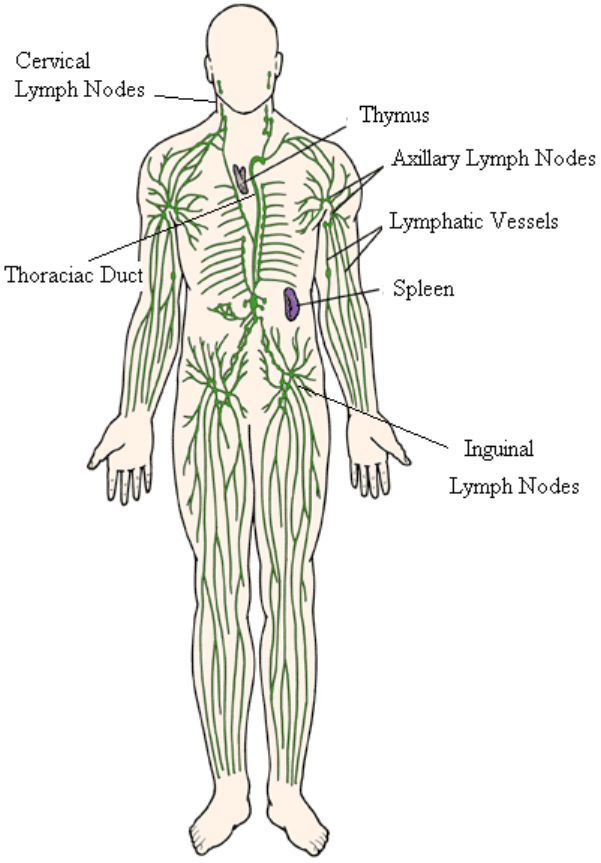

Figure 9- A stylised diagram representing the lymphatic system (adapted from Ellis 2002).

Lymphatic drainage from the breast is primarily to two groups of lymph nodes, the ipsilateral axillary lymph nodes and the internal thoracic nodes (Figure 10). A small percentage of lymph will drain to the supra-clavicular and contra-lateral internal thoracic nodes. Examination of these groups of nodes gives us information about underlying disease within the breast. Infection, inflammation and importantly in this study cancer will result in pathological changes within the nodes. These changes may be determined by clinical examination, radiological imaging or histopathological analysis. Within the context of this study it is hoped that interrogation of the axillary nodes using Raman spectroscopy will help determine whether the breast cancer has metastasised to the lymph nodes.

The axillary nodes are divided according to either their anatomical position or their relation to surrounding structures. Anatomically they may be defined as lateral, central, posterior, anterior or apical (Figure 10). Surgically they are more often defined according to their position in relation to pectoralis minor. They are termed level I if they are inferior to the pectoralis minor, level II if they are posterior to the pectoralis minor and level III if they are superior to the pectoralis minor (Ellis 2002). Within the axilla the lymph nodes lie close to a number of structures including the axillary vein and artery, the long thoraciac nerve, the thoraco-dorsal nerve and the intercostobrachial nerve (Figure 11). Careful identification and preservation of these structures, where possible, helps reduce the morbidity associated with operative dissection of the nodes in this region.

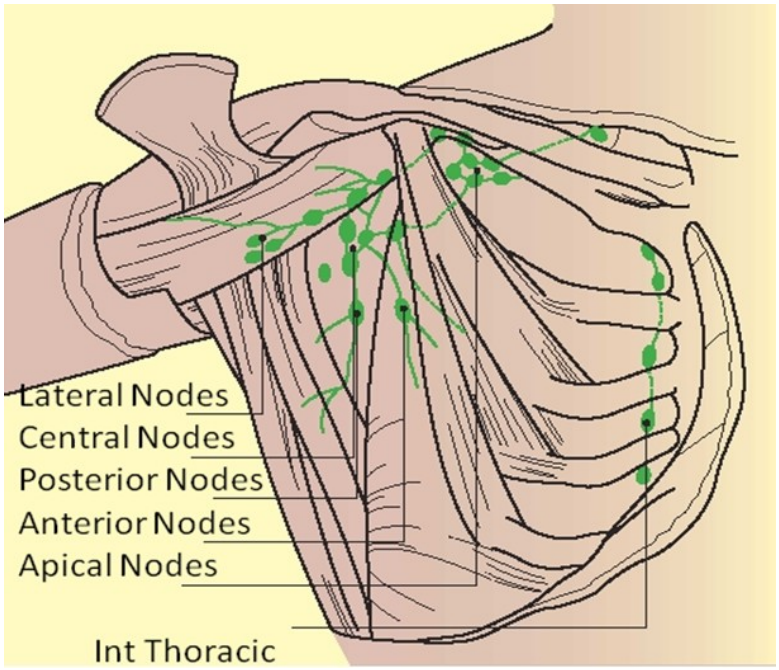

Figure 10- The anatomy of the axillary lymph nodes (adapted from Ellis 2003).

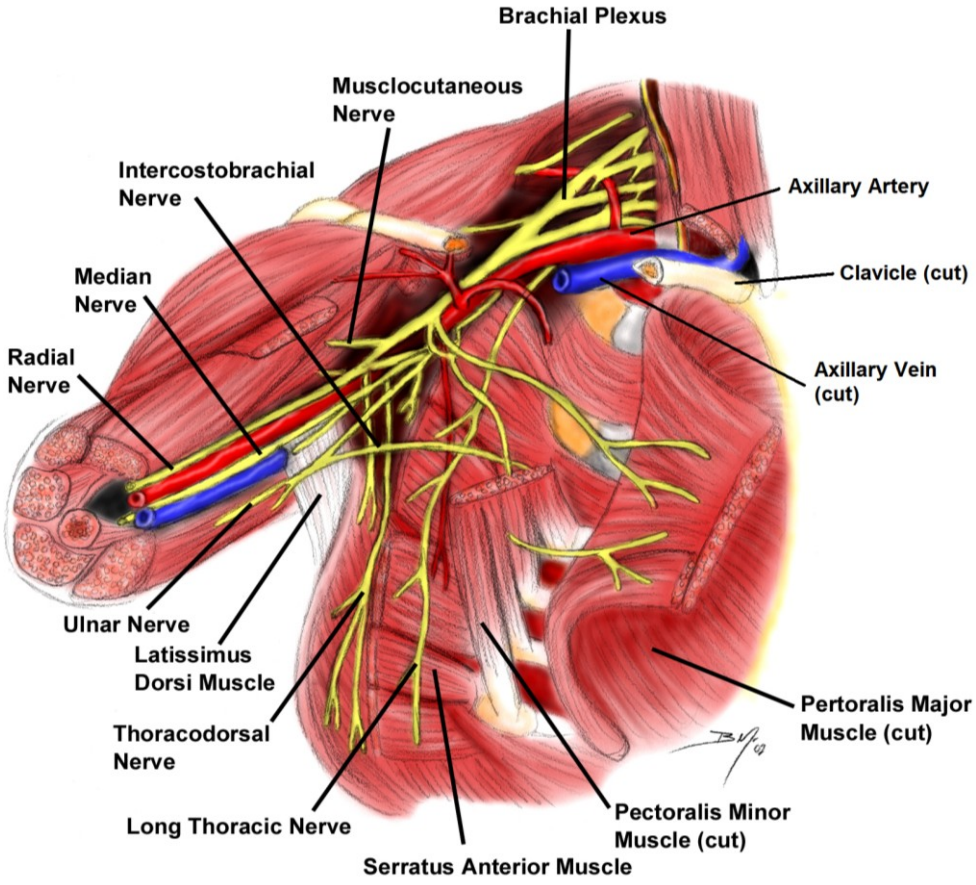

Figure 11- Anatomy of the Axilla

(Adapted from Medscape (http://emedicine.medscape.com/article/880878-overview)).

1.3.2. Histology of the Lymph Node

Lymph nodes are bean shaped aggregations of lymphocytic tissue and can vary from a few millimetres to several centimetres in diameter dependent upon the reactive status of the node at that time (Figure 12) (Obwegeser et al. 2000).

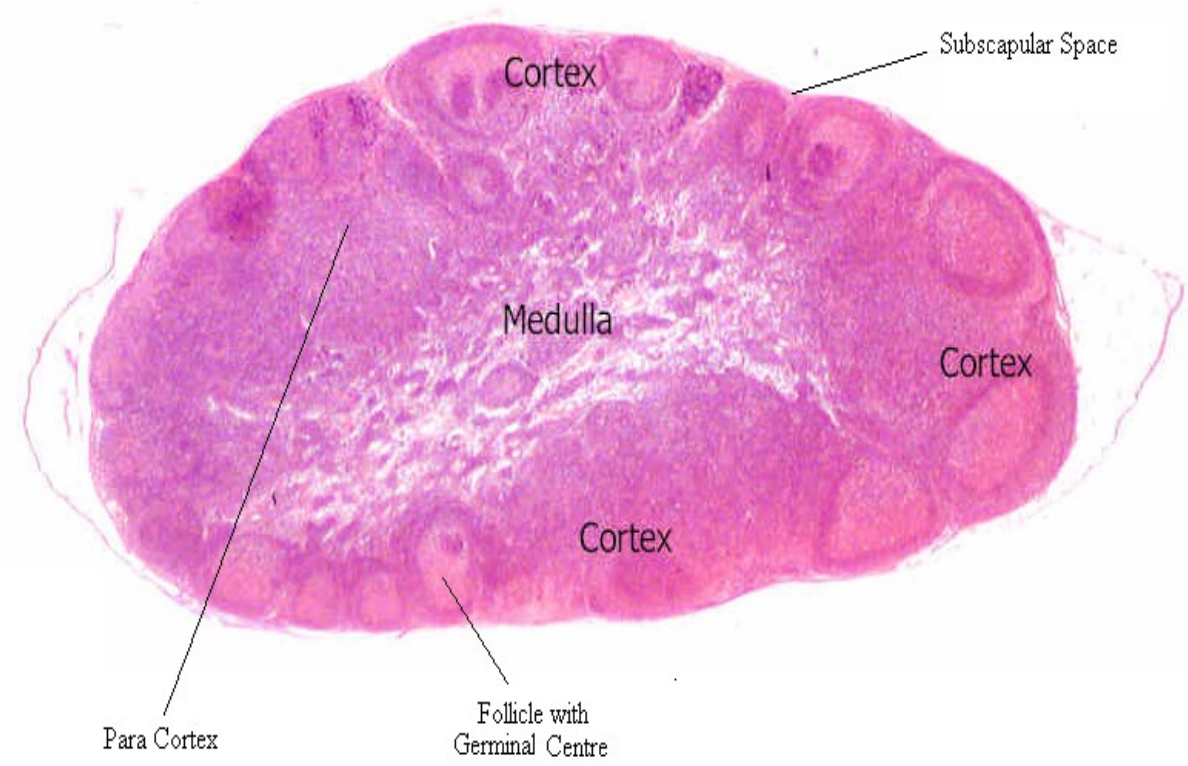

Figure 12- The structure of an axillary lymph node (adapted from Cacaecu 2008).

Lymph nodes are intrinsically involved in both humoral, involving antibodies, and cell mediated immunity. Antigens in the afferent lymphatic fluid will be trapped within the node by either lymphocytes or accessory cells such as dendritic reticular cells, inter-

digitating reticular cells or histiocytes. The antigenic cells are then processed and presented to further lymphocytes which trigger an immune response both locally and further a field (Ioachim and Ratech, 2002).

Each node is surrounded by a fibrous capsule that envelopes an inner core. This inner core may be divided into four contiguous sections, the subscapular space, the outer cortex, the para-cortex and the medulla (Figure 12). This is structurally supported by a framework of reticular fibres, reticular cells and elastin. Lymphatic fluid arriving in afferent vessels on the convex surface of the node will drain through each of these sections in turn before leaving the node at the hilum and draining into efferent lymphatic vessels.

1.3.2.1. The Subscapular Space

The node is surrounded by dense collagenous tissue which extends into the node to form trabaculae. The afferent lymph vessels will converge on the outer surface of the node and drain through this tissue before entering the subscapular space. It is in this space that individual tumour cells, the first sign of metastatic spread, may be found.

1.3.2.2. The Outer Cortex

The outer cortex of the lymph node is just medial to the subscapsular space. It is characterised by the presence of primary lymphoid follicles and contains B lymphocytes, macrophages and dendritic reticular cells. Following antigenic stimulation

this area becomes the source of B cell proliferation. The primary lymphoid follicles, which in a resting state, are composed of homogenous cell populations of dormant lymphocytes, become activated. These, activated, secondary follicles are seen characteristically 4-7 days after antigenic stimulation. Activation occurs due to migration of activated B and T cell lymphocytes to the primary follicle. Their interaction with dendritic reticular cells (DRC) at these sites causes the antigenic sequence to be displayed to the B lymphocytes within the primary follicle. The DRC cells present the antigenic sequence on its surface and produces growth factor which causes B cell activation and the formation of a germinal centre within the follicle. Within the germinal centre B cells divide rapidly and differentiate into either B memory cells, or plasma cells (sometimes referred to as B effector cells). The plasma cells produce antibodies and the B memory cells are stored to help mount a greater response to the antigen if it is encountered again (Ioachim and Ratech 2002).

1.3.2.3. The Para-cortex

Located more medially within the node is the para-cortex where T cells predominate. Inter-digitating dendritic cells (IDCs) are also found in this area and their role is primarily to present antigenic sequences to the T cells so triggering an immune response. T cells go on to differentiate into either TH cells that produce cytokines to recruit and activate further lymphocytes, macrophages and neutrophils or cytotoxic T cells that seek and destroy infected cells by inducing apoptosis (Kuby 1997).

1.3.2.4. The Medulla

The medulla is the innermost part of the lymph node and is the area most sparsely populated with lymphocytes. The majority of cells found within the region are plasma cells that have originated from the germinal centres in the outer cortex. Within the medullary region they differentiate and produce antibodies. These antibodies leave the node in the efferent lymphatics and blood vessels and circulate around the body to target specific matching antigens.

1.3.2.5. Lymph Node Sinuses

The lymphatic fluid drained from individual tissues passes through the different sections of the node via a series of interconnecting sinuses. These sinuses are lined with endothelial cells and lymphocytes. Plasma cells and phagocytes can also be found within the sinus walls. At the cellular level this is an important site for the initial interaction between the antigens and the cells of the immune system.

The result of this complex filtering network is that the lymph node is able to rapidly alter both its own cellular components and the composition of the efferent lymphatic fluid that drain from it. Following immune reactions, in response to both infection and tumour metastasis, the node becomes enlarged and the concentration of lymphocytes and antibodies leaving the node is greatly increased. In the context of metastatic spread this may provide a degree of regional control of cancer cell dissemination. Metastasis to the lymph node is therefore most often seen prior to distant spread to other organs

(Ioachim and Ratech 2002). Within the node itself metastatic cells will first appear in the subscapular space before progressing through the node to the sinuses, medulla and cortex. Once established metastatic disease starts to proliferate from the medulla and eventually the whole node can be over run by self replicating cells (Figure 14).

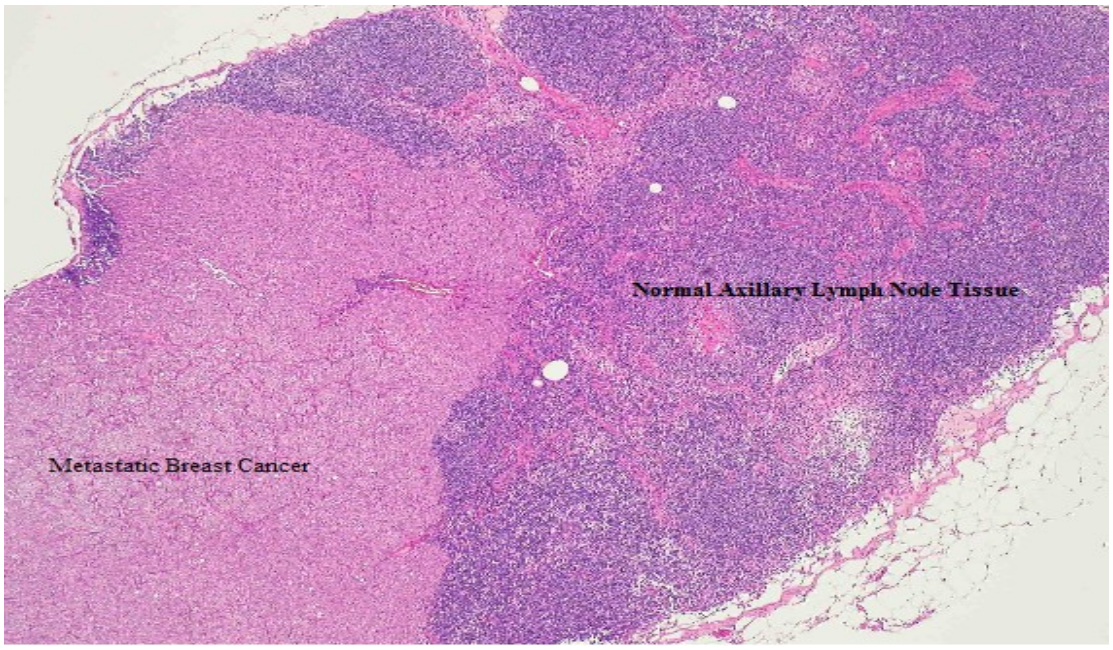

Figure 14- Histological slide (H and E stained) showing normal lymph node tissue and metastatic breast cancer in an axillary lymph node (adapted from Wheater, Burkitt and Daniels 1995).

As will be discussed later, these metastatic deposits may be termed isolated tumour cells, micrometastases or macrometastases. The clinical significance of each of these differs and will be reviewed later in the chapter. The presence of self-replicating metastatic cells with the lymph node activates myofibroblasts and cytokines. In turn this will also stimulate the overgrowth of the surrounding connective tissue which may result in the formation of scar like tissue around the metastases which is referred to as desmoplastic change (Ioachim and Ratech 2002).

The histological changes seen in positive lymph nodes, when metastatic cells replicate, reflects the histology of the underlying tumour. There is a correlation of greater than 95% between the tumour seen in the breast and the changes seen within positive axillary lymph nodes (Ioachim and Ratech 2002). It is argued that if the changes within a positive lymph node do not match those seen in the underlying tumour then further examination of the breast tumour should be carried out to ensure that there is not another primary source.

1.4. Treatment of Breast Cancer

As has been discussed patients may present with breast cancer in one of three ways. They can present with symptomatic changes, via the national breast screening programme, or due to an incidental finding when investigating another problem. The initial role of the team caring for that patient is to confirm the diagnosis, remove the tumour and then stage the disease. Armed with this information a multi-disciplinary team will then plan the optimal treatment for each individual.

Confirmation of the diagnosis of breast cancer is made after a triple assessment. This involves clinical examination, radiological assessment, in the form of a mammogram or an ultrasound scan, and histopathological review of fine needle aspiration samples or core needle biopsy samples of the suspicious area. This assessment most often takes place in secondary care and usually at a one stop clinic. If a diagnosis of invasive breast cancer is made then initial assessment of the axilla for evidence of metastasis should also be offered at this early stage (National Institute of Health and Clinical Excellence

2009). Further details of the assessment and management of the axilla will be discussed in subsequent sections.

The management of breast cancer continues to evolve and varies from patient to patient. In this section a brief overview of the treatment options will be given to help set the scene for this project although it is recognised that this is not an exhaustive review.

1.4.1. Management of Invasive Breast Cancer

The first procedure in the treatment of invasive cancer is the excision of the primary tumour with adequate clear margins. If the tumour is locally advanced or there is evidence of inflammatory breast cancer then a course of neo-adjuvant treatment may be offered (whereby endocrine therapy or chemotherapy is given as the primary modality prior to surgery) (National Institute of Health and Clinical Excellence 2009). Surgical excision may be performed by a number of techniques including breast conserving methods, such as a wide local excision, or by means of a mastectomy (a surgical procedure to remove all of the breast tissue) with or without immediate or delayed breast reconstruction. Assessment of the axillary lymph nodes, if not achieved preoperatively, is also performed during this initial operation.

Further adjuvant treatment in the form of radiotherapy, chemotherapy or endocrine medication (such as Tamoxifen, an oestrogen receptor antagonist or Aromatase Inhibitors, that block production of oestrogen) is offered based on the grade of the tumour, the stage of the disease and the receptor status of the tumour (Table 4).

Nodal Status	Tumour Type (See Table 3)	ER + and HER +	ER +	HER +	ER /HER -
Normal Nodes	T1a	None	None	None	None
	T1b (well differentiated)	None	None	None	None
	T1b (moderate or poorly differentiated)	Endocrine +/- Chemo	Endocrine +/- Chemo	Chemo	Chemo
	T1c	Endocrine + Chemo	Endocrine + Chemo	Chemo	Chemo
	T2 or above	Endocrine + Chemo	Endocrine + Chemo	Chemo	Chemo
Micro Metastases	T1a	Endocrine Treatment	Endocrine Treatment	+/- Chemo	+/- Chemo
	T1b	Endocrine Treatment	Endocrine Treatment	+/- Chemo	+/- Chemo
Macro Metastases	Any T	Endocrine + Chemo	Endocrine + Chemo	Chemo	Chemo

Table 4- Recommendations for the adjuvant treatment of breast cancer dependent on the tumour type and the status of the axilla (National Institute for Health and Clinical Excellence 2009). ER= Oestrogen Receptor, HER = Human epidermal growth factor receptor-2, Chemo=Chemotherapy, Endocrine Treatment = Tamoxifen or Aromatase Inhibitors.

1.4.2. Management of Ductal Carcinoma in Situ (DCIS)

As previously discussed the management of DCIS has become a significant part of the breast services remit. Following the introduction of a national breast screening

programme up to 1 in 5 cancers detected by screening in the UK are proven to be DCIS (National Institute for Health and Clinical Excellence 2009). It is expected that

this number will continue to rise with further technological improvements in imaging and the expansion of the breast screening programme (Patani, Cutuli and Mokbel 2008). Although classified as a pre invasive condition not all patients will go on to develop invasive breast cancer following a diagnosis of DCIS. Estimates of the percentages that will progress to invasive cancer range from 14-75% (Patani, Cutuli and Mokbel 2008). Progression to invasive cancer is most likely to occur in high grade DCIS especially if combined with other risk factors such as a palpable mass at presentation, a family history of breast cancer, wide spread micro-calcifications on mammography and extensive disease.

Similarly to invasive cancer the management of DCIS starts with the excision of the affected area. This is most often achieved with breast conserving surgery but if the tumour is greater than 4 cm, multi-centric or at the site of reoccurrence mastectomy is the preferred option. Adjuvant radiotherapy to the breast has been shown in a meta-analysis of randomised controlled trials to reduce the local recurrence by 60% and should be offered to those patients undergoing breast conserving surgery (Patani , Cutuli and Mokbel 2008).

The investigation and management of the axilla, in DCIS, is more controversial as by definition the tumour cells should not have invaded beyond the basement membrane. However, extensive DCIS may harbour foci of invasive disease and assessment should be offered to patients with either high grade or widespread disease. A retrospective

study of lymph node positive DCIS patients demonstrated that careful examination of the tumour revealed small foci of invasive disease that had not originally seen. Therefore lymph node assessment in DCIS is reserved for patients where extensive disease is present (Sakr et al. 2006). The role of further adjuvant treatment in the form of tamoxifen has been evaluated in the NSABP-B24 trial and the UK/ANZ DCIS trial (Sibbering 2009). These studies report minimal reductions in local reoccurrence and must be balanced against the potential side effects of the treatment.

1.5. The Assessment and Management of the Axillary lymph nodes

The prognostic importance of local metastatic spread to the axillary lymph nodes can not be over emphasised. Indeed it has consistently been shown to be the most important marker of prognosis in patients newly diagnosed with breast cancer (Rovera et al. 2008 ; de Boer et al. 2010). Indeed since the end of the 19th surgical treatment of breast cancer included axillary node dissection as standard (Kurosmi and Takei, 2007; Suami et al. 2008).

The method by which axillary node assessment and hence staging is carried out has altered over time, reflecting the move to increasingly less extensive surgical techniques. Like assessment of the breast, axillary lymph nodes may be examined clinically, radiologically or by histopathological methods. In this section the current methods by which axillary nodes are sampled and assessed will be reviewed. Current controversies in this area will then be discussed and the potential clinical role that Raman spectroscopy could play in lymph node assessment in the future will be highlighted.

1.5.1. Lymph node assessment

Initial attempts at lymph node assessment should take place after the diagnosis of breast cancer is made. It is recommended that all patients newly diagnosed with invasive disease undergo ultrasound examination of the axilla with guided biopsy of areas of suspicion prior to their initial surgery (National Institute of Health and Clinical Excellence 2009). The reported sensitivity (its ability to identify true positives) and specificity (its ability to identify true negatives) of ultrasound scans (USS) at detecting metastatic spread depends on the criterion of positivity (Alvarez et al. 2006). When lymph node size is used the sensitivity is between 66 and 73% and the specificity is between 44 and 98%. If morphological characteristics of the node are used then the reported sensitivity ranges from 55 to 92% and the specificity from 80 to 97% (Alvarez et al. 2006). The recommended technique is USS of the axilla and either FNA (fine needle aspirate) or core biopsy if there are abnormal morphological features. Sensitivity for this approach varies between 31 and 63% with reported specificities of 100% (Damera et al. 2003 ; Alvarez et al. 2006). Factors that influence the success of this technique are the experience of the radiologist, the imaging and biopsy equipment and the number of aspiration or biopsy samples taken (Damera et al. 2003).

If the nodes are found to be positive then the patient is recommended to have an axillary dissection most often at the same time as surgery to excise the tumour in the breast. Due to the low sensitivities of this technique patients with a negative USS still require further evaluation of their axilla.

The use of preoperative positive emission tomography (PET) for staging the axilla has also been investigated. However a recent systematic review and meta-analysis reported wide variations in both sensitivity (20-100%) and specificity (75-100%). Given these results along with the costs and resource implications the authors concluded that the technique should not replace USS as a pre-operative method of evaluating the axilla (Cooper et al. 2011).

The traditional method of axillary node sampling, which took place as part of the operation to remove the breast tumour, involved dissection of the tissue in the axilla, referred to as axillary node dissection (ALND). Between 15 and 20 nodes were excised along with the tissue in that area (Steele et al. 1985; Mansel et al. 2006). An alternative approach was 4 node sampling followed by radiotherapy if they were found to be positive (Steele et al. 1985).

Axillary sampling using these methods carried significant co-morbidities including nerve injury, resulting in parasthesia of parts of the ipsilateral arm, lymphoedema and shoulder stiffness (Mansel et al. 2006). With the emergence of breast conserving surgery in the 1980s focus shifted to developing surgical techniques that reduced the invasiveness of axillary sampling and reduced the risks to the patient. The onset of breast screening programmes and hence the earlier stage of breast cancer at presentation added impetus to this goal.

1.5.2. Sentinel Lymph Node Biopsy (SLNB)

The last decade has seen the emergence of SLNB as the standard of care for the sampling of the axillary lymph nodes. The technique was developed on the principle that cancer cells that have invaded lymphatic vessels draining the breast will initially reach specific (sentinel) lymph nodes.

The principle of the sentinel node and its role in predicting metastases from the primary tumour had been developed in penile cancer and malignant melanoma (Kurosmi and Takei 2007). In many ways a deceptively simple idea it was proposed that all lymph drains via the guardian or sentinel node. Therefore sampling and then assessing this node will predict whether metastases to any of the nodes have occurred (Goyal and Mansel 2008) (Figure 15).

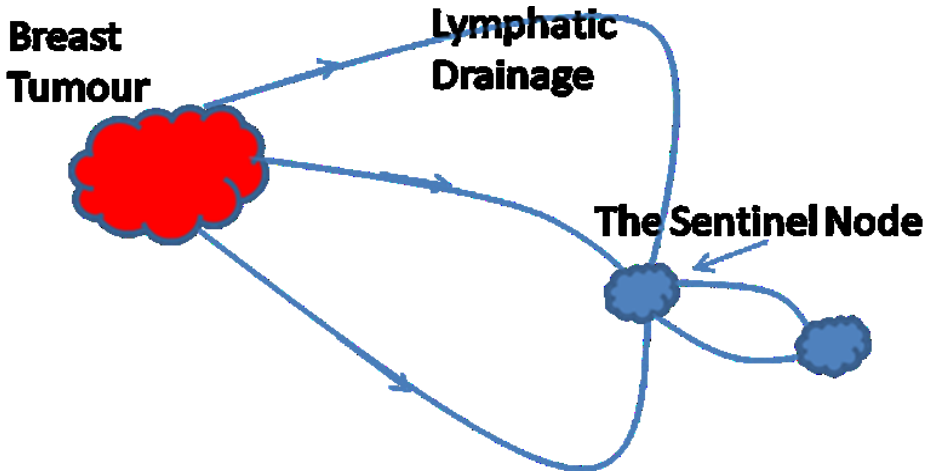

Figure 15- A stylised diagram to illustrate the principles of sentinel lymph node biopsy, whereby lymphatic drainage from a breast tumour drains via the sentinel node.

The status of the sentinel node has been demonstrated to reflect the overall status of the axilla in 97% of cases (Layfield et al. 2011). If the sentinel nodes are negative then the axilla is deemed clear of metastases and the rest of the nodes need not be dissected. This has been shown to reduce the morbidity and complications associated with traditional methods of node sampling (Mansel et al. 2006).

The technique of SLNB was first described in breast cancer in the early 90s (Krag et al. 1993; Giuliano et al. 1994). Since then a number of case series and randomised control trials have been published documenting its use. A meta-analysis of 69 studies published in 2006 pooled data from more than 8000 patients and concluded that the technique was successful at identifying the sentinel node in 95% of cases and had a false negative rate of less than 7% (Kim et al. 2006). These results, combined with the marked reduction in morbidity has meant that SLNB has now been adopted as the standard for the initial sampling of the axillary lymph nodes and is being used more and more widely throughout the UK (National Institute for Health and Clinical Excellence 2009). It is well accepted by patients due to its lower risks and the shorter associated hospital stay (Purushotham et al. 2005).

The procedure involves the patient receiving either a sub dermal or intra dermal injection of Technetium^{99}, a radioactive tracer, to the breast not more than 24 hours prior to surgery. Prior to the operation scintigraphy is performed to help localise the sentinel lymph nodes. At the time of surgery a further injection is made in the peri-areolar region of 2.5% Patent V blue dye (Guerbet, Roissy, France) (Figure 16). The combination of these two markers has been shown to be the most effective method of

correctly identifying the sentinel lymph node (Goyal and Mansel 2008). During the procedure the lymph node position is confirmed using a hand held gamma probe. A small incision is then made over the site and the node is identified visually before being excised.

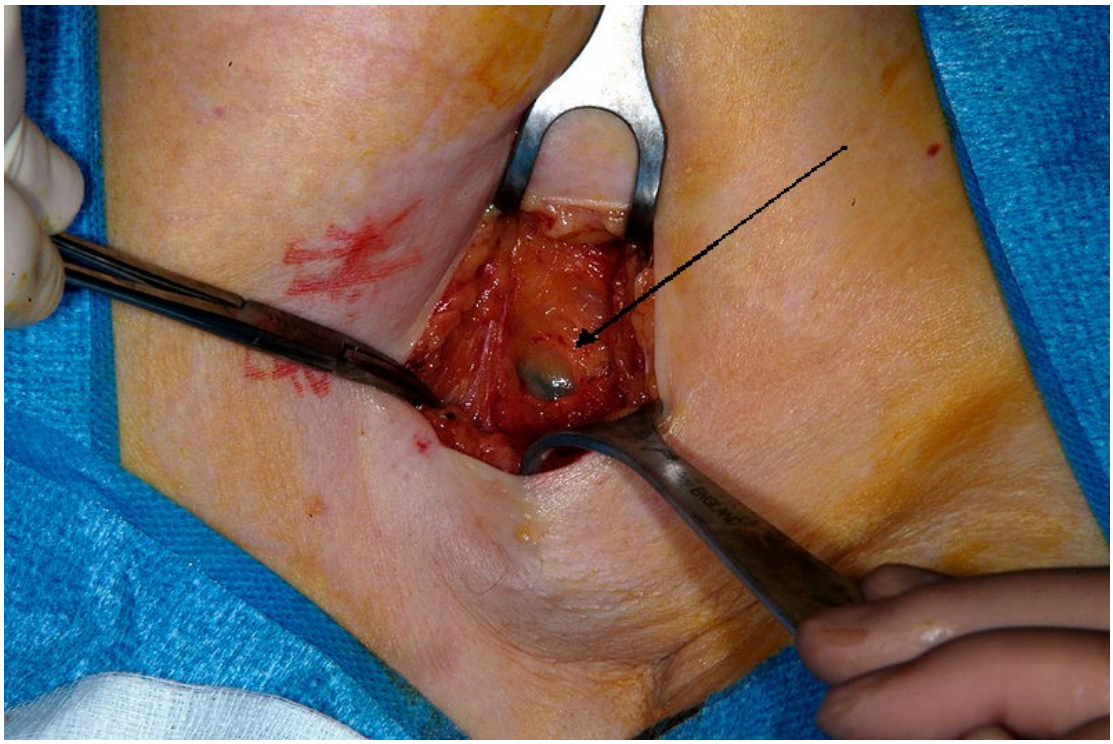

Figure 16- An intra operative photograph of an axillary lymph node (arrow) stained blue identified during a sentinel lymph node biopsy (Authors own copy).

1.5.3. Histopathological Assessment of Axillary Nodes

The presence of metastatic spread within an axillary node may be defined as either macrometastases, cell masses greater than 2 mm in diameter, micrometastases, cell masses between 0.2 and 2 mm in diameter or isolated tumour cells, single cells or clusters of cells less than 0.2 mm in diameter.

The gold standard assessment of lymph nodes following excision is histopathological analysis. Lymph nodes are wax embedded before being cut and stained using haematoxylin and eosin (H and E) stains (Pinder 2009). These stains are widely used in cancer diagnostics. They colour the cell nuclei blue and other eosinophilic structures varying shades or red or pink. Further techniques that aid the identification of either micrometastases or ITCs include immuno-histochemistry staining of cytokeratins and other epithelial markers.

Up until the introduction of SLNB, axillary lymph nodes were assessed by single sectioning of the node whereby a single slice of the node was examined. As a result some metastatic deposits may have been missed as the whole node was not sampled. More intensive serial sectioning of the quantity of nodes collected during an axillary dissection was not practically feasible (de Boer et al. 2010). The reduction in the numbers of nodes collected during a SLNB and the importance of avoiding false negative results has meant that sentinel nodes are now assessed by use of a 2 mm step sectioning procedure often with immuno-histochemical staining (de Boer et al. 2010). Not unsurprisingly this has resulted in an increase in the detection of small metastatic deposits (Quan and McCready 2009; Cserni et al. 2005). Retrospective review of nodes assessed using single slices has demonstrated an up staging of between 7 and 42% (Tan et al. 2008). Slicing the sentinel node into 2 mm sections will identify all macrometastases greater than 2 mm in diameter but will not always pick up micrometastases (Figure 17).

Whilst it is recognised that this technique may miss some micrometastases it is designed to ensure that all macrometastases are detected. More extensive techniques that have a greater sensitivity for micrometastases have been described. The implications these have on resources has meant that they are unlikely to be fully implemented as the low clinical significance of micrometastases and isolated tumour cells (ITCs) becomes more fully understood (Veronesi et al. 2001). New techniques, such as Raman spectroscopy, may therefore have an advantage over standard histopathology as more of the node will be sampled without the associated increased resource requirement.

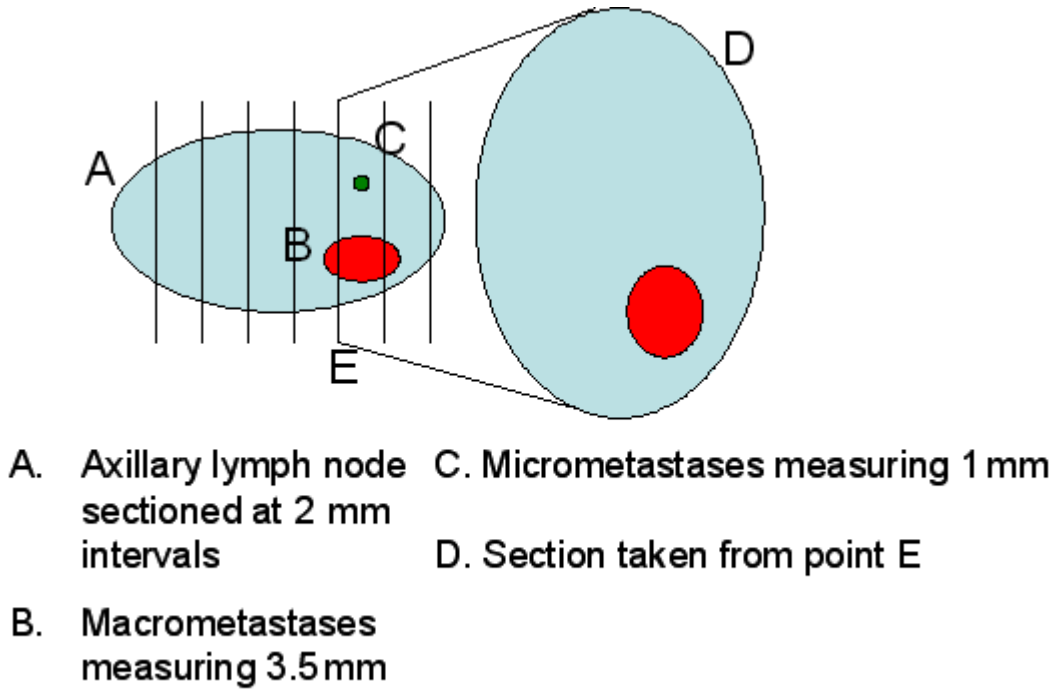

Figure 17- An illustration of the importance of sectioning a lymph node to demonstrate how micro-metastases could be missed.

Before the introduction of SLNB all lymph nodes with metastatic deposits of < 2 mm in diameter were classified as lymph node positive micrometastases (de Boer et al. 2010). However current UK guidelines state that the presence of either macro or micrometastases renders the lymph node positive for metastatic spread but nodes with purely isolated tumour cells are regarded as negative (Pinder 2009).

1.5.4. Management of the positive axilla

The further management of the axilla once positive nodes have been detected depends on the method by which the metastases were detected. A summary based on current NICE guidelines is shown in Figure 18.

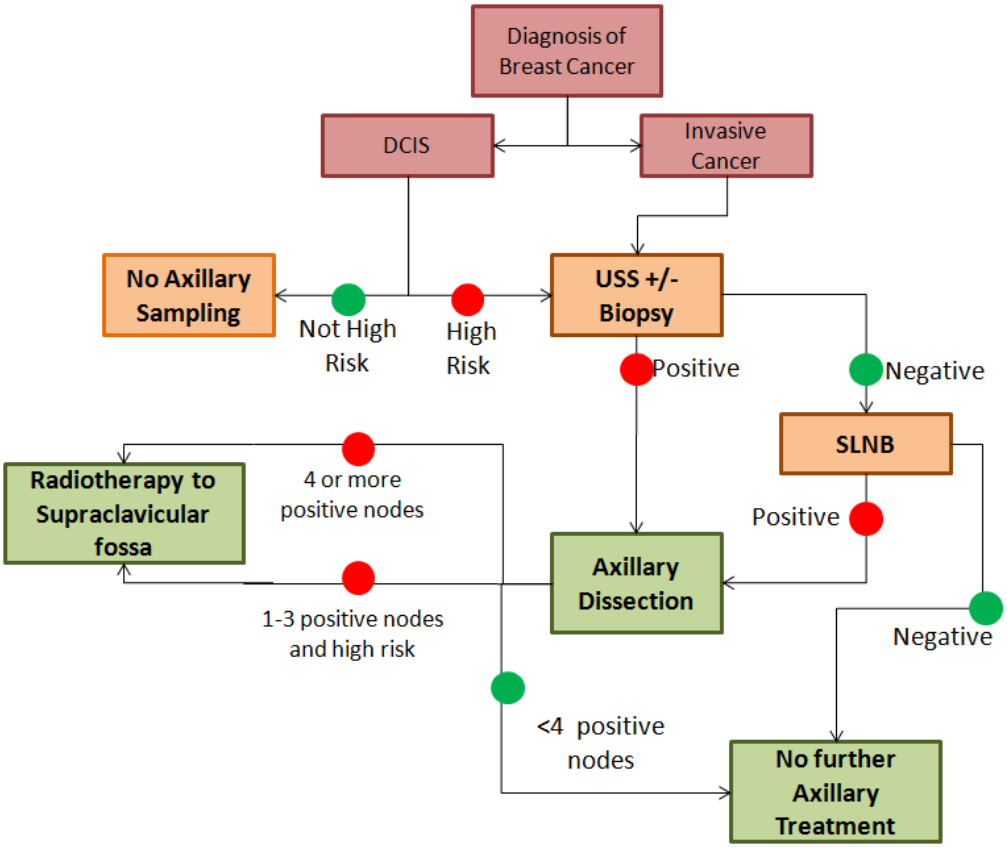

Figure 18- A flow chart demonstrating the management of the axilla in breast cancer.

If there is evidence of metastases from the primary tumour in the SLN then it is recommended that the patient undergoes an axillary dissection to remove all of the lymph nodes in the region (National Institute for Health and Clincal Excellence 2009). Until recently it has been argued that this was necessary for complete staging, improved loco-regional control and perceived improvement in overall survival (Giuliano et al. 2010). It is also worth noting that the current NICE guidelines suggest that all node positive patients receive docetaxal chemotherapy as part of an adjuvant chemotherapy regimen. This is important as a false positive node assessment will result in the patient undergoing both an unnecessary axillary dissection, and if there is no opportunity for post operative result confirmation, a course of chemotherapy (National Institute for Health and Clinical Excellence 2009).

Data from the recently published ACOSOG-Z0011 trial has ignited discussion in this area and questioned our current management of patients with positive lymph nodes. It will be discussed further in subsequent sections (Giuliano et al. 2010).

1.5.5. Intra-operative Assessment of Sentinel Lymph Nodes

Standard post operative assessment of axillary lymph nodes sampled during a SLNB necessitates the need for a second surgical procedure, an axillary lymph node dissection (ALND), at a later date if the sentinel node is positive. Given that 25-30% of patients undergoing a SLNB will have positive nodes a method of intraoperative nodal (IO) assessment has been actively sought (Layfield et al. 2011).

There would be advantages to IO assessment for the patient, the surgeon and the health care system. It has been reported that the delay whilst waiting for results and the effect of requiring a further operation adds to the psychological stress the patient experiences, and a methodology of immediate nodal assessment and ALND, if required, is favoured by patients (Chicken, Sivanadarajah and Keshtgar 2007). Economic analysis carried out in the UK supports the use of intra-operative testing with estimated savings of up to £1000 per patient receiving immediate ALND (Burke and Setters 2010). It has also been argued that further surgery delays the onset of adjuvant treatment which may have an impact on long term outcomes (Snook et al. 2011).

Despite these advantages caution has been expressed because of questions about the true economic benefits of IO assessment, the psychological effect on the patient and the true prognostic role of SLNB detected metastases. It has been argued that the number of patients who could benefit from intra-operative analysis is less than that used in the economic analysis of intra-operative testing (Benson and Wishart 2010). Despite 25-30% of patients having positive nodes data from our own unit suggest that less than 10% of these will return to theatre purely for an ALND (10/121 patients over a 12 month period) (Horsnell et al. 2012). The re-excision of tumour margins, or more significant breast surgery such as a completion mastectomy or breast reconstruction all require second operations during which time an ALND could be performed. Further to this the psychological impact of patients finding out in the recovery room that they have positive nodes by discovering an axillary drain in situ (necessary because of the increased invasiveness of the surgery) has also not been fully explored and will require

careful explanation by the operating surgeon prior to the surgery (Benson and Wishart 2010).

Despite this support has grown for an effective method of intra operative node assessment and has been endorsed by the NHS Technology Adoption Centre (NTAC). The ideal technique in this setting would therefore need to be both sensitive and specific in comparison to the gold standard, quick and user friendly within the theatre setting, economically viable and operable without significant added expertise.

There are currently 3 established techniques for the intra-operative assessment of axillary lymph nodes, frozen section analysis, imprint cytology and molecular assays. Each of these techniques has a number of disadvantages and thus despite the evident potential benefits their use varies. A pan-European survey published in 2004 reported that of the 240 units that responded to the authors, only 60% used some form of intra-operative assessment (Layfield et al. 2011).

1.5.5.1. Frozen Section Analysis

Frozen section analysis is a well established technique that is familiar to all pathologists. It is used in a number of clinical situations where the information derived will be used to guide the patient's immediate management. Current intra operative uses include the differentiation of malignant and benign causes of a frozen pelvis, the identification of resection margins in abdomino-perineal resections or the confirmation of tissue type in parathyroidectomy. Although widely used it has a number of

disadvantages. These include the effect of freezing artefact, the processing time and the need to have immediate access to both an experienced histopathologist and a skilled biomedical scientist (Keshtgar 2009). The sensitivity of this procedure compared to the gold standard, post operative analysis, has been reported as 57-76%, although the specificity is consistently reported as approaching 100% (Creager and Geisinger 2002; Chao 2004; Layfield et al. 2011). Methods of altering the technique to increase the sensitivity have been suggested including multi serial sectioning or the use of rapid immunohistochemistry (IHC) stains (Veronesi et al. 2001). The added workload that this would entail is not thought to be feasible within the UK health care setting (Keshtgar 2009).

1.5.5.2. Touch Imprint Cytology

Touch imprint cytology (TIC) is a simple and rapid method of preparing a cytological specimen for analysis. The excised lymph node is bisected and the cut surfaces are pressed onto a slide which is then fixed and stained. As a result there is no requirement for specialised equipment and there is no loss of tissue that would compromise the gold standard examination of paraffin embedded sections. There does however remain the need for an experienced histopathologist to interpret the slides that have been created (Keshtgar 2009). A meta-analysis of 31 studies where TIC had been used to assess the axillary lymph nodes reported a pooled sensitivity of 63% and a specificity of 99%. This sensitivity was improved to 82% if the presence of micro-metastases were excluded. The authors of the meta-analysis estimated that if all the patients whose nodes were included in the pooled studies had received intra operative TIC node assessment

then over 20% would have proceeded to a primary rather than an interval axillary clearance (Tew et al. 2005). One of the problems with interpreting the results of these studies has been the heterogenity of the sampling techniques used. In the four studies reviewed by Layfield variations in technique occurred in all four centres. However the pooled sensitivity of 63%, which is below that of frozen section, and the added expertise required accounts for why the technique is less widely used than frozen section analysis (Layfield et al. 2011).

1.5.5.3. Molecular Assays

Recently molecular assays using either reverse transcriptase polymerase chain reactions (RT-PCR) or reverse transcriptase loop-mediated isothermal amplifications (RT-LAMP) have been developed to detect metastasis by quantitatively measuring the concentration of tumour specific mRNA markers. The two markers CK-19 (used in both techniques) and mammaglobin (used in the RT-PCR only) are expressed at high levels in cells of breast origin but are absent or a low level in normal axillary nodes. Studies analysing the efficacy of these methods to differentiate between positive and negative nodes have reported sensitivities of between 88 and 98% and specificities of greater than 93% for the RT-PCR technique (Blumencranz et al. 2007; Tafe 2010). An unpublished meta-analysis of 8 similarly run studies carried out within our group, which included a total of 1547 patients, revealed a sensitivity of 88% and a specificity of 95%.

Sensitivities of 95% and specificities of up to 97% have been reported with the RT-LAMP technique (Tamaki et al. 2009; Visser et al. 2008). A four centre study that included 204 patients within the UK using OSNA (the commercially available RT-LAMP equipment) has recently published data with a sensitivity of 91.7% and a specificity of 96.9% (Snook et al. 2011).

The advantages of these molecular assays include the ability to perform the test without the need for a specialised histopathologist to interpret the results and in a time frame that does not delay the surgical procedure. Disadvantages include the need to homogenise the node which prevents subsequent gold standard histopathological analysis. This is a particular danger as the false positives would mean that the patient is condemned to both an unnecessary axillary clearance and a course of chemotherapy as previously highlighted. It is worth noting that GeneSearch ® (Veridex, LLC, Warren NJ, and USA) the first commercially available product to exploit the RT-PCR technique has recently been withdrawn from the market. The high set up costs, logistical difficulties and the level of false positives were all cited for the low demand that prompted its withdrawal from the market (Loftus 2010).

1.6. Controversies

It has always been clear that the status of the axillary lymph nodes in breast cancer is crucial for staging and prognostic prediction. Techniques to both sample and assess these nodes have changed, particularly since the introduction of sentinel lymph node biopsy. However in the modern breast screening era patients are often presenting at an

earlier stage and this has caused many to re-examine the clinical significance of the axillary nodes and the need for an ALND if the nodes are found to be positive. This project is based on the perceived clinical need for a new method of intra-operative lymph node assessment that would allow immediate ALND to take place if required. Therefore an understanding of the nature of the ongoing debate is crucial to appreciate the implications it may have for the future applicability of this research.

1.6.1. What is the significance of positive nodes?

As has been discussed the increased thoroughness of pathological assessment now applied to sentinel lymph nodes has resulted in up to 40% of nodes being "upstaged". Clinicians have therefore asked whether the clinical significance of these positive nodes, particularly micrometastases and isolated tumour cells (ITCs), is the same as the traditional H&E single sliced positive nodes on which their long held prognostic importance is based.

Initially the focus of this debate had been the implication of finding micrometastases and isolated tumour cells. A recent meta-analysis examined 12 cohort studies comparing the 10 year outcomes of patients with single sliced H&E positive nodes (micrometastases and ITCs) against those with negative nodes. This confirmed the traditional view that patients had a poorer disease free survival rate and overall survival at 10 years if micrometastases or ITCs were present on the single slice (de Boer et al. 2010).

This survival difference was less clear in studies that compared an "occult" group of positive nodes (where retrospective pathological assessment of single sliced H&E negative nodes had subsequently identified micrometastases or ITCs) with nodes that remained negative after step sectioning. Overall survival was not reduced in 3 out of 6 studies that used multivariable analysis and disease free survival was not significantly different in eight out of 12 studies that recorded this outcome (de Boer et al. 2010).

Analysis of data published since the advent of SLNB was more difficult as relevant studies were "hampered by small numbers, short follow-up and lack of multi variable analysis". The authors went on to include some of the earlier studies that had included a sub population of patients who underwent SLNB and this suggested a lower disease free survival and overall survival if metastases of less than 2 mm were present (de Boer et al. 2010). This finding is supported by a retrospective cohort study of more than 2500 Dutch women who had a SLNB. Even after adjustment for diagnosis, tumour grade, hormone receptor status and ALND there was an increased risk of events among patients with either micrometastases (hazard ratio 1.56 (95% CI 1.15 to 2.13)) or ITCs (hazard ratio 1.5 (95% CI 1.15 to 1.94)) as compared to node negative women (de Boer et al. 2009) (Figure 19). This increased risk was reduced if patients who had micrometastases or isolated tumour cells received systemic adjuvant therapy.

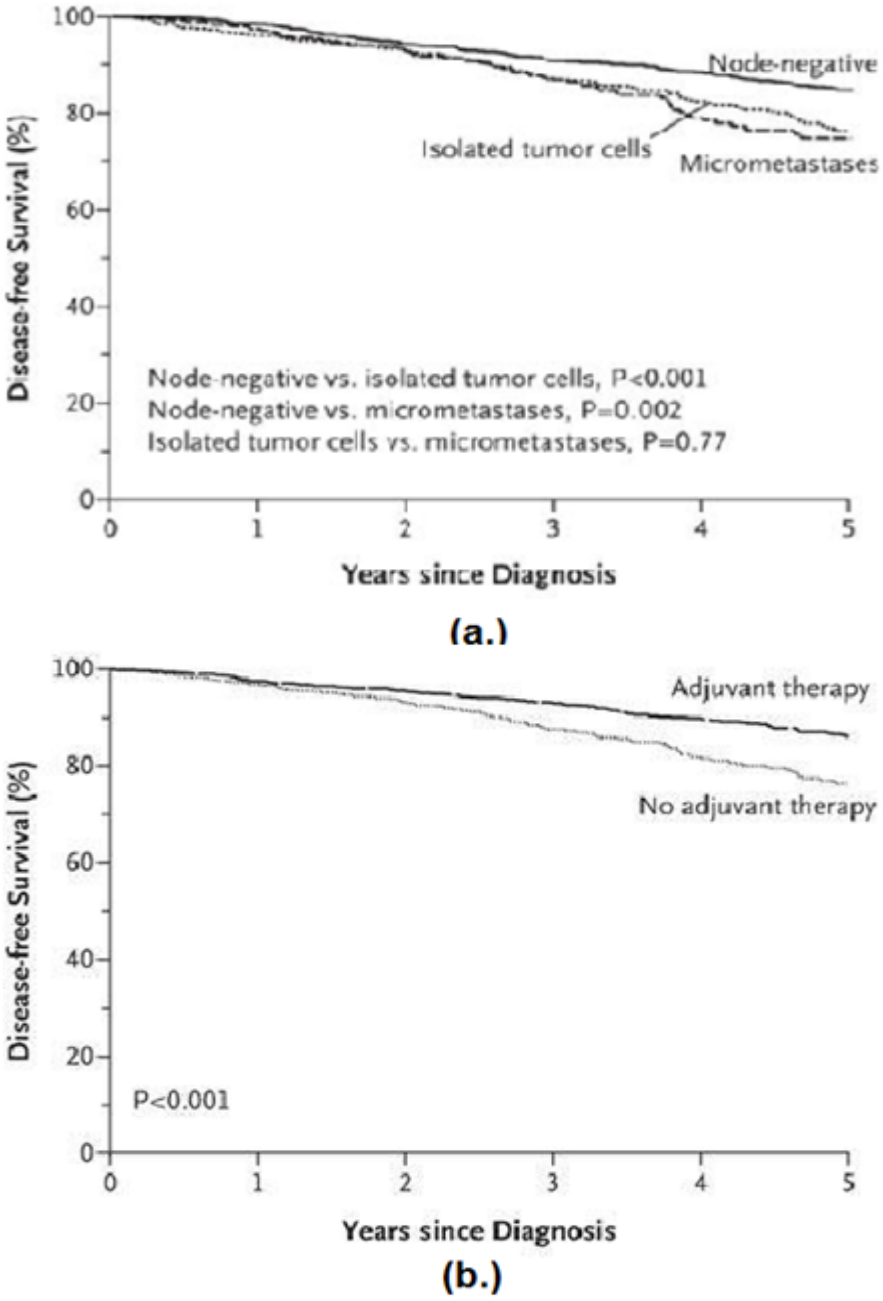

Figure 19- Disease free survival curves over 5 years after diagnosis in patients who are node negative or who have ITCs and micrometastases (a.) with and without adjuvant treatment (b.) This demonstrates the worse outcome in patients who had nodal metastases and how this could be mitigated with adjuvant treatment (adapted from de Boer et al. 2009).

This is important as critics of the retrospective studies argue that much of this data is based on old cohorts of patients who were identified pre-screening programmes and who did not receive adjuvant treatments. A more contemporary American cohort study suggested that there was no added benefit for patients with micrometastases who underwent an ALND after a SLNB in either preventing axillary reoccurrence or overall survival (Bilimoria et al. 2009). Both the local reoccurrence and the overall survival were no different if the patient underwent an ALND or not (disease free survival 98% v 99% at 5 years in ITCs and 90 v 89% at 5 years in micrometastases in the no ALND v ALND groups). This study further went on to show a marked reduction in numbers of patients having SLND if there was evidence of micrometastases or ITCs in the period 2000 -2005.

Two recent studies that have addressed the question prospectively were the American College of Surgeons Oncology Group Z-0010 trial and the National Surgical Adjuvant Breast and Bowel Project (NSABP) - 32 trial. The Z-0010 trial included patients whose clinicians were blinded to the results of immuno-histochemistry and treatment thus relied on the single cut H and E slide. This showed that the 5 year overall survival rates were 95.8% ,in the IHC negative, group as compared to 95.1% in the IHC positive group (Cote et al. 2010). The NSABP-32 trial showed a slight improvement in survival in the IHC negative group (95.8% 5 year disease free survival v 94.6%) (Weaver et al. 2011). The differences remain small and thus the role of these “extra” metastases detected by immuno-histochemistry remains questionable.

Added to this debate are studies that support the concept of ITCs being found in a node for benign reasons. It has been argued that they may be a result of previous manipulation and instrumentation of the breast tumour. Both fine needle aspiration (FNA) and core needle biopsy may displace epithelial cells and either benign or malignant cells have been found in the granulation tissue along the site of the biopsy. Part of the healing process after these procedures involves interstitial fluid draining to the axillary lymph nodes. In this way cells of epithelial type may be transported to the node as a result of a natural healing reaction. Comparison of the cell type may help to clarify this. If the ITCs are different to the primary tumour it is unlikely to be related to the tumour. Further if there is evidence of the debris from tissue trauma such as red blood cells or haemosiderin deposits within the node then a traumatic cause is more likely (Carter et al. 2000 ; Bleiweiss, Nagi and Jaffer 2006).

These studies support the current UK guidelines that nodes with ITCs are deemed to be negative. Within these guidelines the presence of micrometastases, as has been discussed, renders the node positive currently. Based on the studies above this remains a very controversial area and the benefits of further treatment may be questioned. The importance of the MDT in discussing the risks and potential benefits of further treatment in individual patients with these findings is clearly crucial. Thus the place for immediate ALND, following intra-operative diagnosis, prior to MDT discussion in these patients may be questioned.

Until recently the position of macrometastases was much more straightforward. The most recent contribution to the debate has been the results of the Z-OO11 trial (Giuliano

et al. 2011). This was a prospective randomised trial of SLNB and no further axillary treatment versus SLNB and ALND for patients with T1 or T2 tumours and either micro or macrometastases discovered on H&E slides, who were undergoing breast conserving treatment and adjuvant therapy. There were a number of exclusion criteria that included palpable nodal disease, extra nodal spread and more than 3 nodes affected. The results of this study have shown, at a median follow up of 6.3 years, that there were no statistically significant differences in either local or regional recurrence amongst the two treatment groups. The authors suggested a number of possible reasons for this result. Firstly that SLNB removed the nodes with metastatic spread, stating that in 40-60% of cases the sentinel node is the only positive node. Secondly they proposed that not the entire metastatic load in axillary nodes has the ability to develop into clinically significant disease. As a result of this study they suggest that we may be over treating the positive axilla. They do sound a note of caution by explaining that this is only relevant to patients with T1/T2 tumours, undergoing breast conserving surgery with no clinically palpable axillary disease and less than 3 positive nodes. They also concede that all the patients in the study underwent opposing tangential field whole breast irradiation which may well have treated the axilla. Further to this 96% of patients received systemic adjuvant therapy which may confound the results. However as a result of these findings the lead author has suggested that the role of ALND needs to be re-examined and may in the future be eliminated as a requirement for most women with "contemporary" breast cancer.

The latest National Comprehensive Cancer Network guidelines for the management of invasive cancer have thus included a category of patients that meet the criteria for the Z-

0011 trial and should be "considered" for no further axillary surgery (National Comprehensive Cancer Network 2012). Despite the finding of the Z0011 trial, SLNB remains the standard of care for breast cancer patients in the UK and completion ALND is still recommended if there are macro- or micro-metastases within an axillary lymph node. Practice is changing and for the management of micro-metastases the place of ALND is now questioned and thus the role of intra-operative node analysis will be limited if there is no plan to proceed to an ALND. For macrometastases there remains a clear place for ALND even if it is in a smaller group of patients in the post Z-0011 era. This is clearly an issue which will continue to be debated and the results of a number of ongoing trials will help shape the debate. Trials that look at the outcome of axillary node dissection versus no axillary node dissection in patients positive for micrometastases (IBCSG 23-01 Trial) and that assess whether axillary dissection or axillary radiotherapy is the best treatment option for patients with metastatic spread (AMAROS (After mapping of the axilla: Radiotherapy or Surgery) Trial) may add greater pressure onto the advocates of ALND. The results of these trials will be keenly followed and help shape future management of node positive breast cancer.

As the management of breast cancer continues to progress new methods of prognostic assessment may also influence the future management strategies. OncotypeDX (Genomic Health Inc) is a multi gene diagnostic assay based on the gene expression of a tumour specimen. It is currently being marketed to quantitatively predict the likelihood of chemotherapy benefits and distant reoccurrence. Based on the level of expression of 16 genes patients can be stratified into one of three groups. This allows patients to make decisions based on the risk benefit ratio for each sub group, rather than the population

as a whole. As a result those patients who would receive the maximum benefit of systemic treatments can be identified and given the treatment whilst those who would receive minimal benefits could decide against it due to the side effects and toxicity of the treatment. (Paik et al. 2006). Studies to date suggest that these techniques may also be able improve upon standard staging although questions remain with regard to their efficacy at predicting local reoccurrence and their use for rarer sub types (Gelmon 2010).

1.7. Conclusions

Breast cancer remains a significant cause of morbidity and mortality. It is a disease which attracts a great deal of clinical research, of which this Raman based study, is one such example. As a result, the management of the disease will continue to change to embrace new technologies and techniques. It is of the authors' opinion that ALND will continue to retain a place in the management of breast cancer, particularly for patients with nodes positive for macrometastases that fall outside the criteria of the Z-0011 trial. As has been demonstrated in this chapter, determining the nodal status of each patient's axilla remains important both to guide treatment and to achieve the very best clinical outcome.

There are pathological differences that exist between a normal axillary lymph node and one in which metastatic spread has occurred. It is these differences which are exploited by current techniques. As has been discussed they all have their own advantages and disadvantages and have not been universally implemented. As a result there remains a

need for a technique that can provide patients with the benefits of intra-operative axillary node testing, in a cost effective way that could be made available to all. It is hoped that within this study, and thus this thesis, that the potential role of Raman spectroscopy to fill this void will be established. To achieve this experiments performed at a preparatory stage, prior to use within an operating theatre, will be reported before focusing on experiments that were carried out within an operating theatre using fresh tissue, to establish the technique as one that could be used in a real life clinical setting.

2. Raman Spectroscopy and Clinical Diagnostics.

As concluded at the end of the first chapter the aim of this project is to determine whether Raman spectroscopy could be used as a means of assessing axillary lymph nodes intra operatively in patients newly diagnosed with breast cancer. In this chapter the technique and concepts underpinning the use of Raman spectroscopy will be introduced. Evidence supporting its use in this project will be discussed and supported by reviewing previously published work.

2.1. The Ideal Diagnostic Tool.

When considering the development of a new diagnostic tool it is important to first highlight what features would constitute the ideal tool for the scenario in which it is to be used. As previously discussed in Chapter 1 there are a number of techniques that are already being used to assess lymph nodes intra-operatively. They all have significant disadvantages which have prevented their universal use. Analysis of these techniques suggests the key parameters which a new diagnostic tool entering this environment must meet.

Firstly and most importantly the tool must be both sensitive (its ability to detect true positives) and specific (its ability to detect true negatives) in comparison with the gold standard histopathology assessment. The clinical consequences of a false positive result would see a patient undergoing an ultimately unnecessary axillary node dissection and adjuvant chemotherapy. The consequences of a false negative result whilst being less

severe would mean that a patient with a positive node was under-staged and potentially under treated. This can partially be mitigated for by the ability to post-operatively cross check the tests results. This would however mean that a false negative patient needed a second operation and thus negate the very benefit it could provide.

Secondly the diagnostic tool must be able to produce a result without unnecessarily disrupting or delaying the ongoing procedure. It is the author's opinion that the best way to achieve this is for the equipment to be used within the operating theatre. This would reduce the added costs of having separate staff, particularly pathologists, to operate the device outside theatre and help prevent time delays as well as reducing the risk of tissue loss whilst transporting the node to an alternative venue. For the device to be used within theatres it needs to be safe, unaffected by the theatre surroundings and simple to use. It should be the aim that theatre staff can easily produce a result without significant added expertise, either in tissue preparation or diagnostic interpretation.

Finally in the current economic environment it is important that the tool is cost effective. Raman spectroscopy, unlike the other intra-operative methods, has the potential to fulfil these criteria and this will be demonstrated in this project (Table 5).

	Frozen Section Analysis	Touch Imprint Cytology	Molecular Assays	Raman Spectroscopy
• Sensitive				To be determined
• Specific				To be determined
• Post Operative Cross Check				
• Use within theatre				To be determined
• Time Frame				To be determined
• Cost Effective				To be determined

Table 5- The features of an ideal diagnostic tool for intra-operative lymph node assessment. For illustrative purposes the strengths and weakness of current intra-operative techniques are shown, along with the areas that need to be determined for Raman spectroscopy (further details of the non-Raman spectroscopy techniques can be found in Chapter 1).

2.2. Raman Spectroscopy - An Introduction

Raman Spectroscopy is based on the inelastic scattering of monochromatic light as it interacts with molecules. This interaction between light and molecules was first observed by C.V. Raman in 1928. It is one of a number of interactions that may occur when light interacts with matter. Light may be reflected, absorbed or as in the Raman effect, scattered. Each of these modalities may be harnessed to assess matter. To

appreciate these interactions we need to consider that light is a form of electromagnetic radiation and may further be conceptualised as small packets of energy or photons that exhibit wave particle duality. The relationship between the energy (E) of a photon of light and its wave frequency (v) is given by the equation;

$$E=hv$$

Where h is Planck's constant (6.63×10^{-34} J/s molecule^{-1})

The frequency is related to the wavelength (λ) of light by the equation;

$$v = c / \lambda$$

Where c is the velocity of light (2.998×10^{8}ms^{-1})

It is thus apparent that that the energy of a photon of light is inversely proportional to its wavelength.

The majority of scattering interactions are elastic in nature. In this scenario a photon of light interacts with a molecule and causes polarisation of its electron cloud and a rise in its energy state. This new "virtual" energy state is very short lived (approximately 10^{-14} secs.) after which the molecule returns to its initial energy state. As it returns to its initial energy state it releases a photon with the same energy and hence wavelength as the incident light.

In contrast Raman scattering is an inelastic interaction. The incident and emitted photon have different energies and therefore different wavelengths. This occurs because the molecule, having been excited to a virtual energy state from its initial state, does not return to the initial energy state but to a higher (or lower) energy state. Therefore the photon emitted will have an energy which is lower (or higher) than the incident photon. When the emitted photon has a lower energy it is termed Stokes Raman Scatter and when the emitted photon has a higher energy it is termed anti-Stokes Raman Scatter. Many times less than 1% of scattered photons have undergone Stokes Raman scattering, with even less undergoing anti-Stokes Raman scattering (Figure 20).

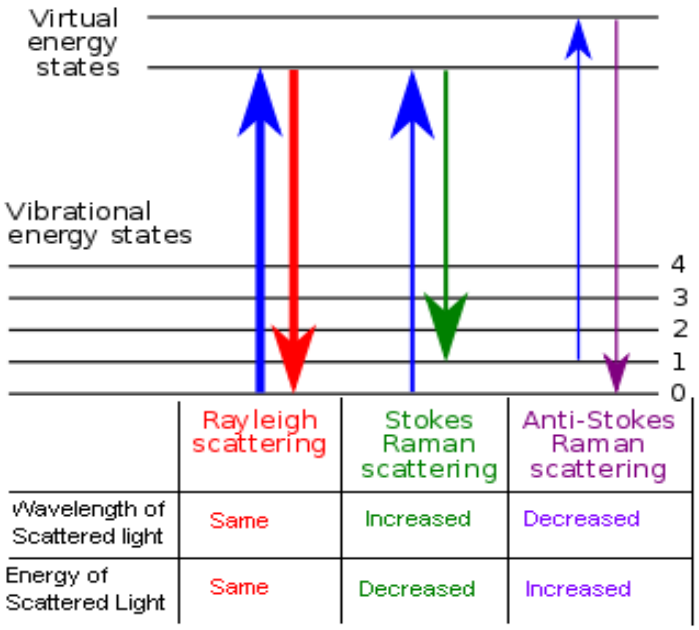

Figure 20- The characteristics of Rayleigh, Stokes and Anti-Stokes light scattering, demonstrating that in Rayleigh scattering the energy level returns to the original state and thus the wavelength of the emitted light is the same as the incident light that caused the temporary energy level shift. In contrast in Raman (Stokes and anti-Stokes) the energy level does not return to the original state and thus emitted light has a different wavelength to the incident light.

Within each molecule there are defined numbers of energy modes. These may be related to the position of electrons in molecular orbits or to the vibrational mode of the molecule. The energy required to alter these energy modes differs for each molecule, dependent on their configuration, however the energy required to alter the vibrational state of a molecule is less than that required to alter the orbital positions of its electrons (Figure 21).

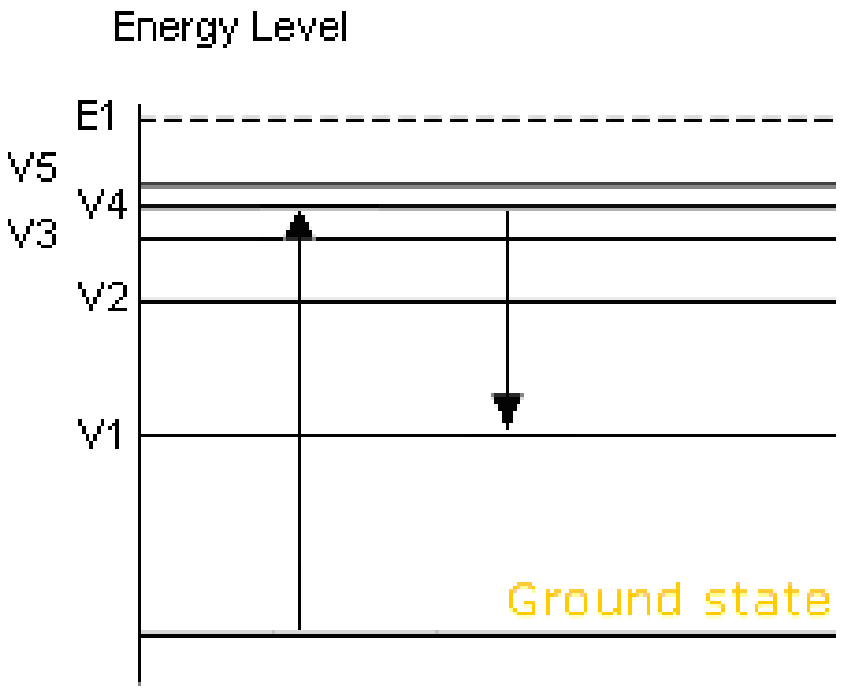

Figure 21- Illustration of the energy levels of different vibrational states of a molecule. Moving from one vibrational energy($V_{1\text{-}5}$) level to another requires less energy than electron position levels (E_x). The arrows indicate the effect of Raman (Stokes) scattering (see also figure 20).

Raman scatter occurs due to changes in the vibrational modes of the molecules that the light interacts with. The number of the different vibrational modes (vm) that each

molecule is capable of adopting is calculated by the equation;

$$vm = 3n-6$$

(where n equals the number of atoms in the molecule and 6 is subtracted to account for the translations and rotations of the molecule itself.)

In ethane (C_2H_4) for example there are 12 vibrations possible: 4 C-H stretching, 1 C-C stretching, 2 H-C-H bending, 2 CH_2 rocking, 2 CH_2 scissoring and 1 twisting mode (Figure 22).

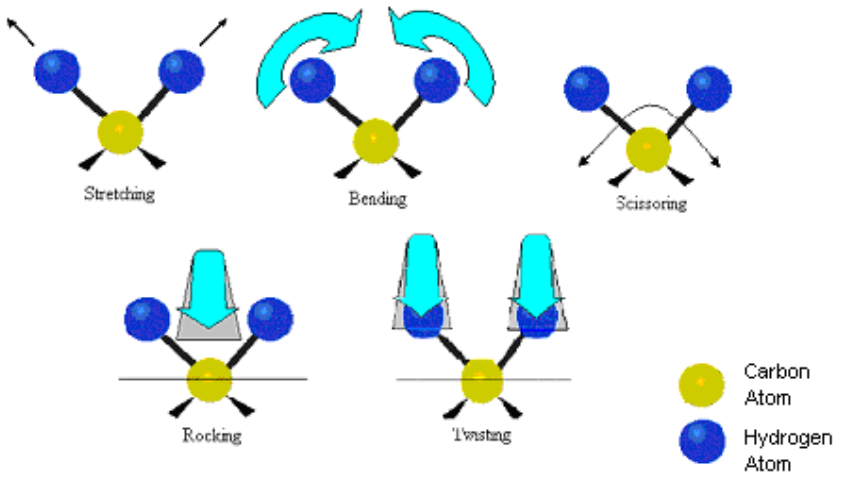

Figure 22- One half of the ethane molecule demonstrating some of the types of vibrational conformations possible (adapted from http://en.wikipedia.org/wiki/Molecular_vibration).

A change in vibrational mode may be detected using Raman spectroscopy but this is not always the case. For a change in vibrational mode to be "Raman active" it must involve a change in the polarisability of the molecule. In its simplest form this means that the volume of the molecule is increased. An example of this is the symmetrical stretch of CO_2 (Figure 23).

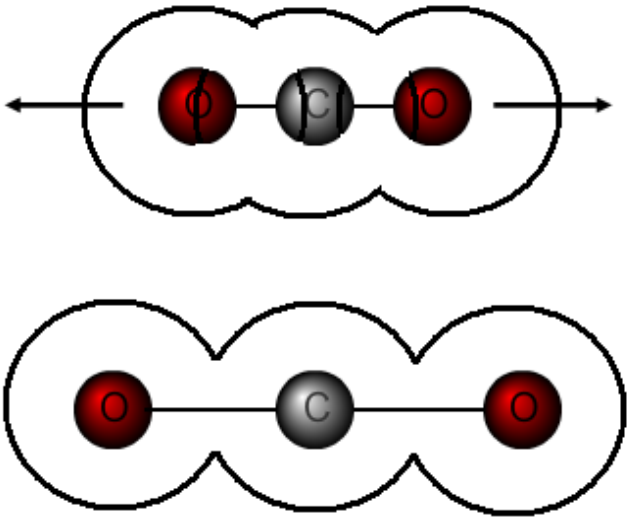

Figure 23- Demonstration of how the distortion of the molecules electron cloud by stretch vibrations will alter the volume and thus the polarisability of the molecule.

By contrast some vibrational mode changes will only alter the dipole moment and not the polarisability of the molecule (Figure 24).

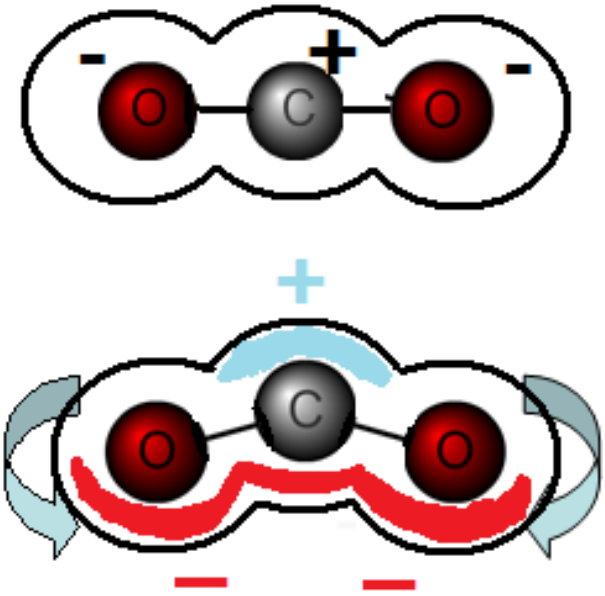

Figure 24- Demonstration of how asymmetrical stretching of a molecule alters the dipole moment of the molecule. Following the stretch part of the molecule (shaded red) becomes more "negative" and part becomes more "positive".

This change is not detected by Raman spectroscopy but is detected using IR (infra-red) spectroscopy and thus the two methods are often said to be complementary to each other. This has important consequences particularly in the measurement of clinical tissue. Water has to be excluded from samples undergoing IR spectroscopy due to the marked dipole effect and the distortion of the spectra produced. This is not the case with Raman spectroscopy and allows the technique to be used on fresh tissue.

Utilising the Raman scatter effect allows spectra to be plotted that are based on the molecular structure of the matter under investigation. The energy requirements required to alter vibrational modes are different for individual molecules and can further be influenced by the interaction with neighbouring molecules. A spectrum produced by a Raman spectrometer plots the intensities of emitted photons (y axis) as a function of the Raman shift (x-axis). The Raman shift is the difference between the energy of the incident photon and the emitted photon. It is measured in wavenumbers (with units of cm^{-1}) that are equal to the reciprocal of the wavelength.

Biological tissue is made up of a combination of different biochemical constituents. Broadly speaking these can be divided into 4 separate groups, nucleic acids, proteins, lipids and carbohydrates. As discussed in Chapter 1, when metastatic colonies establish themselves and proliferate, the proportion of each tissue constituent changes. Cells replicating quickly will increase the nucleic acid component of any tissue spectrum, in combination the immune response will increase the protein contribution and as the metastatic cells replaces the normal tissue then the lipid component will diminish (Ioachim and Ratech 2002). Due to the fact that the features of a Raman spectrum

collected from tissue are based on its molecular structure differences in the biochemical constituents of a tissue can be detected (Figure 25). It is anticipated that the biochemical differences between metastatic and normal lymph nodes will be sufficient to allow separation of the two groups based on their Raman spectral features.

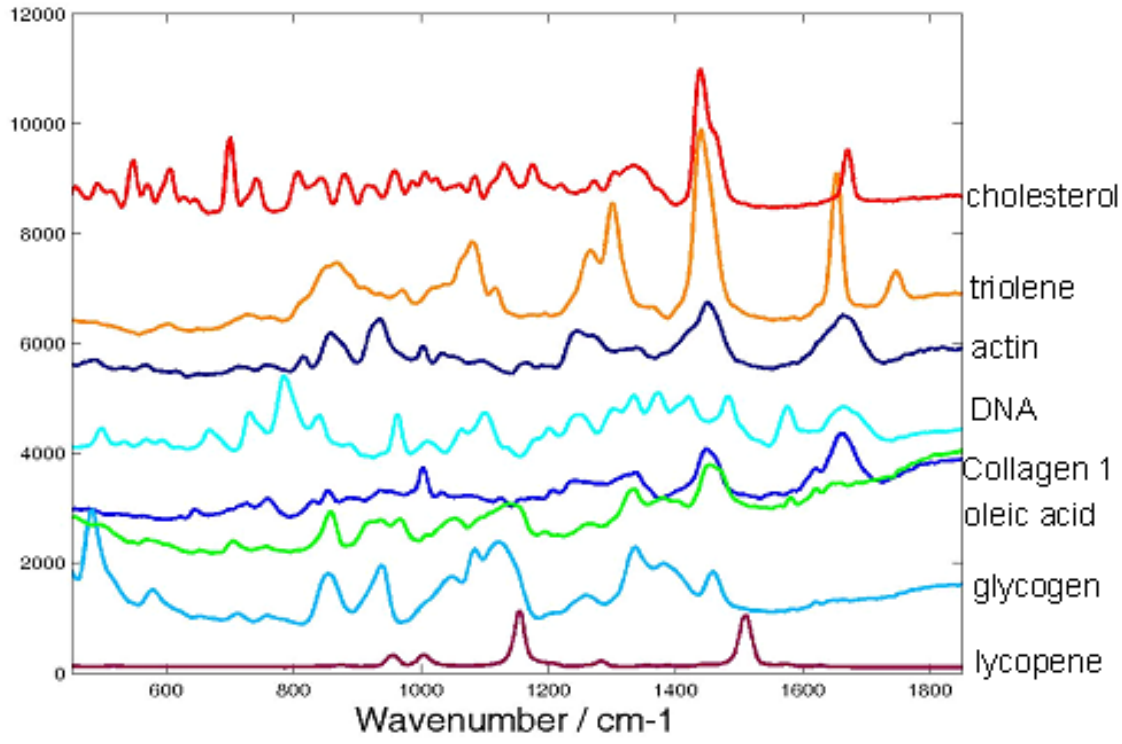

Figure 25- Raman Spectra from different biochemical compounds highlighting the variation in spectral features (Diem, Chalmers and Griffiths 2008).

2.3. Raman Spectroscopy - Technical Considerations

Modern Raman spectrometers are very different to the simple equipment employed by Raman in 1928. Then he used sunlight focused through a telescope as opposed to the high intensity single wavelength laser light sources that are employed now. Much of the previously published work using Raman spectroscopy to assess biological tissue has

used incident light in the Near Infra Red (NIR) region. This wavelength of light is absorbed much less readily by the tissue, causes minimal tissue damage and overcomes the effect of fluorescence seen with visible and ultraviolet light. The wavelength of light that is to be used in this study is 785nm.

A key consideration in Raman spectrometer design is the prevention of interference from elastic scatter. As previously discussed the proportion of all scattered light that is inelastic is very small. Therefore a series of filters are used to reduce this effect. In the spectrometer used throughout this project, the B&W Tek MiniRam II (see Chapter 3), a notch filter allows Raman peaks to be detected as close as $175cm^{-1}$ from the Rayleigh line. Detection of the scattered light is achieved using a charged coupled device (CCD) that allows for the measurement of a whole spectrum at once. Built into the MiniRam II system is a thermo-electric cooler that reduces both the dark current and the background noise. This allows the spectrometer to be used with long collection times and permits the detection of weak optical signals.

A number of techniques have been developed to enhance the Raman signal from tissue of interest. Although it is not intended that these techniques will be used in this project a brief discussion is pertinent for completeness. Examples of this include resonance Raman spectroscopy, surface enhanced Raman spectroscopy and spatially offset Raman spectroscopy.

In resonance Raman spectroscopy the incident light is tuned so that it coincides with the energy required for an electron to move energy level. In this way photons maybe

scattered up to 10^6 times more than using conventional Raman techniques. Thus vibrational transitions which are too weak to be detected normally can be identified. Surface enhanced Raman spectroscopy (SERS) is a further technique that is used to enhance the Raman signal. In this case samples are adsorbed onto Gold or Silver surfaces. This results in an increase in the intensity of the Raman scatter particularly when combined with resonance Raman spectroscopy (DoItPoms 2010). The exact mechanism for this action is still debated. It has been postulated that it may occur either due to an increase in the electromagnetic field that then increases the interactions with the incident light or due to the metal altering the electron energy levels of the molecule and thus providing a resonance effect (DoItPoms 2010). The *in vivo* use of this technique is currently limited by concerns about the ability of the body to excrete the markers and thus the long term effects of retained metals. Spatially offset Raman spectroscopy collects Raman scatter from a position several millimetres offset from the point of excitation. This overcomes the high intensity Raman scatter from the area of excitation which ordinarily dominates the spectra obtained. As a result this technique has been used to probe tissue many millimetres in depth (DoItPoms 2010).

2.4. Raman Spectroscopy in a clinical setting

The use of Raman spectroscopy to identify primary tumours and differentiate them from normal non malignant tissue has been demonstrated in a number of organs including oesophageal (Kendall et al. 2003), laryngeal (Stone et al. 2000), bladder (Stone et al. 2004), prostate, (Stone et al. 2004) and colon (Molckovsky et al. 2003). A review of all

the different tissue types would be beyond the scope of this report but this section will focus on the evidence supporting its use in breast cancer and lymph nodes.

2.4.1. Raman Spectroscopy in Breast Tissue

The first recorded spectra of human breast tissue were published in 1991 (Alfano et al. 1991). They recorded the spectra using FT-Raman spectroscopy and an excitation laser with a wavelength of 1064 nm. Analysis was performed to compare the characteristic spectral peaks of three normal, four benign and seven malignant specimens. They observed differences in both the presence of particular peaks and the relative intensities. Four key peaks were identified in normal tissue at 1078, 1300, 1445 and 1651 cm^{-1}. In comparison there was an absence of these peaks at 1078 and 1300 cm^{-1} in the malignant tissue. Further the intensities of peaks at 1445 and 1651 cm^{-1} where different in all three tissue types. The importance of these peaks was further demonstrated in a number of observational studies published in the 1990s and were attributed to differences in the spectral contribution of fatty acids (FA).

Attempts to quantify what these differences equated to biochemically followed. Initial work attributed the observed changes to contributions of fatty acids and β-Carotene (Redd et al. 1993).

Subsequent work collected 123 spectra from 41 tissue specimens excised during breast surgery procedures. The authors of this study used the data to compare the spectral features of normal breast tissue with those of invasive ductal carcinoma (Frank et al.

1995). The normal tissue demonstrated features consistent with the presence of lipid whilst the malignant tissue had peaks that were suggestive of an increased contribution by proteins. It was particularly noted that the peak in normal tissue at 1439 cm^{-1} (attributed to the CH_2 deformation) was shifted to 1450 cm^{1} in malignant tissue. The authors suggest that this change is consistent with a change from fatty acids to proteins. The previous use of β carotene as a discriminative feature was not evident because of the wavelength of the incident light source, 784 nm (Frank et al. 1995).

A subsequent study that assessed 61 samples from 13 patients similarly compared spectral differences between normal breast tissue and invasive ductal carcinoma. The authors demonstrated that spectra from normal tissue were dominated by fatty acid features whereas spectra from positive samples were dominated by protein peaks. The key differences noted were a shift in the 1445 cm^{-1} peak to 1450 cm^{-1} as shown previously and a widening of the 1650 cm^{-1} band in the positive spectra (Figure 26).

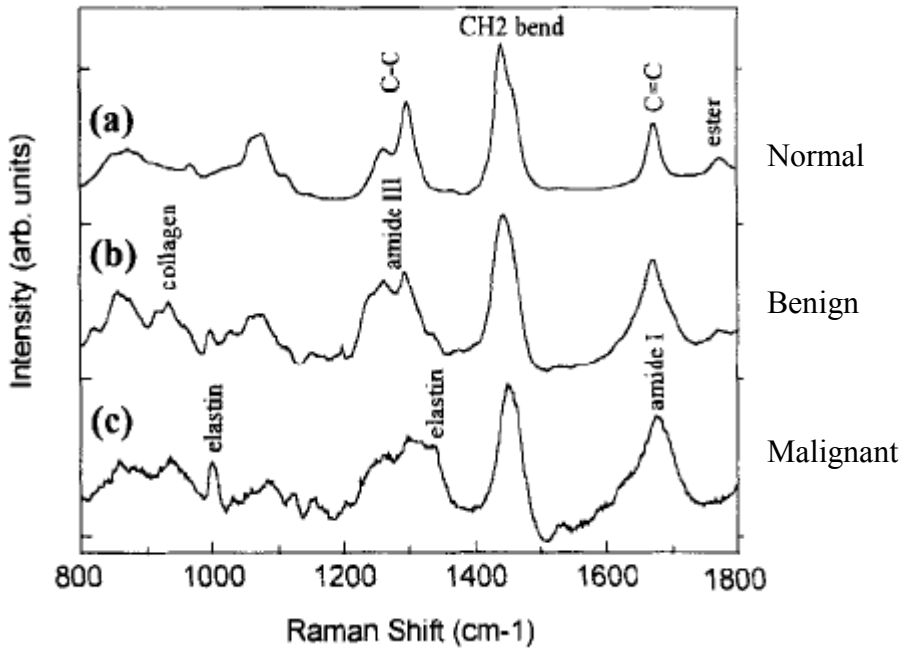

Figure 26- Raman Spectra of three distinct types of breast tissue (Manoharan et al. 1998).

These differences were used to differentiate between normal and malignant tissue. Sensitivities of 100% for identifying malignant tissue, 88% for benign tissue and 94% for normal tissue were achieved using principal component analysis (Manoharan et al. 1998). The authors of the paper accepted that the small number of samples did not allow adequate cross validation to support these results. However the potential for the use of Raman spectroscopy to aid clinical diagnosis of breast cancer was clearly set.

A number of groups have subsequently pursued the use of Raman spectroscopy in the diagnosis of breast cancer. A novel approach to spectral difference analysis was adopted by Haka et al. who in 2005 reported the creation of a breast tissue spectroscopic model. The model was based on the analysis of 130 spectra from 58 patients undergoing breast cancer surgery. They demonstrated that the spectra from different tissue types could be replicated by varying the percentages of the model components, namely collagen, fat, cholesterol, β carotene, cell cytoplasm and nucleus and calcium compounds (Figure 27). The key spectral differences were noted to be the fat, collagen and cell cytoplasm components. Using the component percentages they were able to distinguish between normal and malignant tissue with 94% sensitivity and 96% specificity based on the contributions of collagen and fat (Haka et al. 2005) (Figure 28). The authors recognised that this was an *ex vivo* study based in a laser laboratory on snap frozen specimens but they stated that it was an important step towards the clinical use of Raman spectroscopy in breast cancer.

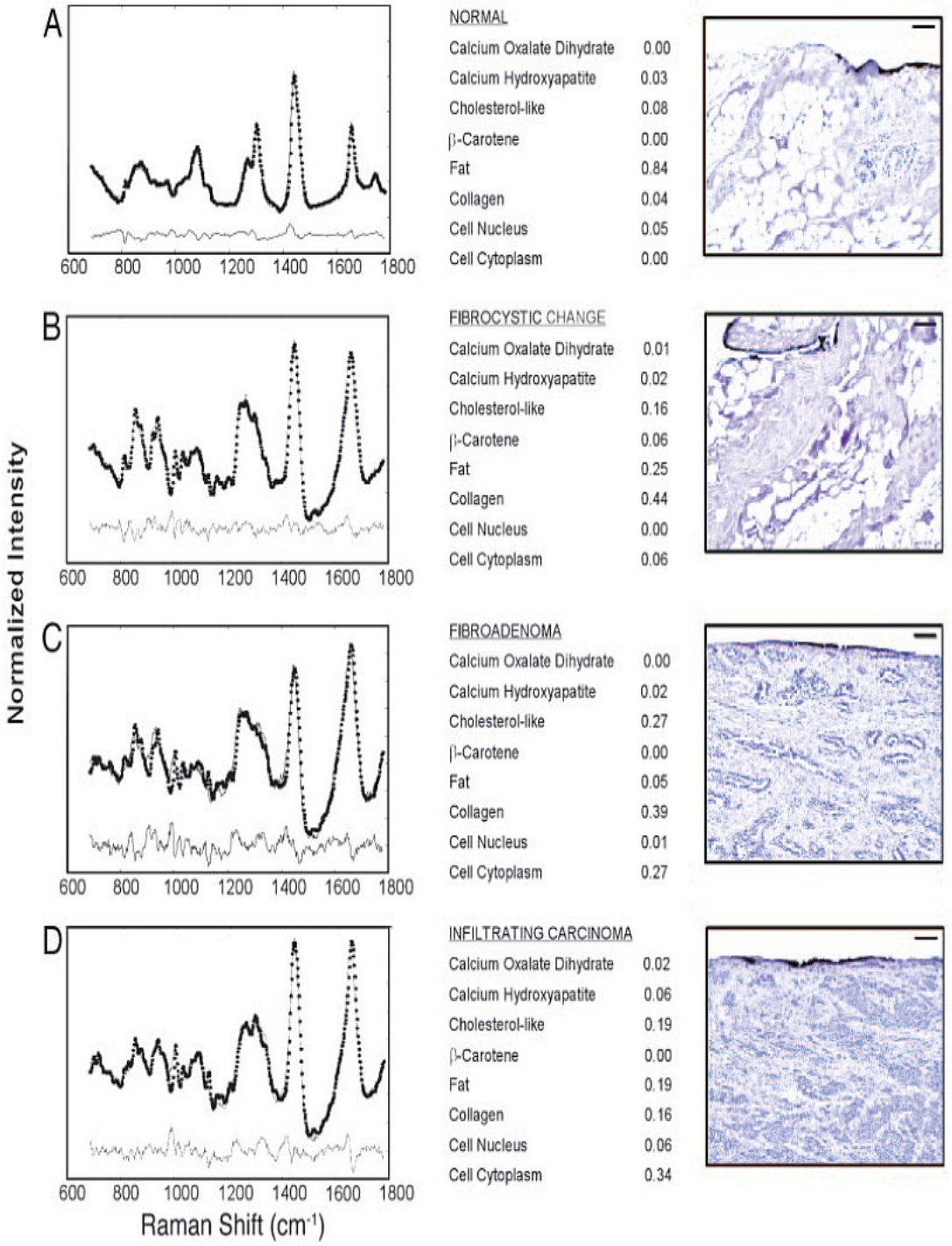

Figure 27- Normalised Raman Spectra and model fits for four distinct tissue types. The percentage of each component included is also displayed, along with the H and E slide of the tissue type being assessed (Haka et al. 2005.)

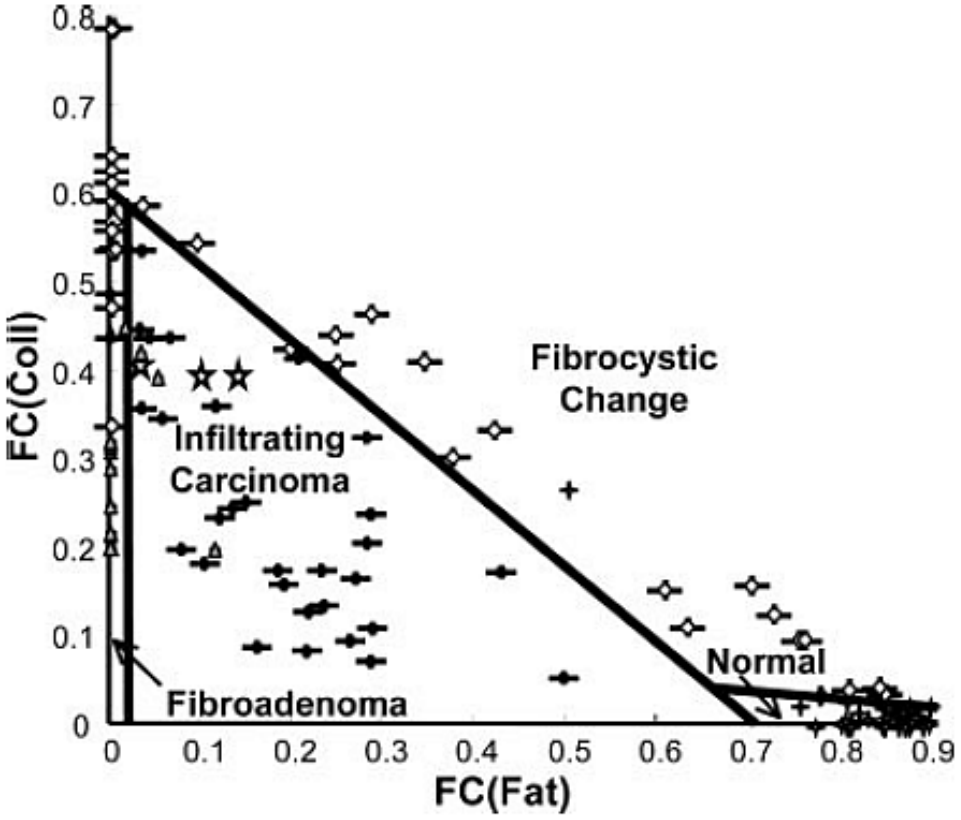

Figure 28- Scatter plot demonstrating the contribution of fat and collagen components in spectra from different breast tissue types (Haka et al. 2005).

The same group went on to use this analytical technique to assess the *ex-vivo* margin status of tumour samples removed during breast cancer surgery. 30 samples were assessed using Raman spectroscopy in the study from a total of 9 patients. 29 of the samples were histopathologically reported as non malignant of which 21 were normal tissue and 8 demonstrated benign fibrocystic change. Only 1 sample was classified as positive , containing areas of ductal carcinoma in situ. The overall accuracy of the algorithm was 93%, with 20/21 normal samples, 6/8 fibrocystic samples and 1/1 DCIS samples being correctly classified. The authors recognised this as a pilot study and accepted the limitations of such small numbers particularly in the positive group. It does

further demonstrate the potential diagnostic capabilities of Raman spectroscopy, based on molecular differences, in the diagnosis of breast cancer (Haka et al. 2006).

A follow up to this study published in 2009 reported the results of real time intra operative analysis of samples from 28 consecutive patients undergoing breast conserving surgery. A total of 220 Raman spectra were collected from 220 samples. Only 129 of these were deemed appropriate for analysis. The 91 that were excluded included samples from patients who had undergone pre-operative adjuvant chemotherapy (n=28), were having repeat surgery due to initial positive margins (n=33), or had pathology that was positive for DCIS (n=20). 10 spectra were excluded due to light contamination of the spectra collected. The remaining 129 spectra were classified based on the contributions of collagen and fat to their spectra. A sensitivity of 83% (5/6) and a specificity of 93% (114/123) was reported for the differentiation between invasive ductal carcinoma and non malignant tissue (normal and benign pathologies) respectively (Haka et al. 2009). However the positive predictive value of the test was reported as only 36%. This was due to the misclassification of 4/73 and 5/9 spectra from tissue with either fibroadenomatous or fibrocystic benign changes. As a result the authors felt that whilst the negative predictive value of 99% was very encouraging larger scale *ex vivo* and *in vivo* studies were required to improve their algorithm prior to clinical implementation.

The biochemical differences between normal and malignant tissue were further demonstrated by Chowdray et al. (Figure 29). They reported the results of 258 spectra collected from 60 samples that were obtained from 60 patients undergoing routine

surgical operations or breast biopsies. A total of 29 normal, 24 malignant and 7 benign samples were included in the dataset. Using spectral difference plots they too demonstrated decreased lipid contributions and increased protein contributions in the spectra collected from positive samples (Chowdray et al. 2006).

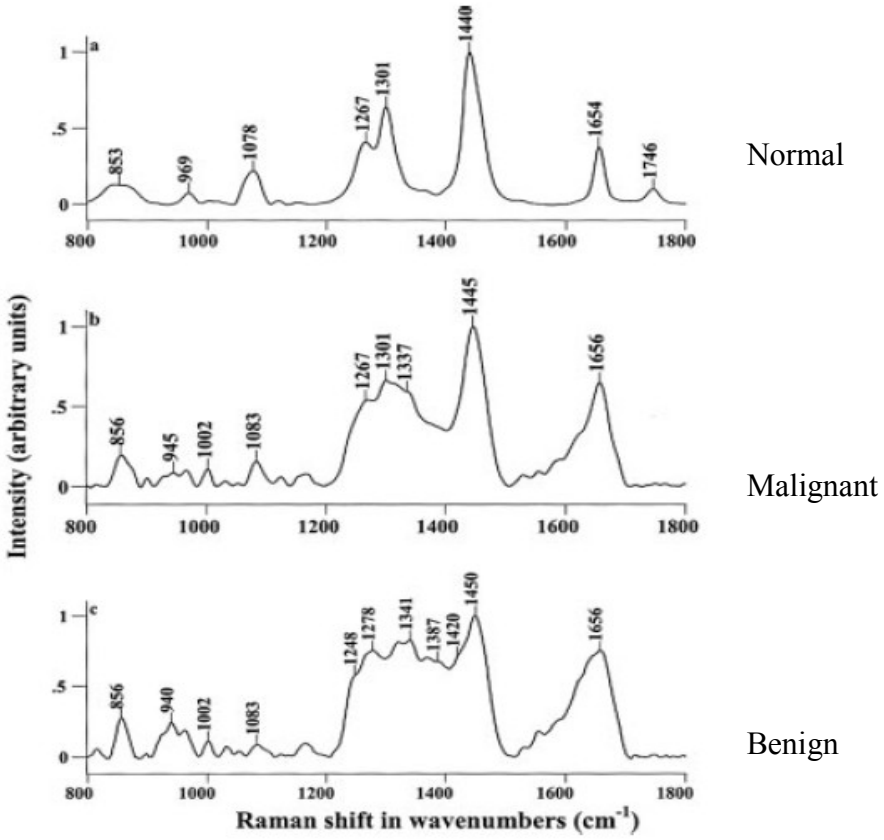

Figure 29- Mean Spectra of normal, malignant and benign breast tissue (Chowdray et al. 2006).

In a later paper the group went on to use the spectral differences between pathology groups in the 1400-1750 cm $^{-1}$ region to prospectively match unknown samples to the training samples from the previous study. Mahalanobis distance and spectral residuals were calculated against the training data and used in a "limit test" match/mismatch approach. In this way 29/30 normal samples, 17/21 cancer samples and 15/18 benign samples were correctly classified.

The spectra were subjected to curve fitting to help understand the biochemical differences between the three groups. This study confirmed that fat (peaks at 1301 and 1440 cm^{-1}), collagen/protein (peaks at 1246, 1271 and 1671 cm^{-1}) and DNA (peaks at 1340 and 1480 cm^{-1}) contributions differed in the three pathology groups (Chowdray 2009) (Figure 33).

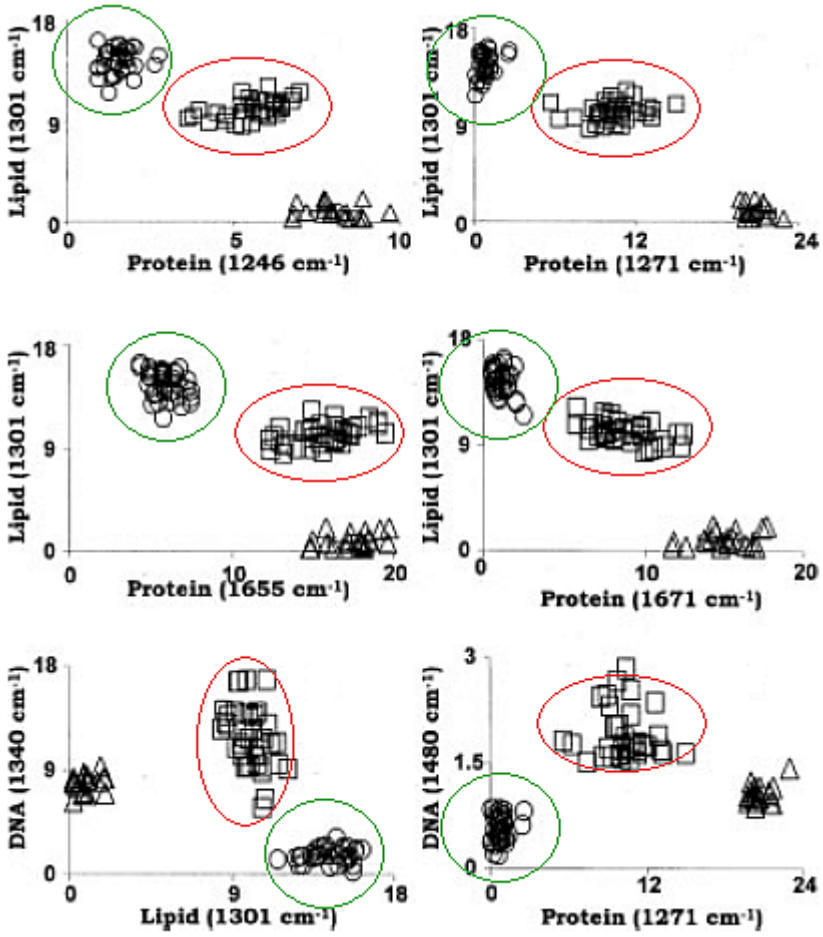

Figure 30- Scatter plots demonstrating the differences in protein, lipid and DNA peaks in malignant (red circles) and normal (green circles) breast tissue (Chowdray et al. 2009).

Two sub-types of Raman spectroscopy, spatially offset Raman spectroscopy (SORS) and transmission Raman spectroscopy, have also been explored as methods of improving the management of breast cancer. A clinical scenario where they have been

used is the problem of positive margins after breast conserving surgery. This is a significant cause of morbidity in breast cancer patients with up to 20% of patients requiring further surgery to obtain adequate clearance (NHS Breast Cancer Screening Programme 2008). One way of reducing the need for a second operation would be the development of a technology that immediately assesses tissue margins. Research performed on tissue models have demonstrated that using spatially offset Raman spectroscopy (SORS) spectral features of breast cancer tumours as small as 1-2 mm in diameter can be distinguished through up to 2 mm of normal tissue (Keller, Majumder and Mahadevan-Jansen 2009) (Figure 31).

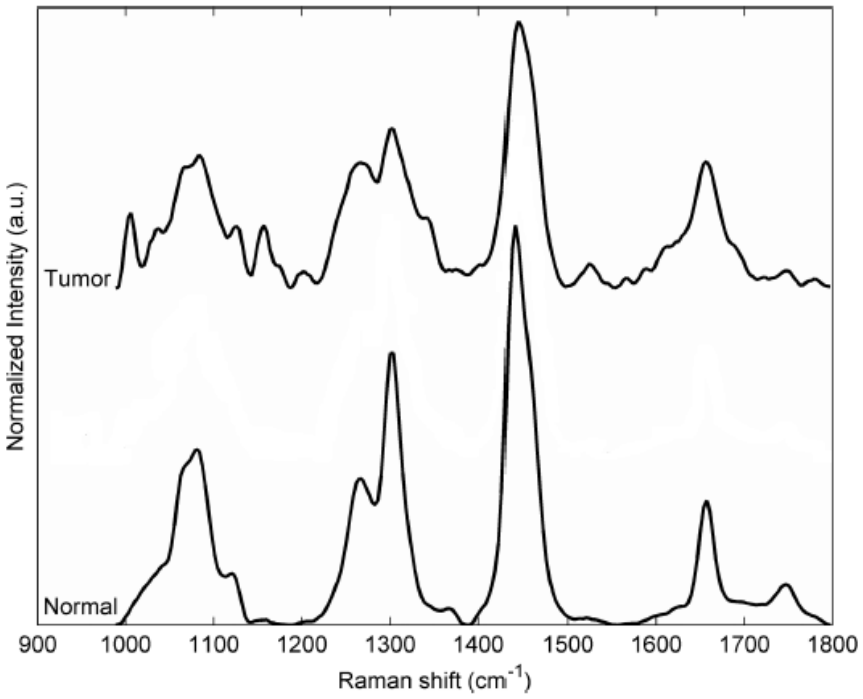

Figure 31- Mean Spectra of normal and breast tumour measured using SORS techniques (Keller, Majumder and Mahadevan-Jansen 2009).

The authors state that the key spectral differences between the two tissue types are the presence of the phenylalanine peak at 1006 cm^{-1}, a decreasing ratio of the 1265 to 1303

cm $^{-1}$ peaks (indicative of an increase in protein content) and an increase in the width of the peak around 1656 cm^{-1} (indicative of an increase in the contribution of amide I) in the cancer spectra. This coupled with the decrease in the relative intensity of the 1445 cm^{-1} peak in the cancer spectra is consistent with the increase in proteins and the decrease in lipids that other groups have demonstrated in breast cancer spectra (Figure 34).

Further work by the group has highlighted a number of confounding factors which need to be overcome before a clinical application is possible. They reported that the results are only achieved with a tumour of 1 mm in diameter which may not be the case if a small focus of cancer is near to the margin. They further state that calculation of the depth of the tumour below normal tissue is difficult without prior knowledge of the tissue geometry (Keller, Majumder and Mahadevan-Jansen 2010).

The use of transmission Raman spectroscopy has and continues to be explored for use in the initial diagnosis of breast cancer. The aim of the work is to develop a means of non invasively probing areas of calcification that are detected during mammography screening. This technique is based on the differentiation of firstly Type I and Type II calcifications and then secondly the carbonate substitutions within Type II breast micro calcifications. These differences have been demonstrated to differentiate between benign and malignant breast disease. To date transmission Raman spectroscopy within the laboratory has been able to determine the amount of carbonate substitutions in type II calcifications and spectral differences between Type I and Type II calcifications through 16 and 27 mm of breast phantom tissue respectively (Matousek and Stone 2007; Kerssens et al. 2010).

These papers suggest that, by exploiting the differences in protein and lipid contributions to spectra collected from normal and malignant breast tissue, Raman spectroscopy could be used in a number of clinical situations pertaining to breast cancer. As has been demonstrated this may include the assessment of margin status after breast conserving surgery or potentially the assessment of core biopsy samples that are used in the initial diagnosis of the disease. Differences in the calcification types can also be detected using Raman spectroscopy and these could reduce the morbidity associated with breast screening.

The ability of Raman spectroscopy to differentiate between normal and malignant tissue is important in this study. Although the tumour itself will not be assessed, metastatic cells that spread from the breast to the lymph nodes have very similar histological properties to the original tumour. It is anticipated that the differences previously described between normal and metastatic tissue will have different spectroscopic features and that these differences can be exploited to differentiate between normal and metastatic nodes.

2.4.2. Raman Spectroscopy in Lymph Nodes

To date there have been very few papers published that document the use of Raman spectroscopy for the assessment of lymph nodes. One of the first papers that reported Raman spectral assessment of axillary lymph nodes used the technique as a method of examining whether silicon breast implants had split. Axillary node tissue specimens were obtained during surgery following silicone implant leak and compared to nodes

from patients with lung cancer that were undergoing lymph node dissection. The authors of the paper did not report in great detail the peak assignments of the spectra that they acquired other than to comment that peaks above 1000 cm^{-1} were due to lipid components. The presence of silicon was clearly demonstrated and the authors concluded that Raman spectroscopy could provide a rapid diagnostic test that could be used in this context (Frank et al. 1993) (Figure 32).

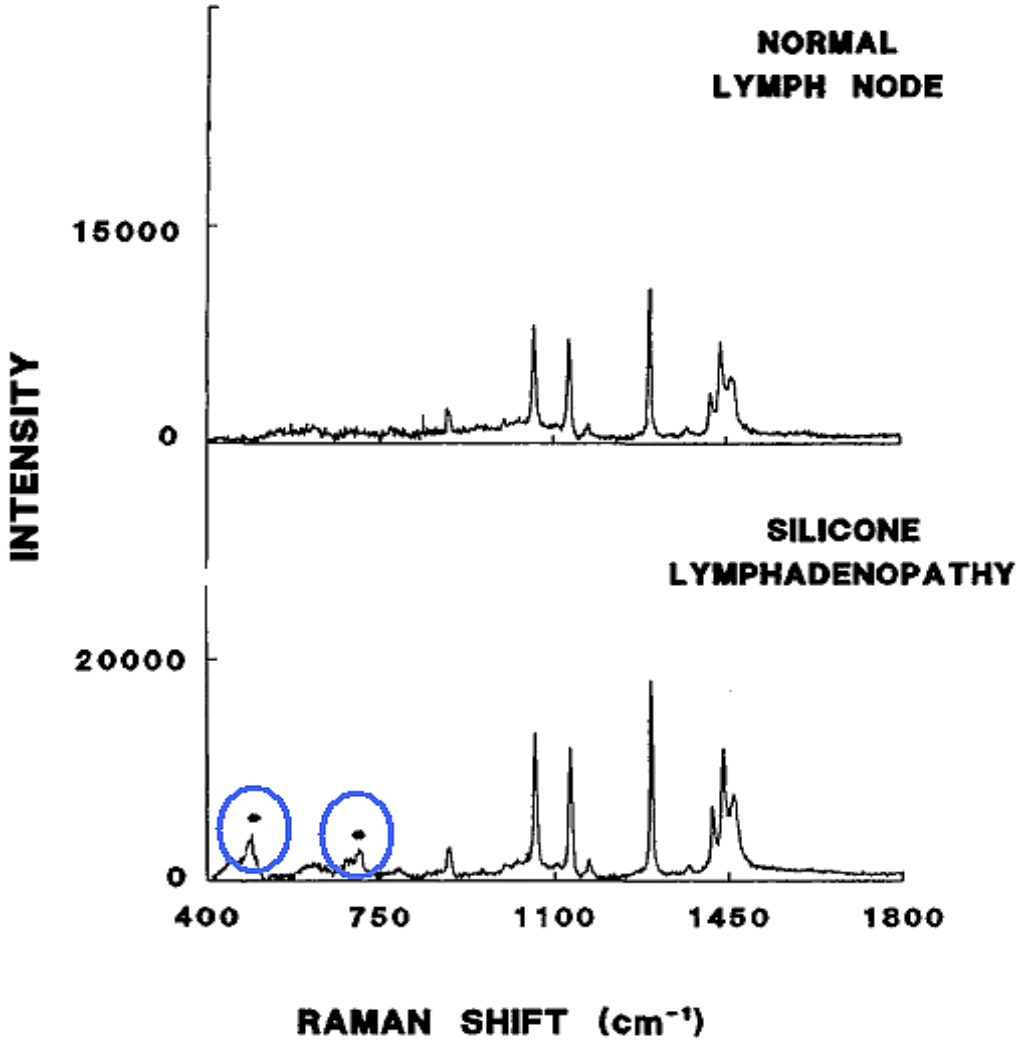

Figure 32- Spectra of normal lymph nodes and those upstream of a silicone implant leak. The added peaks (circled in blue) between 400 and 750 cm^{-1} allow for the differences to be distinguished (adapted from Frank et al. 1993).

A further study published in 2005 used Raman spectroscopy to confirm the presence of silicone within the axillary lymph nodes of 71/96 patients with breast implants. The authors did not comment on the features of the lymph node spectra other than to highlight the presence of polymethysiloxane and polyurethane peaks in the spectra obtained from patients with implants. The sensitivity of Raman spectroscopy at detecting changes in the lymph node associated with silicone implants was worse than standard pathological assessment but was felt to relate to the small area of the node that was assessed using Raman spectroscopy (Katzin et al. 2005).

To date only one group (ours) has used Raman spectroscopy to assess the presence or absence of metastatic cells within human lymph nodes in breast cancer. 59 lymph node samples were collected from 58 patients undergoing axillary lymph node excision due to breast cancer. Raman spectroscopy mapped images were created from 7 μm sections of tissue with a step size of 100 μm in the x and y direction. The differences in the mean spectra of positive versus negative nodes suggested that there were decreases in the DNA and tyrosine contributions within the negative nodes. It was interesting to note that the lipid contribution appeared to be similar in both groups, in contrast to the findings in the breast papers previously reviewed. Principal component fed linear discriminant analysis (PCA fed LDA) was used to create a pathology classification model. This achieved a sensitivity of 91% and a specificity of 93% at differentiating between the positive and negative nodes. Whilst these results were very encouraging the authors recognised that the time taken to produce these mapped images, 12 to 120 hours, was inadequate for intra operative use (Smith 2005).

A potential method of overcoming the disadvantage of mapped images was to use a probe and collect spectra from a greatly reduced but evenly spread area of tissue. The effects of this change were modelled by selecting 5 and 10 points at equally spaced positions across the mapped images of 53 and 47 nodes respectively . The estimated time to collect the spectra obtained from these points was 9 and 18 minutes in the two groups. Sensitivities of 71%, in the 5 probe point group, and 81% , in the 10 probe point group, with specificities of 97% in both groups were achieved based on a cross validated model (Horsnell et al. 2011). These results support the use of a Raman spectroscopy probe for the assessment of axillary lymph nodes as they produced results that were equivalent to both frozen section and touch imprint cytology, in a time frame that would be suitable for intra-operative use. The low sensitivity was attributed to the small total area of the node assessed, 2800μm^3 and 5600 μm^3 in the two respective groups. The authors felt that the increase in sensitivity that was achieved by doubling the total area assessed in the 5 and 10 point group could be further enhanced by using probes that collected spectral data from an even greater tissue area (Horsnell et al. 2011).

Lymph nodes from patients with oesophageal cancer have also been investigated using Raman spectroscopy. 76 halved lymph node samples from 57 patients were collected and snap frozen at the time of surgery. 30 of these samples were said to be positive for cancer and 46 were negative for cancer after histopathological analysis. The samples were then assessed using both Raman and FTIR spectroscopy within a laser laboratory. The mean Raman spectra of positive and negative nodes were compared and demonstrated lipid, carbohydrate and protein peaks in the negative nodes and stronger

nucleic acid peaks in the positive nodes. PCA fed LDA was then used to assess the diagnostic capability of these differences. Cross validated results achieved a sensitivity of 97% and a specificity of 89% for the differentiation of negative and positive nodes. The authors of this study concluded that these results provided a "launchpad" for the development of in vivo applications of Raman spectroscopy in lymph node diagnostics (Isabelle et al. 2008).

The use of Raman spectroscopy as a diagnostic tool for the assessment of axillary lymph nodes remains in its infancy. Whilst the studies to date have been encouraging they have been limited by low sample numbers and have been laboratory based using frozen tissue. This study will be the first to move the spectrometer out of the laboratory into the operating theatre and will assess freshly excised human tissue.

2.4.3. Alternative optical methods of assesing lymph nodes

Other forms of optical spectroscopy have been used to assess lymph nodes. These include elastic scattering and infrared spectroscopy. Elastic scattering spectroscopy (ESS) is a technique that is based on the elastic scattering of light. Short pulses of white light from a source such as a Xenon lamp are delivered to the tissue. Scattered light which has the same wavelength as the incident light is collected by a collection fibre that is offset from the light source. Spectra collected in this way are sensitive to the sizes, refraction indices and structures contained within sub cellular tissue components. A recent study used this technique to create a diagnostic algorithm based on the results of 331 negative and 30 positive lymph nodes. They went on to test an independent data

set of 129 samples at the time of surgery and achieved a sensitivity of 76% (69% with micrometastases) and a specificity of 96% at differentiating between positive and negative nodes (Keshtgar et al. 2010) (Figure 33 and 34).

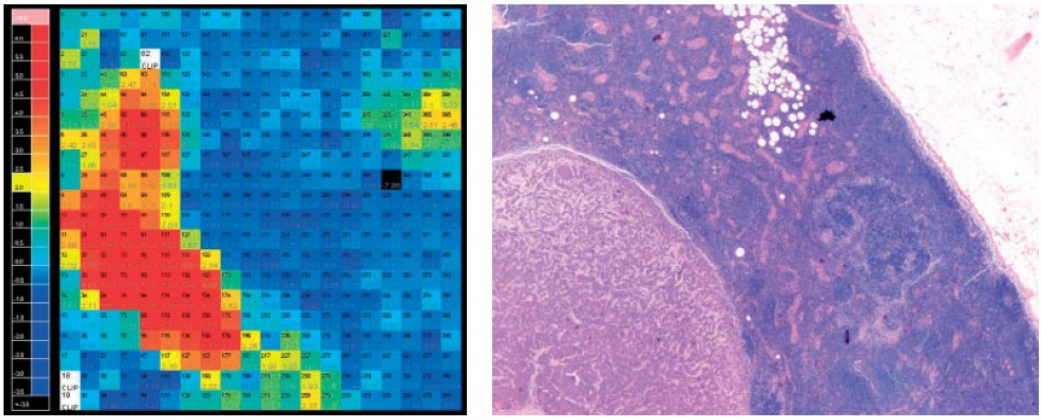

Figure 38- False colour coded scan of a node, using optical spectroscopy, showing a single metastasis alongside its histology (H and E) image (Keshtgar et al. 2010).

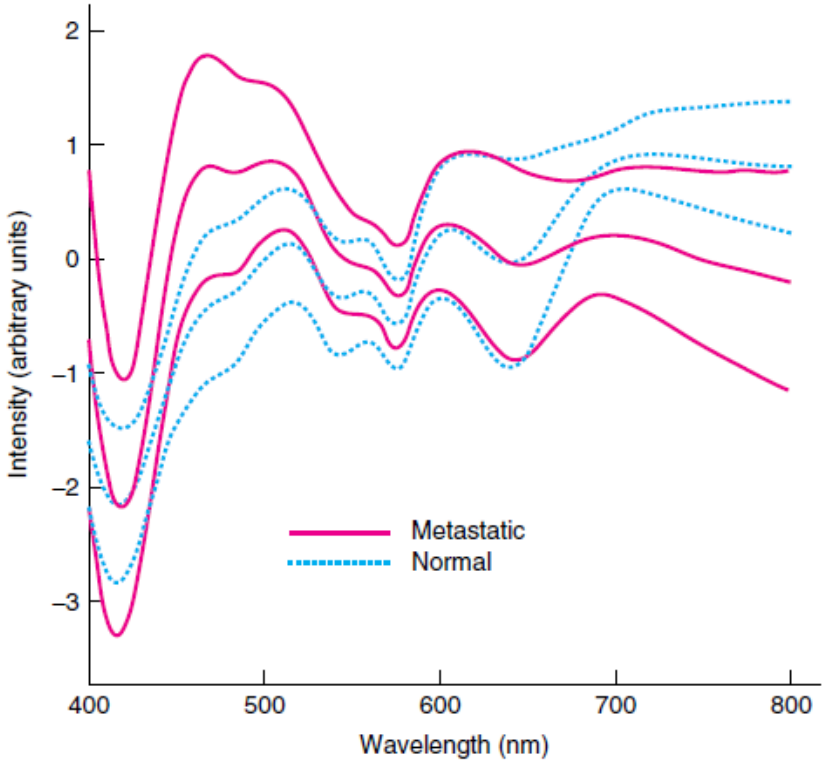

Figure 34- Mean elastic scattering Spectra from 331 normal nodes and 30 metastatic nodes with standard deviations (Keshtgar et al. 2010).

The authors recognised that the level of sensitivity achieved in this study is a potential limitation to the technique although it is comparable to results with both frozen section and TIC. They suggest improving their detection of positive nodes would require sampling of an increased area of the node. The results reported in the paper are based on the measurement of an area 10 x 10 mm x 0.5 mm. Using their current instrumentation this took 8 minutes to assess. If they were to assess multiple lymph node slices then they expect their sensitivity to increase but recognise that this will have a detrimental effect on the total assessment time.

As has been discussed Infra Red (IR) Spectroscopy is often grouped with Raman spectroscopy under the title "Vibrational spectroscopy". As previously noted, unlike Raman spectroscopy, for a molecule to be IR active the molecule must undergo a vibrational change that alters the dipole moment of the molecule. Thus vibrational changes not seen with Raman techniques can be seen with IR spectroscopy. However due to the effect of the IR activity of water the clinical in vivo applications of this technique are limited. However it can be used to interrogate desiccated tissue samples which provides biochemical information that maybe complimentary to that gained from Raman spectroscopy (Figure 34a).

Fourier transform IR (FTIR), so called because of the mathematical technique that converts raw data into spectrum, has been used to analyse axillary lymph node tissue. Recent work highlighted the potential role of this technique in the identification of micro-metastases and isolated tumour cell in the axillary lymph nodes of patients with breast cancer.

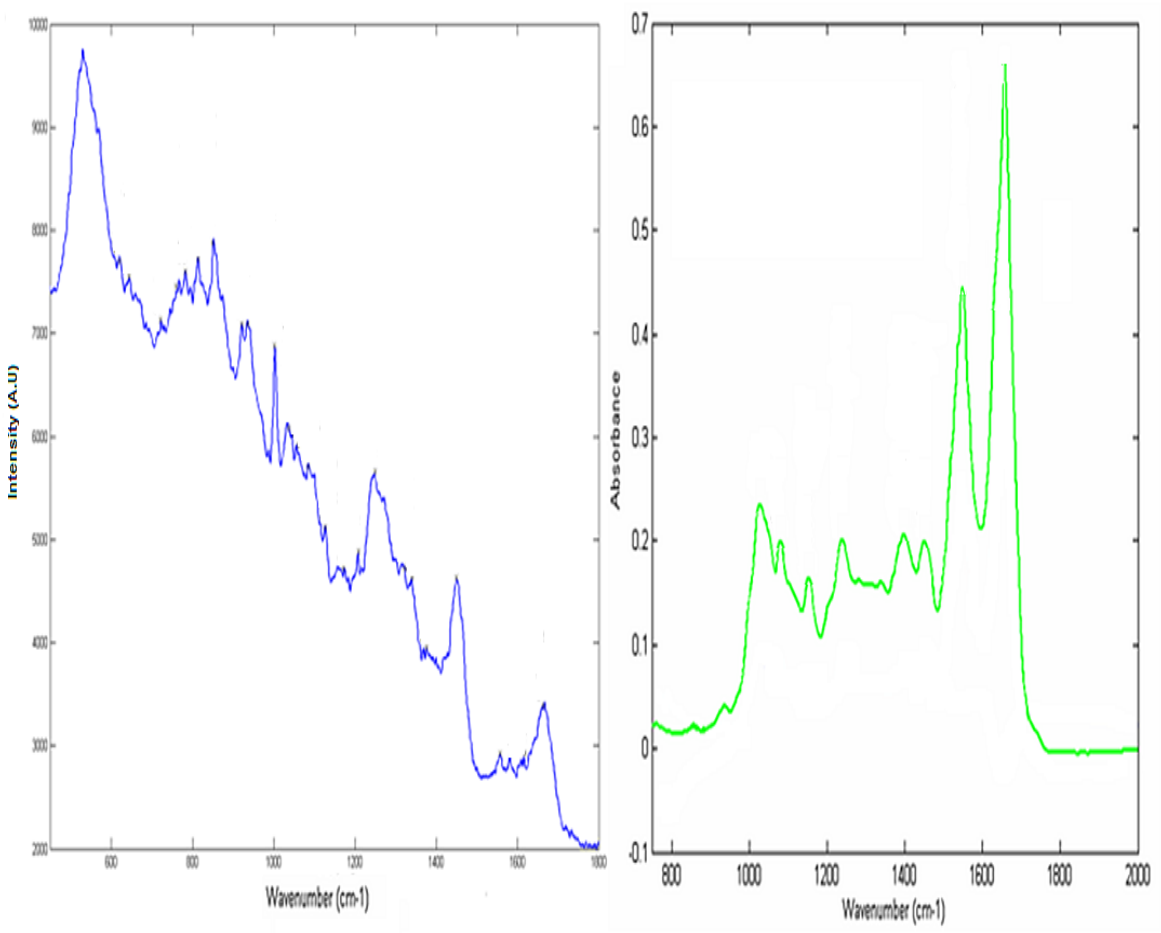

Figure 34a- Spectra obtained from the same sections of human cervical tissue using Raman (blue) and IR (green) spectroscopy. This highlights the very different spectral information available from the two techniques and why they can be used as complimentary tools to each other (Adapted from images held within our own department).

In this study 20 nodal tissue sections from 20 patients were cut from formalin fixed paraffin embedded archived tissue blocks. Spectra were collected in 6.25 µm steps such that a 1 mm x 1 mm tissue black was represented by 160 x 160 spectra. Higher cluster analysis was used to reproduce histological features of the cut lymph node surface (Figure 35) (Bird et al. 2009).

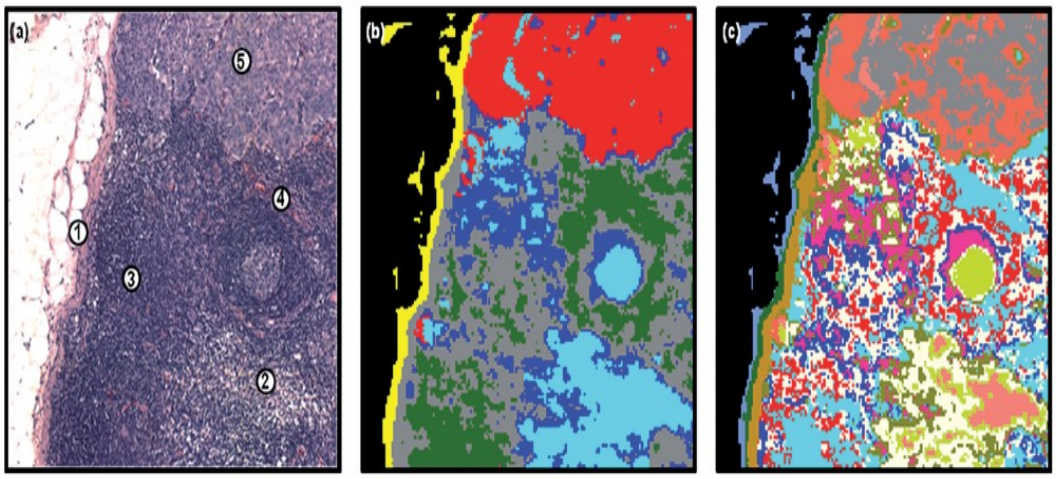

Figure 35 - FTIR Mapped images (centre and right) that show excellent correlation with the associated histology slide (left) (Bird et al. 2009).

Good correlation was achieved in comparison to H and E slides of the same area. Using this technique macrometastases, micrometastases and isolated tumour cells were identified although no attempt was made at creating a classification model based on the results.

The use of FTIR in the assessment of lymph nodes from other areas of the body has also been published. When used to differentiate between positive and negative lymph nodes from patients with oesophageal cancer sensitivities of 91% and specificities of 85% were achieved. Spectra from positive nodes displayed a greater contribution of protein and DNA than those spectra collected from negative nodes (Isabelle et al. 2008). FTIR was also used in a study that assessed the touch imprint samples collected during parathyroid surgery. The ability to correctly identify the parathyroid, thyroid or lymph nodes during a parathyoidectomy is vital and can often only be confirmed by the pathological assessment. Clear spectral differences were evident between these tissue types. In particular it was noted that the lymph nodes displayed strong lipid peaks at

1166, 1380, 1464 and 1748 cm^{-1} (Figure 36). The authors therefore suggest that FTIR could be used in conjunction with TIC to provide an automated and subjective method of tissue analysis (Das et al. 2007).

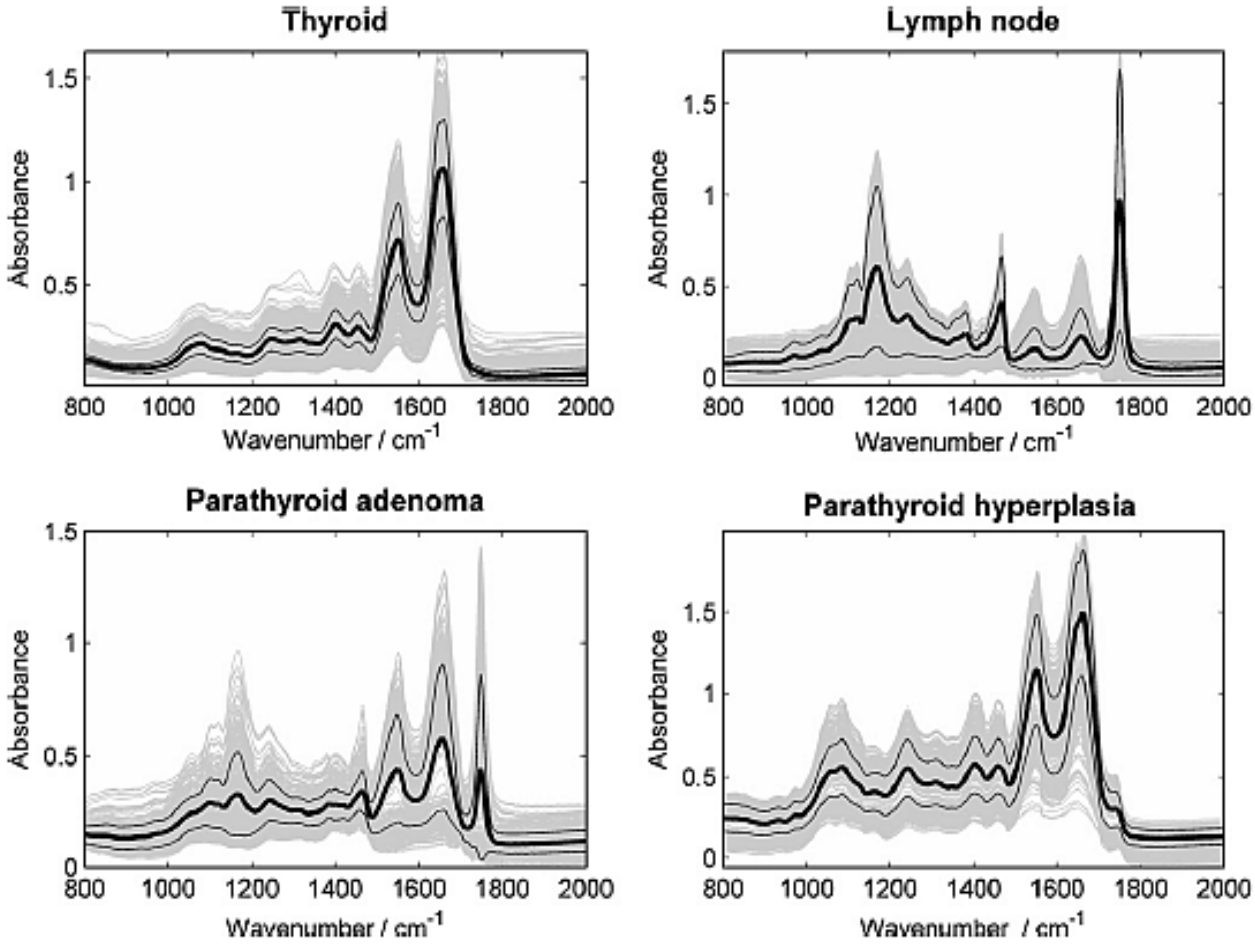

Figure 36 - Mean FTIR spectra (bold black line in each spectra) of thyroid, lymph node and parathyroid tissue highlighting the distinct differences that allow for differentiation of tissue type (Das et al. 2007).

2.5. Conclusions

There is a strong base of knowledge that supports the use of Raman spectroscopy as a method of differentiating between normal and malignant tissue. It has consistently been shown that the key differences in the spectra obtained are an increased contribution of

lipid in the normal tissue relative to malignant tissue and an increased contribution of protein and DNA in the malignant tissue relative to the normal tissue. These results are supported by FTIR results in axillary, oesophageal and head and neck cancers.

A number of groups are now trying to harness these techniques as a means of improving the management of breast cancer. This project will aim to build on these previous studies to demonstrate that Raman spectroscopy could be used within the theatre setting to assess axillary lymph nodes. If this is proven to be the case then Raman spectroscopy has the potential to be the first method that can fulfil all the features that were previously highlighted as the requirements of an ideal method of intra-operative analysis.

3. Towards using a probe in theatre.

3.1. Introduction

As discussed in the previous chapter earlier *in vitro* work has demonstrated the potential for the use of Raman spectroscopy to differentiate between malignant and non malignant lymph nodes in breast cancer (Smith 2005; Horsnell et al. 2011). However this work had a number of significant draw backs that would need to be overcome if Raman Spectroscopy were to be used in the clinical setting.

1. The time taken for spectral acquisition – The mapping images previously used to differentiate between the two pathologies were obtained over time frames that would have precluded their use in an intra operative setting.

2. The equipment used – Previous studies have utilised expensive laboratory based systems that would be beyond the reach of most surgical units. The footprint of the instruments would also have significant implications as safe and suitable storage facilities would be difficult.

3. The environment – The previous work had been performed within a specialised spectroscopy laboratory in standardised conditions. If, as is envisaged, the node assessment were to take place within the operating theatre these conditions could not be easily replicated.

4. Exposure to node markers – The lymph nodes in previous studies were obtained following either axillary sampling procedures or during axillary dissections. At the time of that study SLNB was not routinely performed. As a result there was no dye used to identify the lymph nodes. There is significant concern with regard to the affect this will have on the diagnostic capability of the technique because dyes used to orientate the specimens within the lab demonstrated significant fluorescence.

5. Sample preparation - Previous work has demonstrated the efficacy of Raman spectroscopy using sections of lymph node material. This would significantly add to the overall assessment time as well as render assessment within the operating theatre impossible without significant further investment in equipment and expertise.

In this chapter experimental work will be presented that has been designed to determine if and how these problems could be overcome. A key part in this has been the selection of the spectrometer. Therefore the probe based Raman spectrometer that was selected for use in this project will be described and its capabilities in this setting reviewed. Results of a small feasibility study that was performed using human axillary lymph nodes will be reported before concluding the chapter with some experiments that looked at the effect of the theatre environment on spectral acquisition.

3.2. The Raman Spectrometer

The first and most significant hurdle that had to be overcome in this project was the selection of equipment that could be used outside of the laboratory. As previously discussed mathematical modelling had suggested that a probe based system could be used to assess axillary lymph nodes rather than the more traditional mapping techniques that had been used in the past (Horsnell et al. 2011).

The B&W Tek MiniRam II (B&W Tek, Newark, DE, USA) Raman spectrometer was purchased for use in this project and is utilised in all of the experimental data reported in this thesis. This spectrometer features a 785nm laser with a spot size diameter of 85μm and a maximum power of 300mW at the probe tip. The laser light is delivered via a hand held probe and a distance regulator, that fits the tip of this probe, ensures that samples are positioned 59mm from the tip of the probe. This distance has been determined by the manufacturer as the optimum position for spectral acquisition. Collected light is passed through a spectrometer that provided spatial resolution of $10cm^{-1}$ with a built in thermo-electrically cooled CCD (Figure 37). The nominal ocular hazard distance was calculated at less than 10cm and was a key feature of the local rules that were designed for its use.

The whole system is both lightweight and has a small footprint that would be ideal for use within the operating theatre setting (Figure 38). Further the price of the spectrometer, circa £12000, is significantly less than most laboratory based systems and the equipment used for intra-operative assessment based on molecular assays.

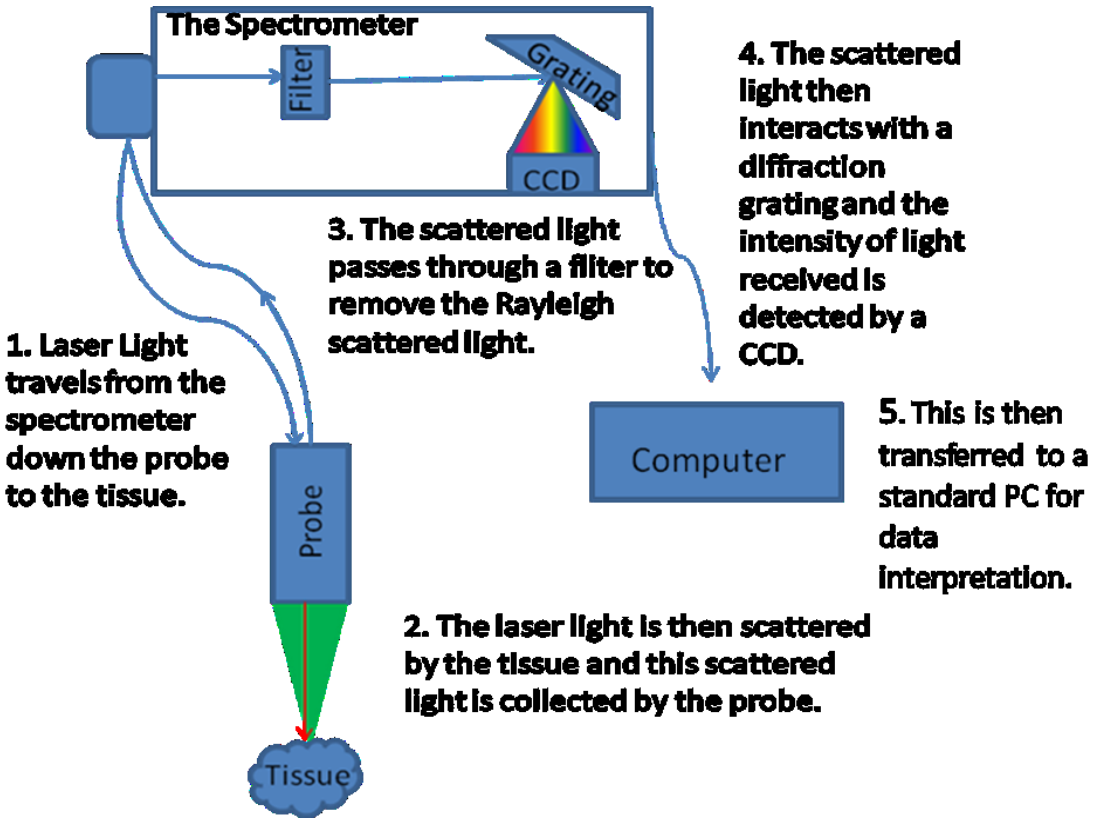

Figure 37 – A stylised diagram of the Raman spectrometer device.

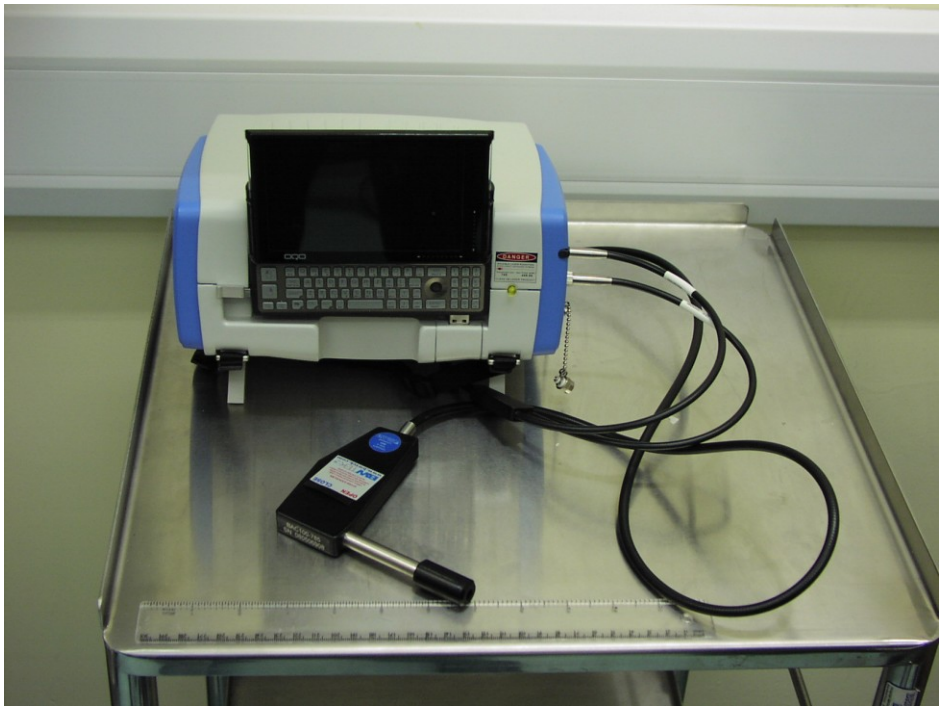

Figure 38- The B&W Tek © Mini Ram II on a standard theatre trolley, with a standard 30 cm ruler in the foreground illustrating the small footprint of the product.

To overcome any daily variation in spectral acquisition standard measurements were collected at each session. Spectra from green glass, pipette tip, and cyclo-hexane were recorded and stored and then used later to calibrate the spectral data. A dark scan was recorded at the start of each session and is subtracted from the spectra recorded in the subsequent session. This overcomes the "hot" pixels on the CCD and is as per the manufacturers recommendations.

3.3. Experiment 1 - Depth of Spectral Acquisition.

Prior to embarking on clinical studies to ascertain the efficacy of the system if was felt that a greater understanding of the capabilities of the probe based system was required. As has been discussed previous work assessing axillary lymph nodes has been performed using Raman spectroscopy systems that collected spectral information from an area of 45 μm^2 and from samples that were only 7 μm thick. This would not be amenable to intraoperative use as the time taken to collect mapped images was between 12 and 120 hours. Further the time taken for tissue preparation would not be acceptable in an intra-operative setting and is one of the disadvantages of frozen section analysis that is used currently.

When designing an ideal diagnostic tool it was felt that minimal tissue preparation would be desirable as this would reduce the time taken to output a result and reduce the need for added expertise and equipment. Thus the design of the clinical part of this study anticipated that the node would simply be denuded of surrounding axillary fat and then bisected. Spectra would then be acquired from the two halves of the node

individually. An appreciation of the depth from which the probe collected scattered light was vital both in samples with macrometastases and micrometastases (Figure 39).

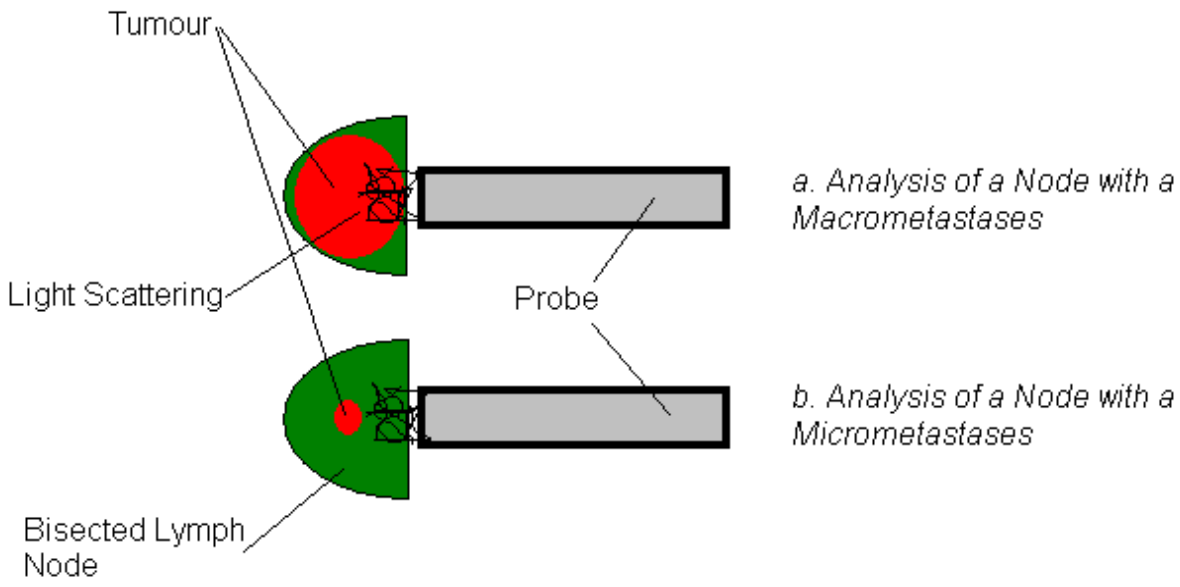

Figure 39- An illustration of the importance of sampling depth using a Raman probe to try and gain an appreciation of what might be "seen" using the system.

3.3.1. Experiment 1 – Methods.

To determine the depth from which the probe receives scattered light an experimental model was created. This was designed such that a standard material could be advanced towards the probe through a variety of different media. As demonstrated in figure 44 a standard 20ml syringe (BD, Oxford, UK) was used to contain the media being tested. Four experimental media, standard room air (i.e. an empty space), sterile water for injection (Baxter, Newbury, UK), standard olive oil (Napolina, Liverpool, UK) and lard (everyday value range, Tesco, UK) were used. 15 ml of each media (aside from the room air) was placed within the syringe whilst in a liquid state. Olive oil and lard were

chosen as they most closely resembled the fat composition of a lymph node. This composition has previously been estimated as containing 29% saturated fats, 57% unsaturated fats, and 9% polyunsaturated fats (Pond and Mattacks, 2003; US and Finnish Food Database 2009).

A 1 mm^3 block of PTFE was then placed on the surface of the media. This was attached to a translation stage (Thorlabs, Ely, UK) that allowed the block to be advanced in 0.5mm steps through the media under investigation (Figure 40).

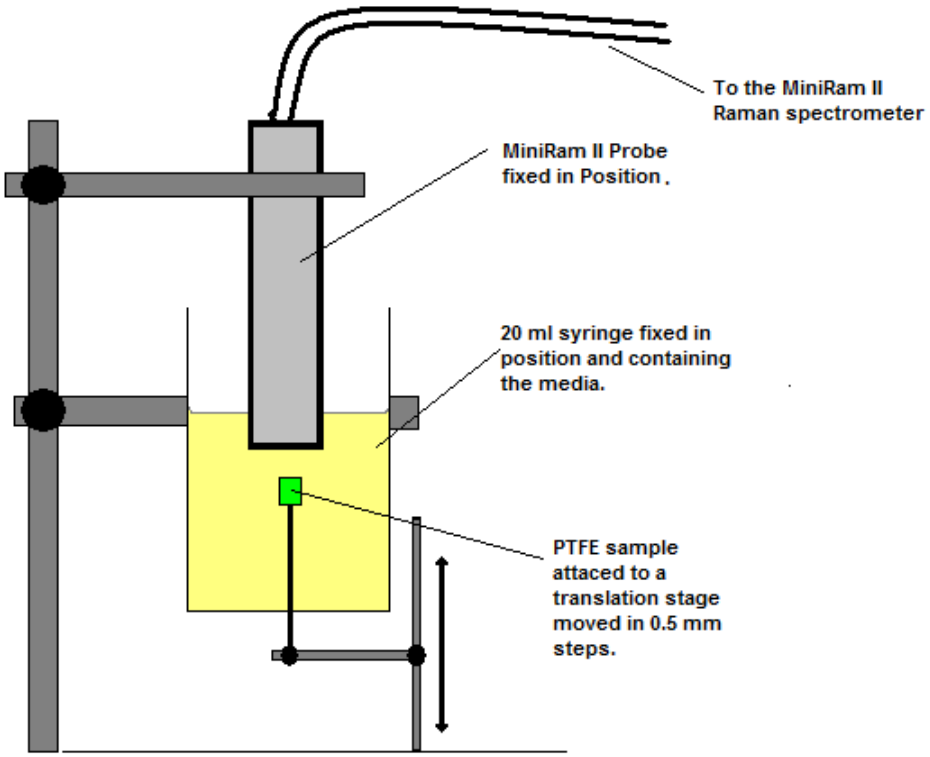

Figure 40- The experimental set up to measure the depth from which spectral information is gathered

In the first part of the experiment the PTFE block was placed at the maximal distance away from the probe tip (14.5mm) and then advanced in 0.5mm intervals. 5 spectra were obtained at each of these positions and the process was repeated for all 4 media.

The MiniRam II was used throughout and each spectra was obtained by combining 16 x 1 sec acquisitions. Control spectra from each of the media and the PTFE were also recorded. In the second part of the experiment an attempt was made to approximate the volume from which spectral information was collected. The experimental set was modified so that the PTFE standard could be moved in both the z (up and down) and y (side to side) plane. The chamber was filled with olive oil, which not only closely resembled the fatty composition of a lymph node but which also, due to its liquid state at room temperature was easiest to handle. 5 spectra were collected from 25 different positions. The PTFE block was moved in 1.0 mm steps to 4 mm from the optimum point in the z direction and 0.25 mm steps to 1mm offset in the y direction. The initial measurement was made with the PTFE block at 0mm offset in both the z and y plane. It was then moved in the y plane before being returned to the initial position and then moved in the z direction. Further spectra were obtained at each y position before returning to the y=0 position and altering the z position again. Spectra were obtained as described for the first part of the experiment and all data was then transferred to a desktop PC for interpretation using Matlab ® software.

3.3.2. Experiment 1 - Results.

Examination of the spectra from the PTFE block revealed a peak at 738cm^{-1} that was not present in any of the other control media. The intensity of this peak was calculated when the PTFE block was at the optimal distance from the probe tip (5.9 mm) in all the media. This figure was then used to calculate the relative intensity of the 738 cm^{-1} peak at increasing distances from the optimal point by calculating an intensity percentage at

each 0.5mm step in the first experiment and each position in the second experiment. These percentages were plotted to produce curves for the change in intensity with increasing offset for each of the four media (Figure 41, 42). In the curves the gradient of the slope has started to level out by 3mm from the optimal point of the probe although the clearest peaks are recorded at less than 1.5mm. The distinct differences seen using lard may have been explained by the solid nature of lard at room temperature. Thus maintaining a consistent volume of the media between the probe tip and the PTFE was difficult. The results of the second part of the experiment were plotted graphically to give a visual idea of the volume of tissue from which spectral information is collected using this system (Figure 44). It was evident that beyond 0.5 mm movement in the y direction there was no discernable contribution of the PTFE block.

3.3.3. Experiment 1 – Conclusions.

Although these results were part of an observational study they do allow some appreciation of the volume from which spectral information could be gathered using this MiniRam II system. Before proceeding to discuss the results further it is important to state that definitive interpretation of the results does need to be carried out cautiously as it is likely that the optical properties of a lymph node and media used in this experiment will differ. In particular the elastic scatter of tissue will cause many more transverse scattering events than these media and thus the results were used as a guide when discussing the technique with clinicians rather than an absolute.

Within this media it is clear that beyond 3 mm depth the contribution of the PTFE block is negligible and that beyond 0.5 mm lateral movement the contribution is non discernable. This is the point beyond which any surface of the block is in line with the laser. In this media as long as a part of the block is in line with the laser then spectral information will be acquired to a depth of 3 mm. Transposing this to tissue the best possible volume from which spectral information from a metastatic deposit could be detected is given by the formula

$$(\pi \text{ x (diameter of the deposit}^2\text{)) x (height of the deposit +3 mm)}$$

If we relate this to a macrometastases, which by definition is at least 2 mm in diameter the maximum size of a node sample that a 2 mm deposit could be detected in is a node visualised as a cylinder of 4 mm diameter x 5 mm depth. The volume of tissue in which it will be detected is 62.8 mm^3 (Figure 43, 44).

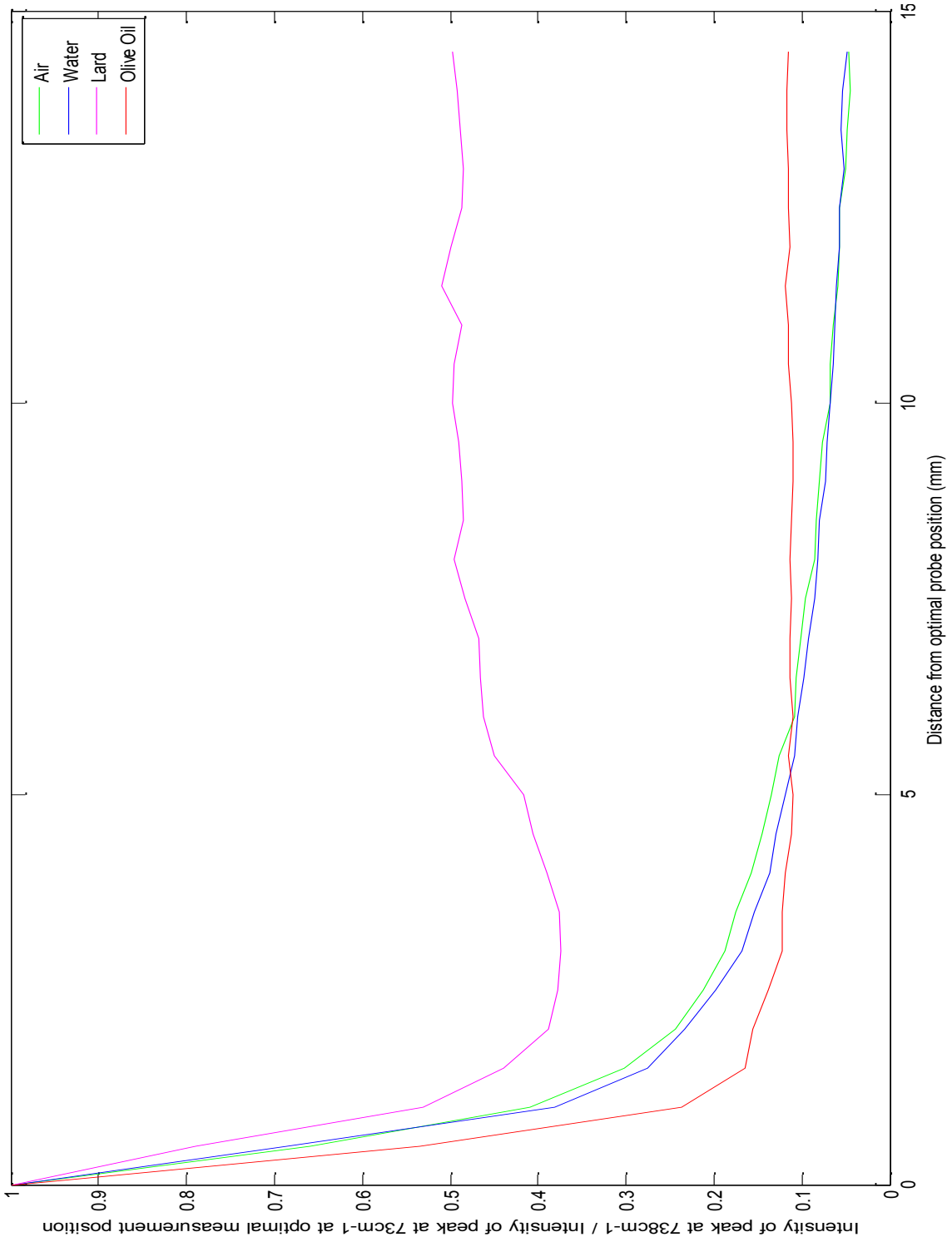

Figure 41- Changes in the Intensity of the 738 cm^{-1} peak at increasing offset from the probe tip in 4 different media over a 15mm range. The clear drop off of the contribution of PTFE beyond 3mm is seen (shown more clearly in Figure 46). The very different plot for Lard may be explained by its solid state at room temp (see text).

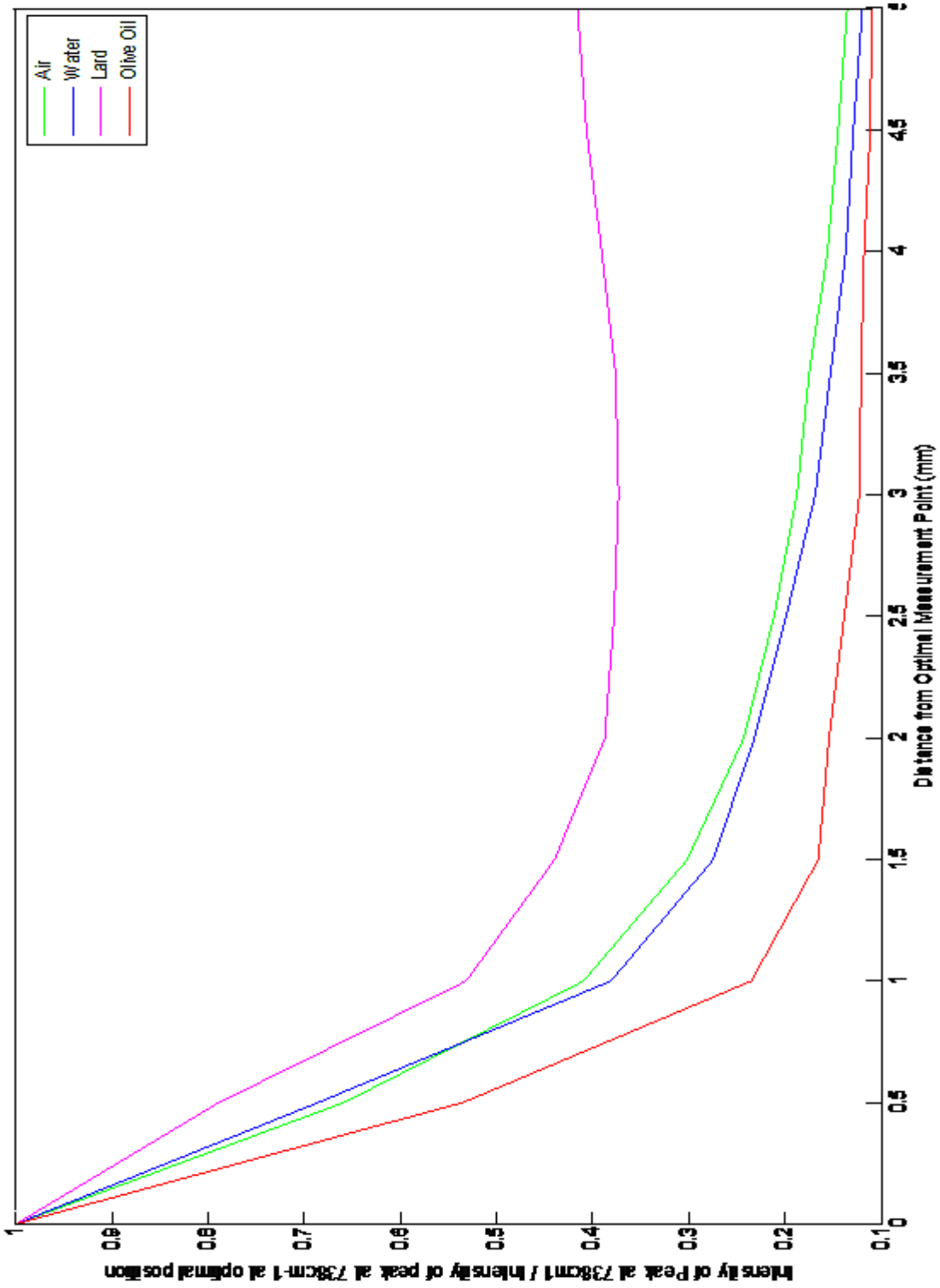

Figure 42- Changes in the Intensity of the 738 cm^{-1} peak at increasing offset from the probe tip in 4 different media as shown in Figure 41. In this figure this is shown over a 5mm range to give greater clarity.

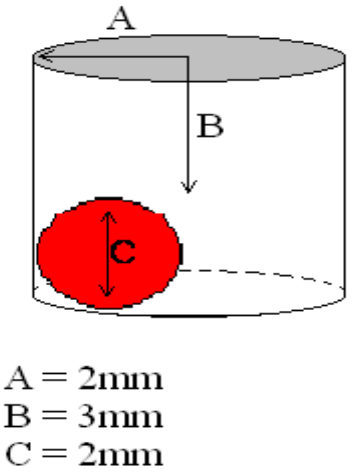

Figure 43- An illustration of the total volume of tissue within which macro-metastases of at least 2mm in diameter could be detected (not to scale).

Lymph node metastases are first found within the medulla of the nodes. It was thus decided that all nodes will be bisected and samples taken from the inner cut surface. Thus the MiniRam II should, if this model is projected forward, be able to detect all macrometastases in lymph nodes that are smaller or equal to 10 mm x 4 mm. This information was used to determine the clinical study design. It has previously been reported in a review of 1249 axillary nodes that 47% were less than 5 mm in diameter , 34% were between 5 and 9 mm in diameter , 17% were between 10 and 20 mm and 2% were greater than 20 mm in diameter (Obweseger et al.2000). Therefore there was obvious concern that as a result macrometastases may be missed in 19% of nodes. It is reasonable to suggest that this situation would be mitigated because the first colonies of metastatic cells will establish themselves within the medulla of the lymph node and that spectra would be collected from the inner cut surface of the node. Further methods of increasing the volume of node assessed would be to divide the node into further sections. The tissue used in the real time clinical part of this study will be relied upon to

guide patient treatment. Further manipulation of the tissue was thus deemed inappropriate. As will be discussed in Chapter 4, an alternative method of increasing the volume tested would be to collect spectra from both the inner and outer surface of the node. In this way it could be anticipated that the depth of collection may be doubled.

Accepting the assumptions commented on above, for micrometastases, of at least 0.2 mm in diameter the total depth of collection from a lymph node sample would be 3.2 mm and the volume from which micrometastases could be detected would be only 0.8 mm^3.

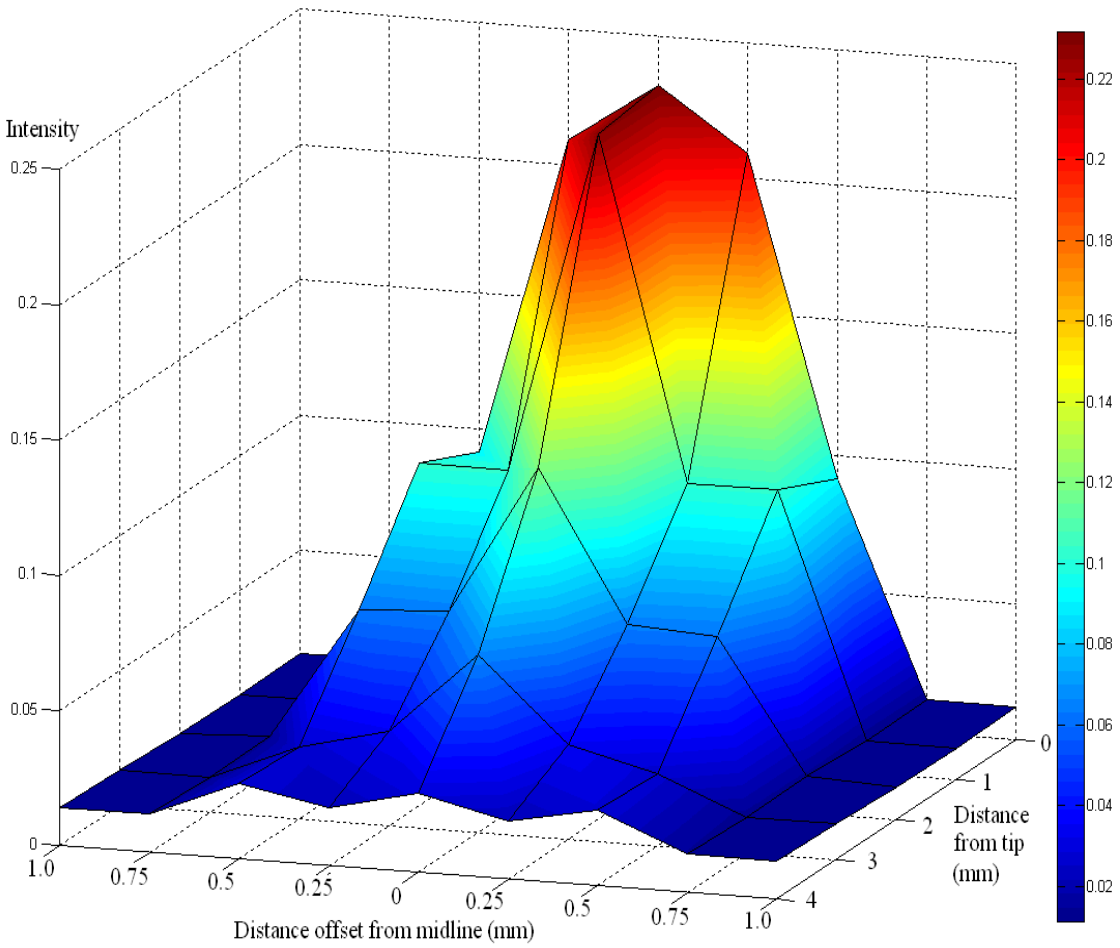

Figure 44- 3D plot demonstrating the intensity profile of the B and W Tek Miniram II as determined in the depth experiment.

3.4. Experiment 2 - Feasibility Study.

Prior to launching into a theatre based study it was felt prudent that a feasibility study should be performed with the equipment that was planned to be used in the theatre setting. This not only allowed confirmation that the modelling studies were reproducible using an actual Raman spectroscopy probe but it also afforded the opportunity to overcome any technical issues prior to carrying out spectral acquisition within the operating theatre environment.

3.4.1. Experiment 2 – Methods.

Following local ethical approval (approval code 01/158G – "The Development of Raman Spectroscopy in the Diagnosis of Breast Cancer") lymph nodes were collected from a small cohort of 20 consecutive patients presenting with newly diagnosed invasive breast cancer. All patients were consented prior to taking part. They all underwent either a sentinel lymph node biopsy or an axillary node dissection as part of an operation that also included a wide local excision or a mastectomy to excise the primary breast tumour. These procedures were performed at Russell Hall Hospital, Dudley by a single consultant surgeon. Pre-operative preparation for the SLNB followed national standards. Not more than 24 hours prior to surgery patients received a peri-tumoral injection of radio-labelled Technetium ^{99m} and immediately prior to surgery the surgeon injected patent V blue dye into the subcutaneous tissue overlying the tumour.

During the operative procedure the node was identified and its status as the sentinel node confirmed by measuring the radioactivity of the node, using a hand held gamma probe. The visual "blueness" of the node was also recorded on an analogue scale of 0-3 (0= not blue, 1= faint blue, 2 = mild blue, 3= strong blue). The node was then excised and denuded of fatty tissue before being divided into two halves. One part was sent for routine histopathological examination and the other half was used for research purposes.

The sample for research use was placed in a cyrovial, labelled and immediately immersed in liquid nitrogen. The sample was then transported to the histopathology laboratory at Russell's Hall Hospital, Dudley. Here it was stored at approximately -48ºC prior to being transferred to the research department at Gloucestershire Hospitals NHS Trust. Once in Gloucester the nodes were stored within the pathology laboratory freezer at a temperature of -80ºC. Sections of each node were cut, according to local protocols, by staff within the pathology department for preparation of a standard H&E slide. These slides were examined by a consultant histopathologist to define the "gold standard" result for each of the nodes.

The remaining tissue was transferred to the research laboratory where it remained frozen at temperatures of approximately -80ºC. This tissue was used for experiments using the portable Raman system. All samples used in these experiments were defrosted for 30 minutes at laboratory temperature (21ºC) prior to spectroscopic analysis within a laser laboratory. Following this spectra were collected as described in Chapter 4.2 for freshly excised nodes. Data was then transferred to a desktop PC and all spectra were pre-processed by a standard set of processes which will be discussed in more detail at

the start of Chapter 4. Matlab® software was then used to interpret the spectra. Mean spectra were calculated for each pathological group. Peak assignment was performed based on tables held within the department. The statistical significance of differences between the intensities of these peaks in each group was calculated using the Student's t-test. Principal component analysis (PCA) and linear discriminant analysis (LDA) (details described further in Chapter 4) was then used to split the two groups and mimic a diagnostic process.

3.4.2 Experiment 2 – Results.

A total of 38 nodes were analysed in this study from 17 different patients (mean 2.35 nodes, range 1-4). 25 of the nodes studied were reported by histopathology as negative (i.e. no metastases) and 13 were reported as positive (i.e. metastases present). All of the positive nodes were be defined as macrometastases. A total of 3602 spectra were obtained from the 38 lymph nodes assessed. A mean of 95 spectra were obtained from each node (range 25 -100 spectra) (Table 6).

Nodal Status based on H and E assessment	Total Number of Nodes	Total Spectra Numbers	Mean number of Spectra per node
Negative	25	2384	95.4 (Range 95 -100)
Positive	13	1218	93.7 (Range 25 -100)

Table 6- Details of data included in the feasibility study split into two groups based on H and E assessment.

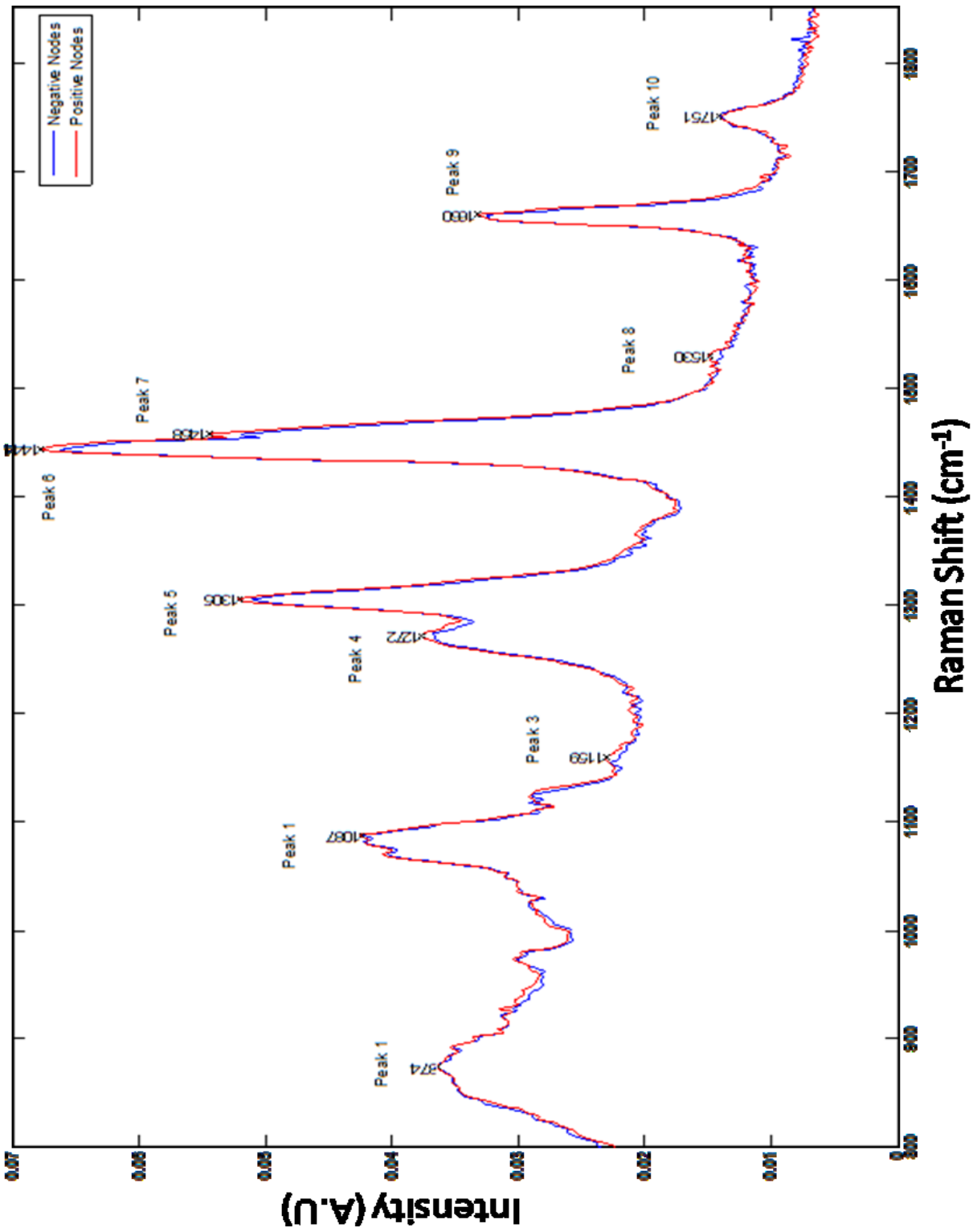
Negative Nodes
Positive Nodes
Peak 1
374
Peak 1
1087
Peak 3
1159
Peak 4
1272
Peak 5
1305
Peak 6
1448
Peak 7
1428
Peak 8
1530
Peak 9
1660
Peak 10
1751
Intensity (A.U)
Raman Shift (cm-1)

Figure 45- Mean spectra for nodes defined as normal (i.e. negative) (n=25, spectra=2384) and positive (i.e. contains metastases) (n=13, spectra=1218) by H and E assessment in the feasibility experiment. 10 peaks identified using tables held within the department marked.

The first stage in the analysis of this dataset was to calculate mean spectra for each of the two histological groups (Figure 45). 10 peaks across the spectra were identified and the intensities of these peaks were analysed to determine differences between the two histological groups (Figure 45). The statistical differences between the intensities of the ten peaks in the two histological groups were calculated using the Student's t-test (Table 7).

Peak Number	Peak Position (cm^{-1})	Mean Intensity of the peak in H and E defined negative samples (spectra no. = 2384) (SD and SEM)	Positive Intensity of the peak in H and E defined positive samples (spectra no. = 1218) (SD and SEM)	P Value (Student's t-test)
1	874	0.0367 (0.003,0.00006)	0.0366 (0.002, 0.00006)	0.2593
2	1087	0.0421 (0.0063, 0.00013)	0.0426 (0.005, 0.00015)	0.0209
3	1159	0.0222 (0.0028,0.00006)	0.0232 (0.0026, 0.00007)	0.0001
4	1272	0.037 (0.0053, 0.0001)	0.0379 (0.004, 0.0001)	0.0001
5	1305	0.051 (0.01, 0.00024)	0.0522 (0.01, 0.0003)	0.0033
6	1444	0.0663 (0.02, 0.0004)	0.0677 (0.017, 0.0005)	0.0039
7	1458	0.0521	0.0546	0.0001

		(0.0132, 0.0003)	(0.01, 0.0003)	
8	1530	0.0142 (0.0032, 0.00007)	0.0152 (0.0028, 0.00008)	0.0001
9	1660	0.0327 (0.0067, 0.00014)	0.0331 (0.0051, 0.00015)	0.0754
10	1751	0.0142 (0.0011, 0.000023)	0.0142 (0.001,0.00003)	1.0

Table 7- The mean intensities of the 10 peaks labelled in figure 45 for H and E defined negative and positive nodes.. The p-values given by a Student's t-test represent the statistical significance of the difference between the means of the intensities of each peak in the two histological groups (SD= standard deviation , SEM= standard error of the mean)

Statistically significant differences were calculated for the intensities of 7 of the ten peaks. These peaks were at 1087, 1159, 1272, 1305, 1444, 1458 and 1530cm^{-1}. These peaks may represent a variety of biochemical constituents including lipid, protein and nucleic acids. The implications of these differences will be discussed in greater detail when the results of the larger intraoperative study are discussed.

In the second stage of spectral interpretation principal component analysis (PCA) was used to help separate the two histological groups. As is explained in Chapter 4.4.1.2 PCA allows simplification of the data into fewer variables (loads) whilst retaining the overall information. Self programmed Matlab® functions were used to determine the loads and the contribution that they made to each spectra (scores). Differences in the scores for the first 10 principal components of each histological group where analysed

using a Student's t-test and differences between the first 9 were shown to be statistically significant (Table 8).

Principal Component (PC)	Mean Value for the score of each PC in H and E defined negative nodes (spectra no.= 2384) (SD and SEM)	Mean Value for the score of each PC in H and E defined negative nodes (spectra no.= 1218) (SD and SEM)	p value
1	-0.0053 (0.1588, 0.0032)	0.0117 (0.1348, 0.004)	0.0019
2	-0.0056 (0.121, 0.002)	0.0125 (0.0113, 0.00034)	0.0001
3	-0.0015 (0.014, 0.000281)	0.0034 (0.009, 0.0003)	0.0001
4	-0.0018 (0.0125, 0.0003)	0.0041 (0.0067, 0.0002)	0.0001
5	-0.0009 (0.0122, 0.0002)	0.002 (0.0063, 0.0002)	0.0001
6	0.0007 (0.0097,0.0002)	-0.0016 (0.007, 0.0002)	0.0001
7	-0.0009 (0.01, 0.0002)	0.002 (0.0046, 0.0001)	0.0001
8	-0.0017 (0.0069, 0.0001)	0.0038 (0.0076, 0.0002)	0.0001
9	-0.0011 (0.0067, 0.0001)	0.0024 (0.0073, 0.0002)	0.0001
10	0 (0.0033, 0.0001)	-0.0001 (0.01, 0.0003)	0.6649

Table 8- The mean value for the score of each principal component (PC) in H and E defined negative and positive nodes in the feasibility study. The p-values given by a Student's t-test represent the statistical significance of the difference between the means of the score for each PC in the two histological groups.(SD=standard deviation and SEM=standard error of the mean)

The loads relating to each of the principal components were plotted and although spectral features became increasingly difficult to differentiate from noise beyond the first 3 principal components (PCs) clear features were seen in the loads of the first two principal components (Figure 46, 47 and 48).

The plot for the load of principal component (PC) 1 bears distinct similarities to spectrum of fatty acids, particularly mono-unsaturated fatty acids such as oleic acid. This is consistent with previously published work (discussed in Chapter 2) that demonstrated a difference in the concentration of fatty acids in malignant tissue. This is explored more in the intra-operative work in Chapter 4.

The key question that this feasibility study sought to answer was how successful the test was at differentiating between negative and positive nodes. Initially an attempt was made to split the two groups based on the scores of the most statistically significantly principal component, PC2. Whilst there was a degree of overlap this PC alone achieved a sensitivity of 69.3% and a specificity of 77.2% at differentiating between the two pathological groups (Figure 49).

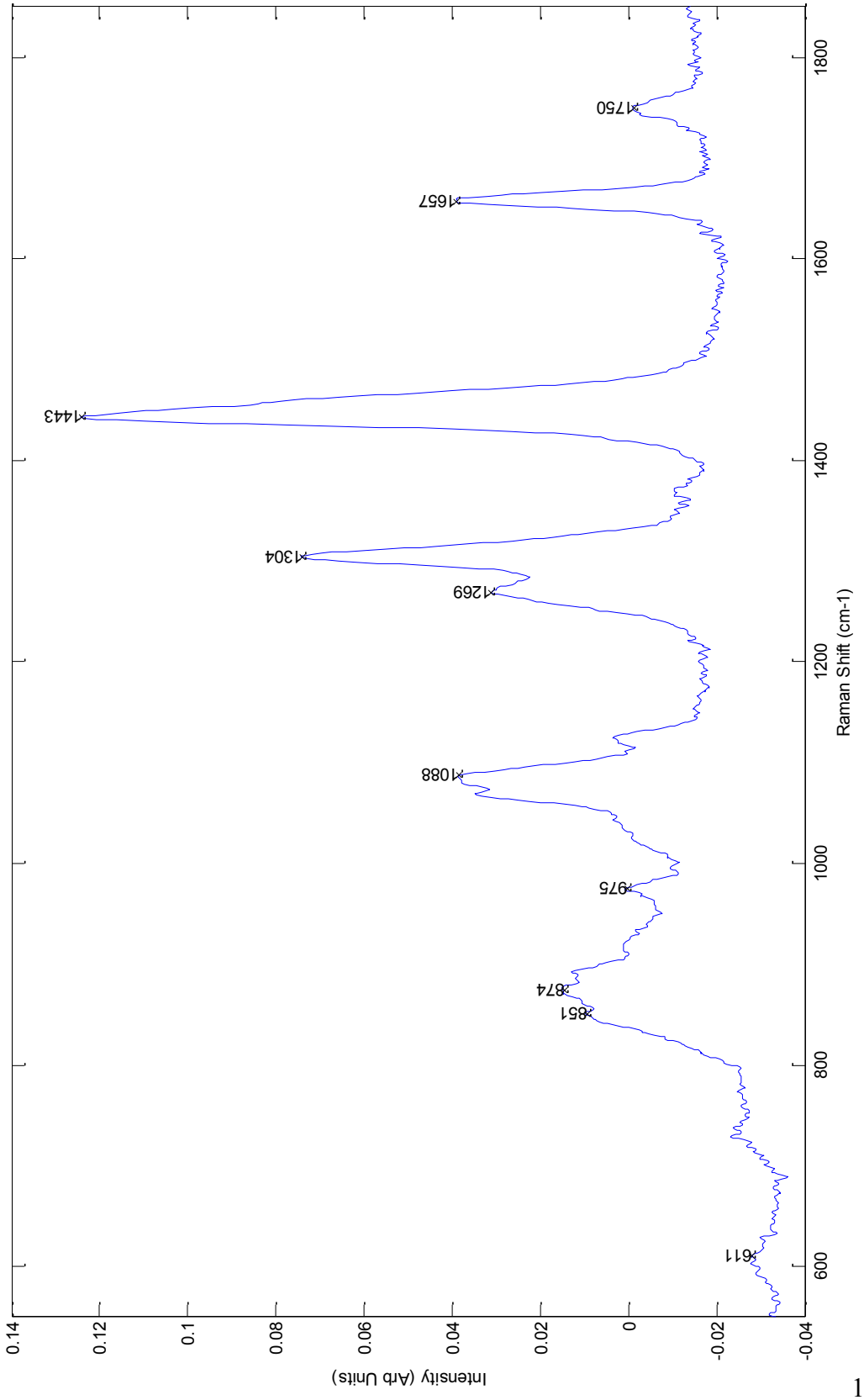
Intensity (Arb Units)
Raman Shift (cm-1)
0.14
0.12
0.1
0.08
0.06
0.04
0.02
0
-0.02
-0.04
600
800
1000
1200
1400
1600
1800
611
851
874
975
1088
1269
1304
1443
1657
1750

Figure 46- Spectral plot of the load for principal component 1 in the feasibility study, some peaks marked for clarity. The contribution that this load made to the overall spectra is given by the scores (see table 8).

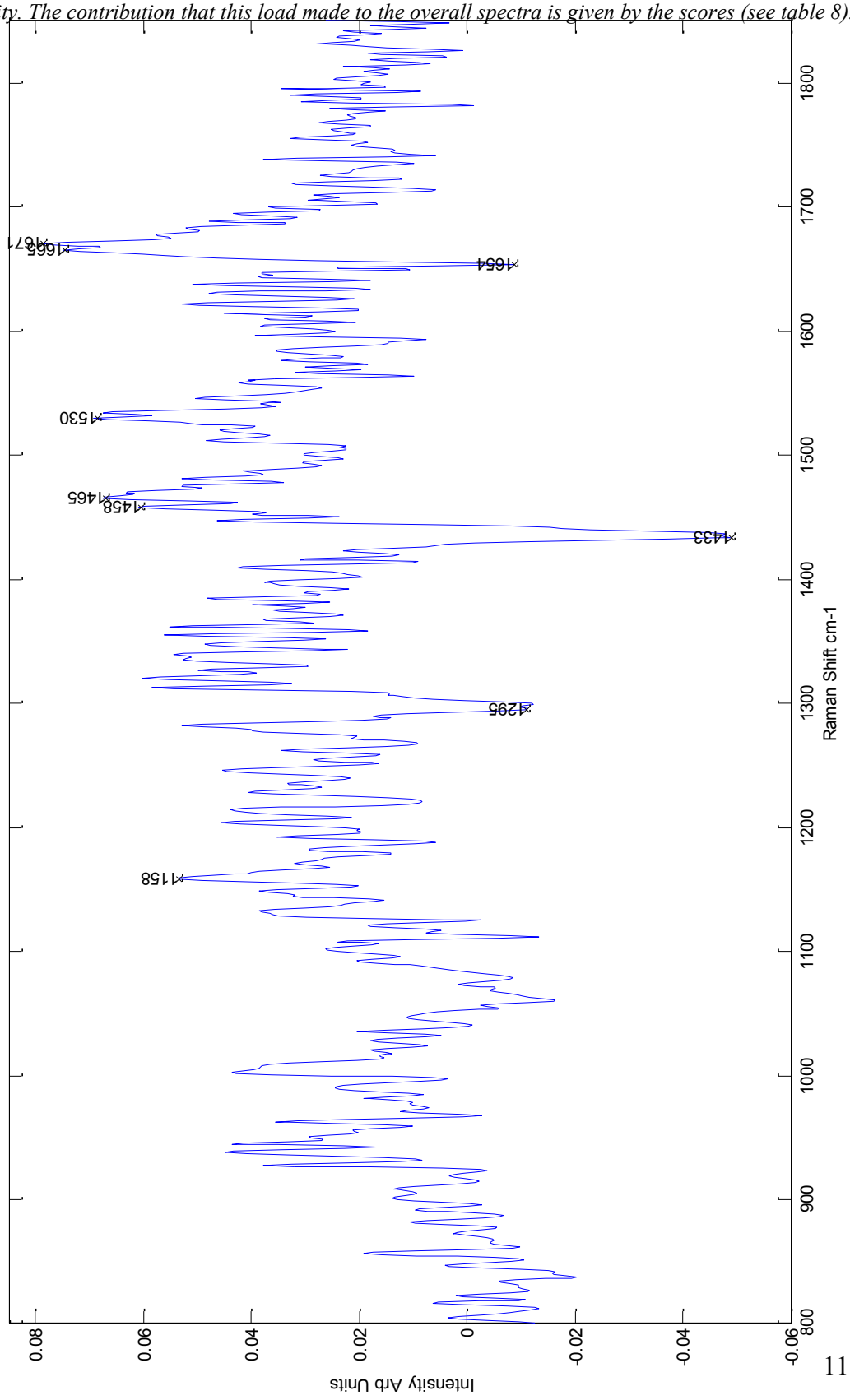

Figure 47- Spectral plot of the load for principal component 2 in the feasibility study, some peaks marked for clarity The contribution that this load made to the overall spectra is given by the scores (see table 8).

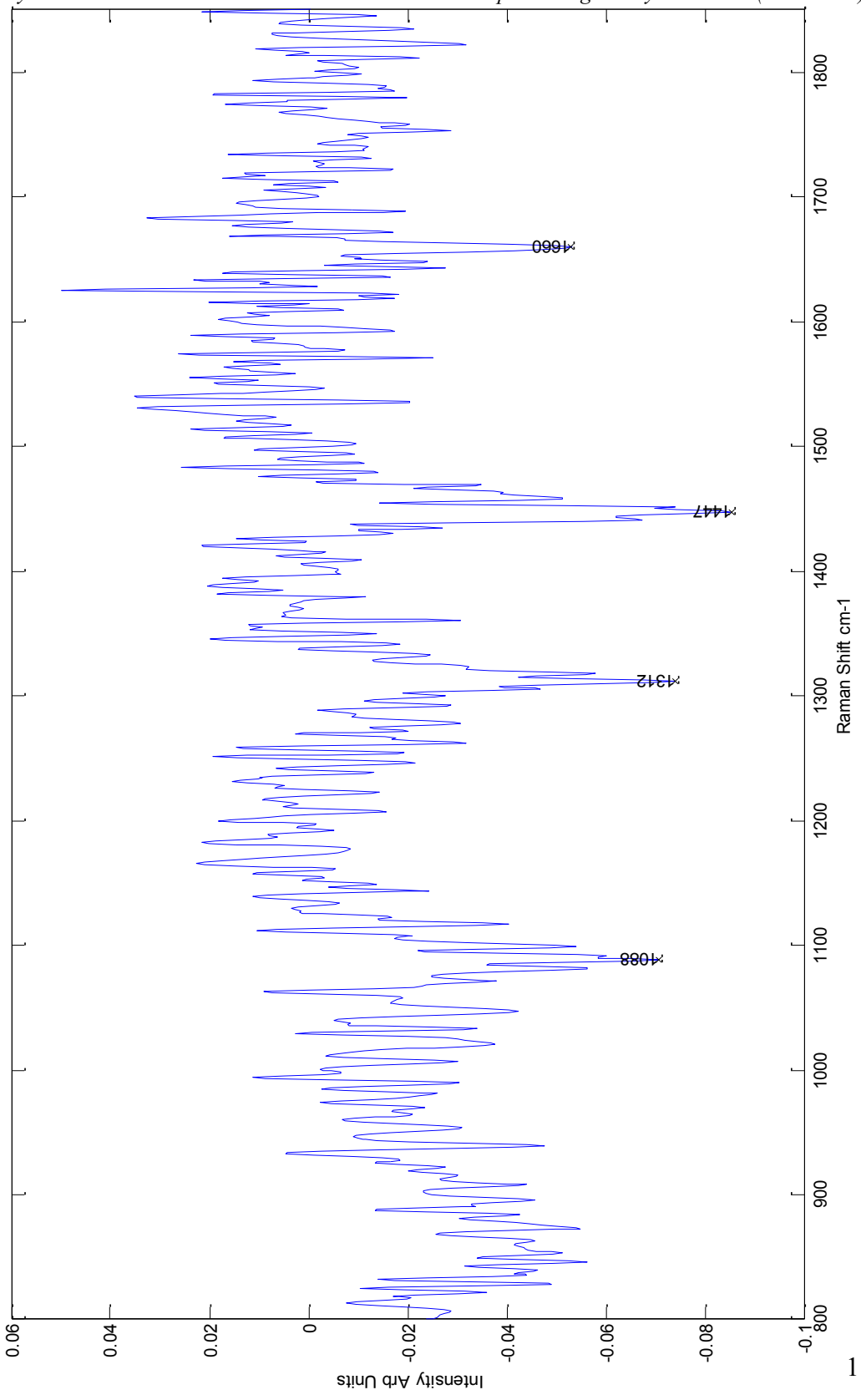

Figure 48- Spectral plot of the load for principal component 3 in the feasibility study some peaks marked for clarity. The contribution that this load made to the overall spectra is given by the scores (see table 8).

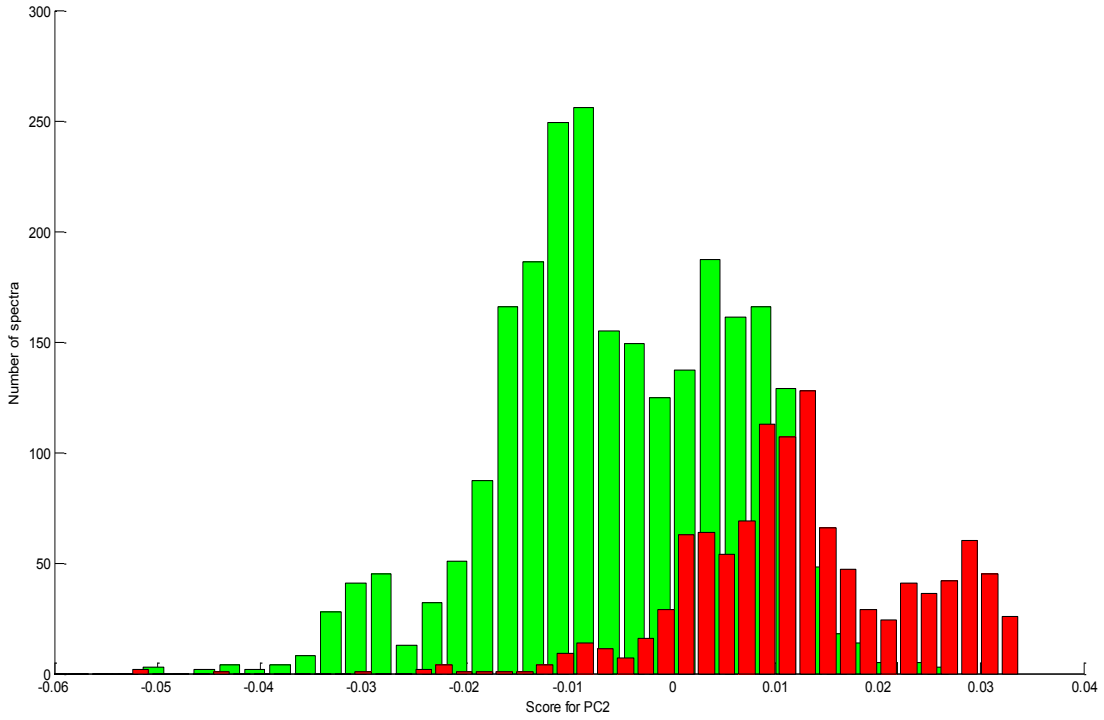

Figure 49- Histogram plotting the scores for principal component 2 of both H and E defined negative nodes (green) and positive nodes (red) in the feasibility study to demonstrate its ability to divide the two groups.

In the third phase of spectral interpretation linear discriminant analysis (LDA) fed by the principal components was used to improve the separation of the two pathological groups by providing a supervised classification algorithm (as is explained further in Chapter 4). In this calculation the first 25 principal components were used. The results of this analysis revealed a sensitivity and specificity of differentiation between the two groups of 95.7% and 98.9% respectively (Table 9) (Figure 50). This is clearly

comparable with many of the current methods of intra-operative analysis and strongly supports the potential of this technology in that role.

	H and E defined Positive Nodes	H and E defined Negative Nodes
Raman Spectra (Positive)	1166	26
Raman Spectra (Negative)	52	2358
	Sensitivity =95.7%	**Specificity=98.9%**

Table 9- The sensitivity and specificity achieved in the feasibility study on an individual spectral basis using linear discriminant analysis fed by the principal components.

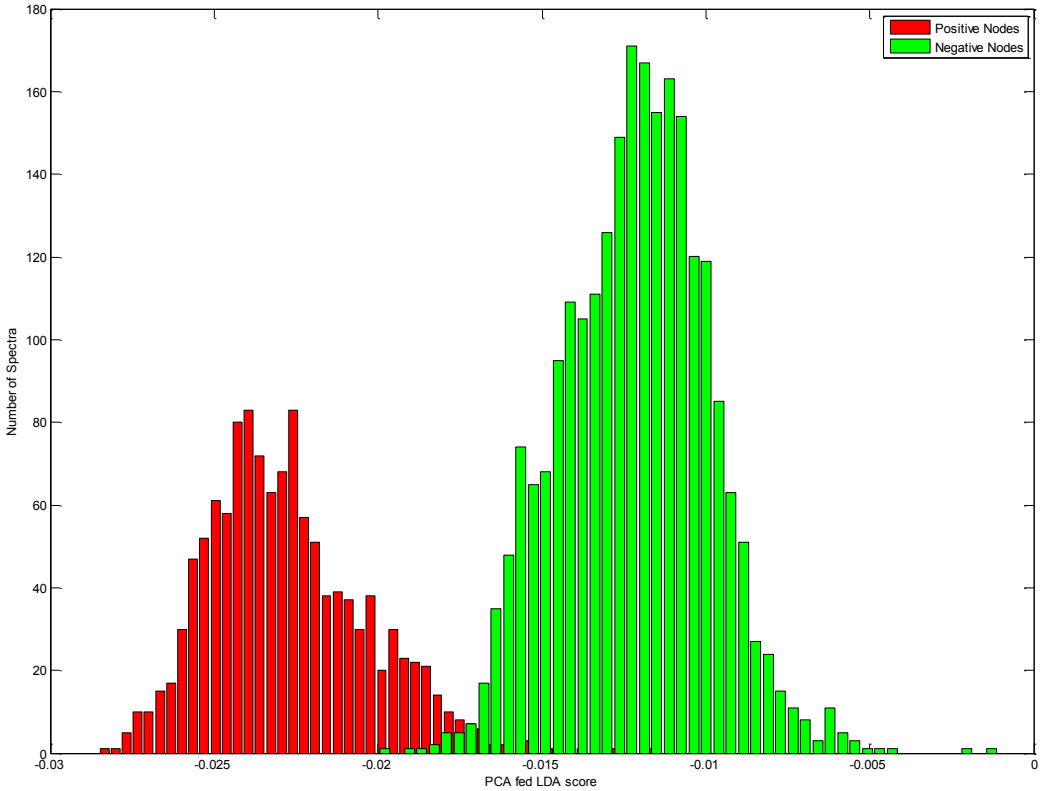

Figure 50- Histogram plotting the scores for the linear discriminant analysis fed by the principal components of both H and E defined negative (green) and positive (red) nodes in the feasibility experiment .

The influence of each of the principal components in achieving this result were assessed by repeating the LDA calculation with increasing numbers of PCs , starting with just the first PC. These training results achieved a sensitivity and specificity of >90% using only the first 8 PCs although the best results were achieved when all 25 PCs were included (Figure 51).

In the fourth stage of spectral interpretation the strength of these findings were scrutinised using a leave one node out validity test. Initially all spectra from one node were removed and individual spectra projected onto the training set using 25 principal components. This demonstrated that Raman spectroscopy was 75% sensitive and 94% specific when differentiating between normal and metastatic tissue for this dataset. This remains comparable to the sensitivities and specificities achieved for other intra-operative techniques; particularly frozen section analysis and touch imprint cytology, but a larger dataset would be expected to improve upon these results.

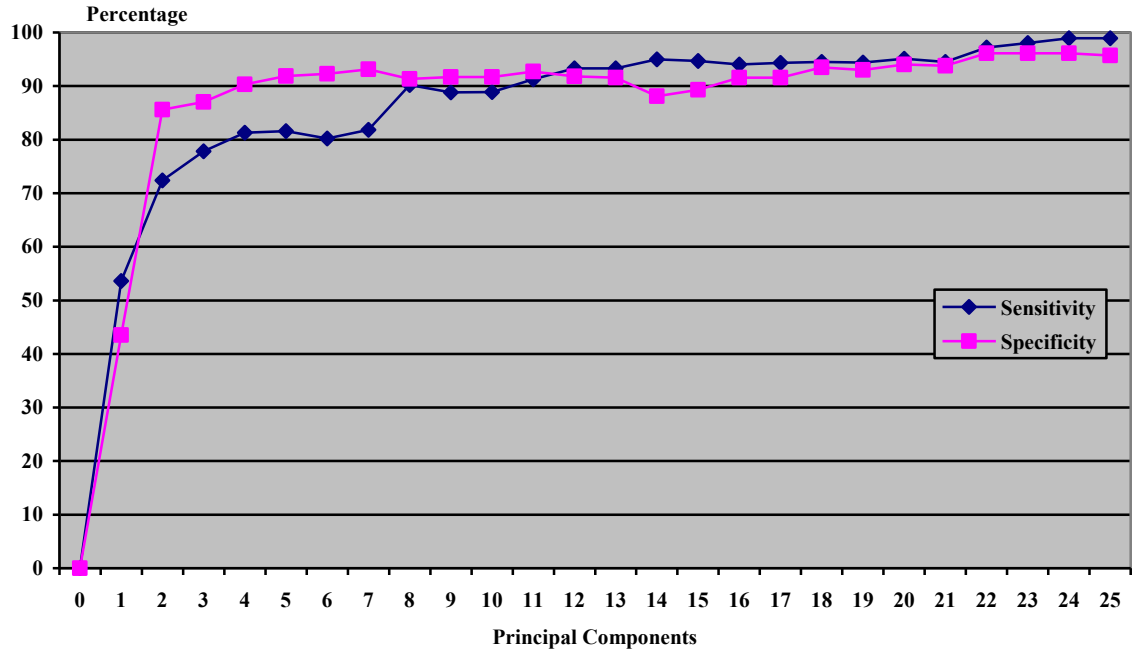

Figure 51- Sensitivity and specificity at splitting H and E defined negative and positive nodes in the feasibility study using increasing numbers of principal components in the linear discriminant analysis.

To help simulate acquisition of data in a time frame that was suitable for intra-operative use the next section of analysis went on to alter the numbers of spectra from each node that were included in the analysis. 5, 10 and 25 spectra from each node were randomly selected from the total spectra acquired from each node. These numbers were selected following discussions with the clinicians involved in the project. Data related to current techniques and surgical experience suggests that there would be approximately 40 minutes per patient to process and assess all the nodes sampled. If up to 5 nodes were sampled from each patient and divided into two then there would be less than 4 minutes to prepare and assess each sample It was important therefore to appreciate the affect that smaller spectral numbers would have on the results achieved.

A Matlab® programme was written that randomly selected 5, 10 and 25 spectra from the total spectra sampled from each node. These were then used to create a mean spectrum for each sample. The sensitivity and specificity of the test based on the results of PCA fed LDA and leave one node out cross validation was then calculated based on mean spectra containing 5, 10 and 25 spectra each (Table 10).

	5 spectra per node	10 spectra per node	25 spectra per node
Sensitivity	77% (10/13)	85% (11/13)	92% (12/13)
Specificity	96% (24/25)	100% (25/25)	100% (25/25)

Table10-The sensitivity and specificity achieved in leave one node out cross validity testing using a range of spectra per node.

In the final stage of analysis the above results from 5 spectra per node (Table 10) were used to mimic the clinical scenario in which the system might one day be used. Of the 17 patients included in the feasibility study, 11 had a negative axilla (i.e. all nodes negative) and 6 had at least one node positive (range 1-4). If any of these nodes sampled were found to have evidence of metastases then an axillary node clearance would have been recommended. Using the data presented here, 5 out of the 6 patients who were advised to have an axillary clearance post operatively would have been successfully identified and been able to receive the benefits of an immediate rather than a delayed axillary clearance. One patient with a single positive node would initially been deemed to have a negative axilla only to have this changed on post operative H

and E analysis. Of the 11 patients with negative axilla none would have been recommended an axillary clearance based on the Raman results (Table 11). The only false negative was in a node from a patient with other positive nodes. One possible explanation for this could be that the H and E analysis had missed a metastasis which was then picked up by the Raman analysis.

	H and E defined Positive Axilla	H and E defined Negative Axilla
Raman Positive Axilla	5	0
Raman Negative Axilla	1	11
	Sensitivity = 83%	**Specificity=100 %**

Table 11: The sensitivity and specificity achieved in the feasibility study at identifying positive and negative axilla using Raman spectroscopy.

3.4.3 Experiment 2 – Conclusions.

Given the sensitivity and specificity achieved both with PCA fed LDA (supervised testing) and leave one node out cross validation (unsupervised testing) it was felt that these results support the potential of a hand held Raman spectroscopy device for use in the intra-operative assessment of axillary lymph nodes. Importantly the feasibility study also enabled one to demonstrate that equivalent results could be achieved by selecting a smaller subset of spectra from each node. Even when only 5 spectra per node were

assessed the sensitivity and specificity remained consistent. Given the pressures on time that are going to be evident when using fresh tissue in a clinical setting this is an important concept to demonstrate. Importantly if Raman spectroscopy had been used to guide management 5 patients would have benefited from immediate axillary surgery and none would have been advised to have an axillary clearance that later was deemed to be unnecessary.

3.5. Experiments 3 and 4 - Overcoming the effects of operative theatre lighting

Encouraged by the results of the feasibility study planning of an intra-operative study using the portable probe Raman spectroscopy system continued. One of the key problems that needed to be overcome if this was going to be possible was the effect of theatre lighting on the spectra obtained. The first step in this process was understanding the nature of theatre lighting. Lighting within the operating theatre includes both the general illumination as well as the operating lights. The illumination of the surgical site is vital to optimise the surgeon's view of the operating field and operating lights are therefore specifically designed to meet this goal.

The majority of operating field illumination is provided by overhead lights. These are often white fluorescent but may also be incandescent. Whilst the level of general illumination should be at least 200 foot candles (2095 lux) to allow the theatre staff including the anaesthetist to work safely the surgical lights should be in the range of 2500-27,000 foot candles (26,190-290,628 lux) (Berry and Kohn 2000). These lights need to be able to provide contrast between both tissue types and tissue depths without

casting shadows and focused in such a way as to avoid a dark centre. There are a wide variety of different lights marketed by an array of different companies. Not only do the lights in different theatres vary but the way the lights are set up and used also varies. 41% of German surgeons report that they use a single main light with a smaller satellite, 43% use two equally sized large lights and 16% use three equally sized large lights (Matern and Koneczny 2007). Further complicating this is the preference of some surgeons to operate with low levels of ambient or general light whilst others maintain the general lighting throughout the procedure. Many UK hospitals have developed in stages over a number of years with new operating suites added as the need arose. As a result operating suites will have a variety of different theatre lights within a single hospital.

Background lighting has an adverse effect on Raman spectroscopy as it is recorded at intensities that swamp the low intensity of Raman scattered light. The spectral acquisition from biological tissue is often performed in darkened laser laboratories. Providing mechanisms to exclude background light is vital to the effective functioning of an intra operative Raman device.

Potential solutions included switching all the theatre lights off to create a darkened environment or applying filters to all the lights. Creating a darkened theatre was rejected due to the potential negative consequences this may have for the patient and the safety implications for the theatre staff. The application of filters to all the theatre lights was considered impractical because of the variety of theatre light designs in use, as well as the problems with infection control and the possibility of surgical site contamination

if the filter were to become loose. An alternative was theorised based on excluding the light from the immediate area around the probe tip. In this way the device could be used in all lighting conditions within the operating theatre without the potential deleterious side effects.

3.5.1. The Light Eliminator design

The basis of the design was the standard film case used to prevent light contamination. This was modified to allow the Raman probe to be housed within it. The design of the probe includes a tip that ensure the optimal positioning of the matter being investigated when it is in contact with the tip. A removable lid allows the matter to be positioned in the correct position (Figure 52, 53).

3.5.2. Experiment 3 (The Light Eliminator Experiment, Part A) – Methods.

The light eliminator was first tested within the operating theatres at Gloucestershire Royal Hospitals NHS Foundation Trust. Prior to its use within this environment local rules were designed to ensure safe use and the experiments were carried out at times when the operating theatres were not in clinical use.

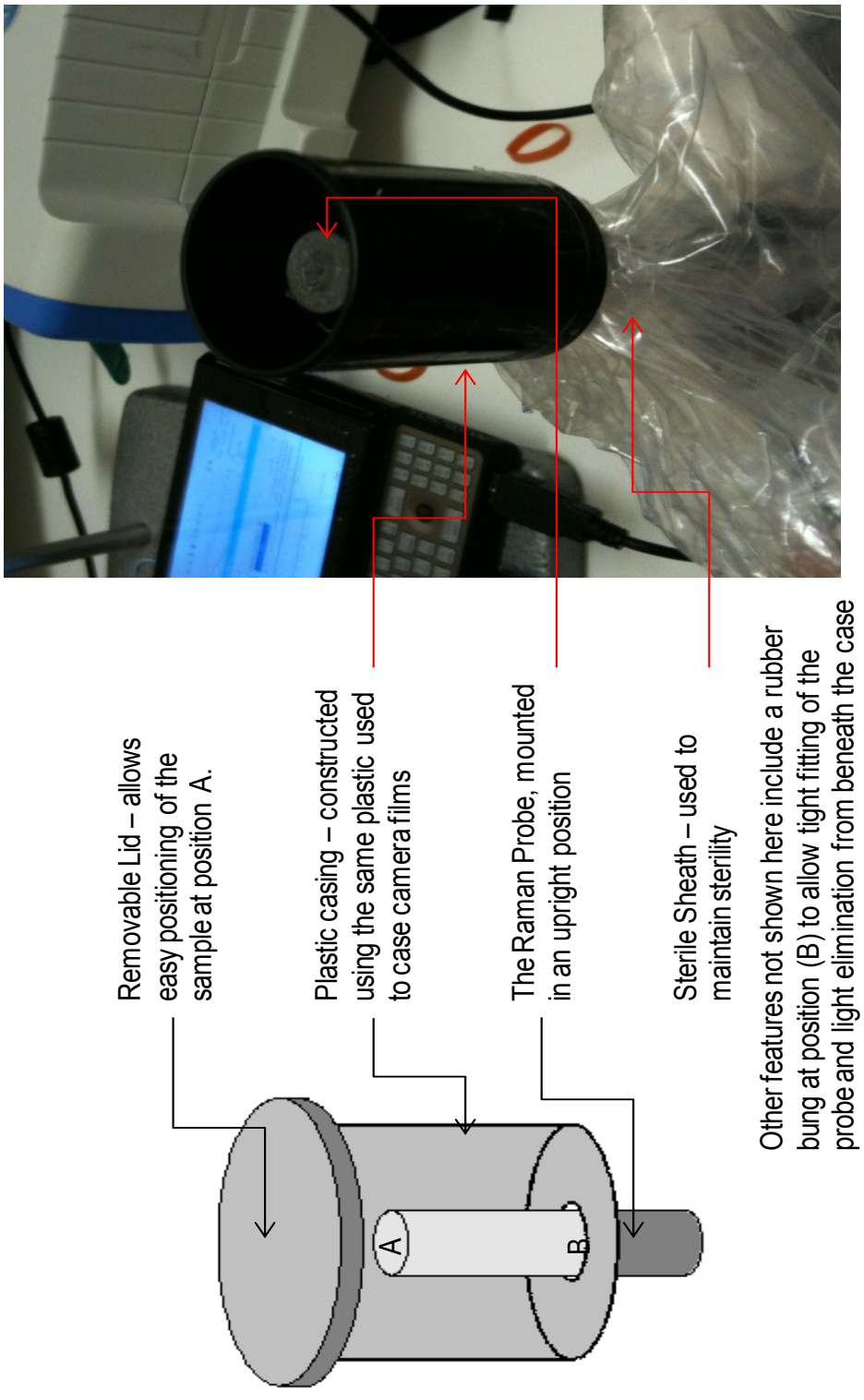

Figure 52 Outline design drawings for a light eliminator (not to scale)(left) and photograph of the Light eliminator in place over the end of the probe tip(right). The probe is held facing upwards. The sterile sheath is placed around it and the eliminator is then placed over this. The tissue can then be placed on the central flat surface and a light resistant lid placed and secured. .

Using the MiniRam II Raman spectrometer spectra were obtained from a standard block of PTFE. This block measured 2cm x 1cm and was used due to its clear and characteristic peaks. This is used as a standard measurement by the research group. Theatre temperature was maintained at 22 ºC throughout the experiment and the laminar ventilation system was switched off. The spectroscopy device was placed on a standard theatre trolley in the corner of the theatre approximately 3m away from the operating table, a position that may be mimicked when the device is used in the intra-operative setting.

Spectra were obtained in four lighting conditions.

1. Background lights and operating lights on.
2. Background lights on and operating lights off.
3. Operating lights on and background lights off.
4. All lights within the theatre switched off.

In each of these situations 10 spectra were recorded (by combining 16 1s acquisitions) both with and without the light eliminator device in situ. The data were transferred to a desktop PC and analysed using Matlab® software.

3.5.3. Experiment 3 – Results.

The mean plots of spectra obtained without the eliminator demonstrated the deleterious effects of both the background and operating lights (Figure 54). The spectra obtained when the operating lights were on demonstrated saturation of the CCD and there were

multiple additional peaks in the spectrum obtained with only the general lights on. These results confirm that both the theatre lights and the general lighting make interpretation of the PTFE spectra either very much more difficult or impossible. Given the relatively high intensities of the PTFE peaks it is likely that this would be replicated or indeed made worse when using biological specimens.

The effect of the eliminator in this observational study was evident when the mean spectra of the data were plotted for the four lighting settings both with and without it in place (Figure 55). It was thus hoped that the light eliminator would facilitate the use of the MiniRam II Raman spectrometer within the operating theatre. Due to the prominent PTFE peaks further experiments were designed to assess the effect of the light eliminator when using biological tissue.

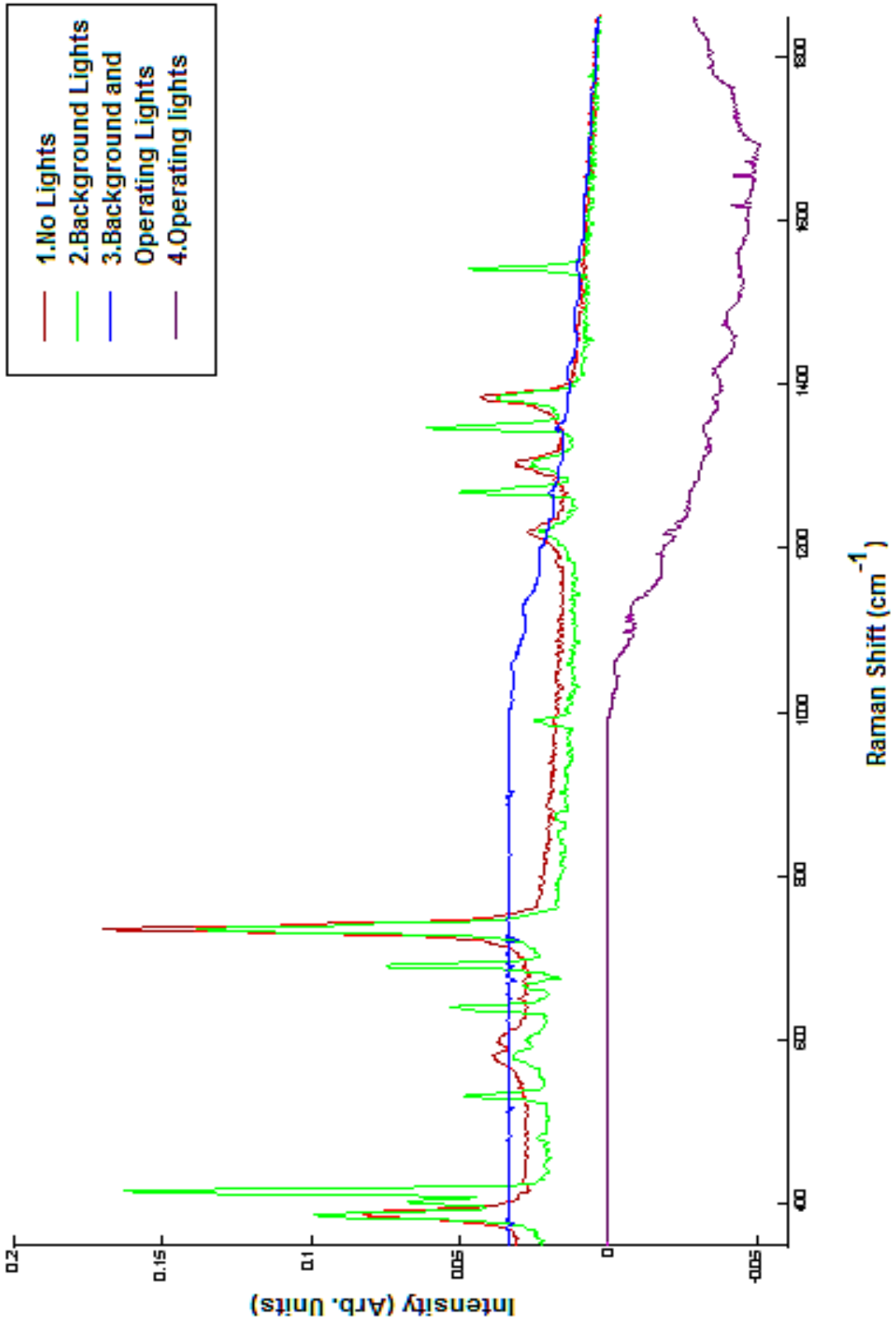

Figure 54- Mean spectra (n=10) for PTFE from four lighting conditions collected in an operating theatre to demonstrate the deleterious effects of background and operating lights.

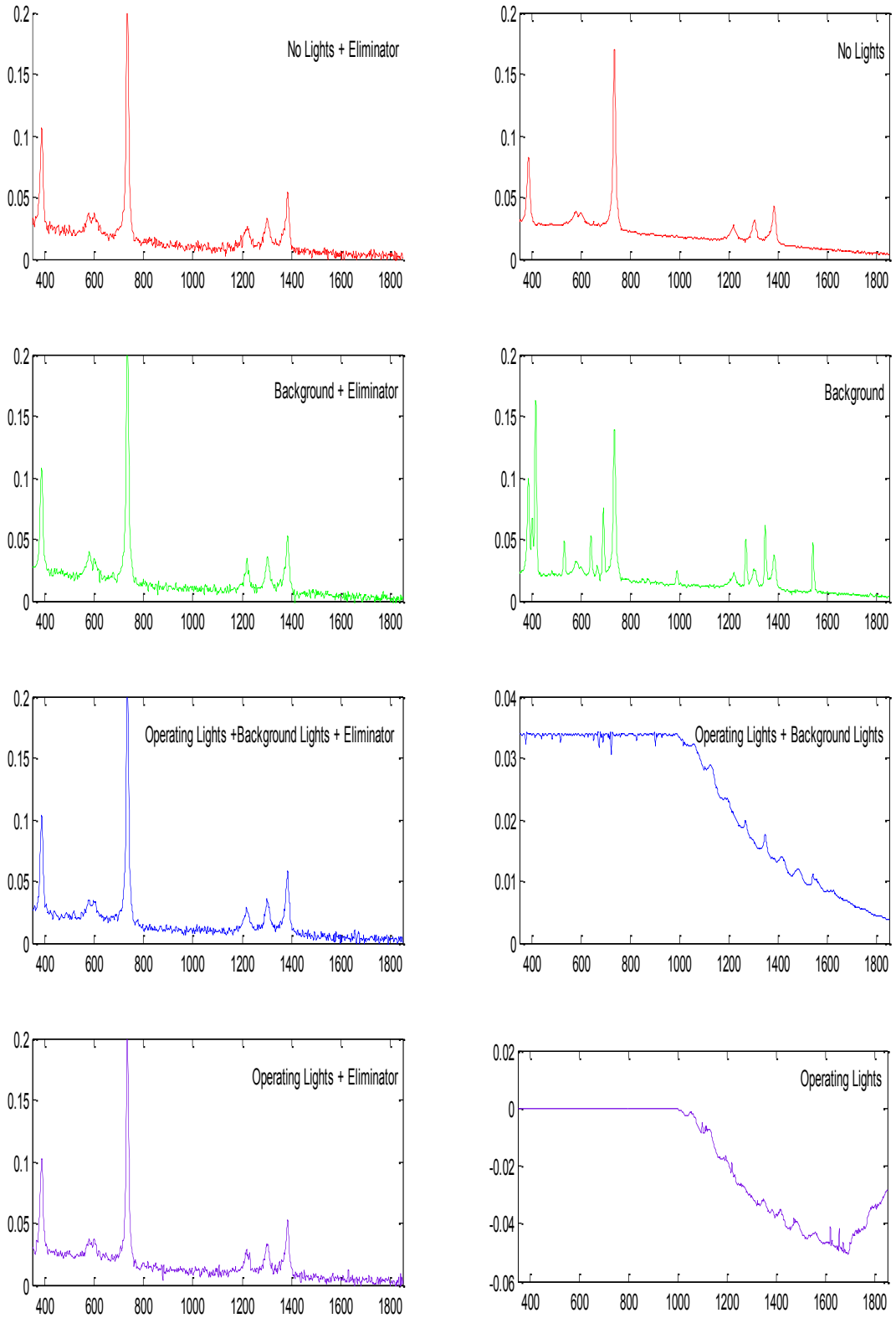

Figure 55- Mean spectra (n=10) for four lighting conditions both in the presence of the light eliminator (left) and without it (right) (y axis = intensity AU and x axis = Raman Shift cm^{-1}).

3.5.4. Experiment 4 (Light Eliminator Experiment Part B) – Methods.

To determine the effect of the eliminator when obtaining spectra from biological tissue the device was tested within the laser laboratory using axillary lymph node tissue rather than PTFE. A single lymph node that had been collected and stored as part of the feasibility study was used. This node was not included in the feasibility study but its handling both at the time of collection and during the experiment was a described in Chapter 3.4. Standard laboratory conditions were maintained except for the switching on of all the lights as required by the experiment.

16 x 1 second acquisitions were used to collect 5 spectra from the node using the MiniRam II Raman spectrometer. These were obtained in the following conditions;

- Standard laboratory conditions (all lights off).
- Standard conditions with lights on.
- Standard conditions with lights on and using the eliminator device.

The data was then transferred to a standard desktop PC and interpreted using Matlab ® software. Principal component analysis, ANOVA analysis and Student's t-tests were used to assess the results.

3.5.5. Experiment 4 – Results.

Examination of the resulting spectra demonstrated that the spectra obtained in standard laboratory conditions were markedly different to the spectra obtained with the lights on. As expected the spectra obtained with the lights on, but without the eliminator, were overwhelmingly dominated by peaks resulting from the laboratory lights (Figure 56).

The spectra obtained with the eliminator in place appeared very similar to the spectra obtained under standard laboratory conditions. There were differences in intensity and it was felt that this may represent the different orientation of the node which had been repositioned during the experiments (Figure 57a).

The principal components of the three sets of spectra were then calculated using self built programmes in Matlab®. An ANOVA calculation was performed on the scores of each principal component to determine which the most significant principal components were. PC 1 and 2 were calculated to have f values of 110686 and 115 respectively. The loads that pertained to these PCs were plotted and it was evident from inspection of these plots that PC1 related to that of the laboratory lights and that PC2 related to that of the lymph node spectra (Figure 58).

When the scores for PC1 were plotted it could be seen that the eliminator had been successful at eliminating the light as the scores for both the spectra taken with the light turned off and those taken with the lights on were very similar (Figure 59).

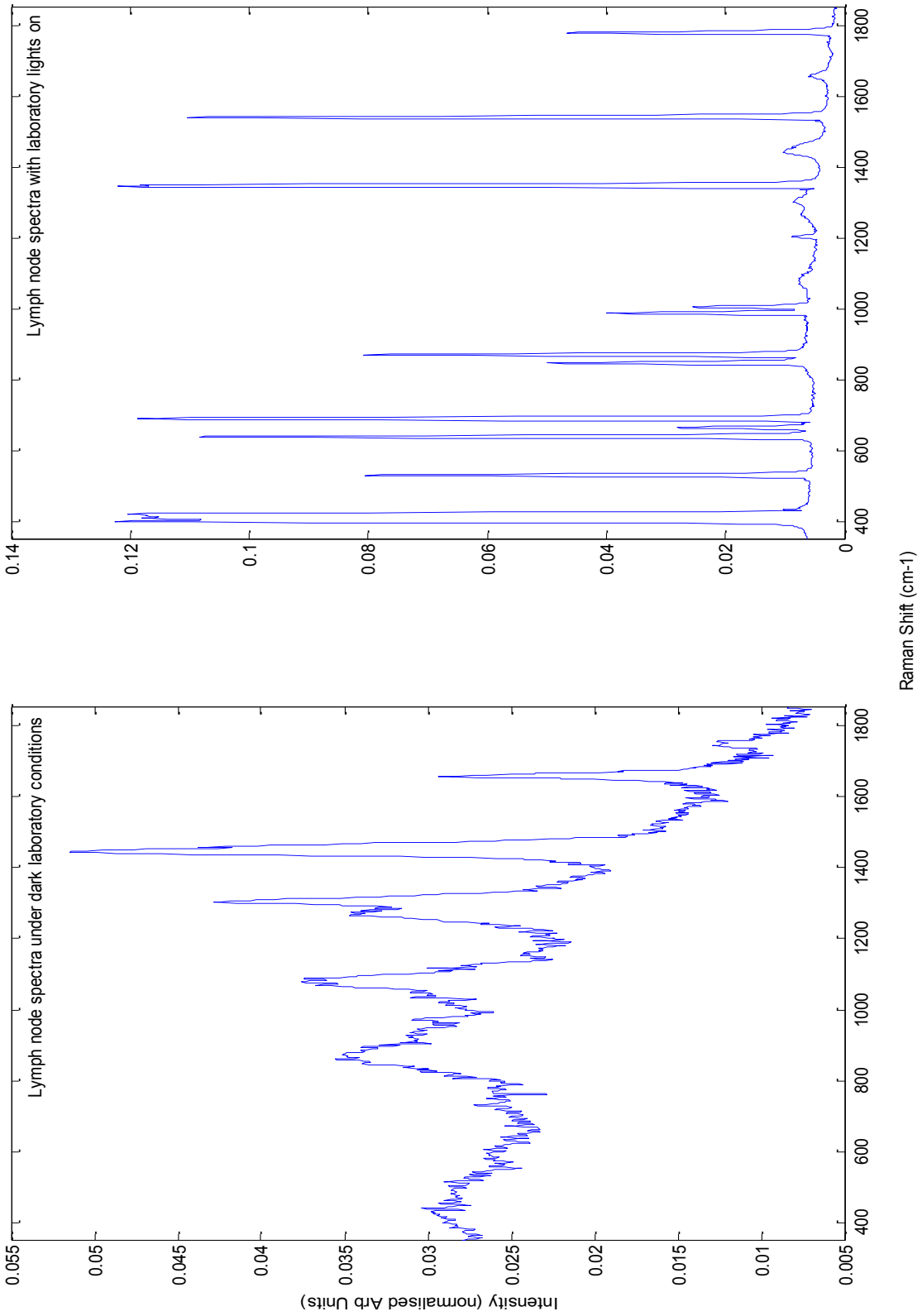

Figure 56- Mean spectra collected from an axillary lymph node (n=5) under standard laboratory conditions and with lights on.

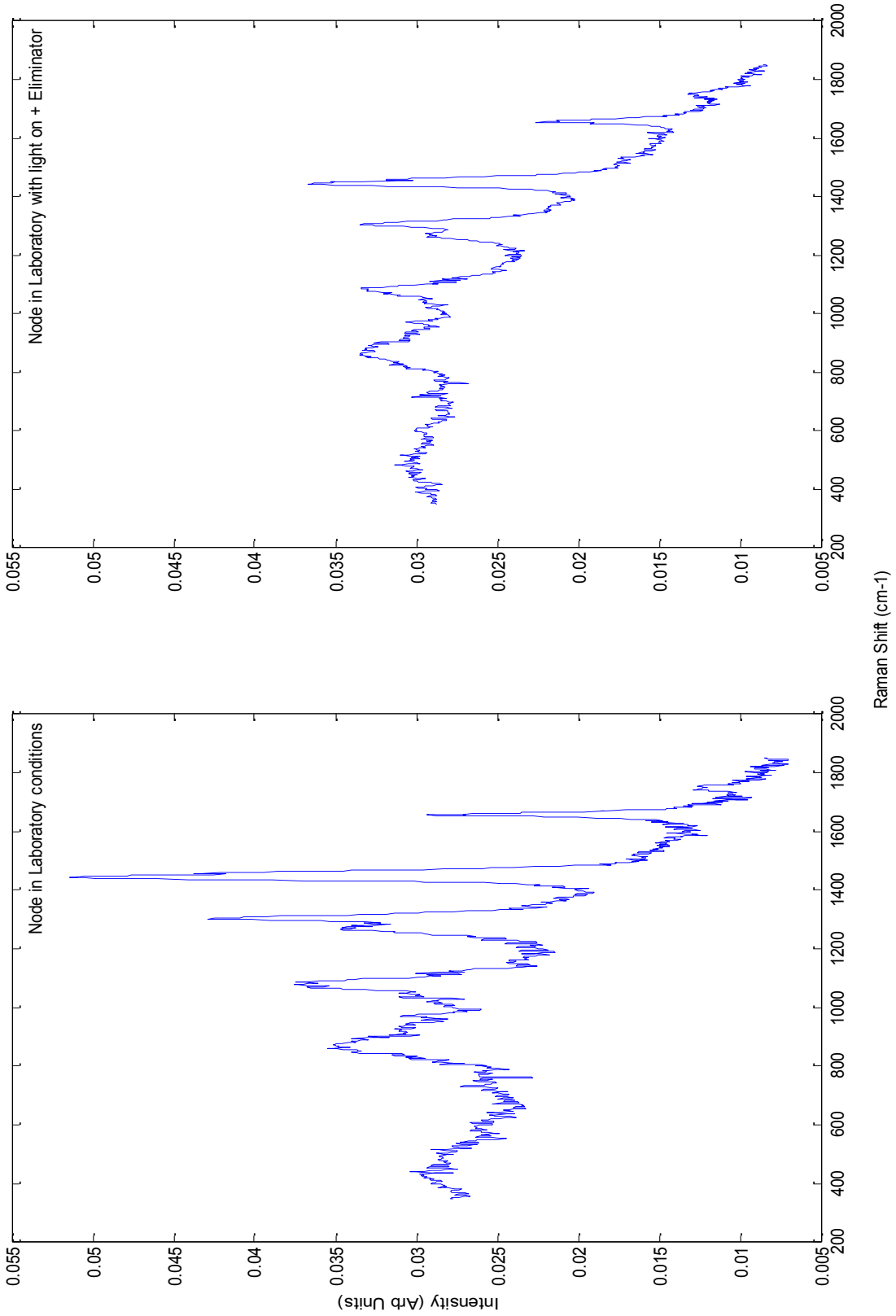

Figure 57- Mean spectra (n=5) collected from an axillary lymph node under standard laboratory conditions and with the laboratory lights on with the light eliminator.

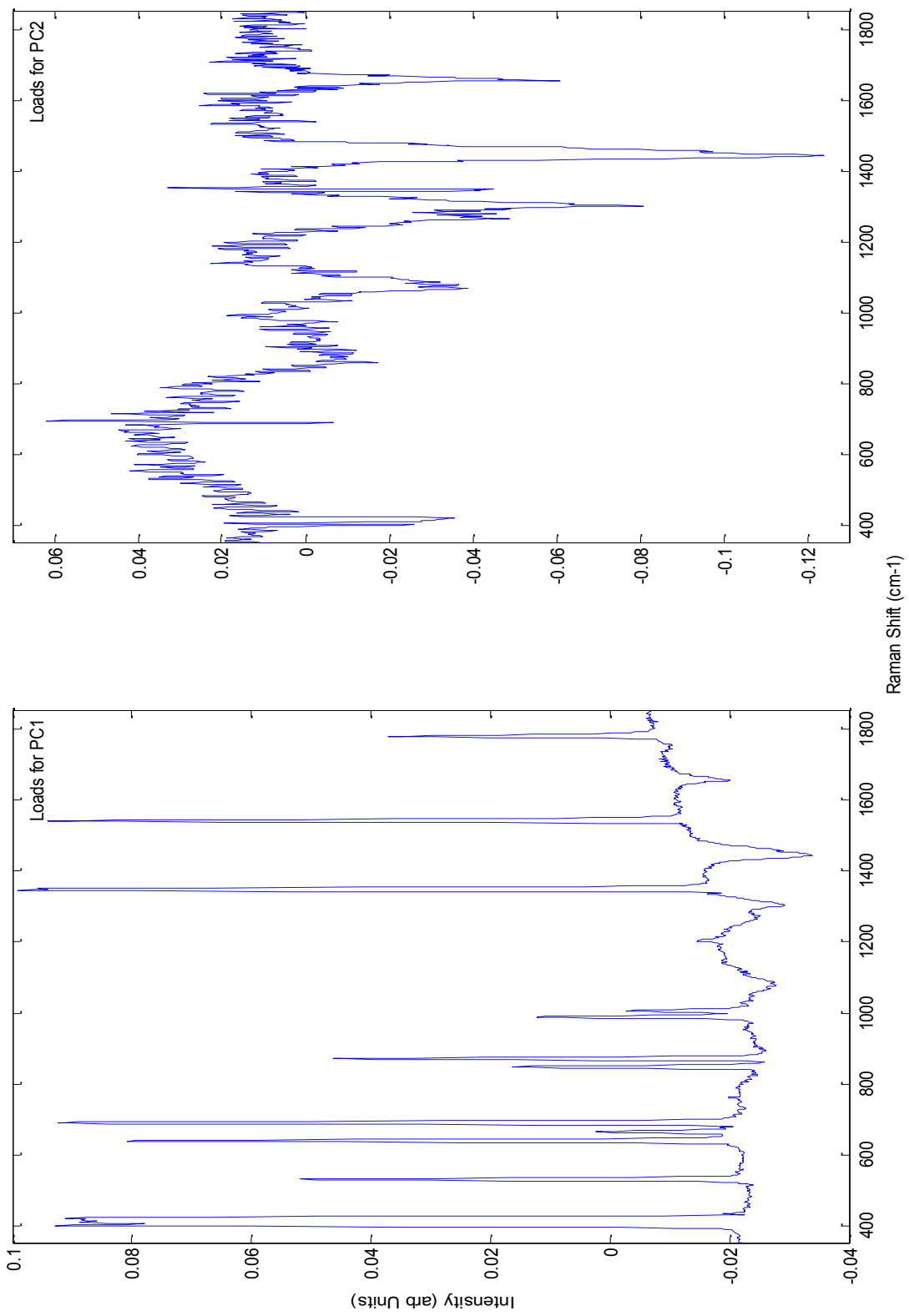

Figure 58- Spectral plots of the loads for principal components (PC) 1 and 2 in experiment 4. PC1 appears to be representative of the laboratory lights and PC2 resembles the spectra that are obtained from an axillary lymph node.

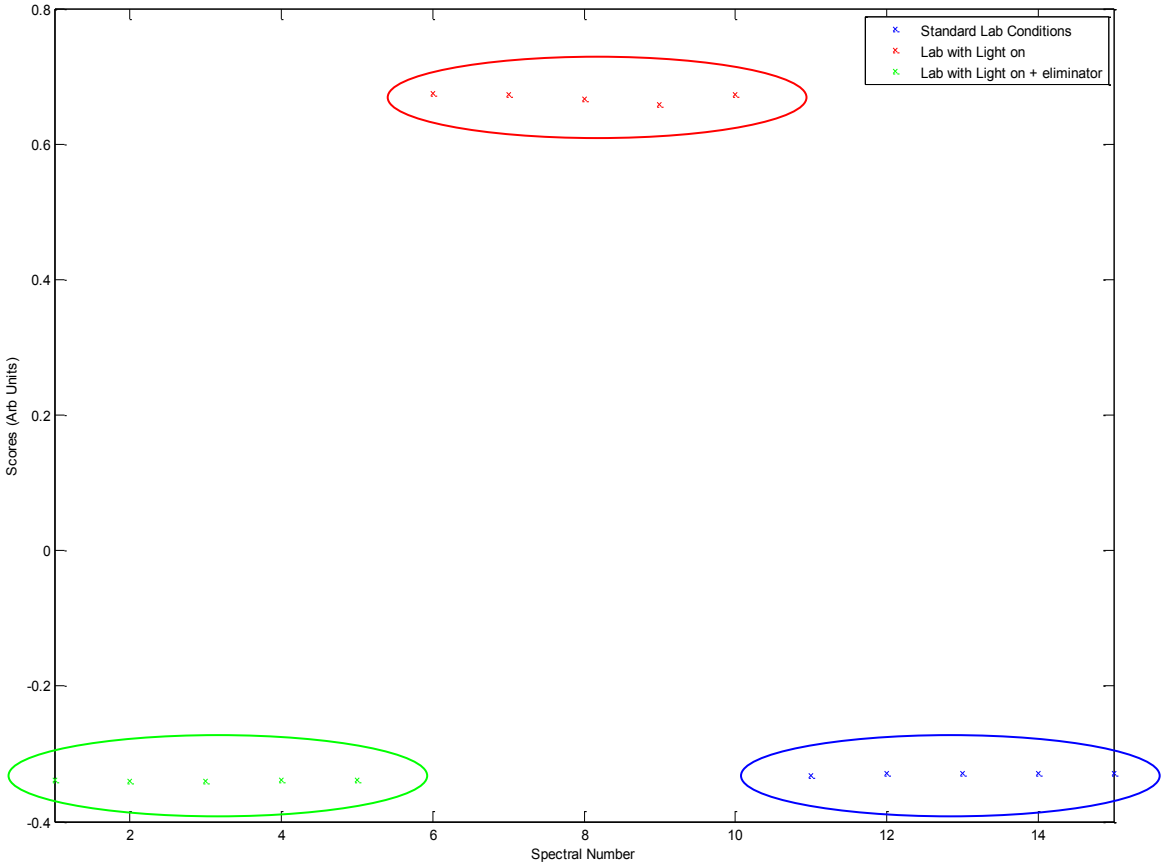

Figure 59- Plot of the scores for PC1 in all lighting conditions in experiment 4. The circles are to emphasise the differences and similarities in the data plotted. The results of the statistical analysis of these results are shown in table 12.

Statistical analysis using Students t-test confirmed that there was no statistically significant difference between the score for PC1 in the standard laboratory and lights on and eliminator group (p=0.13). There was however statistically significant differences between both of these groups and the lights on and no eliminator group (Table 12).

It was thus felt that these results demonstrated that the eliminator would allow the portable Raman spectroscopy device to be used in theatre without the need to turn the lights in the whole theatre off.

Comparison	Mean for the score of PC1 in each group (n=5) (SD and SEM)	p value
Standard laboratory conditions v. Lights on (no eliminator)	0.349 (0.001, 0.00045) v 0.661 (0.004, 0.002)	p<0.0001
Standard laboratory conditions v. Lights on (with eliminator)	0.349 (0.001, 0.00045) v. 0.347 (0.005,0.001)	p= 0.1303
Lights on (no eliminator) v. Lights on (with eliminator)	0.661 (0.004, 0.002) v. 0.347 (0.005,0.001)	p<0.0001

Table 12: A comparison of the mean score (n=5) for PC1 in each of the three lighting conditions in experiment. The results of statistical analysis, using a Student's t-test, to compare these results are shown (SD= standard deviation, SEM= standard error of the mean).

3.6. Experiment 5 -Effect of theatre temperature variations.

Having determined an effective way of overcoming the effects of theatre lighting the next variable that needed to be explored was that of temperature variations within the operating theatre. Previous work using Raman spectroscopy to assess axillary lymph nodes has been carried out in a laser laboratory where the temperature was regulated to remain at 21ºC. The ambient temperature of an operating theatre may vary as a result of the need to maintain the patient's temperature throughout an operation. The importance of altering the theatre temperature is demonstrated by figures that suggest that up to 70% of patients may experience a degree of inadvertent hypothermia during an

operative procedure (Burger and Fitzpatrick 2009). Not maintaining a suitable ambient temperature within the operating theatre was one of the key factors linked to this inadvertent hypothermia (Young and Watson 2006).

A review of the literature pertaining to ambient temperature published in 2006 suggested that an ambient temperature of at least 22°C should be maintained with some authors suggesting temperatures of up to 26°C (Young and Watson 2006). The importance of maintaining the balance between the patient's core temperature and the ability of the surgical team to operate is recognised by the authors especially as the temperature rises above 22°C. Most surgeons prefer to operate at temperatures between 18.5 and 22°C (Brock 1975). American guidelines for the prevention of surgical site infection published in 1999 suggest a slightly higher ambient temperature of between 68-73°F (20-23°C) (Mangram et al. 1999). Given these competing interests it may be that ambient theatre temperature would vary both throughout a single operation and across different days.

3.6.1. Experiment 5 – Methods.

This experiment investigated the effects of varying the temperature across a range of 18-28°C so as to over represent the anticipated ambient temperature range that intra operative spectral analysis would take place within. All experimental measurements were recorded within a laser safe laboratory which has a temperature control facility that allowed the room to be both cooled and heated. The instrumentation within this system allowed both the room temperature to be selected and then monitored to

maintain the desired setting. The temperature of the room is normally set at 21°C. Spectra of cyclo-hexane were obtained across the seven temperatures starting at 18°C and rising in 2°C intervals to reach 28°C. The temperature within the room reached the new temperature setting within 15 minutes. A period of 30 minutes was allowed between temperature alterations to ensure that a stable temperature had been achieved. All other factors within the room were kept stable. Five spectra of cyclohexane were recorded at each of the six temperature settings. Data analysis was performed using Matlab® mathematical software. The statistical significance of any observed differences was tested using ANOVA analysis.

3.6.2. Experiment 5 – Results.

Inspection of the mean spectra for each temperature revealed very few changes. As expected for cyclohexane four very distinct peaks were visible in the range of 750-1500 cm^{-1} (Figure 60). The position of each of the 4 most prominent peaks (labelled in Figure 60) were recorded to ensure there was no peak position drift over the temperature range (Figure 61).

To assess the mean peak position at 6 different temperatures ANOVA, a statistical test that simultaneously compares two or more means, was employed to determine the statistical significance of the small shifts that had been observed. In this test the null hypothesis was that there was no difference between the peak positions at the six different temperature points. Using standard tables the critical "f" value at which the null hypothesis would be rejected can be calculated.

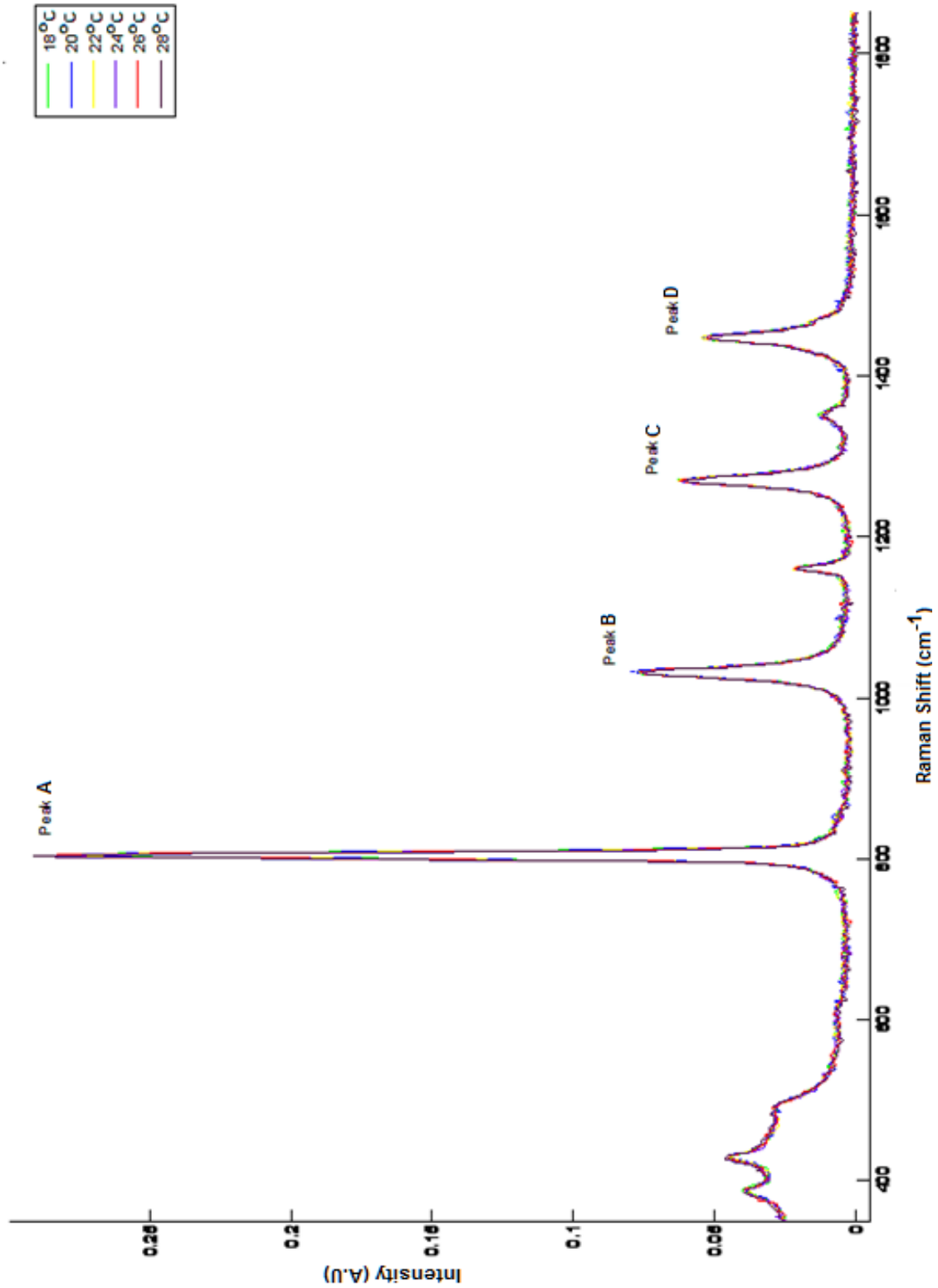

Figure 60- Mean spectra (n=5) of cyclo-hexane recorded at 6 different temperatures. The four prominent peaks are labelled A-D.

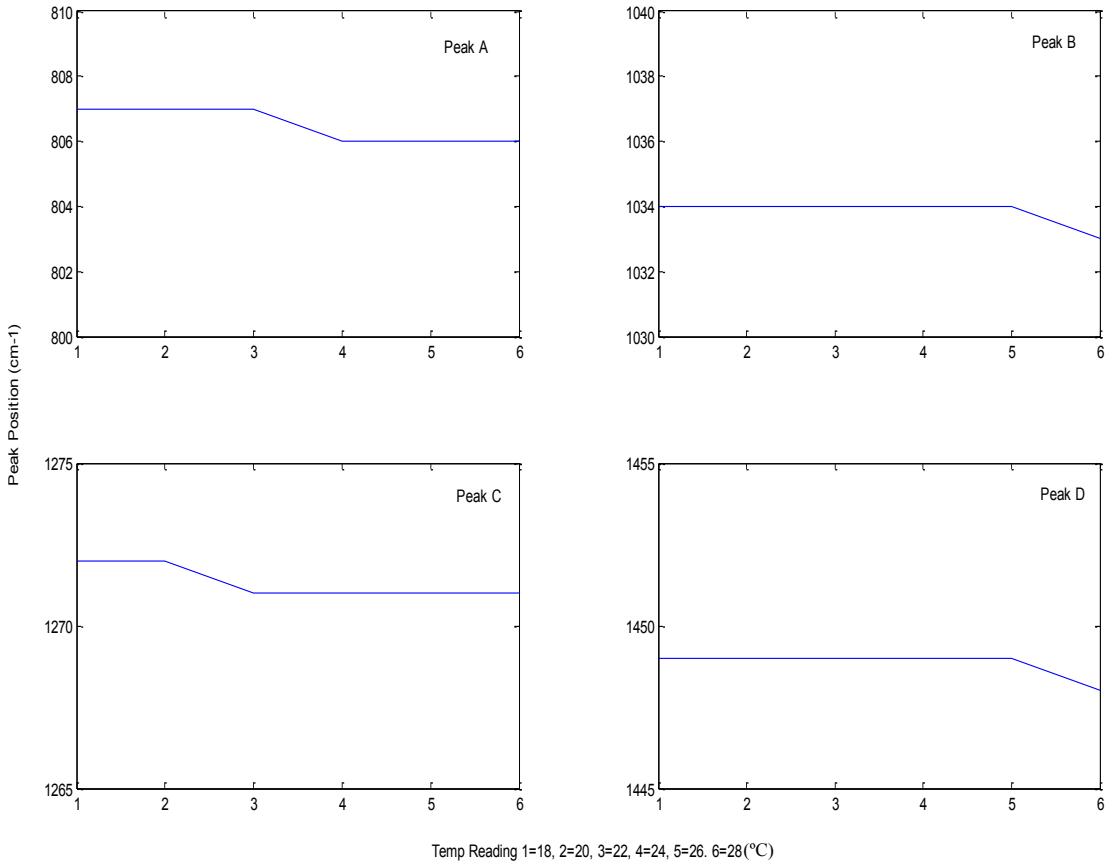

Figure 61- Mean peak position (n=5) of the 4 cyclo-hexane peaks (labelled in Figure 60) across the temperature range 18 -28°C).

The position of peak A was the only one that recorded an f value greater than the critical value. The relative peak positions of the 4 peaks were then calculated. The null hypothesis that there was no difference between the relative positions of the 4 main peaks at the level of $p<0.01$ was not rejected in any of the calculations (Table 13).

This data demonstrated that across a range of temperatures, that correlate with those found in the operating theatre, the positions of each of the four main cyclo-hexane peaks did not significantly differ in relation to each other. Indeed the position of peak A,

which was shown the only peak to record a statistically significant shift only, alters by $1cm^{-1}$. Discussion within the research group suggested that this degree of shift is not significant when comparing spectra recorded on multiple occasions. It was therefore concluded that the equipment could be used without significant peak shifts due to variations in theatre temperature.

Relative Peak Position	f -value
D:A	1.5417
D:B	0.3655
D:C	1.6857
C:B	0.7158
C:A	2.5333
B:A	2.7733
The critical f-value above which the null hypothesis is rejected = 4.1	

Table 13- F values for the relative positions for each of the four cyclo-hexane peaks. As all the f values were less than 4.1 the null hypothesis, that there no difference between the relative peak positions related to temperature changes, was accepted.

3.7. Experiment 6 - Maintaining Sterility.

One of the significant concerns of the surgeons involved with this study was the need to maintain sterility particularly if the device was to be used in an intra-operative setting. This is of course vital to ensure there is no cross contamination from one lymph node to the next as this could lead to false results. Further to this it is anticipated that in the long term the device will be held by the operating surgeon possibly with the node *in situ*. It must therefore also remain sterile to prevent cross contamination of the operative field.

3.7.1. Experiment 6 – Methods.

To meet the requirement for sterility a sterile sheath that is designed for use with a hand held ultrasound probe was identified. The JAD01 ultrasound cover (Jade Medical, RG8 9EX, UK) was used as it was readily available and due its primary purpose had a design that was easily adapted for the Raman probe. It is made of latex free polyurethane and measures 6 x 33 inches (Figure 62).

The sheath was placed over the whole Raman probe and secured in place with sterile rubber bands that are supplied in each pack. The light eliminator was then placed over the top of this. Any material being measured is only in contact with the sterile sheath. An added advantage of mounting the sheath in this way was that small nodes could be placed over the aperture of the inverted probe spacer without risk of them falling though into the space above the probe tip.

Figure 62- The JAD01 sterile sheath used in experiment 6.

Spectra (made up of 16 x 1sec. acquisitions) were obtained from a standard block of PTFE using the B&W Tek MiniRam II within a laser laboratory. The first ten spectra were obtained under standard conditions and the second 10 spectra were obtained with the sterile sheath in place (Figure 63). Data were transferred to a standard desk top PC and interpreted using Matlab® software. ANOVA statistical analysis was then performed to assess the positions of the 4 most prominent peaks in the PTFE spectra.

A further study was set up to ensure that there was no variation between the use of different sheaths as it was envisaged that a separate sheath would be used for each patient. 5 spectra were acquired from the same standard block of PTFE with the sheath in place. This was repeated with 10 different sterile sheaths from two different batches. Data interpretation took place using Matlab® software.

3.7.2. Experiment 6 – Results.

Analysis of the data from the first part of the study, using ANOVA, revealed no statistically significant shift in the PTFE peaks. There were no additional peaks present in the spectra obtained whilst using the sterile sheath. Similarly analysis of the 50 spectra collected in the second part of the experiment revealed that there was no significant shift in the position or intensity of the 4 most prominent PTFE peaks (labelled A, B, C, and D in Figure 63). Further there was no additional peaks evident for any of the 10 different sheaths used.

It was thus concluded that the sterile sheath had little or no effect on the spectra collected. It would therefore be used throughout the intra operative work and to maintain sterility and avoid cross-contamination it would be changed after each patient.

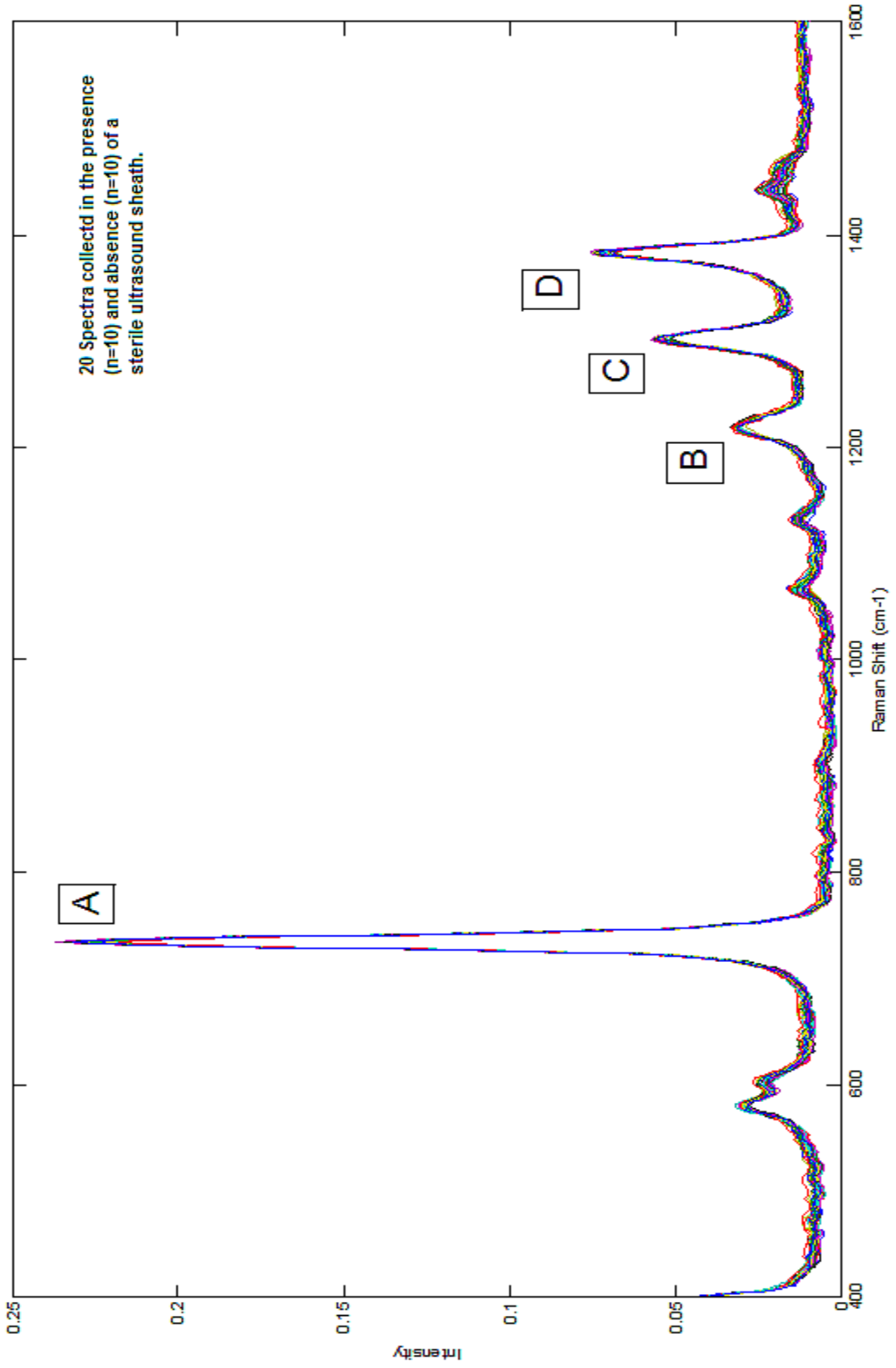

Figure 63- All spectra (n=20) of PTFE collected in the presence and absence of a sterile sheath to demonstrate the consistency of the spectra obtained. The 4 most prominent peaks of PTFE are labelled (A-D). There was no significant difference between the position or intensity of these peaks.

3.8. Experiments 7 and 8 -The effect of Patent V Blue Dye.

A critical part of the SLNB procedure is the correct identification of the axillary sentinel node. As has been described, the identification of the node involves a combination of a radio-labelled colloid and a visible dye. Locally a combination of technetium^{99m} labelled colloid and Patent V blue dye is used as per the national guidelines (Somasundaram, Chicken and Keshtgar 2007). Previous work has demonstrated that the presence of marker dyes used to orientate samples saturated the spectra obtained (Smith 2005). At that time sentinel node biopsy was not being performed routinely and the nodes used in that study had not been exposed to blue dye. Given that the use of Patent V blue dye is a standard part of the procedure it was vital to assess the effect that its presence would have on the spectra that we obtained.

3.8.1. Experiment 7 – Methods.

Samples of the Patent V Blue Dye (2.5%) (Guerbet, Roissy, France) routinely used in SLNB were obtained. There is no published data documenting the concentration of the blue dye within the axillary lymph node itself after it passes from the breast down the lymphatic channels. Clinically surgeons refer to the nodes on an analogue scale of 0-3 dependent on the degree of "blueness" of the excised node. The only previous work which estimated the concentration of dye in breast tissue reported a concentration of 0.08% of methylene blue in the tissues after injection of 0.1 ml of 1% of this dye (Hirsch et al. 1989). It is likely that the concentration of blue dye will be further diluted by the time it reaches the lymph node. Given that there was no definitive data

documenting the concentration of blue dye within the node experiments were planned that used concentrations greater than and including 0.08%.

To help determine the effect of this blue dye an experiment involving thirty 1cm^3 cubes of chicken breast (Tesco, UK) that had been dissected to mimic the size of a newly excised lymph node was set up. The 2.5% Patent V Blue Dye was diluted using Water for Injection (Baxter, Newbury, UK) to 1.25%. 0.63%, 0.31%, 0.16%, and 0.08%. Five chicken cubes were placed in a tube containing 10 mls of one of the five solutions and a further five cubes were placed in 10 mls of water for injection. These tubes were then left at room temperature for a period of 24 hours. At the end of this period the chicken cubes were removed from the tubes and placed on a new Petri dish.

9 spectra were obtained from each of the 30 chicken cubes using the same technique as for axillary lymph nodes described in Chapter 4. The spectra were then transferred to a desktop PC and interpreted using Matlab® software. Principal component analysis and ANOVA was used to assess the differences between the different blue dye concentrations and the controls. An unpaired t-test was used to determine the statistical significance of the differences in the PC scores between the groups.

3.8.2. Experiment 7 - Results.

A total of 270 spectra were included in data interpretation. The mean spectra (n=45) for the different concentrations of blue dye were calculated and compared to spectra of blue dye previously published (Stropp et al. 2003) (Figure 64). Analysis of this spectrum,

obtained with an excitation wavelength of 514.5nm using surface enhanced Raman spectroscopy techniques, revealed significant peaks at 1210 cm^{-1}, 1432 cm^{-1} and 1620 cm^{-1}. Similar peaks were observed in the spectra recorded from the chicken samples that had been prepared in Patent V blue dye (Figure 64). Analysis of the spectra obtained from the controls without the presence of blue dye was characteristic of that from chicken breast with three evident peaks at 1328, 1455 and 1660 cm^{-1} (Beattie et al. 2006; Beattie et al. 2007) .

Following principle component analysis statistical testing using ANOVA calculations revealed that the first principal component was the most significant at differentiating between those spectra obtained in the presence of blue dye and those without (f value >1700). The scores obtained for the first principal component were plotted and showed a clear difference between the two groups (Figure 65). This was confirmed with statistical analysis (Table 14).

Mean value (and SD and SEM) of the score for PC1 (all blue dye concentrations) (n=225)	Mean Value (and SD and SEM) of the score for PC1 (all controls) (n=45)	p Value
-0.0359 (0.0121, 0.0008)	0.1673 (0.015, 0.0022)	<0.0001

Table 14: The mean value for the score of PC1 in experiment 7 in samples exposed to blue dye v controls. The difference was highly statistically significant using an unpaired t-test. .

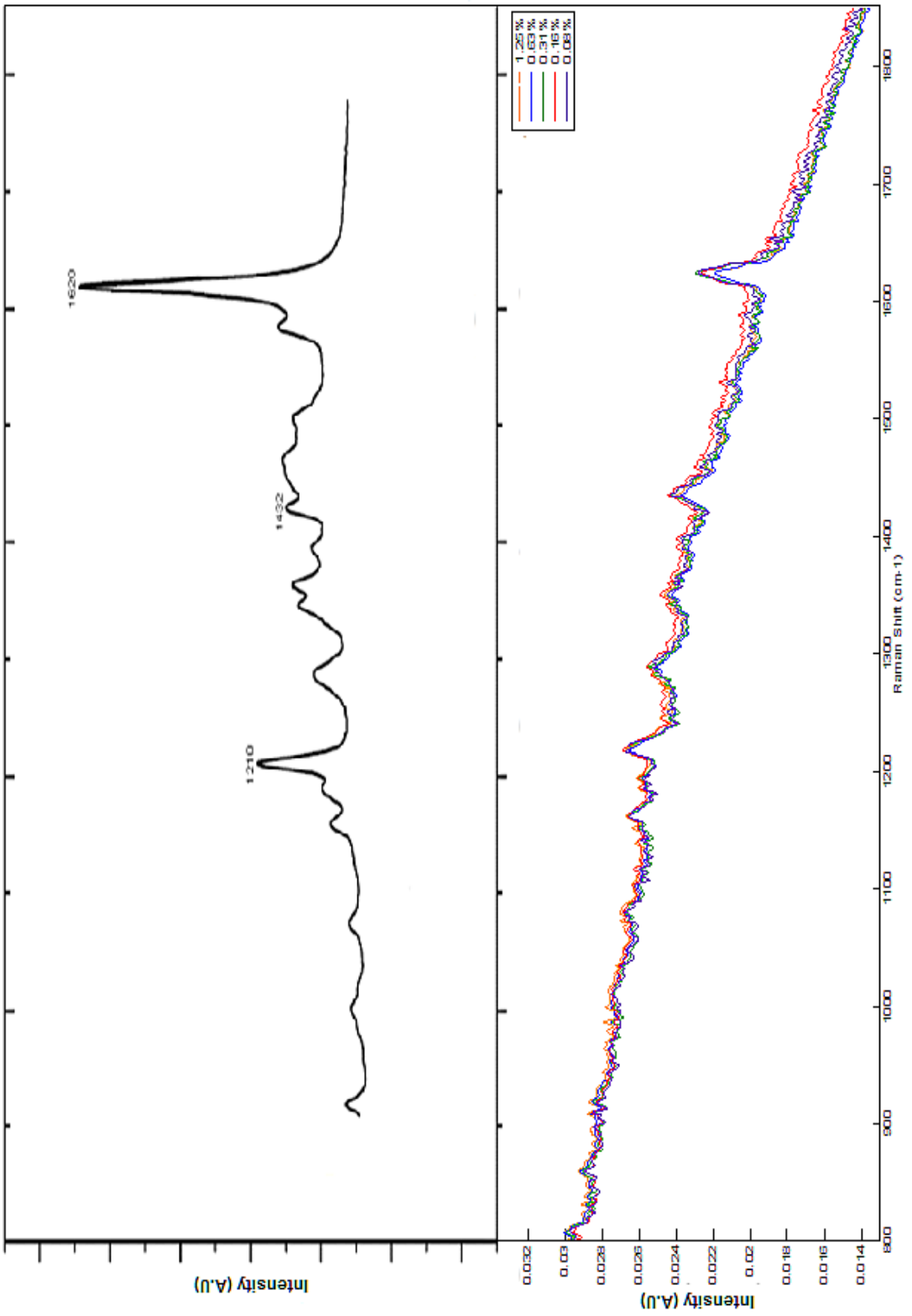

Figure 64- Mean spectra (n=45) obtained from 1 mm^3 chicken breast after 24hours in 5 concentrations of Patent V blue dye (right) compared to published spectra for patent V blue dye (left) (Stropp et al. 2003).

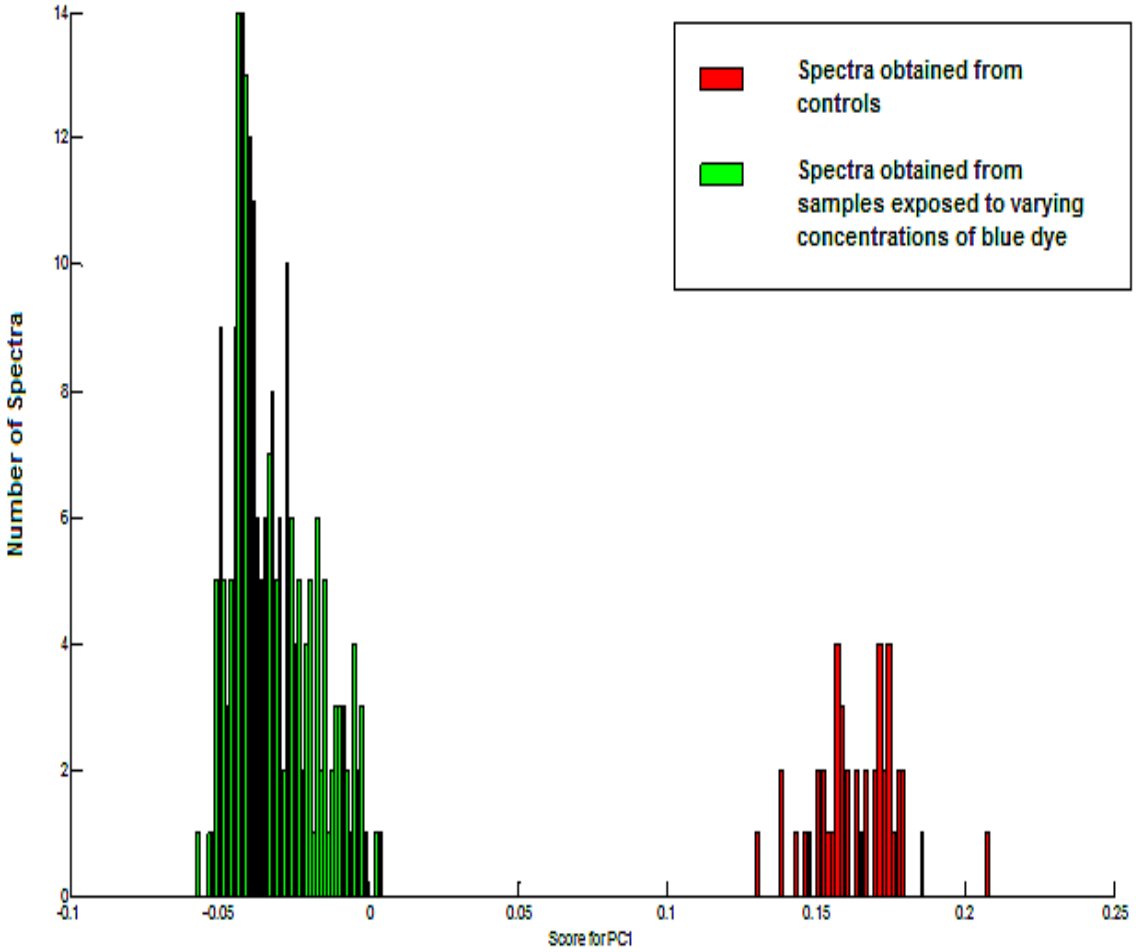

Figure 65- Histogram plotting the score for PC1 for all spectra (n=270) in experiment 7. This demonstrates the clear separation of the scores for PC1 between the controls (red, n=45) and those exposed to blue dye (green, n=225).

Analysis of the load associated with this principal component was very similar to that obtained from the control chicken cubes (Figure 66). This data suggested that all the spectra obtained in the presence of the blue dye were representative of the dye alone and this masked the spectral features of the underlying chicken breast. This would have a hugely detrimental effect on the proposed study as in the presence of blue dye the underlying spectral features of the tissue might be lost and any spectral differences seen in the tissue itself would be difficult to appreciate.

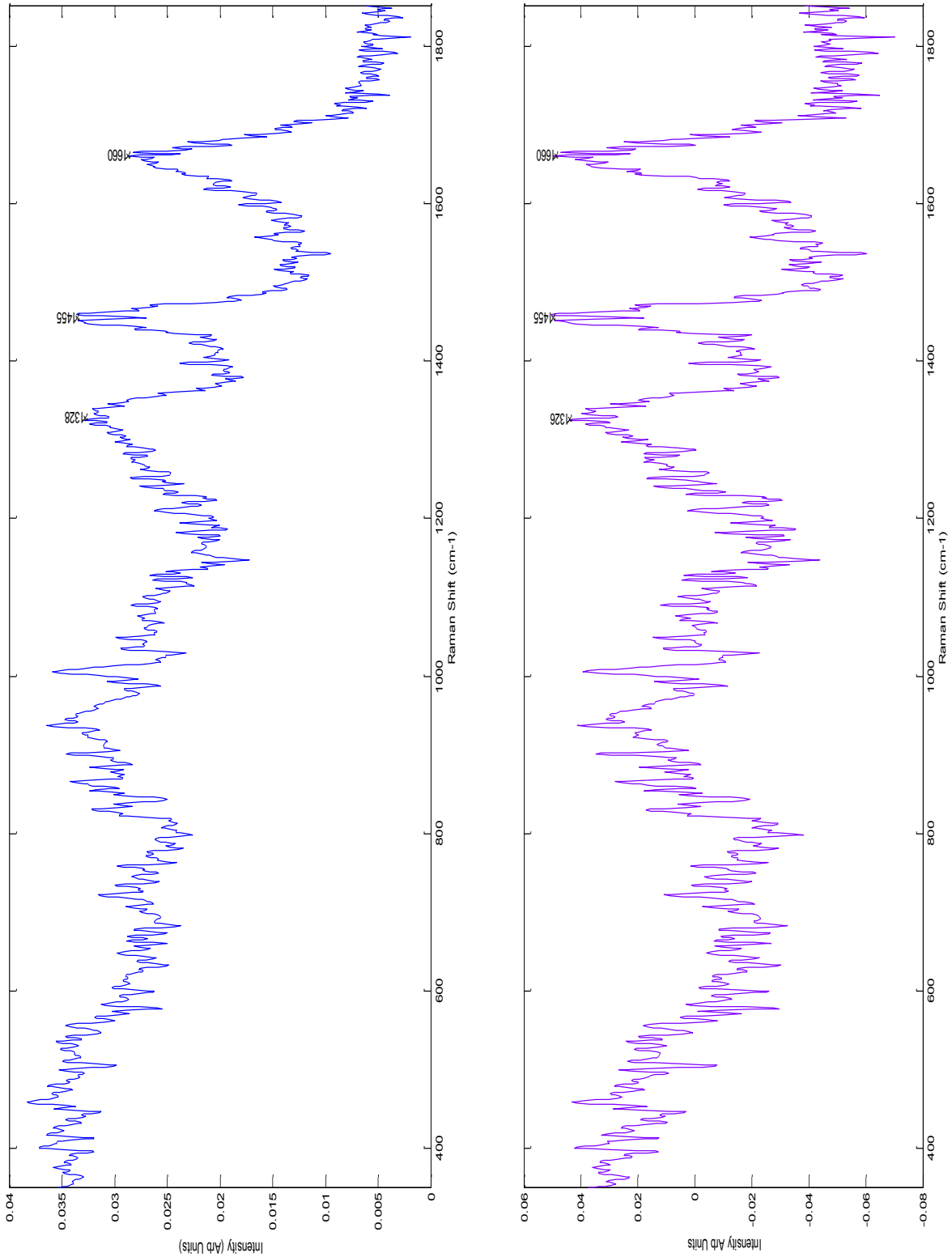

Figure 66 Mean spectra for controls (n=45) (blue) and plot of the load for principal component 1 in experiment 7.

These data cast significant doubt on the validity of Raman spectroscopy at differentiating between abnormal and normal lymph nodes in the presence of blue dye. However the method of preparation of the tissue in this experiment is very different to the processes which would transport the blue dye to the lymph node in vivo. It may be that the spectral features related to the blue dye on the surface of the chicken specimens rather than that which had diffused into the chicken tissue itself. This situation would not occur in the lymph node where the blue dye will arrive via the lymphatic system and then percolate its way through the node.

3.8.3. Experiment 8 – Methods.

Further studies to investigate this effect were evidently required. The results of the feasibility study were therefore reviewed to assess the affect of the patent V blue dye used (further details of the methodology of collecting and assessing the lymph nodes are contained in Chapter 3.4). In the feasibility study 11 nodes had been acquired during a sentinel lymph node biopsy and 27 had been collected during an axillary dissection. As part of the standard SLNB procedure the "blueness" of the node is recorded after it is excised from the patient. All the nodes in the feasibility dataset were rated on an analogue scale of 0 to 3 by the lead surgeon at the time of surgery (0 = no blue, 1 = faint blue, 2 = moderate blue and 3 = strong blue). It was therefore possible to create a dataset that included nodes that had no exposure to blue dye at all and those with visually increasing concentrations of blue dye (Table 15). In addition to this 60 spectra were obtained, by the same methodology, from standard samples of 2.5% Patent V blue dye (Guerbet, Roissy, France). All the spectra were assessed using Matlab® software.

Principal component analysis was performed along with ANOVA statistical testing to determine which of the principal components was statistically most significant at differentiating between the groups. The statistical significance of the difference in the mean scores for this PC was then confirmed using an unpaired t-test.

Blueness of Node	Number of Nodes	Number of Spectra
0	27	2448
1	4	394
2	3	291
3	4	391

Table 15- Numbers of nodes and total spectra in each group in experiment 8 (blueness measured at the time of surgery by the operating surgeon; 0 = no blue on visual inspection or not exposed to it, 1 = faint blue, 2 = moderate blue and 3 = strong blue) .

3.8.4. Experiment 8 – Results.

A total of 3584 spectra were included in the dataset. Principal component analysis was performed on the dataset to identify the principal component that was associated with blue dye. The statistical significance of each of the PCs in differentiating between the four different node groups and the blue dye was determined using ANOVA statistical calculations. Principal component 2 was the most statistically significant with an f value

of 2103. The plot of this PC closely resembled the mean spectra of Patent V blue dye with peaks at 1165,1219,1288 and 1610cm^{-1} being present in both plots (Figure 67). Examination of the mean scores for each group supports PC2 as the PC associated with the blue dye. This is firstly because the mean score for the pure dye spectrum is very positive and secondly that the mean score increases as the "blueness" of the nodes increases (Figure 68) (Table 16). The differences between the mean scores were then assessed using an unpaired t-test (Table 17).

Group	*Total Number of Spectra*	*Mean score for PC2 (standard deviation and standard error of the mean)*
Blue dye score 0	2448	-0.0070 (0.015,0.0003)
Blue dye score 1	394	-0.0083 (0.014, 0.0007)
Blue dye score 2	291	-0.0054 (0.01, 0.0006)
Blue dye score 3	391	0.0004 (0.006,0.0003)
Patent V blue dye 2.5%	60	0.14 (0.0008, 0.0001)

Table 16 - Mean value for the score of PC2 in the 5 groups in experiment 8. Standard deviation and standard error of the mean are also shown (blueness measured at the time of surgery by the operating surgeon ; 0 = no blue or not exposed to blue dye, 1 = faint blue, 2 = moderate blue and 3 = strong blue).

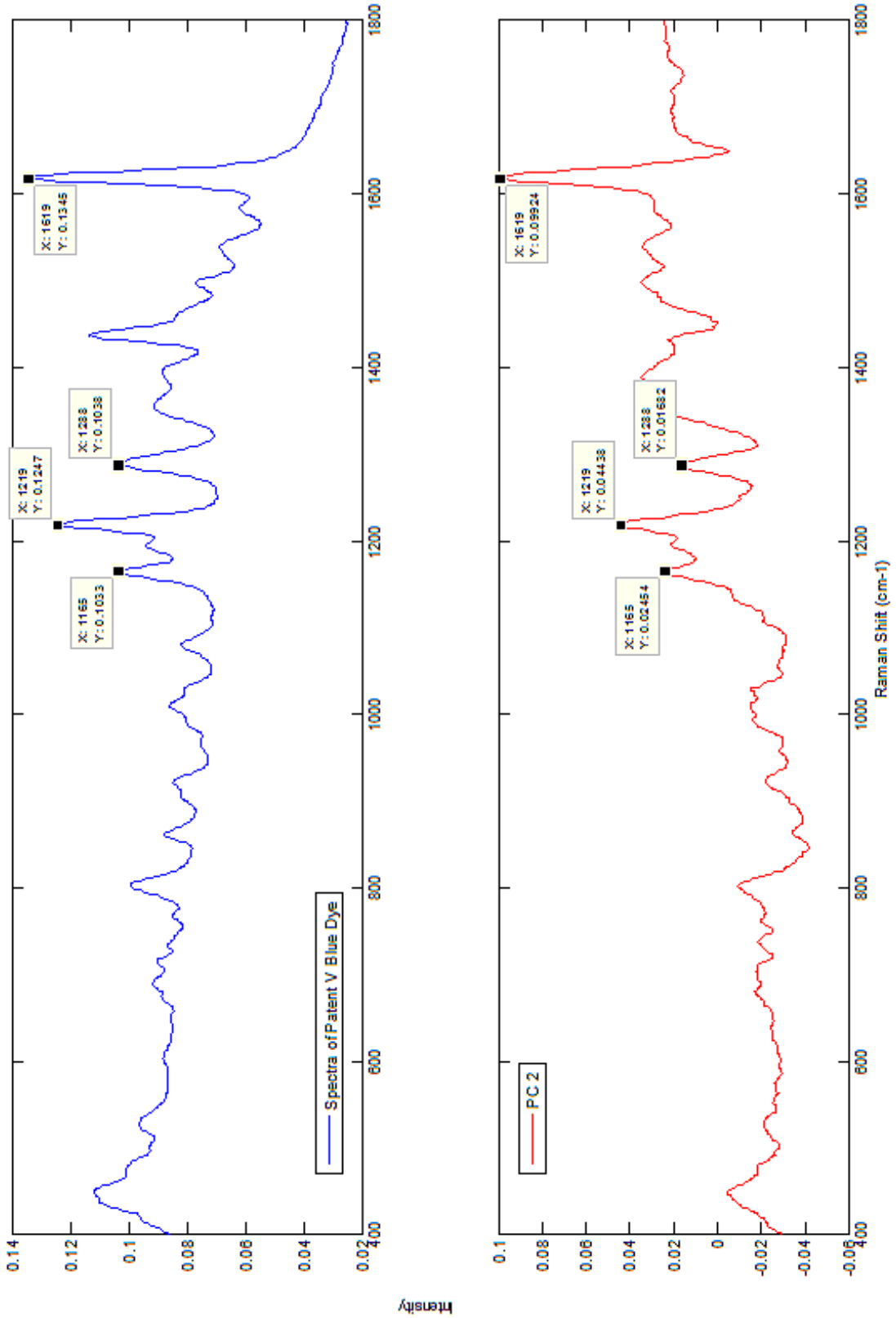

Figure 67- Mean spectra (blue, left) of Patent V blue dye (n=60) and the load of PC2 (red, right) in experiment 8 with the distinct similarities between the two highlighted.

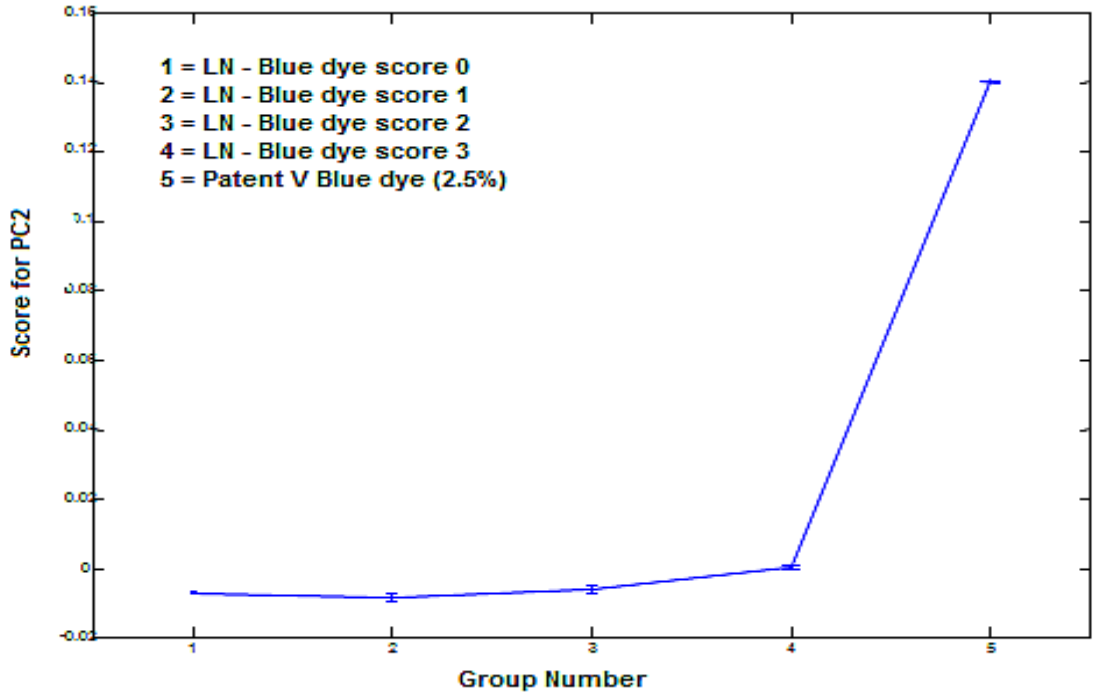

Figure 68- Mean score with standard error bars for PC2 in experiment 8 in the five separate groups across the range of blueness (blueness measured at the time of surgery by the operating surgeon ; 0 = no blue (or not exposed to blue), 1 = faint blue, 2 = moderate blue and 3 = strong blue)(for numbers in each group see table 15).

Groups being compared	*P value (unpaired t-test)*
0 v 1	0.107
0 v 2	0.076
0 v 3	p<0.001
0 v 4	p<0.001
1 v 2	0.002
1 v 3	p<0.001
1 v 4	p<0.001
2 v 3	p<0.001
2 v 4	p<0.001
3 v 4	p<0.001

Table 17: Statistical significance of the differences in the mean value for the scores of PC2 between each group using an unpaired t-test in experiment 8. (Group 0 = No dye, group 1= faint blue, 2=moderate blue, 3 = strong blue and 4=Patent V blue dye 2.5%).

None of the loads for the other principal components appeared to have peaks suggestive of blue dye. Further they were neither as statistically significant using ANOVA analysis or displayed the same change in mean score as was demonstrated for PC2. This principal component was thus deemed to most closely represent the contribution of blue dye.

To assess the effect of this component on the ability of the system to differentiate between the different pathologies PCA fed LDA was performed both in the presence of and in the absence of this PC. When PC fed LDA was calculated for all the scores trained on gold standard histopathology results the sensitivity and specificity of the Raman system at differentiating between cancer and normal tissue was 95.7% and 98.9% respectively as discussed previously. When the same calculation was performed using all the scores except for that from PC 2 the sensitivity and specificity remained virtually unchanged at 95.1% and 99.6%.

Given these results it was felt, despite the results of experiment 7, that the presence of blue dye of varying concentrations would have little effect on the spectra obtained. Indeed further it does not significantly adversely affect the ability to differentiate between normal and metastatic lymph nodes.

4. Intraoperative Analysis of Axillary Lymph Nodes

Having demonstrated that the Mini Ram II could be used within the operating theatre context to differentiate between positive and negative nodes the next phase of the project moved onto using the equipment within the operating theatre, on freshly excised tissue, in real time. Prior to embarking on this phase both ethical and laser safety approval needed to be achieved.

Ethical approval was granted by the Gloucestershire Local Ethics Committee (approval code 01/158G – "The Development of Raman Spectroscopy in the Diagnosis of Breast Cancer"). Patients were eligible for inclusion in the study if they had a diagnosis of breast cancer and were undergoing lymphatic surgery as part of the management of this condition. Patients were excluded from the study if they were unable to give informed consent. A leaflet explaining the nature of the study was distributed to eligible patients at the time of their pre-admission clinic. Consent forms were signed by all patients who agreed to take part in the study prior to the operative procedure. As involvement in the study did not change patient management in any way recruitment was fairly straightforward and well received by patients.

To satisfy laser safety requirements the portable Mini Ram II system was used in a room situated next to the operating theatre. This room was chosen as it was both windowless and had a lockable door. It was deemed that despite the relative safety of the laser within the spectrometer this location would further mitigate against potential risk. Whilst in the future it is hoped that the tissue will be assessed and thus remain in

the operating theatre it was felt that this was a suitable interim step during the evolution of the technique.

4.1. Materials and Methods

Axillary lymph nodes were analysed in the study from patients who were undergoing either a sentinel lymph node biopsy (SLNB) or an axillary clearance. Samples were obtained from a total of 72 operative procedures (57 SLNB and 15 axillary clearances). 6 patients had nodes assessed during both an initial SLNB and a subsequent axillary clearance. Thus 66 individual patients were included in this phase of the study. Of these, 55 (83%) had an invasive ductal carcinoma of the breast, 6 had lobular carcinoma, 2 had mucinous tumours, 1 had a tubular adenocarcinoma, 1 had a metaplastic tumour and 1 was having a SLNB because of extensive DCIS. Of the 55 patients with invasive ductal carcinoma 23 (42%) had grade III disease, 27 (49%) had grade II disease and 5 (9%) had grade I disease. These numbers were broadly consistent with the UK population as discussed in Chapter 1.

19 (29%) patients included in the study had lymph nodes positive for either macrometastases (n=13) or micrometastases (n=6). 15 of these patients had their positive nodes discovered following SLNB and 4 had received preoperative diagnosis following an USS and core biopsy. A total of 176 axillary lymph nodes were assessed during the 72 operative procedures. To minimise the risk of nodes being assigned to the wrong patient all analysis was performed before another patient entered theatre. Prior to spectral analysis nodes were cleared of surrounding fat and cut into two equal halves. If

the node was too small for this to be done easily then the node was measured as a whole node. This occurred in 13 cases and in all cases the maximum diameter of the node was 5 mm. As a result 339 samples were assessed. All samples were assessed post operatively by standard histopathological protocols. Nodes sampled during SLNB were cut at 2 mm intervals and underwent H and E and immuno histochemistry staining. Nodes sampled during axillary clearance were cut in two planes and exposed to H and E staining only. Histopathology classification was provided for each separate node sample.

In the clinical context of deciding further treatment for each patient included in the study the node was assessed based on the results from both halves of the node. Thus the overall status of a node with a macrometastases in only one half was macro metastasis positive. However within the context of this study the results from each separate node half were used.

Of the 176 nodes assessed, 139 were defined as negative on histological examination, 18 were positive for macrometastases, 5 were positive for micrometastases, 8 were positive for ITCs and 6 samples were reported as having no lymphoid tissue present within the sample (Table 18). When the node halves were examined, 276 were negative, 32 were positive for macrometastases, 8 were positive for micro metastasis, 10 were positive for ITCs and 13 had no evidence of lymphoid tissue present (Table 18). The negative halves were further sub-divided into 160 that were from patients who had no other positive nodes, N_0 patients, or 116 that were from patients who had at least one other positive node.

	Number of Nodes	Number of separate tissue samples (*either halve a node or a whole small node)*
Negative	139	276
Positive – Macro	18	32
Positive – Micro	5	8
ITCs	8	10
Non Lymphoid	6	13

Table 18- The number of samples and nodes in each classification group. The whole nodes were classified according to their highest group (i.e. a node which had a macrometastases in one halve and an ITC in the other half was classified as a macrometastases) and the halve node samples were classified according to their halve only. The majority of nodes were divided into two halves. However due to their small size 13 nodes were assessed as a whole.

4.1.1. Spectral Acquisition.

After excision and preparation each node was placed on the upturned probe. Prior to assessment, a sterile sheath had been placed over the probe tip to prevent cross contamination. The node was placed in an approximately central position and spectra were obtained by combining 16 1s acquisitions. A total of 2627 spectra were collected from the 339 samples. (Mean 7.2 spectra per node, range 5-25 per sample). Once collected, spectral data was uploaded into Matlab® for spectral analysis.

Three standard spectra were collected during each session as is routine within the research group. Standard spectra were obtained from a green glass standard, cyclohexane, and a plastic pipette tip. Data was stored within a password protected database that recorded patient details, the type of tumour, hospital number, the date of surgery, the operating surgeon, the surgical procedure, the size of the node and the final pathology data.

4.1.2. Spectral Analysis.

Spectra were collected from the lymph node samples at the time of surgery as described previously. No spectra were removed during data processing as any spectra that were either saturated or contained cosmic rays were identified and removed during collection.

Each spectrum was subjected to a stepwise sequence of processing. Initially all raw spectra (Figure 69) were corrected for peak position and intensity. This was performed using in house Matlab® functions and based on the calibration standards that were recorded at the start of each session (Figure 70). Peak position calibration was first performed based on the peak positions of the four highest intensity Cyclohexane peaks. The Matlab® programme used cropped the spectra to 400-1800cm^{-1}. The resulting spectra were then intensity corrected based on the spectra recorded from the green glass standard.

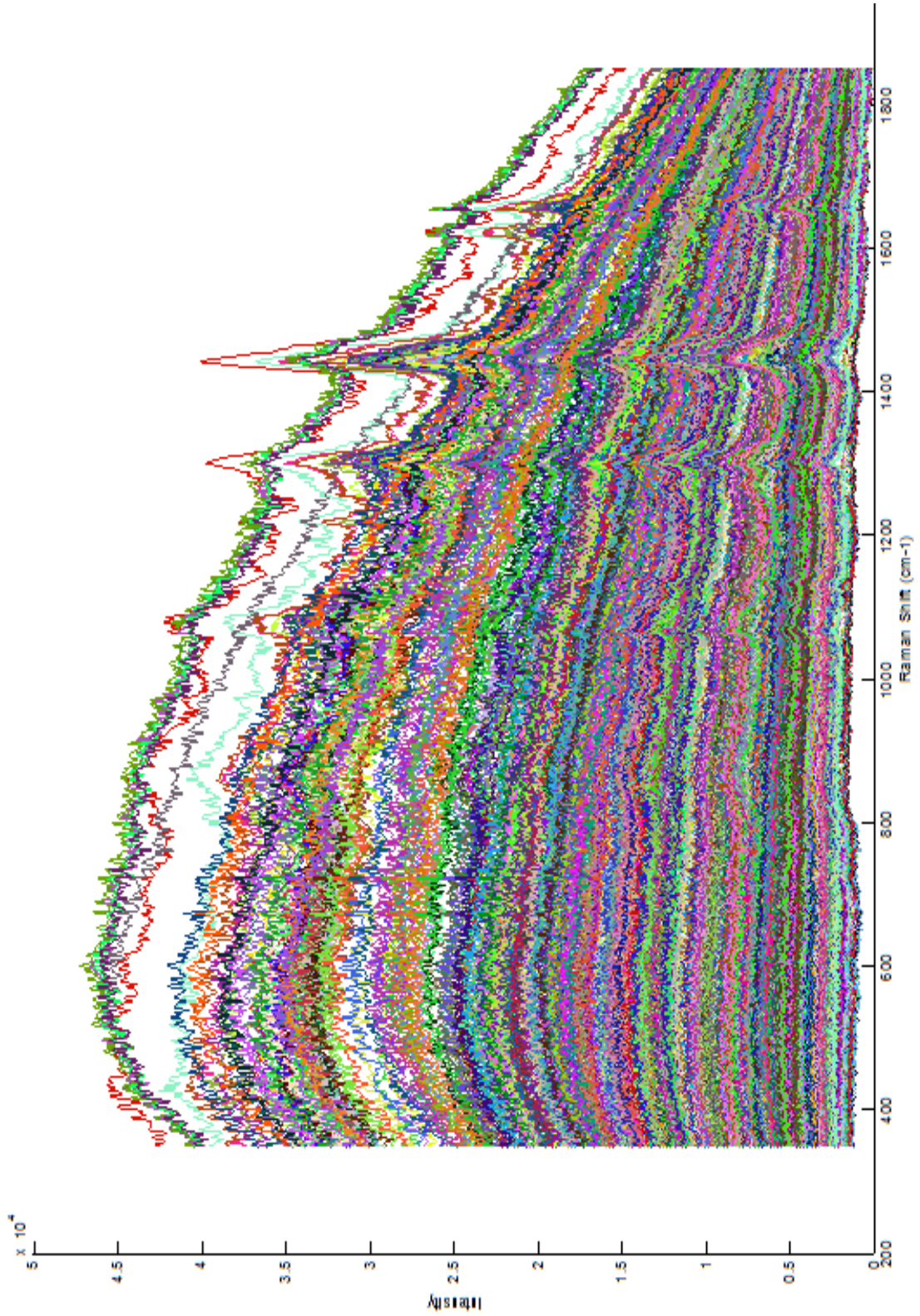

Figure 69 – Raw spectra collected from all lymph node samples in the intra-operative series (n=2627). This demonstrates the wide range of background intensity of the samples collected.

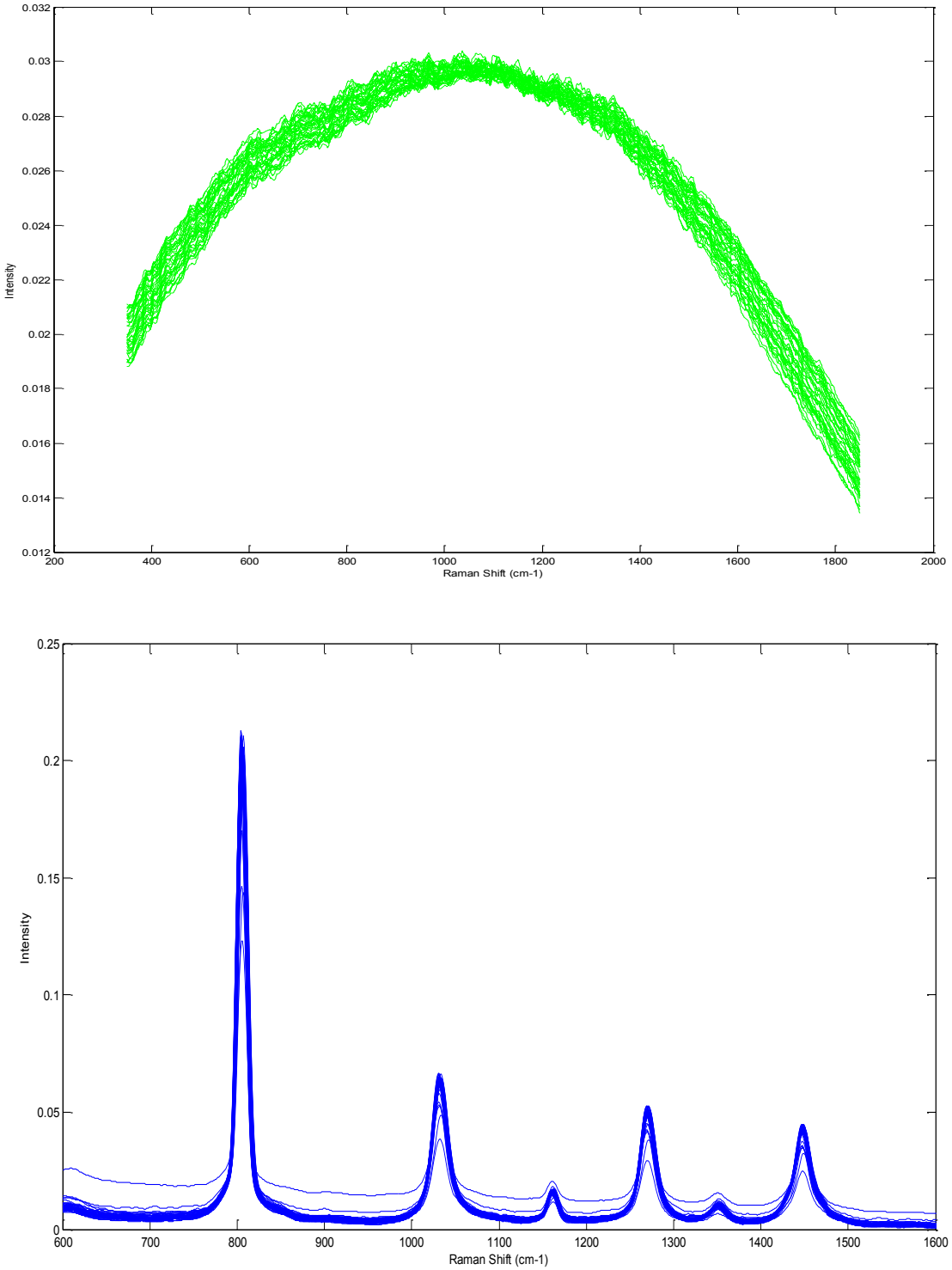

Figure 70 – Raw spectra for green glass (above) and cyclohexane (below) standards obtained in the Cheltenham series demonstrating the stability of the system over the course of the study (y axis intensity is arbitrary units).

Following these steps the spectra were baseline corrected, smoothed and finally normalised using in house and self programmed Matlab® functions. A mean spectrum was then calculated for each of the nodes analysed (Figure 71).

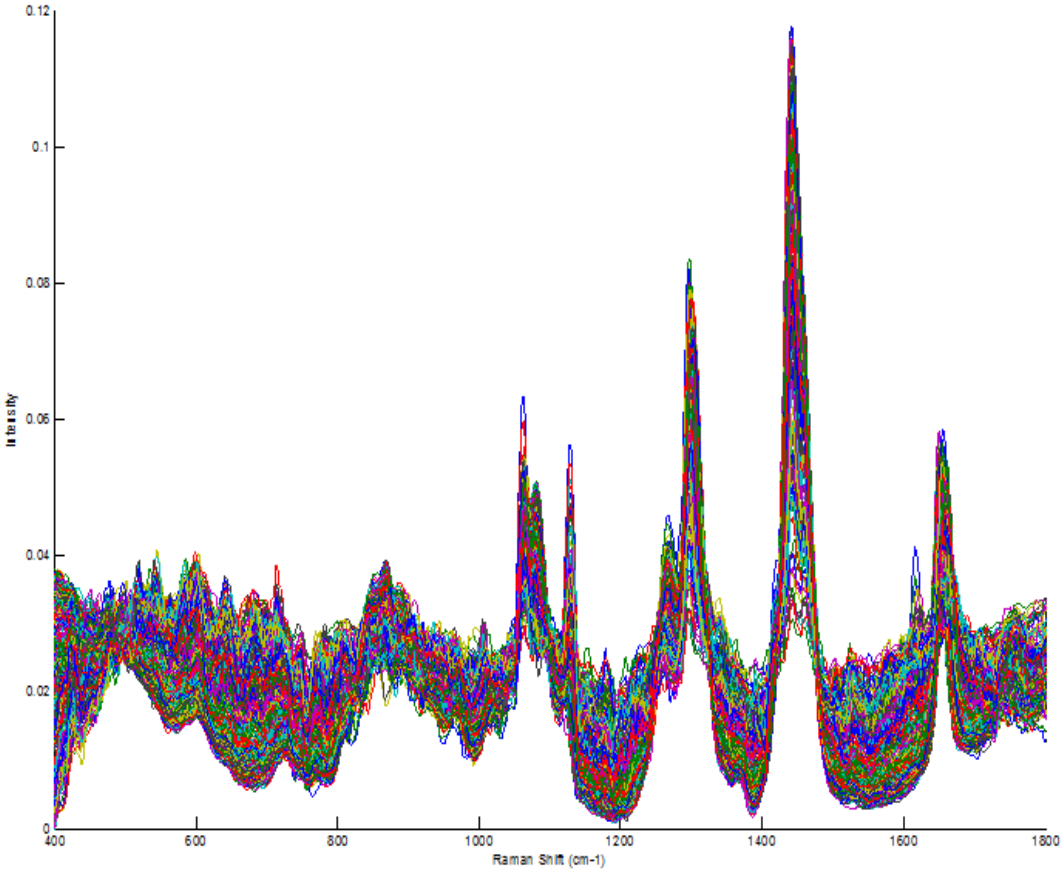

Figure 71– Mean corrected spectra for all node samples (n=339) in the intra-operative study.

Using this methodology a dataset that pertained to the 339 samples was created that had been corrected in a uniform and consistent way. This dataset was organised so that it could easily be manipulated based on individual patients, node pathology or date of spectral acquisition. This was referred to the "overall dataset" and separate pathology subgroups and sub-datasets were created from it.

4.2. Results - Dataset 1: Macrometastases v. Negative N_0 Nodes.

Of the five pathology groups identified from the histopathology results the two with the greatest histopathological differences were the groups that were identified as containing macrometastases (n=32) and the group that were defined as negative nodes from N_0 patients (n=160). It was anticipated that the spectral differences between these groups would be the most significant. Initial comparison of the spectra for these two subgroups was performed after calculating the mean spectra for each one (Figure 72).

Significant areas of difference were evident simply on inspection of the mean spectra and this was emphasised by plotting the mean spectra with 95% confidence intervals either side of the mean value for each wavenumber (Figure 72, 73). This change was enhanced when we subtracted the mean positive spectra from the mean negative spectra. A plot of the result of this manipulation for each wavenumber gave further clarity to the distinct differences (Figure 74). Those peaks that remained positive were representative of increased relative concentrations within the N_0 node subgroup and those peaks that were negative indicated increased relative concentration within the macrometastases subgroup of nodes.

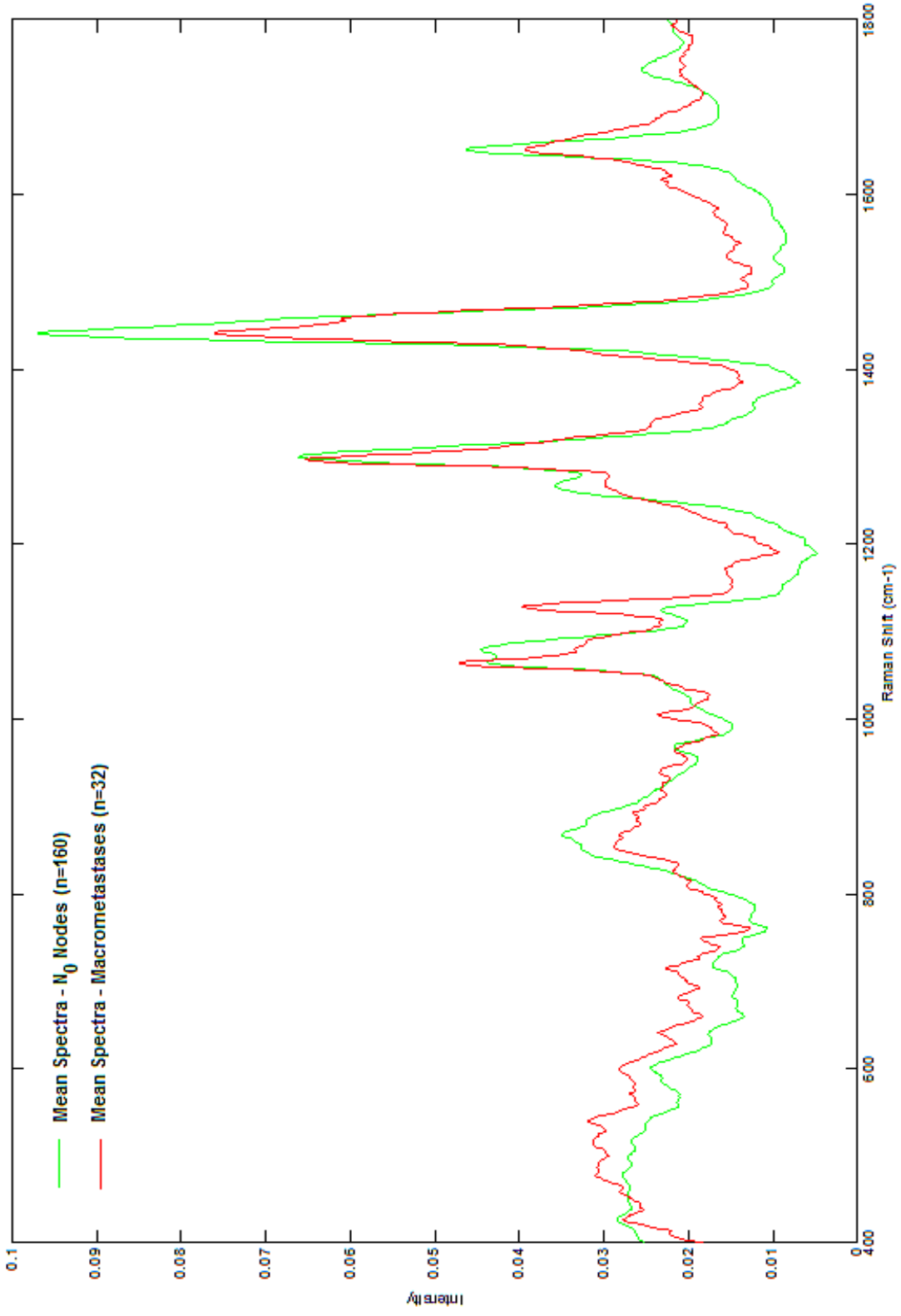

Figure 72 – Mean spectra of N_O Nodes (green, n=160) and macrometastases (red, n=32) in the intra-operative study.

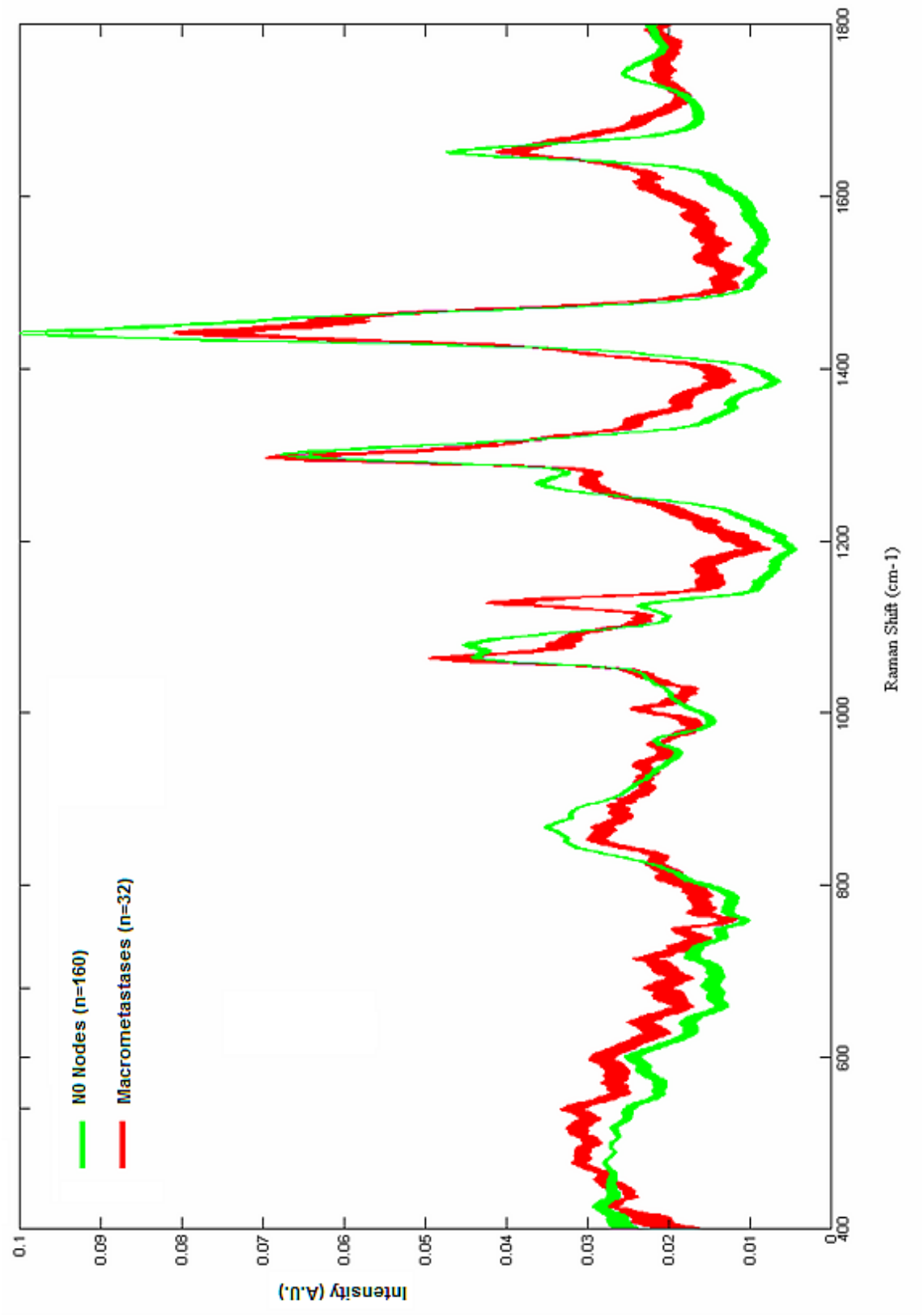

Figure 73 – Mean spectra of N_0 Nodes (green, n=160) and macrometastases (red, n=32) with 95% confidence intervals in the intra operative study.

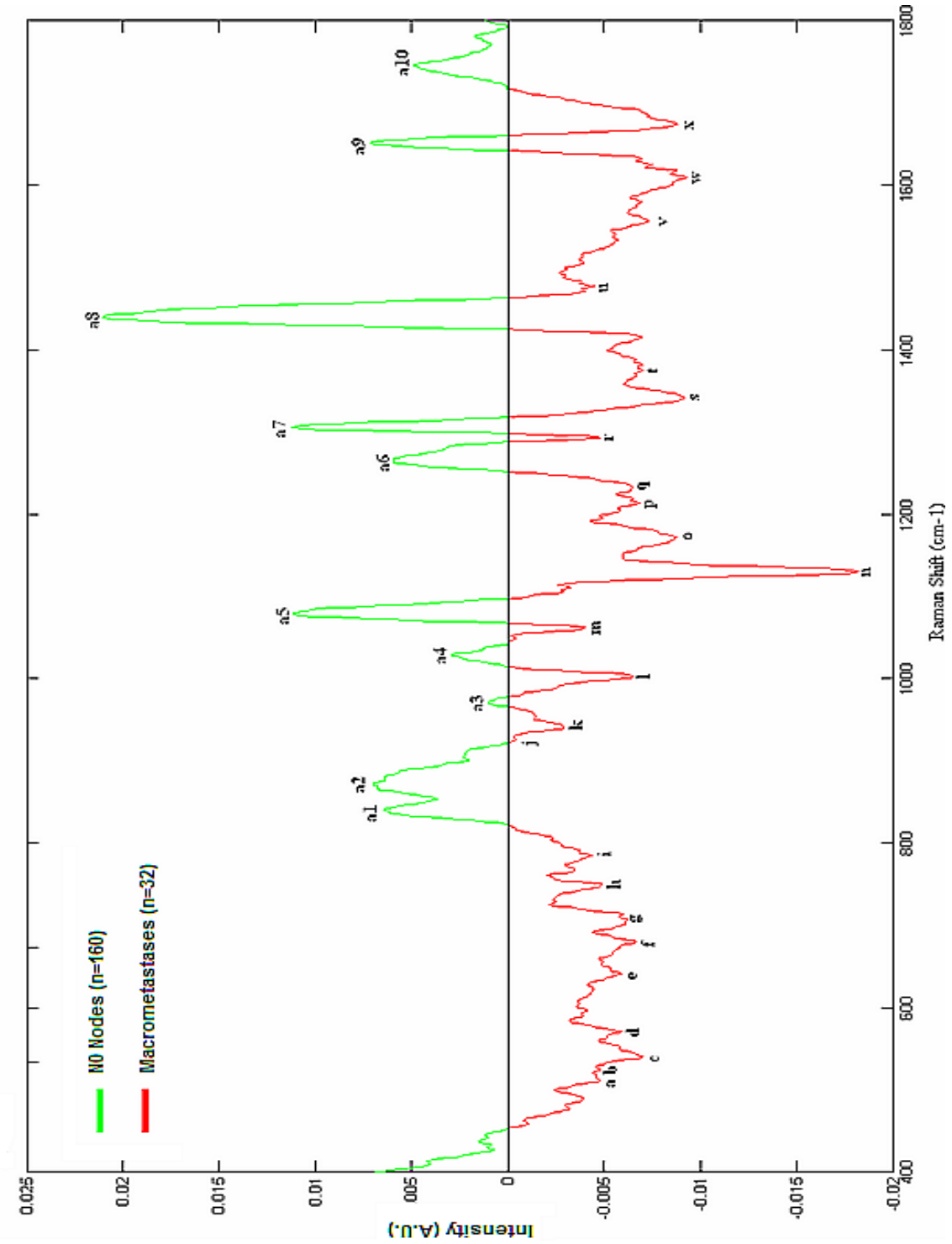

Figure 74 – Plot of spectral subtraction to demonstrate key areas of spectral differences between N_0 Nodes (n=160) and macrometastases positive nodes (n=32) in the intraoperative study . Where the plot is green the peaks are more prominent in the N_0 spectra and where the plot is red the peaks are more prominent in macrometastases spectra. Labelled peaks are discussed further in table 19.

Examination of the plots of the subtracted differences enabled us to identify the wavenumbers associated with each of the positive and negative peaks. Peak labelling and assignation was performed using Matlab® programmes and compiled tables of peak assignments held within the department (Kendall 2002). In this way a total of 34 peaks that appeared significant were labelled and their biochemical association recorded (Table 14).

Peak Label in Fig. 79	Peak Position (cm^{-1})	Biochemical assignation	Mean peak intensity N_0 nodes (SD and SEM)	Mean peak intensity macrometastases (SD and SEM)	t Value	p Value
a	510	Disulphide	0.026 (0.002, 0.00016)	0.031 (0.0021, 0.0007)	12.8	p<0.0001
b	525	Disulphide	0.026 (0.003, 0.00026)	0.030 (0.0032,0.0006)	6.3	<0.0001
c	540	Disulphide	0.025 (0.005, 0.0004)	0.032 (0.0039,0.0007)	7.5	p<0.0001
d	571	Trytophan	0.021 (0.006, 0.0004)	0.027 (0.0038, 0.0007)	5.7	p<0.0001
e	642	Tyrosine	0.018 (0.008, 0.0006)	0.023 (0.0042, 0.0007)	3.5	p=0.0007
f	681	Guanine	0.015 (0.008, 0.0006)	0.021 (0.005, 0.0009)	4.1	p<0.0001

g	710	Adenine	0.016 (0.007, 0.0004)	0.021 (0.004, 0.0007)	4.8	p<0.0001
h	749	Thiamine	0.014 (0.0055, 0.0004)	0.018 (0.0028,0.0005)	4.01	p<0.0001
i	787	Cysteine	0.012 (0.006, 0.0005)	0.016 (0.0032, 0.0006)	3.78	p=0.0002
A1	840	Glucose	0.030 (0.0024,0.0002)	0.023 (0.0026,0.0005)	14.9	p<0.0001
A2	876	C-C Stretch	0.033 (0.003, 0.0002)	0.026 (0.0033, 0.0005)	11	p<0.0001
j	926	DNA	0.023 (0.0026,0.0002)	0.023 (0.0024, 0.0004)	0	p=1
k	941	C-C (protein)	0.020 (0.0033, 0.0003)	0.023 (0.0026, 0.0005)	4.9	p<0.0001
A3	971	=C-H	0.021 (0.0023, 0.0002)	0.020 (0.0024,0.0004)	2.6	p=0.01
l	1004	Phenylalanine	0.017 (0.004,0.0003)	0.023 (0.0026, 0.005)	8.1	p<0.0001
A4	1029	Proline	0.020 (0.002, 0.0002)	0.017 (0.0016, 0.0002)	8.0	p<0.0001

m	1062	?DNA ?Lipid	0.042 (0.004,0.0003)	0.046 (0.0053,0.0009)	4.8	p<0.0001
A5	1079	C-C Stretch Lipid	0.044 (0.007, 0.0005)	0.033 (0.0054, 0.0009)	8.4	p<0.0001
n	1130	C-N protein	0.021 (0.007, 0.0005)	0.038 (0.009, 0.0002)	12.1	p<0.0001
o	1172	C-O stretch/ Tyrosine	0.007 (0.005,0.0004)	0.016 (0.004, 0.0007)	9.5	p<0.0001
p	1205-1213	Thiamine/ Tyrosine/ Phenylalanine	0.006 (0.005,0.0004)	0.012 (0.004,0.0007)	6.4	p<0.0001
Q	1231	Amide III	0.012 (0.005, 0.0004)	0.018 (0.004, 0.0007)	6.4	p<0.0001
A6	1263	Lipid (=C-H)	0.034 (0.004, 0.0003)	0.029 (0.003, 0.0005)	6.7	p<0.0001
R	1293	Amide III	0.055 (0.007, 0.0005)	0.059 (0.009, 0.0002)	2.8	p<0.0001
A7	1306	Lipids	0.060 (0.012, 0.0009)	0.049 (0.007, 0.001)	5.0	p<0.0001
S	1348	Nucleic Acid/ Tyrptophan/ Adenine	0.014 (0.005, 0.0004)	0.022 (0.004, 0.0007)	8.5	p<0.0001

T	1376-1397	Thymine/ adenine/ guanine	0.010 (0.005,0.0004)	0.017 (0.003, 0.0005)	7.6	p<0.0001
A8	1440	Lipids	0.095 (0.022, 0.0012)	0.07 (0.013, 0.002)	6.2	p<0.0001
U	1479	Purine Bases	0.019 (0.002, 0.00016)	0.023 (0.002, 0.0004)	10.3	p<0.0001
V	1536	Tryptophan	0.009 (0.006, 0.0005)	0.015 (0.003, 0.0005)	5.5	p<0.0001
W	1609	Tyrosine	0.013 (0.006, 0.0005)	0.022 (0.004, 0.0007)	8.2	p<0.0001
A9	1652	Lipid	0.046 (0.007, 0.0005)	0.039 (0.005, 0.0009)	6.2	p<0.0001
X	1673	Amide III	0.021 (0.006, 0.0005)	0.029 (0.004, 0.0007)	7.22	p<0.0001
A10	1746	C=O stretch lipid	0.025 (0.002, 0.0002)	0.020 (0.003, 0.0005)	11.7	p<0.0001

Table 19- Peak assignments of the key spectral differences highlighted by spectral subtraction and labelled in Figure 74 (Kendall 2002). The mean intensity for each of these peaks in N_0 nodes and macrometastases is also given, along with their standard deviation and standard error of the mean. The results of an unpaired t-test are also shown (both the t value and the p value) (SD=standard deviation, SEM= standard error of the mean).

To add a degree of robustness to this process and to ensure that any significant peak differences had not been missed statistical analysis of the mean intensity of each wavenumber in the two groups was performed. An unpaired t-test was performed and the degree of freedom for the analysis was calculated. The unpaired t-test was chosen as it is a statistical test that compares the mean of one variable between two groups.

A null hypothesis was defined which stated that there was no difference in the mean peak intensity between the two groups. The t value was compared to standard tables of significance to determine whether the difference between the means was unlikely to have occurred by chance alone. The level of statistical significance was set at 99%, thus if the t value was greater than the published value for this significance level with 190 degrees of freedom, 2.6, then the null hypothesis could be rejected. All but 2 of the previously identified peaks had t values which allowed us to reject the null hypothesis. The two peaks that did not achieve this were those labelled A3 and J at 971 and 926cm-1 respectively. These were then excluded from further evaluation.

The t values for each wavenumber were examined and used to identify further significant differences between the two groups. It was evident that three further wavenumbers, that had not been initially selected, recorded highly significant t values. These were found;

- below peak *a* at 488cm^{-1} (N_0 mean = 0.027 (standard deviation (SD) = 0.001, standard error of the mean (SEM) 0.0001) v. macrometastases mean 0.031 (SD = 0.001, SEM = 0.0005)).

- above peak *a2* at 889cm^{-1} (N_0 mean = 0.031 (SD = 0.002, SEM = 0.0002 v. macrometastases mean 0.026 (SD = 0.003, SEM = 0.0005)).
- above peak *t* at 1419^{cm-1} (N_0 mean = 0.025 (SD = 0.002, SEM = 0.0002) v. macrometastases mean 0.031 (SD = 0.003, SEM = 0.0005)).

The t values for these peaks were 13.7, 11.8 and 14.2 respectively. Potential peak assignments of glycogen, CH_2 rock and adenine/guanine were made based on available tables. The t values for the 32 peaks identified initially and the 3 further wavenumbers identified confirm that there are statistically significant differences between the two groups. As spectrum recorded in Raman spectroscopy is based on the molecular composition of the tissues being assessed these spectral differences can be assigned to molecular differences between the two groups.

Evaluation of the different peaks associated with each pathology subgroup suggests significant differences in the biochemical composition. Analysis demonstrated that the positive nodes had increased relative levels of protein and nucleotides in comparison to the true negative nodes. This is supported by the peaks associated with disulphide and C-N bonds (510, 525, 540 and 1130 cm^{-1}) amide III (1293 and 1673 cm^{-1}) as well as those associated with amino acids such as phenylalanine (1004 cm^{-1}), tryptophan (1348 and 1546 cm^{-1}) tyrosine (642, 1172, 1609 cm^{-1}) as well as the region 1205-1213 cm^{-1}. Peaks associated with adenine (710 and 1348 cm^{-1}), cystine (787 cm^{-1}), thiamine (749 cm^{-1}) and guanine (681 cm^{-1}) and in the region 1376-1397 cm^{-1} all support the increased intensity of DNA within metastatic nodes. Within the negative nodes peaks at 876, 1079, 1263, 1306, 1440, 1652, and 1746 cm^{-1} are associated with lipids and support the

relative increased levels of lipids within negative nodes. The peak at 840 and 894 cm^{-1} suggest that there may also be increased levels of glycogen and glucose in the normal nodes. These findings are both consistent with previous studies of lymph nodes using Raman spectroscopy and with the histological changes that occur during cancer cell metastases. In areas where metastatic cells predominant their large nuclei account for the increased levels of DNA and the decreased levels of lipid associated with normality. The increased protein levels correlate with an up regulation of the immune response due to the presence of foreign cells and the decrease in energy stores maybe accounted for by the energy requirements of rapidly replicating cancer cells that have lost their normal cell regulatory mechanisms.

These initial results confirmed that there were significant differences between the two pathological groups. Further, using peak assignment, it was demonstrated that these differences appeared to represent biochemical changes within the node. These results were consistent with previous work, presented in Chapter 2, which has shown decreased lipid and increased protein and DNA spectral contributions in malignant tissue.

4.2.1. Dataset 1- Diagnostic Tool.

4.2.1.1. Molecular Differences.

The next stage in the analysis of the data was to determine if the results could be used to differentiate between the positive (macrometastases) and the N_0 nodes. An initial model was based on the relative intensities of the lipid, protein and DNA peaks that had been

highlighted above. The combined intensity of the 9 peaks attributed to lipids, the 15 peaks related to proteins and the 10 peaks attributed to DNA were combined for each node to give a lipid, protein and DNA score. Separation of the two groups was then attempted based on each of these three values and finally the combined value of the three intensities. As it was expected that the lipid value would be higher in the negative nodes and that the protein and DNA value would be higher in the positive nodes an overall score was calculated based on the formula given below. The lipid score was subtracted from 0.5 as no node achieved a value of greater than 0.45.

Overall Score= (Protein score + DNA score) + (0.5-lipid score)

Plots of each of these composition scores highlighted the differences between the macrometastases and N_0 samples (Figure75-79). Although these compositional scores demonstrated statistically significant differences between the two pathology sub-groups, using an unpaired t-test (Table 20) (Figure 80) they were not sufficient to separate them with a sensitivity and specificity sufficient for clinical use.

It is interesting to note the negative nodes appear to separate into two further subgroups based on the protein score. It is postulated that this may reflect either a greater immune response in nodes earlier in the nodal chain or that it may represent a response to recent breast biopsies or due to isolated histopathologically undetected metastatic cells.

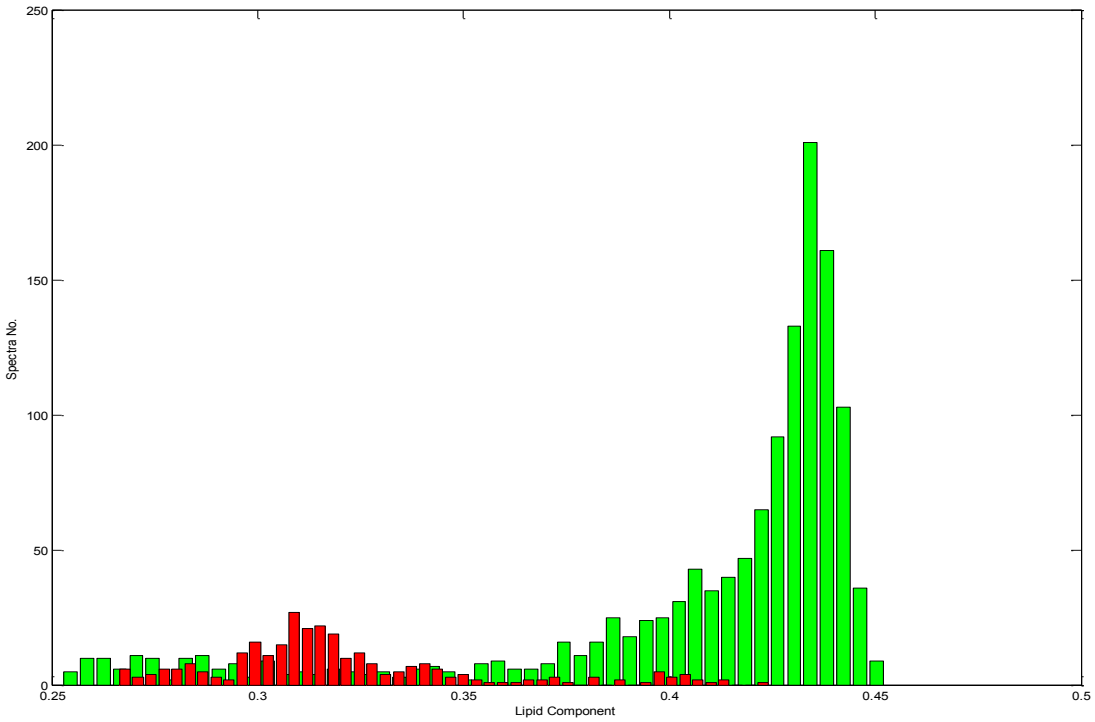

Figure 75 – Histogram demonstrating the combined intensity of all lipid related peaks for each spectra in dataset 1 (green = N_0 negative nodes, red= macrometastases positive nodes).

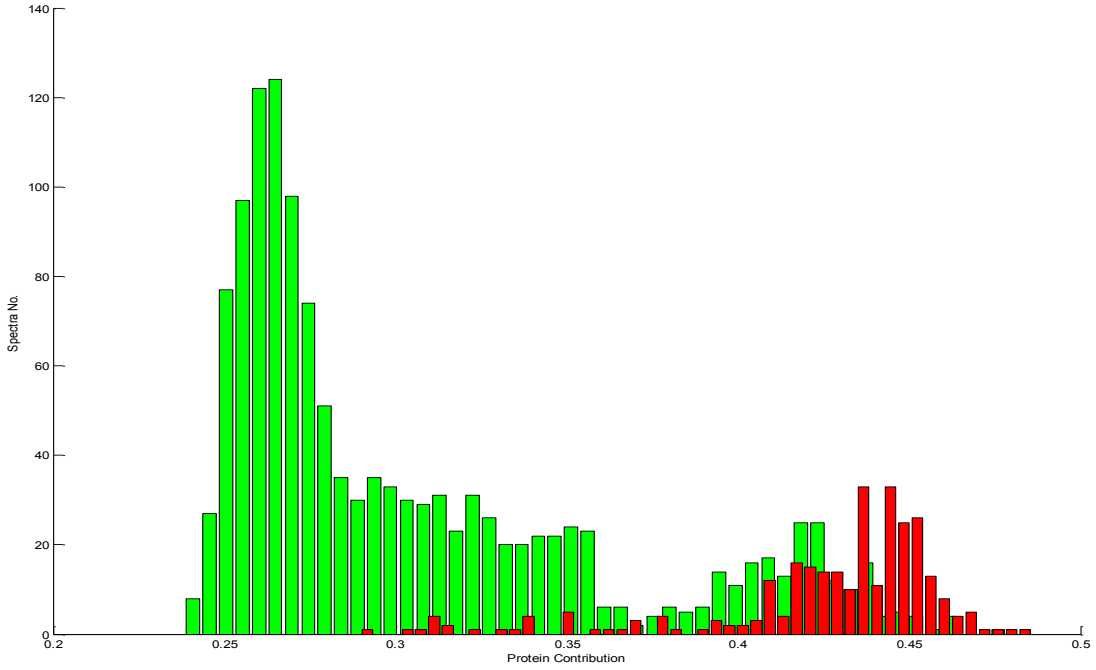

Figure 76 – Histogram demonstrating the combined intensity of all protein related peaks for each spectra in dataset 1 (green = N_0 negative nodes, red= macrometastases positive nodes).

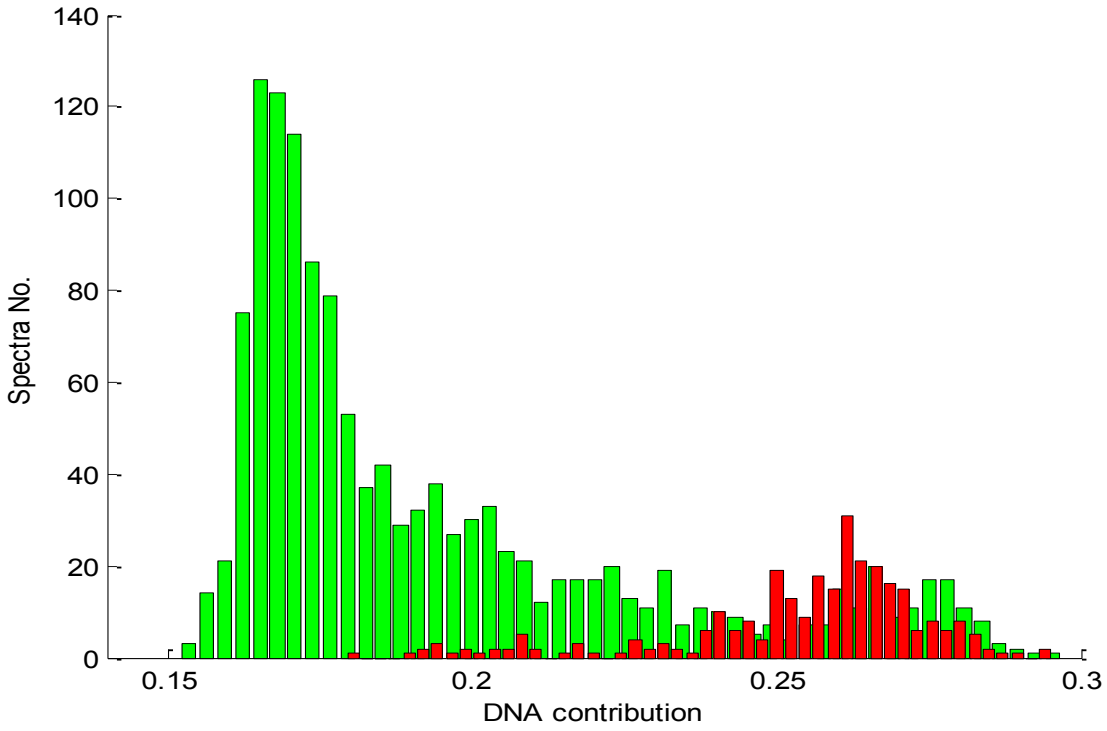

Figure 77 – Histogram demonstrated the combined intensity of all DNA related peaks for each spectra in dataset 1 (green = N_0 negative nodes, red= macrometastases positive nodes).

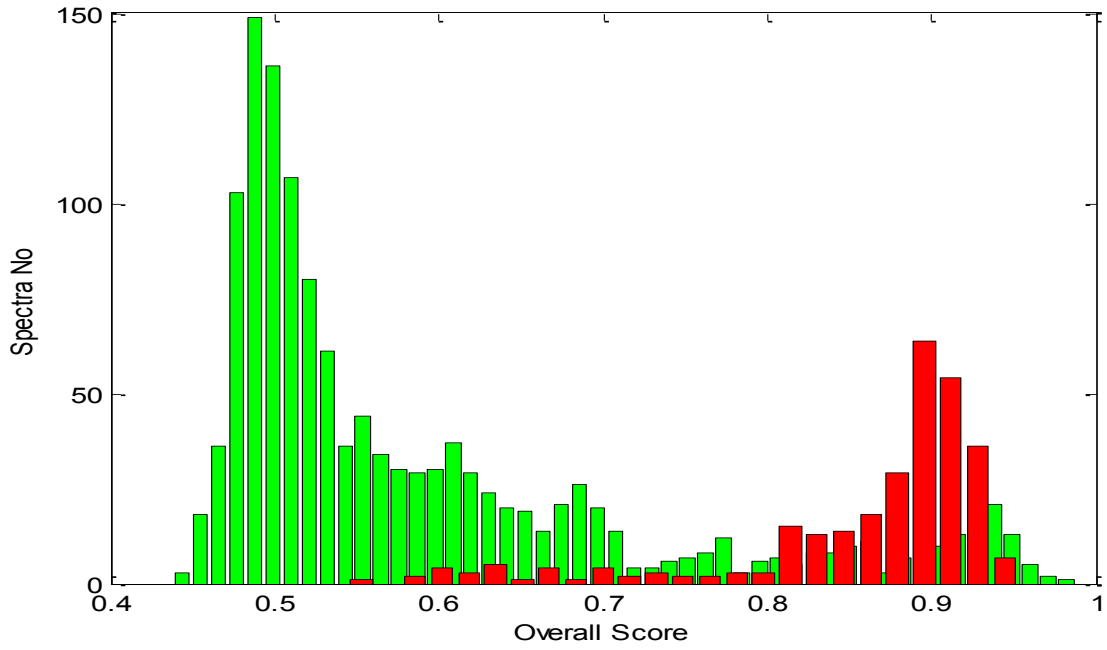

Figure 78 – Histogram demonstrating the overall score for positive and negative nodes for each spectra in dataset 1(green = N_0 negative nodes, red= macrometastases positive nodes).

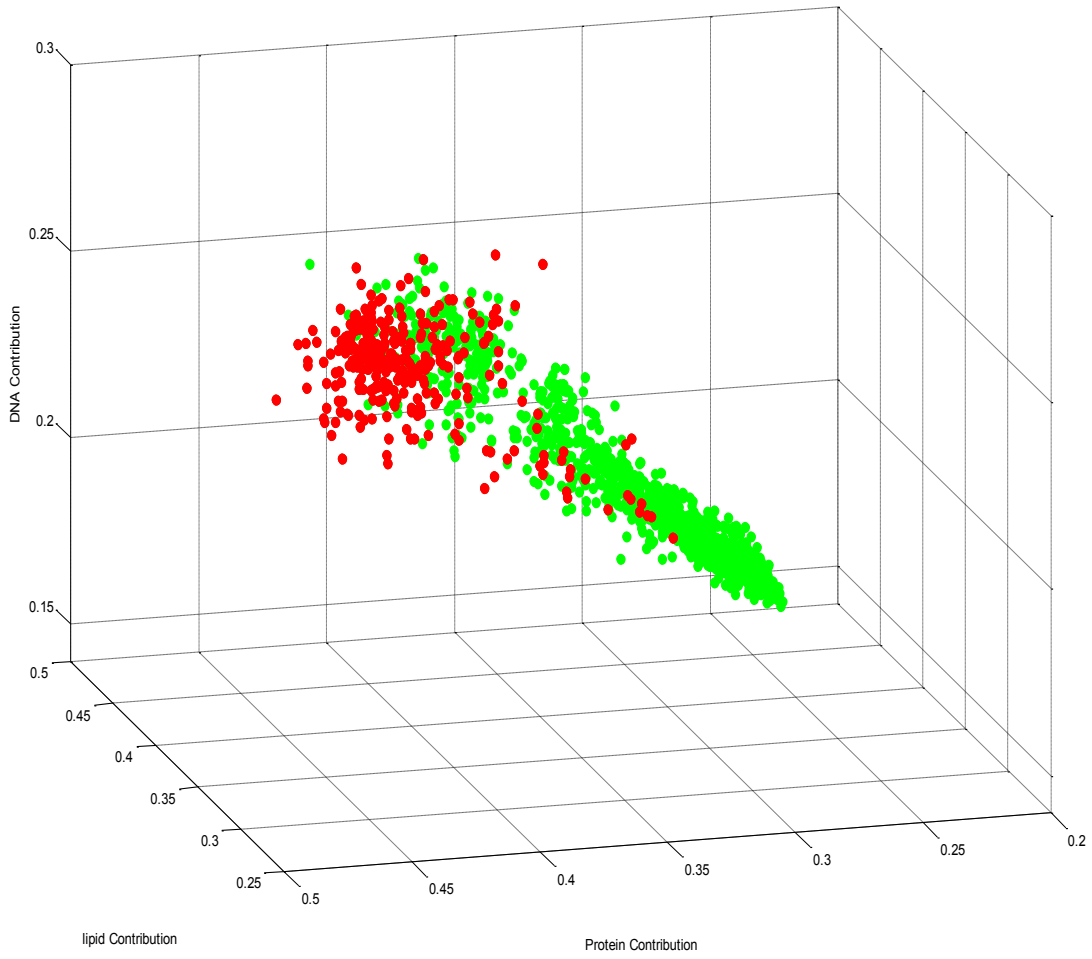

Figure 79 –3D plot demonstrating the ability of the three scores (lipid, protein and DNA contribution) to separate macrometastases positive nodes (red) from N_0 negative nodes(green) in dataset1.

	Mean Lipid Score (SD, SEM)	Mean Protein Score (SD, SEM)	Mean DNA Score (SD, SEM)	Mean Combined Score (SD, SEM)
Macrometastases (n=32)	0.32 (0.03, 0.005)	0.40 (0.04,0.007)	0.24 (0.02, 0.004)	0.82 (0.06, 0.01)
N_0 Negative (n=160)	0.40 (0.05, 0.004)	0.30 (0.06,0.005)	0.19 (0.04, 0.003)	0.59 (0.04, 0.003)
Unpaired t-test	p<0.0001 t=8.29	p<0.001 t=9.02	p<0.001 t=6.9	P<0.001 t=27

Table 20: The total intensities of peaks attributable to lipid, protein and DNA in the macrometastases and N_0 groups. Results of an unpaired t-test confirm the statistical significance of these differences.

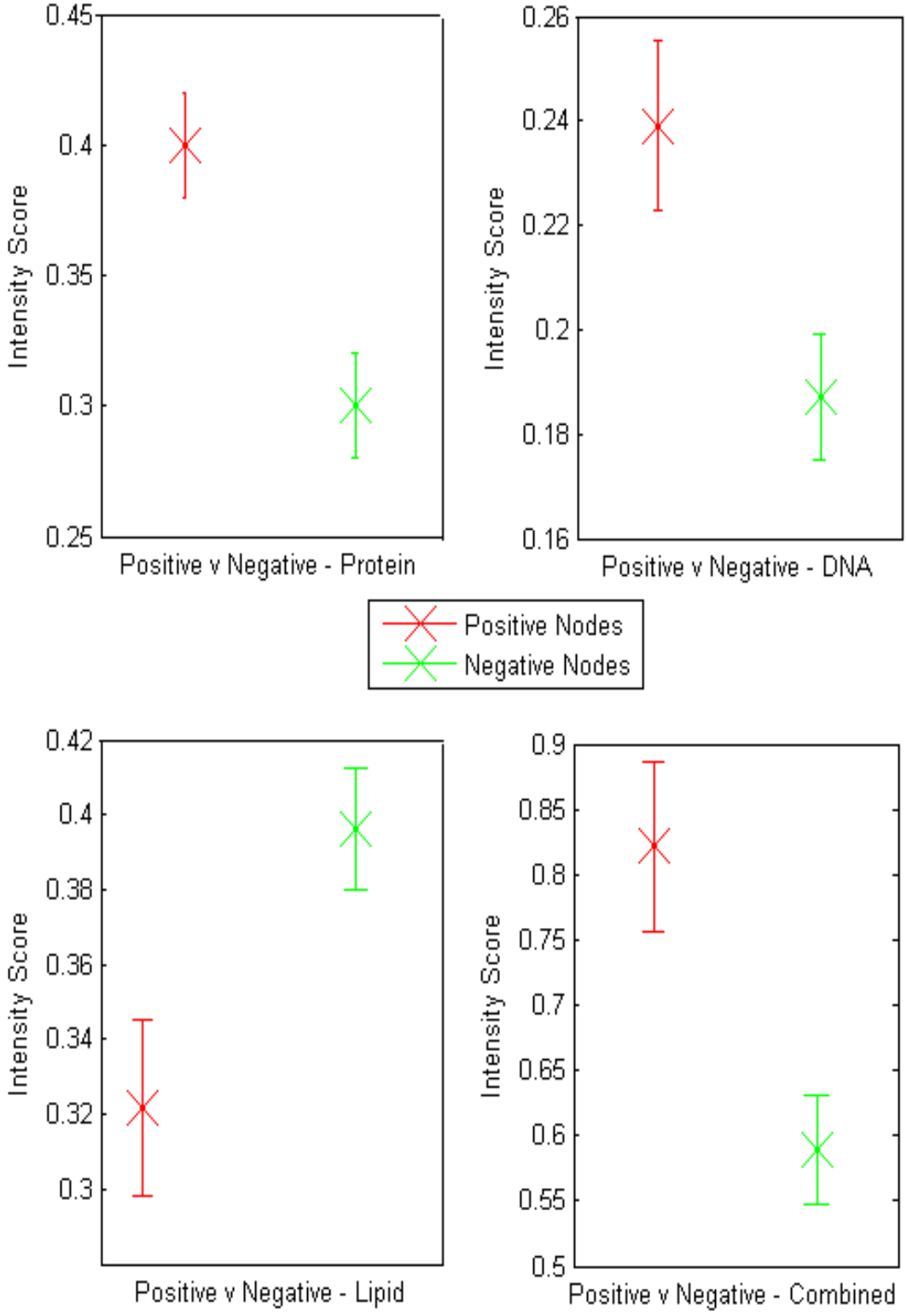

Figure 80 – Box and Whisker plots demonstrating the mean and 95% confidence intervals for the contributions of lipid, protein and DNA peaks as well as the overall molecular score for macrometastases (positive, green) v N_0 (negative, green) nodes (see also table 14a).

The combined compositional score was then used to assess whether it could be used to discriminate between positive and negative nodes. Analysis of the data suggested that the "score" which best discriminated between the two groups was 0.75. If a node had a combined score of greater than 0.75 it was defined as positive and if the combined score was less than 0.75 it was defined as negative. Using this score a sensitivity of 81% (27/32) and a specificity of 84% (128/160) was achieved. Whilst the sensitivity is at least comparable to current intraoperative techniques the specificity is significantly worse. As has been discussed this is clinically of most significance to avoid ultimately unnecessary axillary dissections and adjuvant chemotherapy. To investigate how the specificity could be improved the calculation was repeated with separation scores of 0.7 to 0.9. As the score was raised the specificity did indeed improve but at the expense of the sensitivity (Table 21).

Combined Score Diagnostic Cut Off Point (if > cut off = positive)	Sensitivity (%)	Specificity (%)
0.7	84	80
0.75	81	84
0.8	72	86
0.85	56	91

Table 21- Change in sensitivity and specificity at differentiating between macrometastases nodes and N_0 nodes using a combined biochemical score ((protein + DNA contribution) + (0.5 – lipid contribution)) as the diagnostic cut off point is altered.

Whilst these results are encouraging it was felt that they would not acceptable for a diagnostic test within this clinical scenario. Therefore further methods of data analysis were required to develop the technique as a diagnostic tool.

4.2.1.2. Principal Component Analysis fed Linear Discriminant Analysis (PCA fed LDA)

Due to the complexity of the data contained within a spectrum many authors have used chemometric recognition techniques to help interpret the information. A widely used technique is linear discriminant analysis (LDA) fed by principal component analysis (PCA). Using PCA allows one to simplify the data into fewer variables whilst retaining the overall spectral information. Each dataset is split into a number of components (loads) which contribute to each of the spectrum within the dataset. The contribution of each component is different for each spectrum and is defined by the principal component score. Each original spectrum has a different score for each load. The scores for each principal component (PCs) can then be used to simulate a linear boundary between the classes in the model (Sattlecker et al. 2010).

Initial data analysis used all spectra that had been collected from the nodes in the two groups. Thus a total of 1325 negative spectra and 290 positive spectra were included. When PCA fed LDA was performed a specificity of 99% and sensitivity of 95% was achieved. However it was felt that in a clinical scenario all spectra acquired from a single sample would be combined to provide a single output for each node. Therefore the mean of the spectra collected from each sample was subsequently assessed.

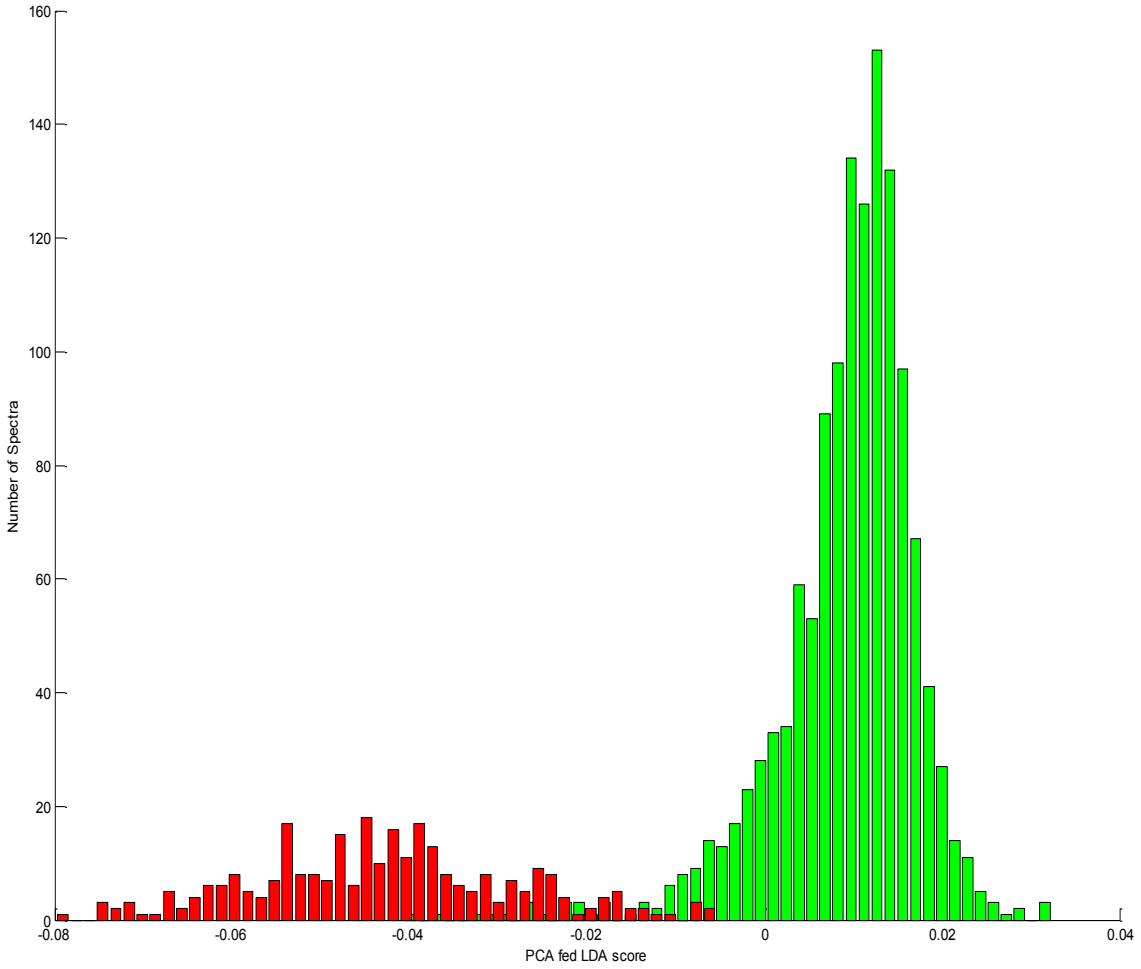

Figure 81 – PCA fed LDA scores for spectra from macrometastases positive samples (red) and N_0 negative samples (green) in dataset 1.

After mean centring the processed spectral data, principal component analysis was performed to generate 25 PC loads and scores. An unpaired t-test was performed to assess the statistical significance of the differences between the mean of the 25 scores for both positive and negative nodes. For each of the principal components the null hypothesis was that there was no difference between the mean score in the two groups. With 188 degrees of freedom the null hypothesis could be rejected at the 99% confidence level if the t score generated was greater than 2.6. Only 4 PCs achieved this level of significance, PC 1, 2, 11 and 12 (Figure 82, 83).

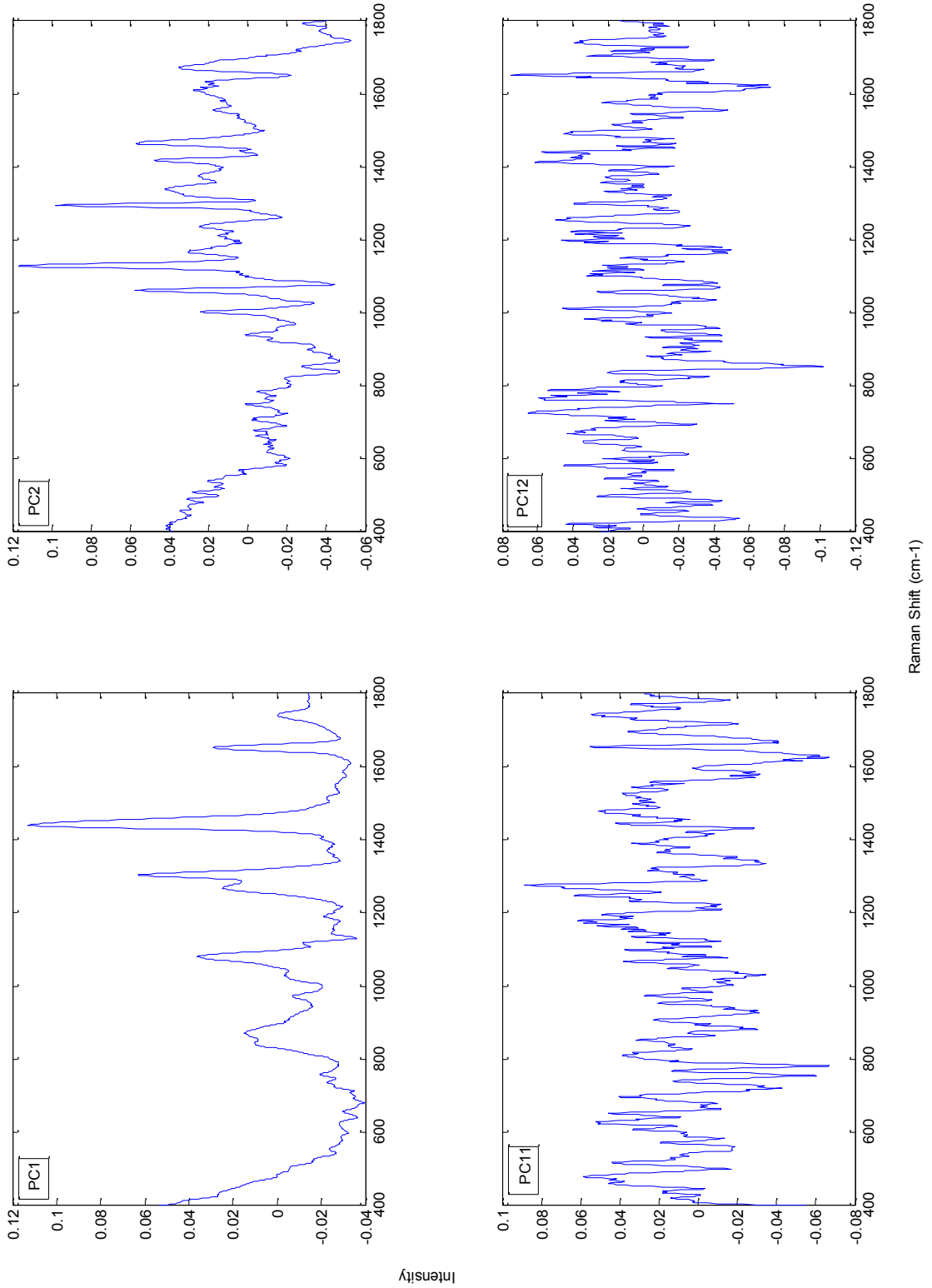

Figure 82 – Plots of the loads of the 4 most statistically significant PCs in the intraoperative study, as demonstrated in figure 83.

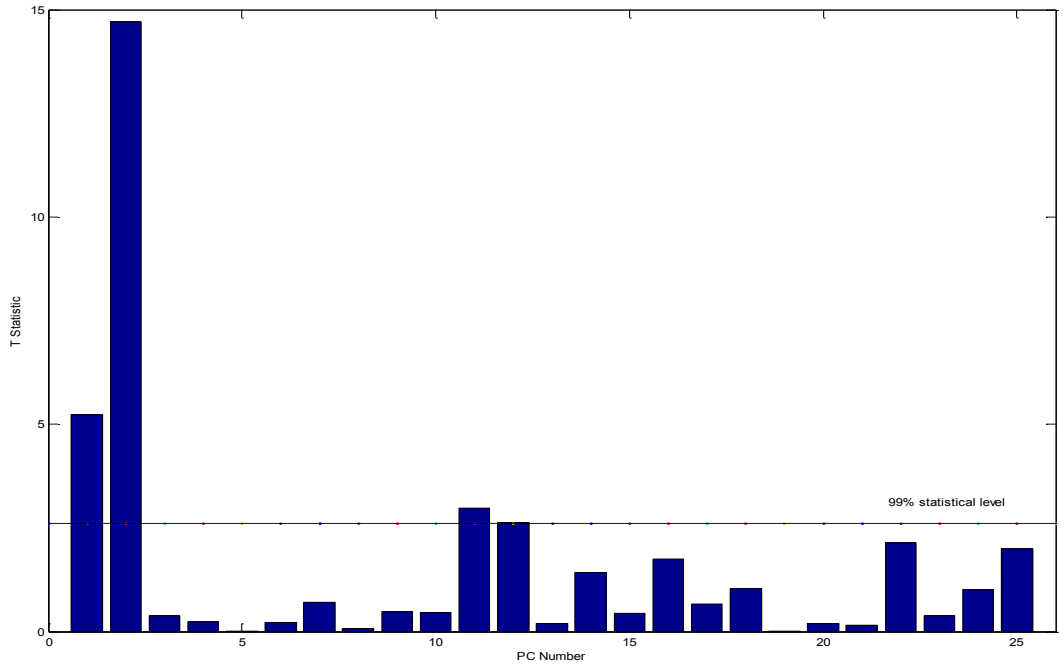

Figure 83 – t score from an unpaired t-test to assess the statistical significance of differences in the mean value of the scores for the first 25 PCs between macrometastases and N_0 node (n=32 and n= 160 respectively) .The horizontal line represents the 99% statistical level.

Closer examination of PC1 revealed peaks at positions identical or very similar to those previously identified as representative of negative nodes (Figure 84). Examination of PC 2 revealed that there were 20 of the peaks previously identified as positive evident in the plot (Figure 85). It was postulated that PC1, resembling lipids, represented negative nodes and that PC2, representing a combination of protein and DNA, was representative of positive nodes. This is supported by the finding that the mean score for PC1 amongst the positive nodes is -0.155 whereas that of the negative nodes is 0.03. Similarly for PC2 the mean score for the negative nodes is -0.17 and for the positive nodes it is 0.085.

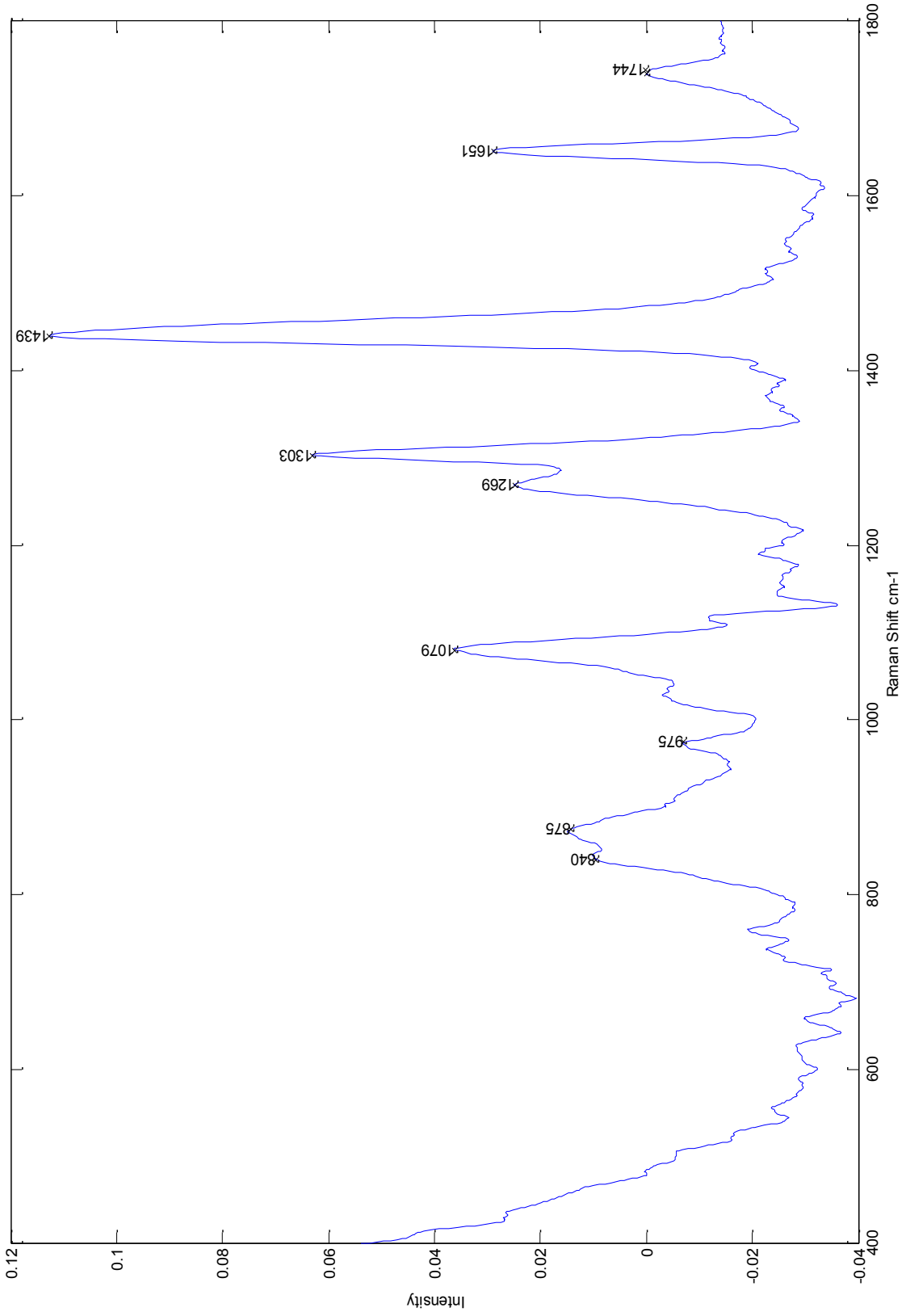

Figure 84- Plot of PC1 from principal component analysis of the dataset N_o and macrometastases nodes with key peaks marked for clarity.

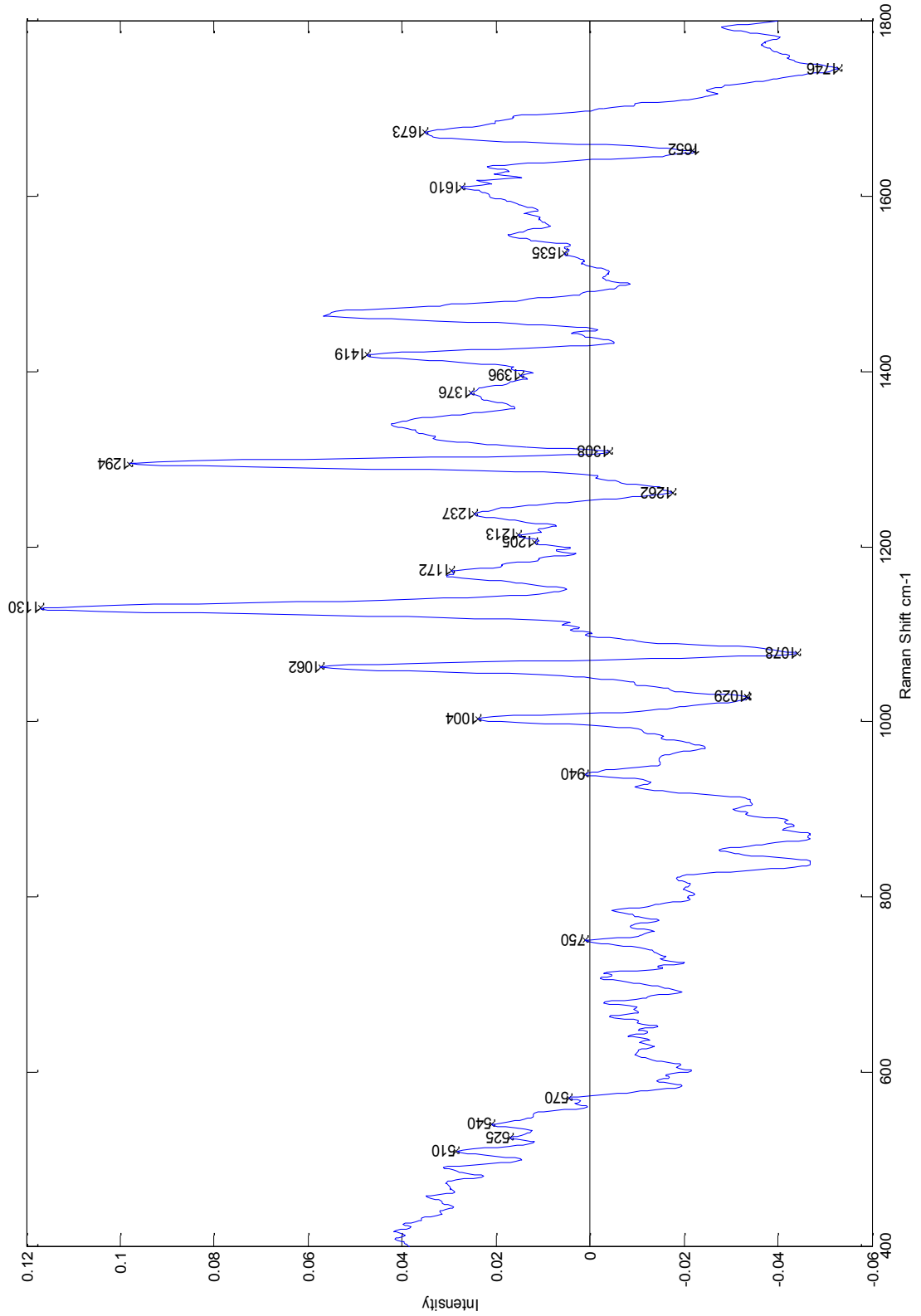

Figure 85- Plot of PC2 from principal component analysis of the dataset N_o and macrometastases nodes with key peaks marked for clarity.

The four most significant PCs from the T test analysis were then used to develop an LDA classification model. The training performance of this model achieved a sensitivity of 94% (30/32) and a specificity of 99% (158/160) (Figure 86).

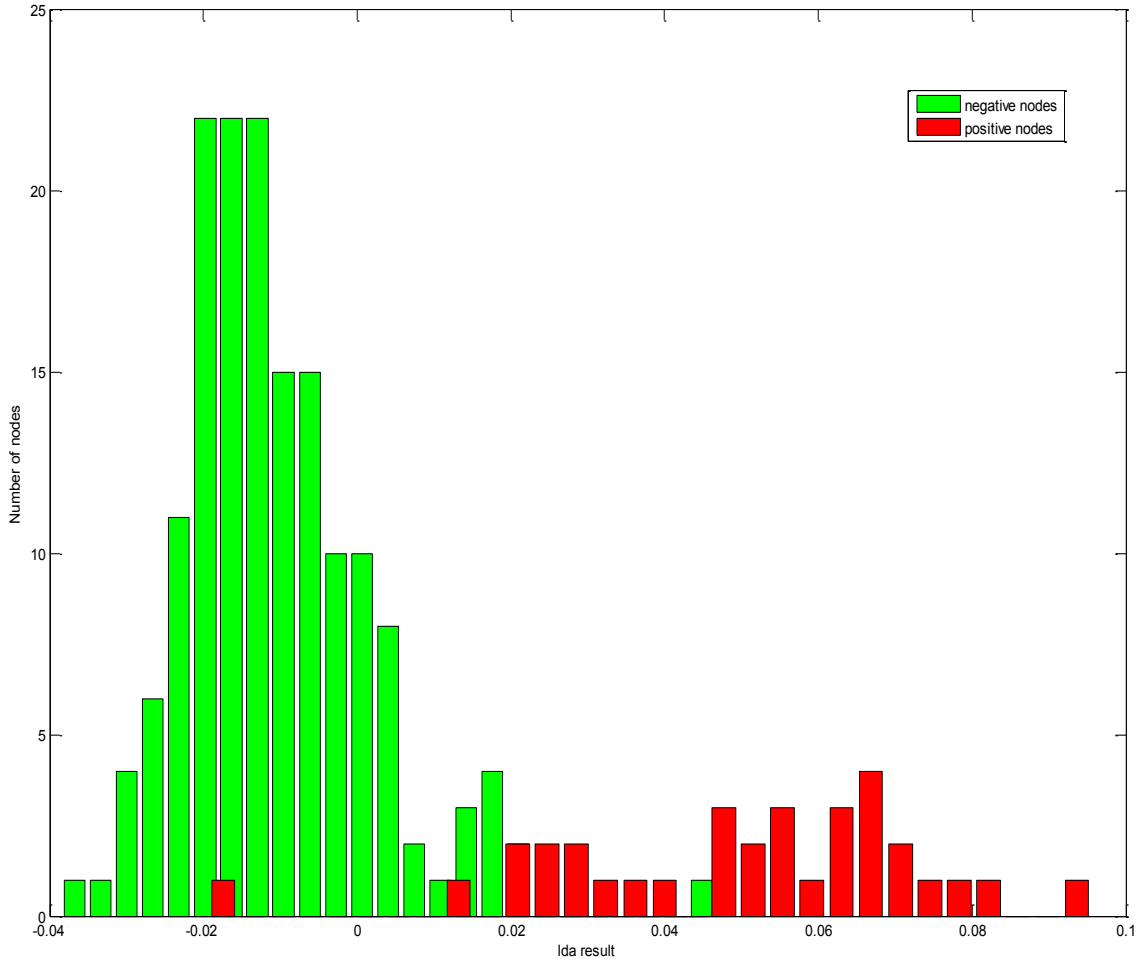

Figure 86- Histogram demonstrating the ability of the 4 most statistically significant PCs to separate the two tissue groups (N0 negative nodes, green, n=160, and macrometastases positive nodes, red, n=32) based on the LDA result generated using PCA (principal component analysis) fed LDA (linear discriminant analysis).

This analysis was then repeated using all 1 to 25 PCs to determine the optimum result that could be achieved (Figure 87). The best result was achieved when the first 14 principal components were included in the model, although only small improvements

are made beyond the first two PCs. Using PCs 1 to 14 to train the LDA model a sensitivity of 96.9% (31/32) and a specificity of 99.4% (159/160) was achieved in the training model.

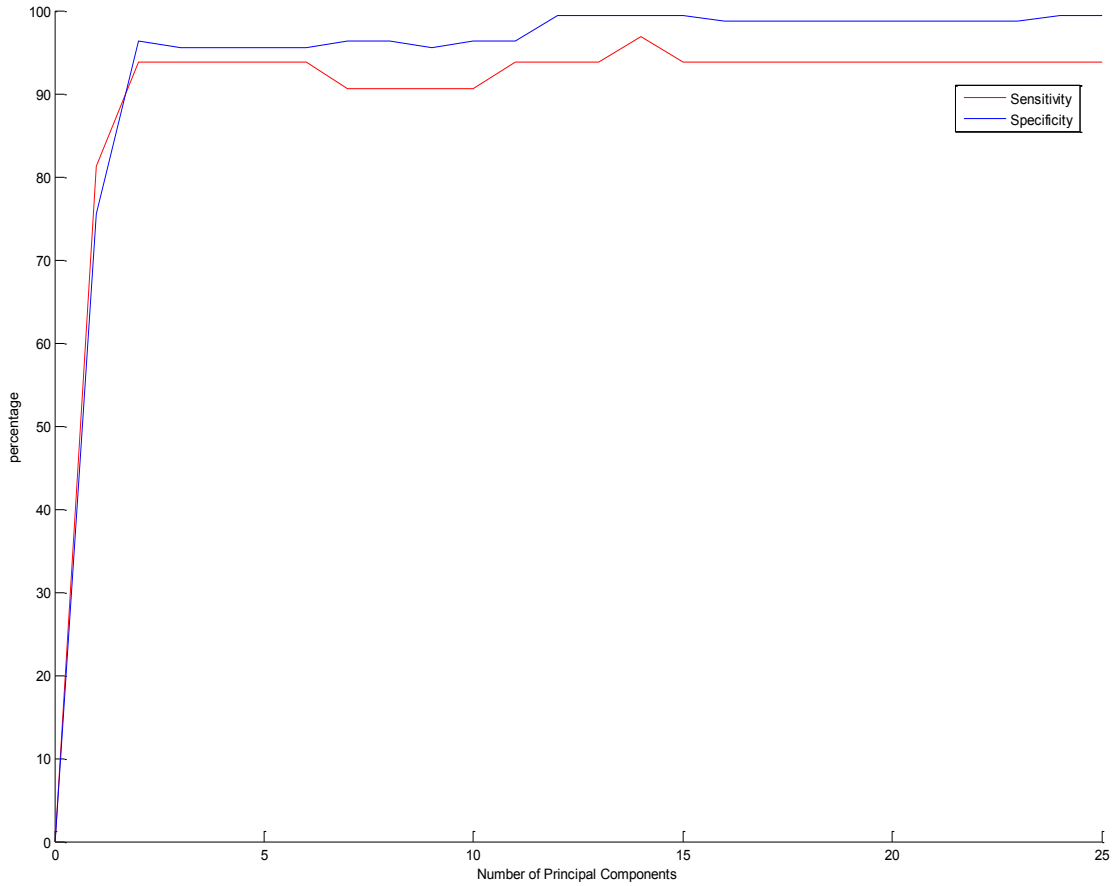

Figure 87– Improvement in the sensitivity(red) and specificity (blue) with increasing numbers of PC in dataset 1 (N_0 negative and Macrometastases positive nodes) .

The robustness of this data was further tested by using leave one node out cross validation. In this test the data from one sample is left out and the data from the remaining samples is then used to build a training set. This training set is split according to known pathology results and is used to predict the group membership, in this case positive or negative node, of the sample that had been left out. The leave one node out testing achieved a specificity of 99.4% (159/160) and a sensitivity of 93.8% (30/32)

when using all 25 PCS. When using only 14 PCs which we have previously shown achieved the best training set result using LDA a specificity of 98.8%(158/160) and a sensitivity of 90.6% (29/32) was achieved (Fig 88).

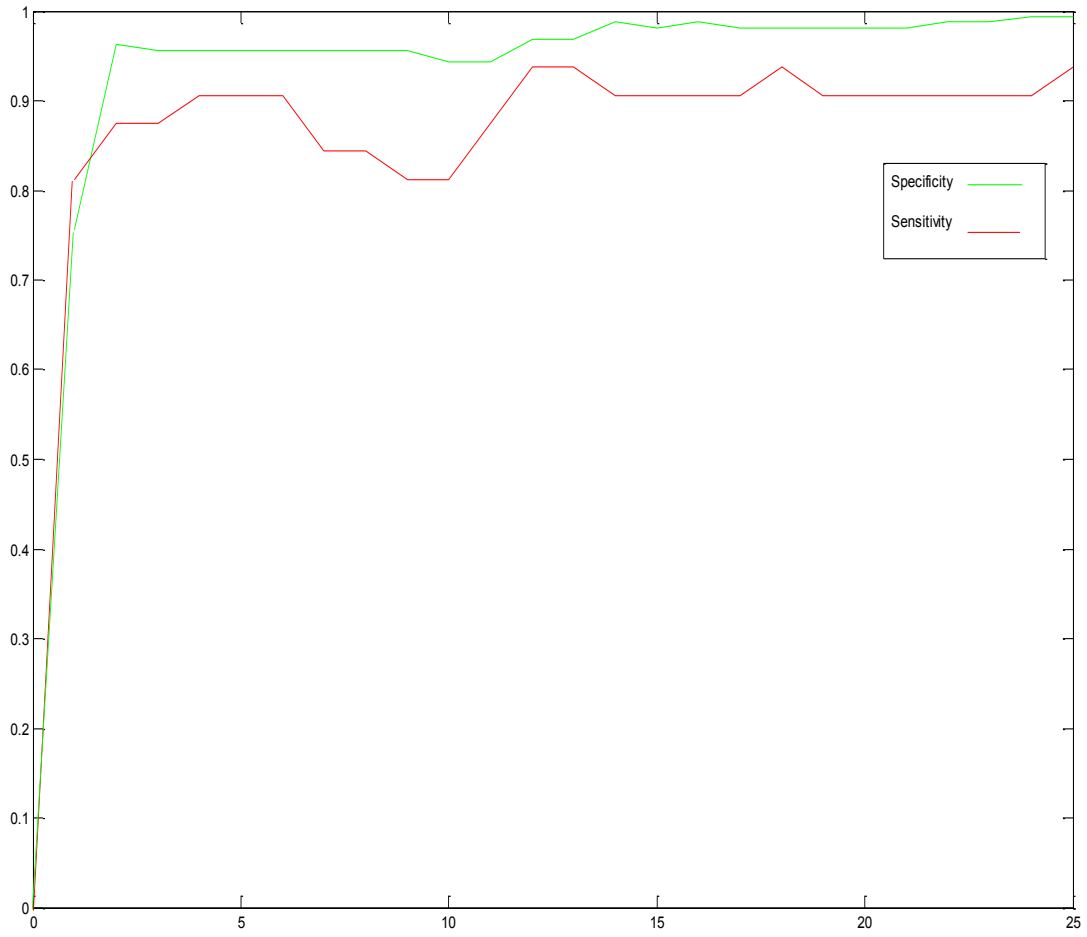

Figure 88- Improvement in the cross validation based sensitivity (red) and specificity (green) with increasing numbers of PC in dataset 1 (N_0 negative and Macrometastases positive nodes) .

This data was then used to assess the clinical impact it would have had on the patients involved in the study had it been used to guide clinical decisions. This dataset included nodes samples from 48 patients undergoing a SLNB. On subsequent histopathological testing Of the 57 sentinel lymph node biopsies performed 40 a negative axilla and 8 had evidence of macrometastases. If the results of the leave one node out cross validation

testing had been used, 38 out of 40 (95%) patients with a negative axilla would have been correctly identified. 6 out of 8 (75%) patients with an axilla containing macrometastases would have been correctly identified and would have benefited from an immediate axillary clearance. Thus 2 patients would have suffered from a false positive result and had an unnecessary axillary clearance. The two patients with false negatives would have been identified following post operative gold standard node assessment and recommended a delayed axillary clearance. These results are comparable to both other Raman spectroscopic studies (outlined in Chapter 2) and the current techniques used in the intra-operative assessment of axillary lymph nodes in breast cancer. However it needs to be remembered that these results are for the comparison of the two groups, macrometastases and normal nodes from N0 patients which would be expected to demonstrate the most significant pathological differences.

4.3. Results - Dataset 2: Macrometastases v all Negative nodes.

In the second dataset a larger group of negative nodes were assessed. This included both the negative nodes from N_0 patients (n=160) and the non-N_0 group (n=116). As stated previously these nodes are those that were histopathologically negative but that came from patients with other positive nodes. Mean spectra of the two groups were plotted and the intensity of the same 34 peaks, that had previously been used to examine the differences in the protein, DNA and lipid spectral contributions were calculated (Figure 89). These, along with the combined score were used to compare both between the positive and negative groups, as well as the two negative groups.

The results revealed that there were slightly higher levels of DNA and protein and slightly lower levels of lipid within the non-N_0 negative group in comparison to the N_0 negative group (Figure 90) (Table 22). An unpaired t-test revealed statistically significant differences between the Non-N_0 nodes and both the N_0 and macrometastases nodes (Table 23).

	Mean Lipid Score (SD, SEM)	Mean Protein Score (SD, SEM)	Mean DNA Score (SD, SEM)	Mean Combined Score (SD, SEM)
Non N_0 negative nodes (n=116)	0.38 (0.05, 0.004)	0.32 (0.07,0.007)	0.20 (0.04, 0.004)	0.63 (0.03, 0.003)

Table 22: The intensities of peaks attributable to lipid, protein, DNA and a combined score in the non N_0 negative nodes. For comparison to N_o nodes and macrometastases see table 20 (SD=standard deviation and SEM= standard error of the mean).

	Lipid Score	Protein Score	DNA Score	Combined Score
N_0 v. Non- N_0 negative nodes	p=0.009 (t=2.63)	p=0.0073 (t=2.70)	p=0.01 (t=2.60)	p<0.001 (t=9)
Macrometastases v. Non- N_0 negative nodes	p<0.001 (t=8.29)	p<0.001 (t=9.02)	p<0.001 (t=6.9)	p<0.001 (t=24)

Table 23: Results of unpaired t-tests comparing the mean lipid, protein, DNA contribution and a combined score for N_0, non-N_0 negative and macrometastases nodes (n=160,116 and 32 respectively). See also tables 20 and 22 for mean, standard deviation and standard error of the mean for each group.

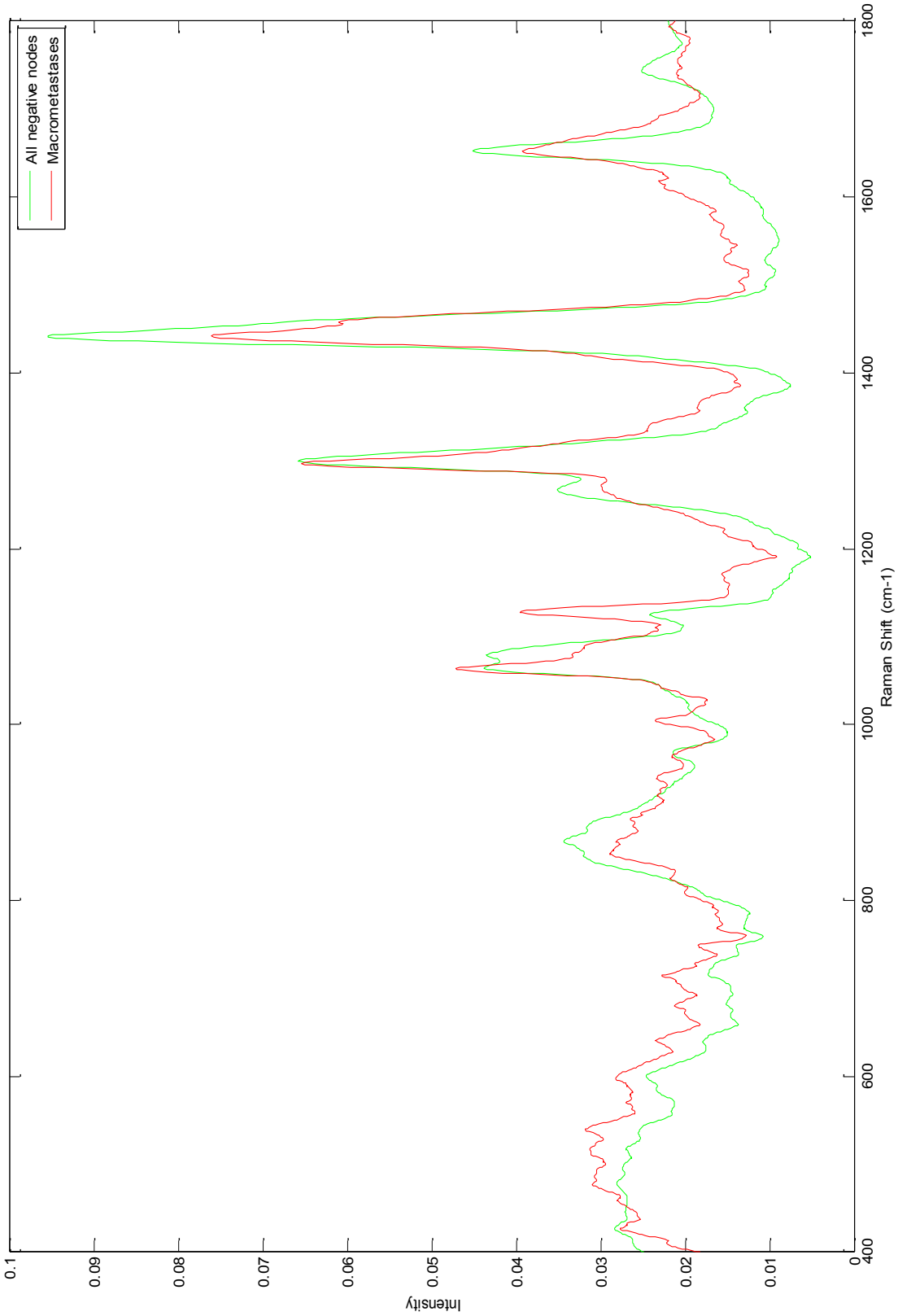

Figure 89– Mean spectra of the two tissue groups in dataset 2 (all negative nodes, green n=276 and macrometastases positive nodes, red n=32).

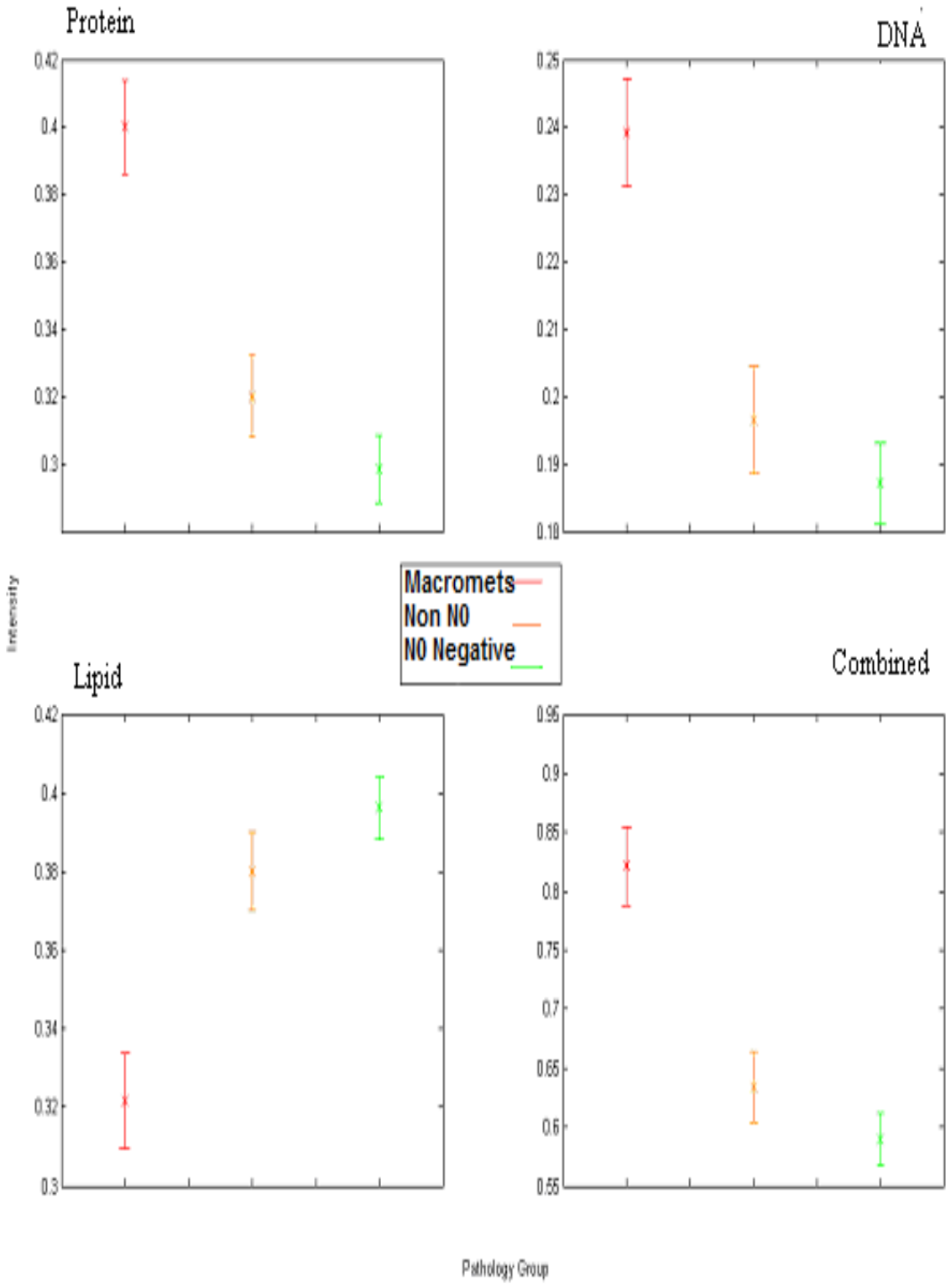

Figure 90- Mean intensity scores (with 95% confidence intervals) for peaks related to Protein, DNA and lipid and a combined score in dataset 2. (N_0 (green,) non-N_0 negative (orange) and macrometastases (red) nodes (n=160,116 and 32 respectively)).

If a combined score of 0.7 was used as a diagnostic cut of a sensitivity of 84% and a specificity of 76% was achieved. As previously demonstrated in the first model if the score required to differentiate between the two groups rose then the sensitivity fell and the specificity rose (Table 24).

Combined Score Diagnostic Cut Off Point	Sensitivity	Specificity
0.7	84	76
0.75	81	80
0.8	72	84
0.85	56	89

Table 24- Change in sensitivity and specificity as the diagnostic cut off point is altered in dataset 2.

As outlined earlier in this chapter principal component fed linear discriminant analysis was then used to differentiate between the negative and macrometastases groups. The best sensitivity achieved was 91% (29/32) and the best specificity achieved was 98% (270/276) when using 25 PCs. Leave one node out cross validation testing was performed and a specificity of 96% (265/276) and a sensitivity of 84% (27/32) were achieved. Whilst still very acceptable this result is poorer than that achieved in the true negative v macrometastases model.

This result prompted questions as to why this was the case? It could be postulated that there are changes in the non-N_0 negative group that are due to the immune response to metastases in another node, as detailed in Chapter 1. This is supported by the results of

the individual component analysis that demonstrated that the differences in the protein score were the most statistically significant between the N_0 negative nodes and the non-N_0 negative groups. The mechanism behind this difference may be explained by immune mediators produced in response to metastatic deposits in other nodes being filtered through nodes higher in the chain. These differences would not render the node "positive" pathologically but could alter the spectral features of the sample sufficiently to influence the classification model. This is an important finding to be aware of in the future particularly if models are created based on this data. Misclassification of these non-N_0 nodes is in itself not likely to be clinically important as other nodes would already have seen the patient classified as having a positive axilla. Their role however in altering the model classification could render positive nodes negative as it has done in this dataset and increase the false-negatives.

4.4. Results - Dataset 3: All Positive nodes (Macro+Micro+ITCs) v Negative Nodes.

The final dataset included the macrometastases (n=32), the micrometastases (n=8), the isolated tumour cells (n=10) and all the negative nodes (n=276). As the micrometastases and ITC group sizes were so small these were combined into one group term "non-macrometastases positive nodes" (n=18).As discussed previously the protein, lipid and DNA scores for each sample were calculated (Table 25). The differences between the macrometastases and the "non-macrometastases" positive nodes were statistically significant for lipid, protein and DNA. Although none of the changes were statistically significant for "non macrometastases" positive nodes versus N0 negative nodes and non

N0 negative nodes there did appear to be a trend from macrometastases to N0 negative nodes (Table 26) (Figure 91).

	Mean Lipid Score (SD, SEM)	*Mean Protein Score (SD, SEM)*	*Mean DNA Score (SD, SEM)*	*Mean Combined Score (SD, SEM)*
Non Macrometastases Positive Nodes (n=18)	*0.38 (0.05, 0.012)*	*0.32 (0.04,0.01)*	*0.195 (0.04, 0.01)*	*0.63 (0.09, 0.02)*

Table 25: The combined intensities of peaks attributable to lipid, protein, DNA and a combined score in non-macrometastases. For comparison to N_o nodes, non N_0 negative nodes and macrometastases see table 20 and 22.

	Lipids	Protein	DNA	Combined score
N_0 v. Non Macrometastases Positive nodes	p=0.1915 (t=1.3)	p=0.1402 (t=1.48)	p=0.42 (t=0.8)	p=0.1 (t=3.4)
Non- N_0 negative nodes v. Non Macrometastases Positive nodes	p=1 (t=0)	p=1 (t=0)	p=0.628 (t=0.5)	p=1 (t=0)
Macrometastases v. Non Macrometastases Positive nodes	p<0.001 (t=5.17)	p<0.001 (t=6.8)	p<0.001 (t=5.3)	p<0.001 (t=8.9)

Table 26: Results of unpaired t- tests comparing the mean lipid, protein DNA contribution scores and a combined score for N_0, non-N_0 negative and macrometastases nodes v. non-macrometastases positive nodes (n=160,116, 32 and 18 respectively). For further details see Tables 20, 22 and 25.

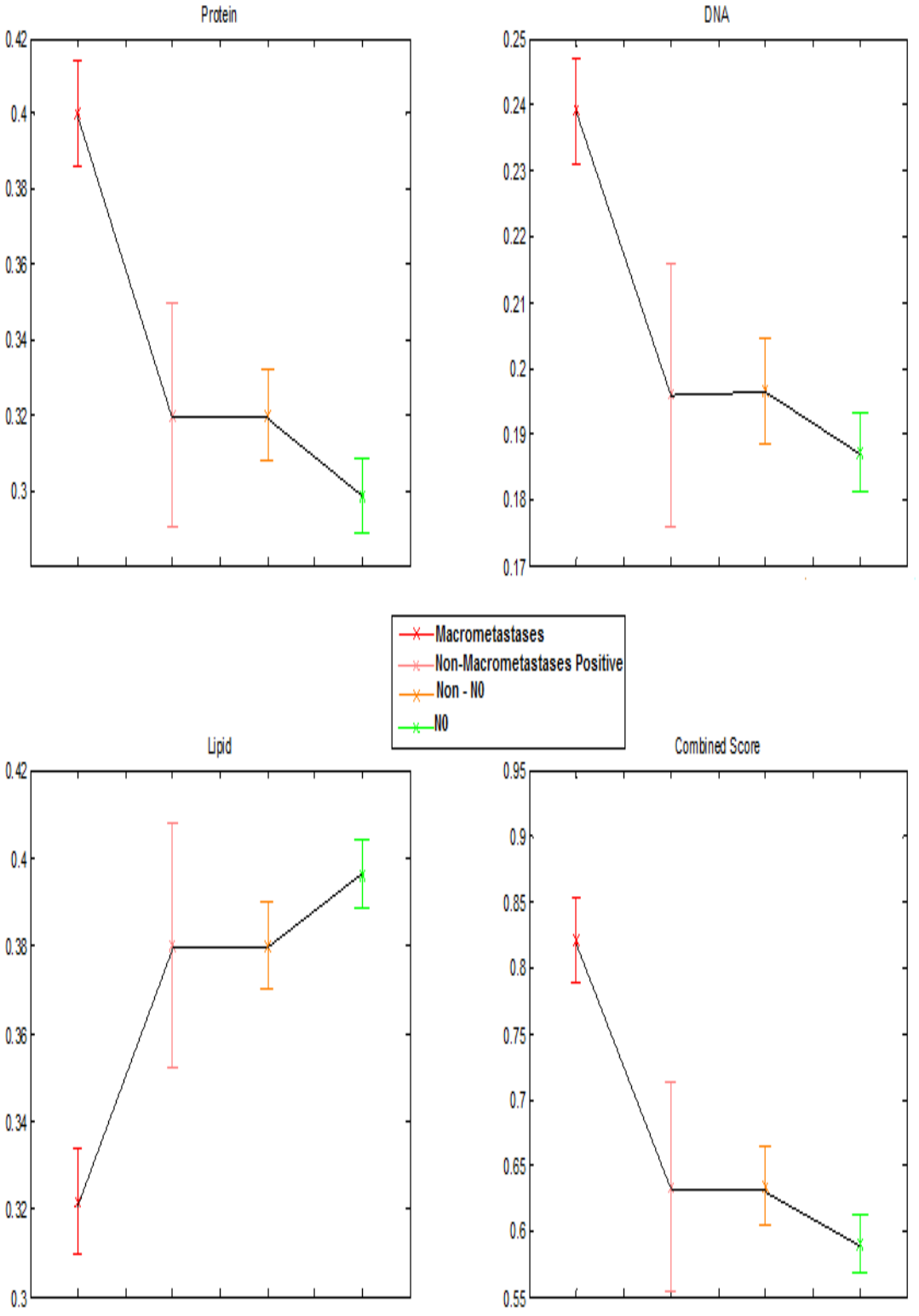

Figure 91- Mean intensity scores (with 95% confidence intervals) for peaks related to Protein, DNA and lipid and a combined score in N_0 (green,) non-N_0 negative(orange), non-macrometastases positive nodes (light red) and macrometastases(dark red) nodes (n=160,116,18 and 32 respectively)

The width of the standard error bars for the non macrometastases positive nodes is partly explained by the small group size but may also be explained by the presence of what appear to be two distinct subsets within the data (Figure 98). In one subset there are high levels of lipid with low levels of protein and DNA (resembling negative nodes) and in the other there are low levels of lipid with high levels of protein and DNA (resembling the macrometastases nodes). These two subsets are not related to a comparison between the ITCs vs. Micrometastases. Chemometric analysis revealed that only 50% (4/8) of the micrometastases and 40% (4/10) of the ITCs were correctly categorised. The small group size made further evaluation of this finding difficult but it could be suggested that one reason for the difference was that an insufficient volume of the node is being sampled to detect the small areas of change associated with either micrometastases or isolated tumour cells in those samples that appeared similar to the negative nodes. It is not altogether surprising that those eight samples that were correctly categorised were the eight that had features most closely resembling the positive nodes and thus would be examples of where the nodal change was identified from the volume of tissue analysed (Figure 92).

These results demonstrate the difficulties that may be experienced detecting micrometastases and isolated tumour cells using this technique. As was discussed in Chapter 1 it is likely that a decision to proceed to an ALND would not be clear cut and that MDT discussion would be required prior to proceeding to an ALND.

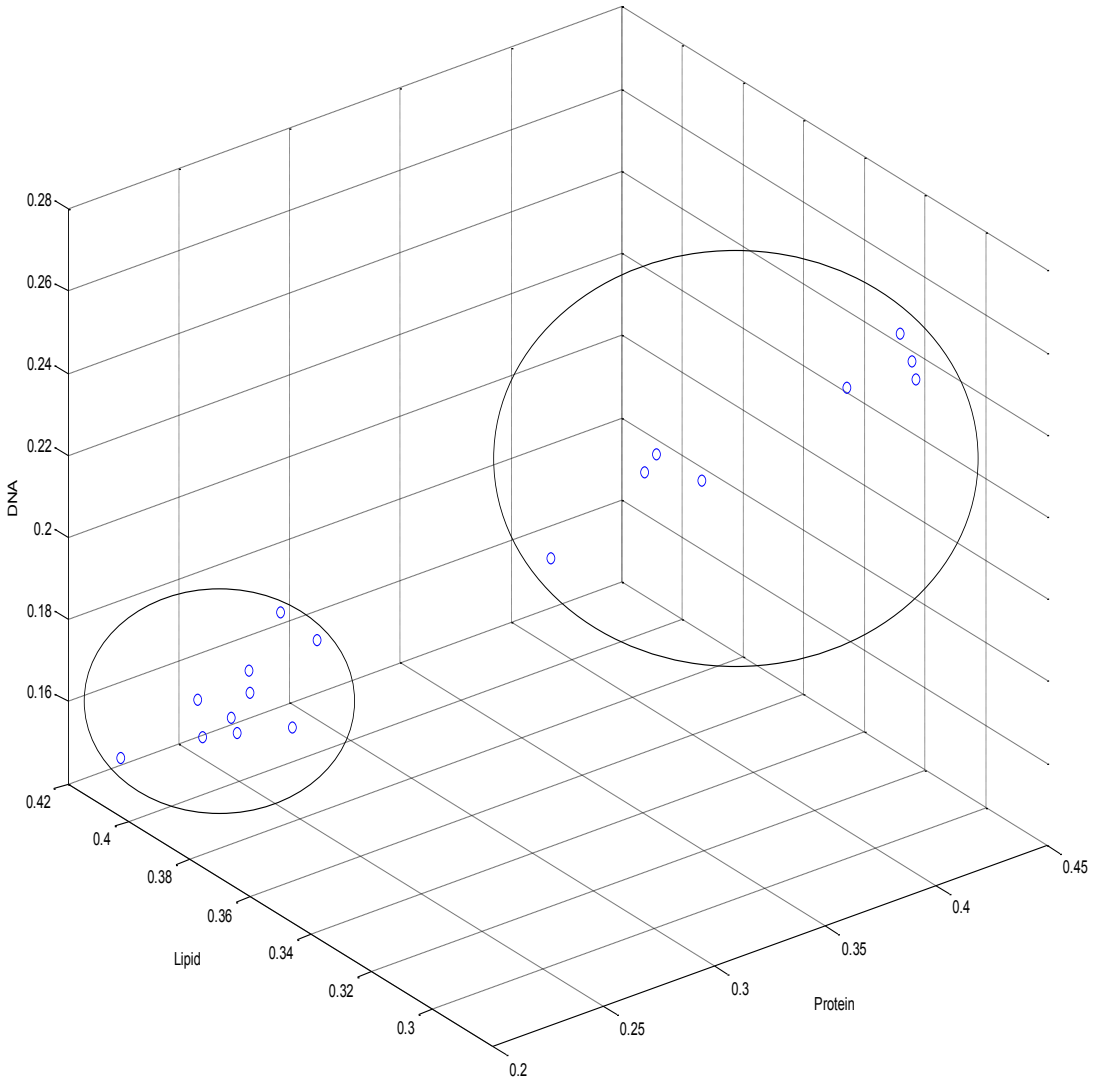

Figure 92- 3d plot of the lipid, protein and DNA contributions in micrometastases and ITC demonstrating two clear groups, one with high DNA and protein contributions and low lipid contributions (consistent with a positive node) and one group with lower DNA and protein contributions and high lipid contributions (consistent with a negative node). This supports the suggestion that in the micrometastases and isolated tumour cell samples because of the small volume of disease this was not being "seen" by the Raman technique in all of the nodes investigated.

4.5. Measurements from the inner cut surface versus those from the outer surface.

Discussion within the group at the outset of this study questioned whether spectra needed to be obtained from the cut inner surface of lymph nodes, as had previously been performed, or whether spectra could be collected from the outer surface of the node without altering the sensitivity and specificity of the test. Looking forward this would mean that lymph node analysis might be able to be performed with the node still *in situ* and negate the need to excise the lymph node if it were negative. Various groups throughout the world are beginning to develop either minimally invasive lymph node sampling or in a few centres laparoscopic sampling techniques (Lim and Lam 2005). If Raman spectroscopy could differentiate between positive and negative nodes based on spectra obtained from the outer surface of the node this technique would be further enhanced and the invasiveness of the procedure further reduced. Further, analysis of the results, as discussed above, suggested that further volume sampling may help improve the detection of micrometastases and isolated tumour cells.

4.5.1. Inner vs. Outer Experiment - Methods.

282 of the samples collected during the study described at the start of Chapter 4 were assessed both from the inner cut surface and also from the outer surface. At the time of analysis 5 spectra were obtained from the inner cut surface and then the node was simply turned 180° and further spectra were acquired. Spectral acquisition and tissue handling was as described at the start of Chapter 4. Data analysis was performed using

Matlab® software. Statistical analysis was performed using a paired t-test to compare the mean intensity of each wavenumber in the two datasets. The null hypothesis was that there was no difference between the two groups at each wavenumber. The null hypothesis was rejected if the t value was greater than 2.33 (the critical value for a test with >500 degrees of freedom at the 99% level). More detailed analysis of the biochemical differences was performed by examining the mean intensity of the peaks attributable to lipid, protein and DNA as described earlier in this chapter. Further analysis using PC fed LDA was then performed as has been discussed earlier in this chapter.

4.5.2. Inner vs. Outer Experiment - Results.

Of the 282 samples which were assessed in this way. 132 were negative nodes from N_0 patients, 90 were negative nodes from non-N_0 patients, 31 were samples with macrometastases, 8 were samples with micrometastases, 9 had ITCs and 12 were from fat (thus not included in further analysis). For comparative purposes two datasets with spectra obtained from either the inner or the outer surface of each sample was created. Mean spectra (n=270 in both groups) from the two datasets looked very similar on initial inspection and this was confirmed by performing a paired t-test on each of the wavenumbers (Figure 93, 94).

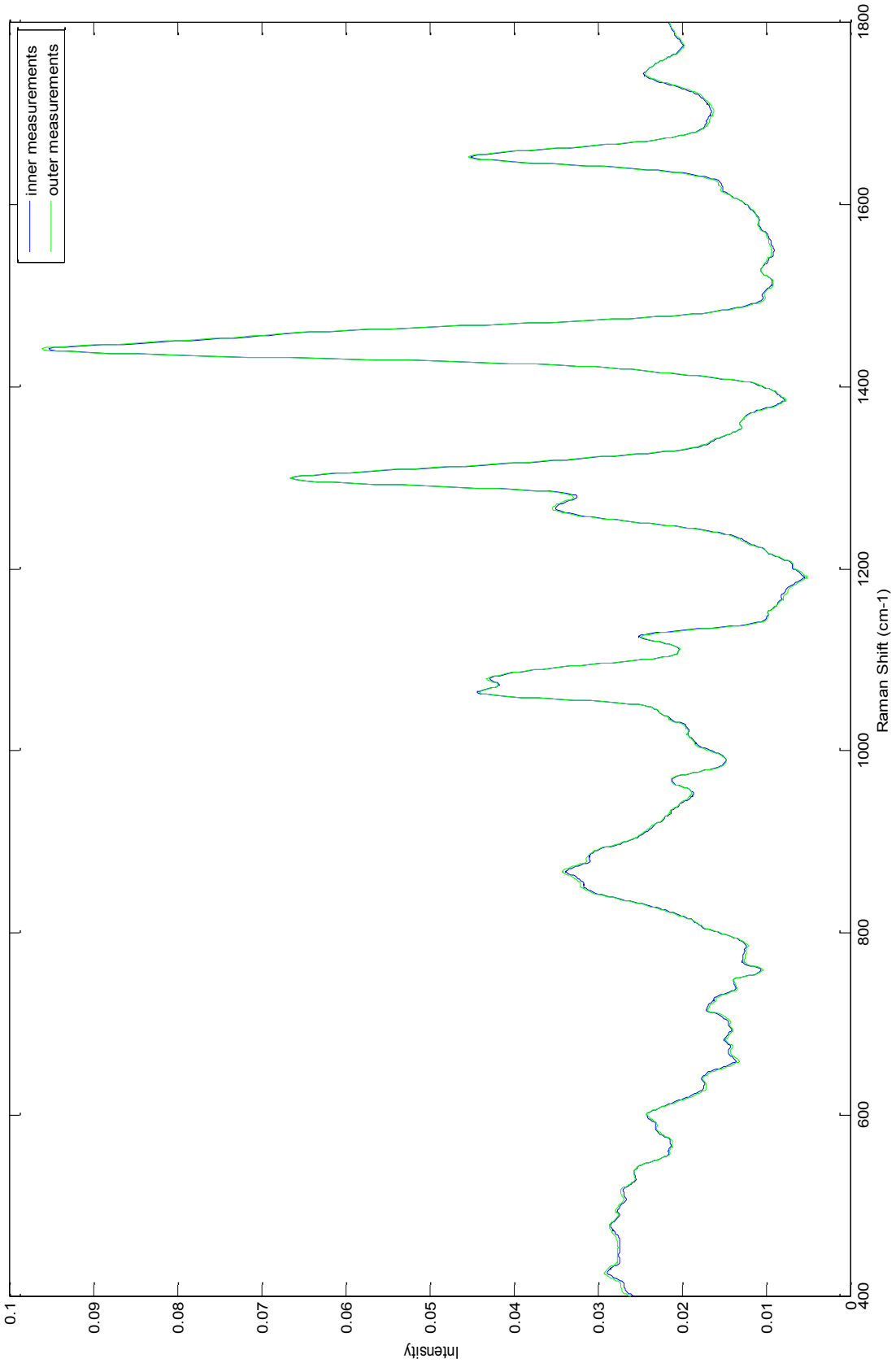

Figure 93 – Mean spectra collected from the outer (n=270, green) and inner surface (n=270, blue) of the lymph nodes.

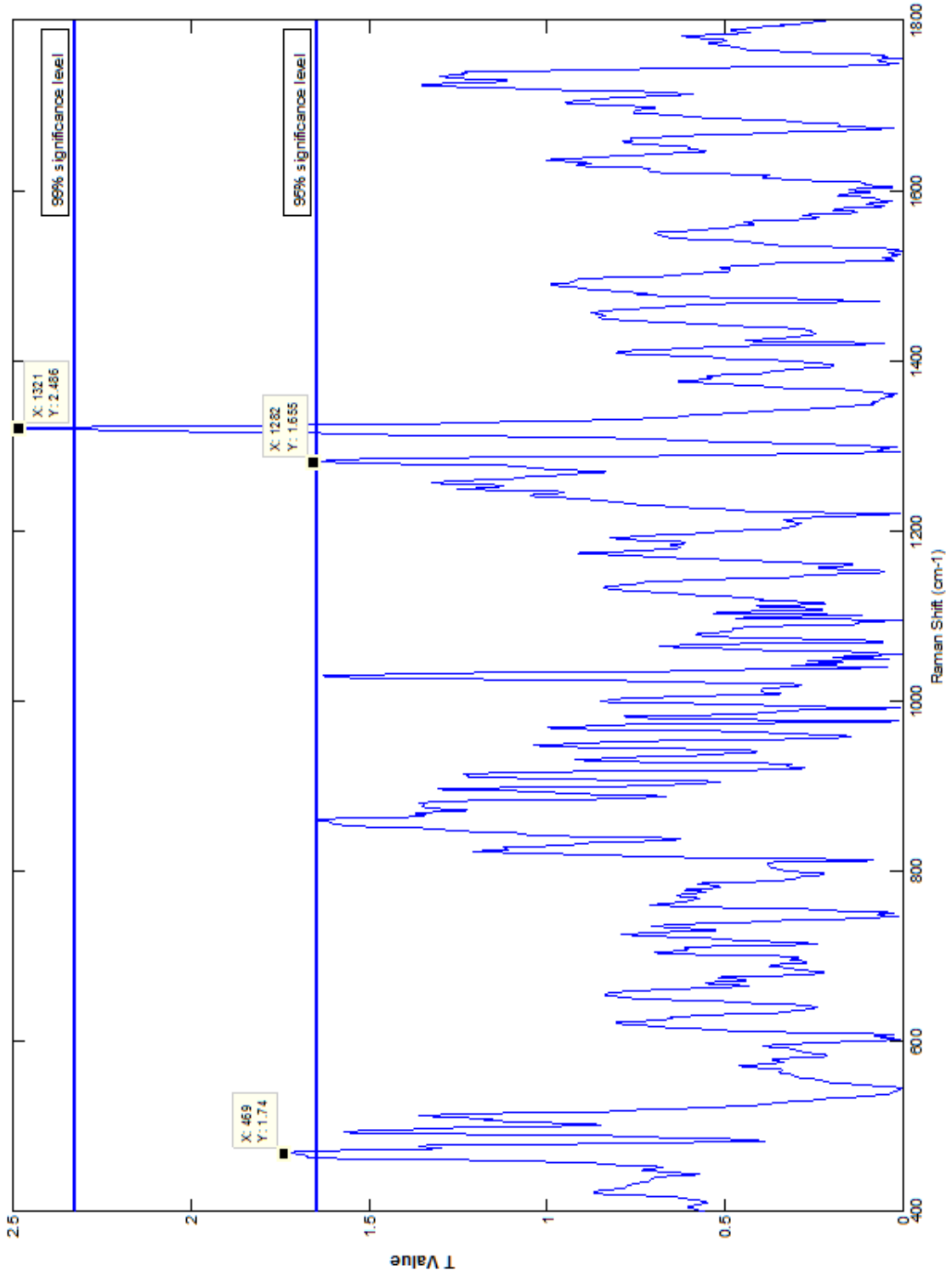

Figure 94 –The results of the t-test for each wavenumber to demonstrate the statistical significance of the differences between the mean intensity of each wavenumber for spectra from the inner and outer surface of each lymph node. Statistical significant differences were only present if the t-value was above 1.66 (95% significance level) or 2.33 (99% significance level).

The null hypothesis was only rejected for one wavenumber at 1321 cm^{-1}. Even if the significance level is reduced to 95% the null hypothesis is rejected at only two further wavenumbers at 469 and 1282 cm^{-1}. Chemometric analysis was then performed on the data to calculate whether the two sets of data could be categorised. The differences between the two groups were not sufficient to differentiate between the spectra obtained from inner or outer surfaces. The overlap between the two groups was very evident when the scores for the LDA analysis were plotted (Figure 95). These findings therefore support the statement that there is little difference between the mean spectra acquired from the outer and inner half of the lymph node.

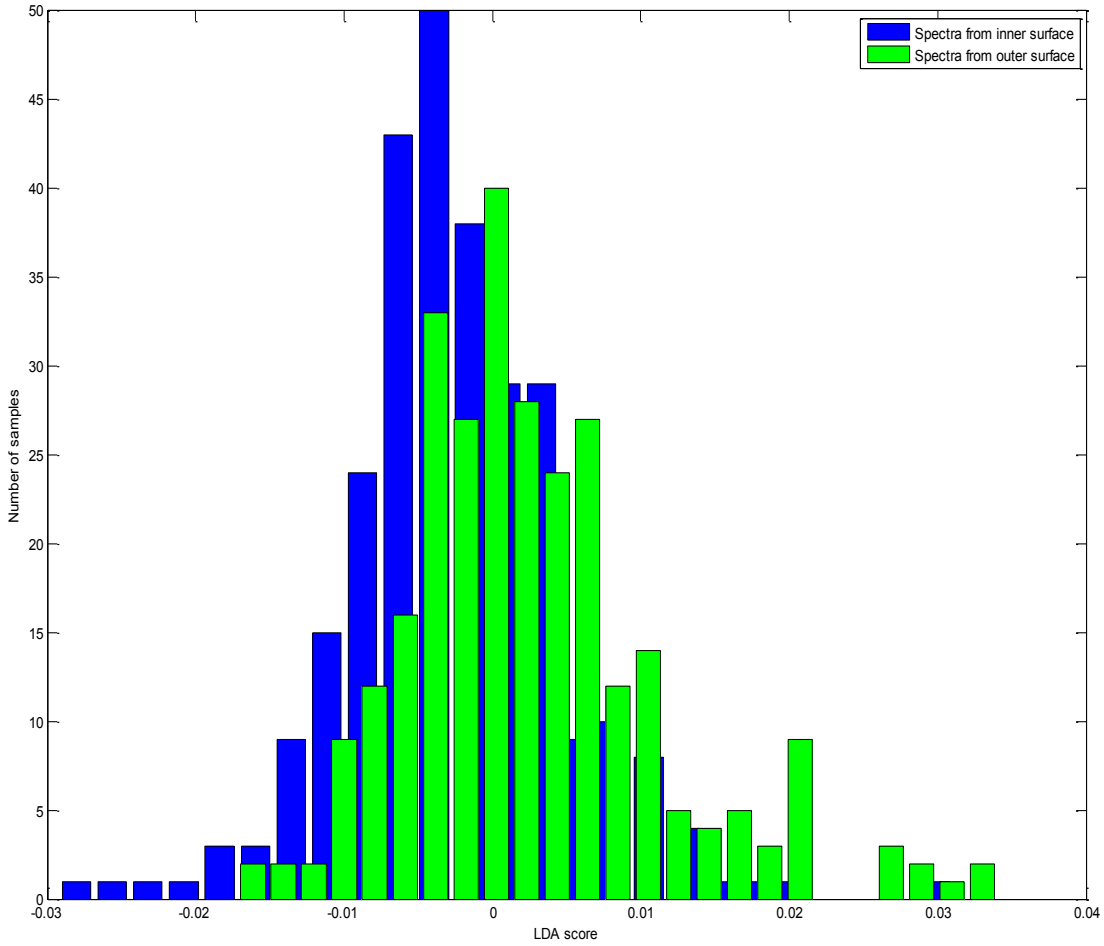

Figure 95–PCA fed LDA scores for spectra from the inner (blue) and outer (green) surface of each node demonstrating the difficulty separating the two datasets.

Whilst the results from the overall mean spectra were encouraging it was theorised that greater differences may be seen in the nodes with metastatic disease. As previously discussed metastatic cells that have spread to axillary lymph nodes are first found in the subscapular sinuses before passing to the medullary sinuses from where they penetrate the medulla, then the cortex, and eventually can result in parenchymal replacement (Iochim and Ratech 2009). Thus although isolated metastatic cells may be found near to the outer surface of the node large macrometastases are more likely to be found in the centre of the node.

Thus a dataset was created that included the spectra from the macrometastases positive nodes (that had been acquired from both the inner and the outer surface of the node) and the spectra obtained from the inner surface of the N_0 negative nodes. When the mean spectra of the macrometastases samples acquired from the inner surface were plotted with the mean spectra of the macrometastases samples acquired from the outer surfaces clear differences are evident. If the mean spectra acquired from the inner surface of the N_0 negative nodes were plotted on the same graph it is clear that the mean spectra from the outer surface of the macrometastases nodes has shifted towards the mean spectra from the true negative nodes (Figure 96).

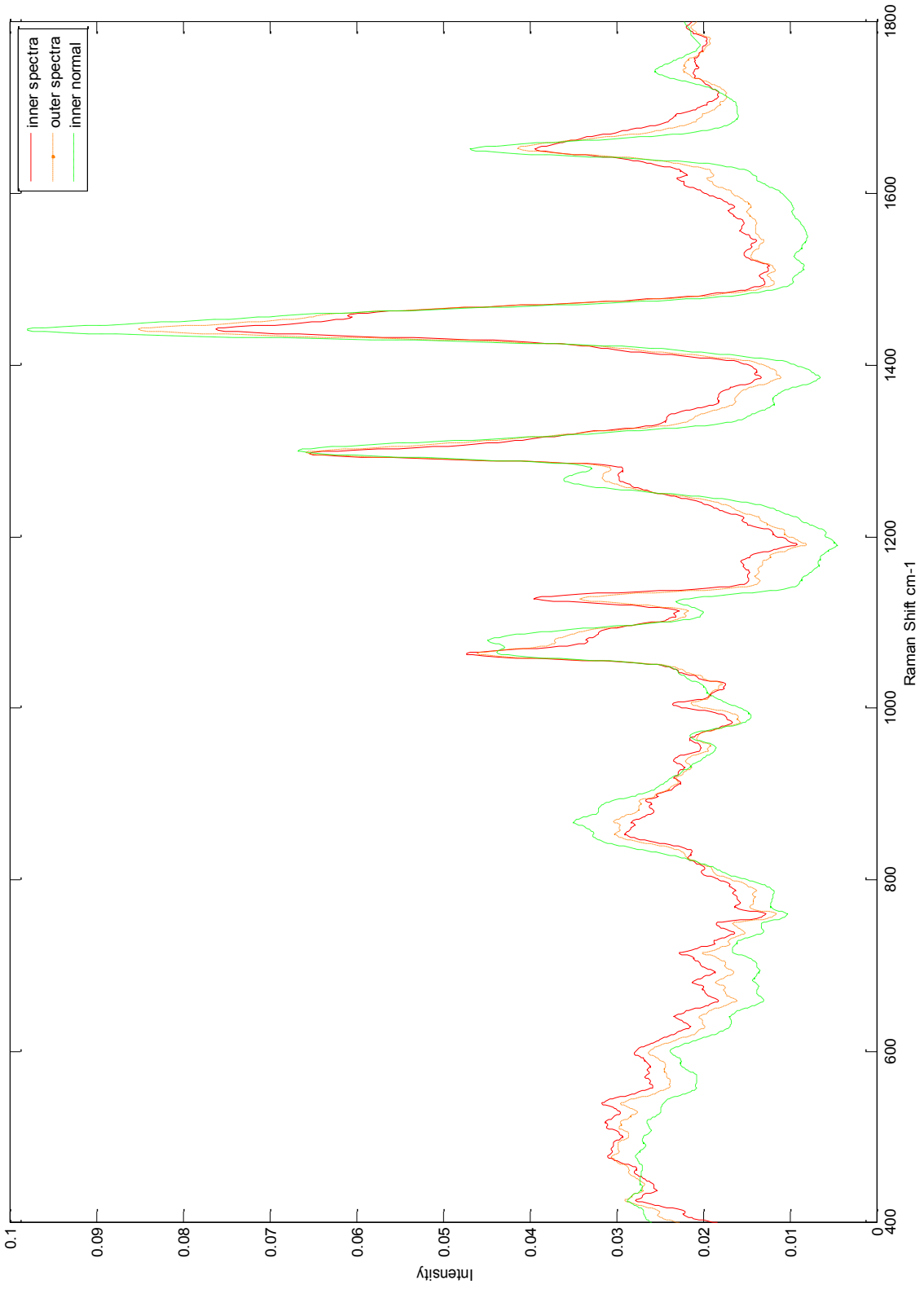

Figure 96 – Mean spectra collected from the outer (orange dash, n=31) and inner (red, n=32) surface of the lymph nodes with metastatic spread and the inner surface of normal nodes (green, n=160).

This is further demonstrated when the contributions of the 34 key peaks described at the start of Chapter 4 are assessed. There were statistically significant differences in the contribution of protein, DNA and lipid. The results demonstrate a shift away from the N_0 nodes but not quite to the level achieved when sampling from the inner cut surface (Figure 97) (Table 27).

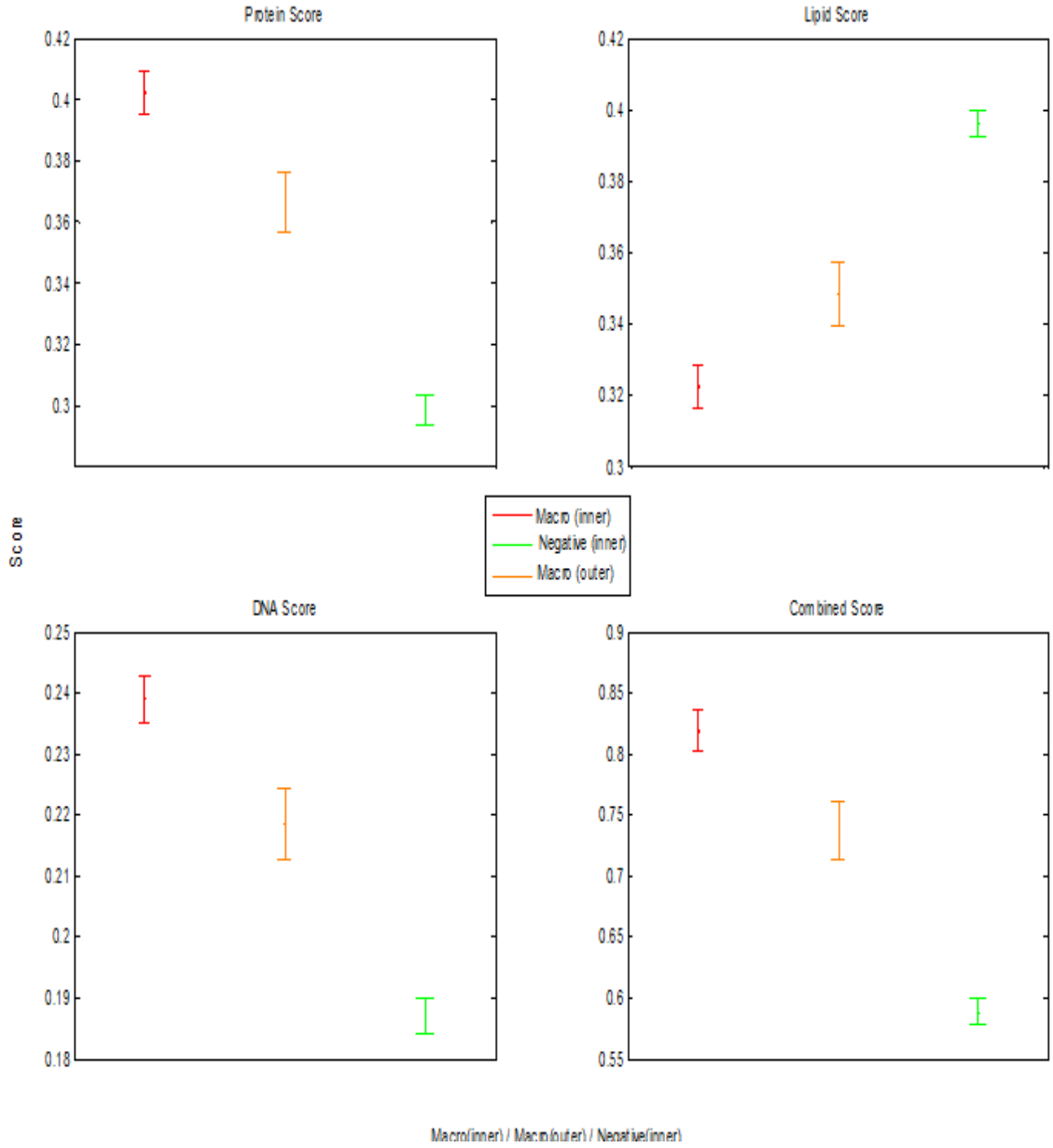

Figure 97 –Mean intensity scores (with 95% confidence intervals) for peaks related to protein, DNA and lipid and a combined score for N_0 inner surface (n=160,green), macrometastases outer surface (n=31,orange) and macrometastases inner surface (n=32, red.)

	Mean Lipid Score (SD, SEM)	Mean Protein Score (SD, SEM)	Mean DNA Score (SD, SEM)	Mean Combined Score (SD, SEM)
Macrometastases Inner (n=32)	0.32 (0.03, 0.005)	0.40 (0.04,0.007)	0.24 (0.02, 0.004)	0.82 (0.06, 0.01)
N_0 Negative (n=160)	0.40 (0.05, 0.004)	0.30 (0.06,0.005)	0.19 (0.04, 0.003)	0.59 (0.04, 0.003)
Macrometastases Outer (n=31)	0.35 (0.03,0.005)	0.368 (0.03, 0.005)	0.2185 (0.02,0.004)	0.73 (0.05, 0.01)
1.Unpaired t-test Inner v. Outer	p=0.004 t=3.74	p=0.007 t=3.6	p<0.001 t=4.3	P<0.001 t=6.5
2.Unpaired t-test N_0 v. Outer	p<0.001 t=4.9	p<0.001 t=6.3	p<0.001 t=4.3	p<0.001 t=17

Table 27: The combined intensity of peaks attributable to lipid, protein and DNA in the macrometastases (inner and outer spectral collections) and N_0 (inner spectral collection) groups. Results of unpaired t-tests confirm the statistical significance of these differences and are also shown.

This effect was further interrogated by using the data to differentiate between the positive and negative samples. PCA fed LDA and leave one node out cross validation was again used as discussed earlier in the chapter.

Using leave one node out cross validation testing the test achieved a specificity of 97.7% (129/132) and a sensitivity of 81% (25/31) at differentiating between N_0 negative nodes (spectra from the inner surface) and macrometastases samples (spectra from the outer surface) (Table 28). This was then compared to the results of the leave one node out cross validation testing of the samples acquired from the inner surface of the macrometastases samples which in this dataset achieved a sensitivity of 93.6% (29/31) and a specificity of 99.2% (131/132).

		Pathology	
		Positive	Negative
Raman	Positive	25	3
	Negative	6	129
		Sensitivity =81%	**Specificity=98%**

Table 28- The sensitivity and specificity table with spectra from the outer surface.

An explanation for the compositional analysis results is that there is greater contribution to the spectra from normal areas of the node when they are acquired from the outer surface. Therefore in the 6 false negatives it could be argued that the spectral features of the metastases were either masked by the normal areas of the node or the probe simply did not collect information from a deep enough volume to detect them. This will have also affected the overall model and may explain the slightly worse specificity. The histopathology reports for these nodes demonstrate that the 6 false negative samples have a mean diameter of 9.33mm which is beyond the sampling depth of the probe, and that there is no evidence of extra nodal spread in any of them. Neither of the false

negatives from the inner surface analysis were correctly placed by assessment of the outer surface. This suggests that currently lymph node assessment from the outer surface of the node is not only, not as sensitive as assessment from the inner surface, but that it may not be complimentary to the inner surface testing either. It should however be noted that the sensitivity remains higher than that reported for frozen section and touch imprint cytology. It therefore appears that whilst not as good as inner surface testing then this might be worth pursuing following the establishment of an effective testing model if the benefits of *in situ* testing were clear.

The dataset was then used to examine the spectra for micrometastases and ITCs Potentially because ITCs are found in the outer capsule of the node it is possible that spectra acquired from the outer surface of the node would be better able to detect these small deposits than those obtained from the inner surface. This however proved not to be the case. Using chemometric analysis a specificity of 99% (159/160) but a sensitivity of only 33% (3/9) was achieved when differentiating ITCs from. When differentiating between micrometastases and N_0 nodes with a specificity of 99.2% the sensitivity was 37.5% (3/8). These are broadly consistent with the results of the spectral analysis of those collected from the inner surface. Again none of the false negatives, from analysis of the inner surface, were correctly placed using the outer surface spectra.

Based on these results nodal analysis based on spectra obtained from the outer surface of the node as opposed to those obtained from the inner surface of the node could not be supported. The results are poorer both for the identification of macrometastases but also micro metastasis and ITCs. Complimentary assessment of both the inner and outer

surface would have not improved the correct classification of the node as the false negatives were present in both groups. If spectral analysis from the outer surface is to be improved then either the benefits of in-situ testing need to be significant enough to overcome the poorer sensitivity or probes with a greater sample depth will be required to overcome the effects of normal tissue which surrounds the metastatic deposits.

4.6. Intraoperative Work - Conclusions

The results in this chapter for the first time demonstrate the efficacy of a portable Raman spectroscopic device at differentiating between positive and negative nodes for patients undergoing axillary surgery for breast cancer, in real time. They are also some of the first results that use Raman spectroscopy at the patient "bed side" to assess tissue.

The results of dataset 1 comparing N_0 negative nodes to nodes positive for macrometastases are unsurprisingly, most promising. The best results achieved are easily comparable, if not better, than many of the currently available techniques. The demonstration of the molecular differences that underpin these results by both interpretation of peak positions and evaluation of the principal components generated using PCA adds further weight to these results. Differences in the protein, DNA and lipid concentrations within nodal tissue are consistent with the anticipated changes that would be expected when a colony of metastatic cells invades an axillary lymph node. The results achieved when including the negative samples from non-N_0 patients and those with micrometastases and isolated tumour cells were less encouraging. They are however important findings as it demonstrates that future models should be built on data

from samples from N_0 patients and samples positive for macrometastases only. Clinically the need to discover either micrometastases or especially ITCs is questionable. If it was felt clinically important then samples used in future studies may need to be multiply sectioned before spectra were acquired to help overcome the issue of sampling depth. The results in the final section suggest that until portable devices with greater sampling depth become available that spectral acquisition from the cut inner surface will remain the mainstay of assessment.

5. Reproducibility

A key concern associated with the introduction of a new diagnostic technique is the reproducibility of the results that it produces. This chapter will examine this by altering key factors in the assessment of tissue using a portable Raman spectrometer. Discussion amongst the project investigators identified three modifiable factors which could influence the results obtained. The first of these is the time between tissue excision and assessment using the Raman device. This along with the second factor identified, the effect and implications of using different spectrometers, was investigated using the nodes collected as part of the series reviewed in Chapter 4. The final factor, the effect of different individuals using the equipment to assess the same tissue was assessed using animal tissue within the laboratory setting. In this chapter the methods and results of the experiments carried out to investigate the effects of altering these three factors will be introduced and discussed.

5.1. Reproducibility Experiment 1 - The effect of alterations in the time from excision to the time of assessment.

5.1.1. Reproducibility Experiment 1 - Methods

The project protocol, discussed in Chapter 4, stipulated that following excision of the node, any fat would be dissected free from the node and the node would then be bisected and assessed using the Raman spectrometer. The tissue was then returned to theatre before the end of the case to reduce the risk of samples being mislabelled. As a result the maximum time that tissue could be assessed post excision was estimated to be

40 minutes. As often more than one sample was collected from each patient the exact time at which the sample was assessed post excision varied. To assess the effect of this time delay on the diagnostic ability of the system an experiment was set up such that nodes were assessed immediately post excision, and then at time delays of 10, 30 and 60 minutes.

8 of the node samples collected from 8 different patients and on 6 different days were included in this study. Following the techniques described in the methods section of Chapter 4, 5 spectral measurements were made immediately after excision and then again 60 minutes later. For 7 of the eight samples intermediate measurements were also made at 10 and 30 minutes after the initial spectrum had been acquired. In between sample acquisitions the tissue was placed on a clean Petri dish. Acquisition of spectra from other samples continued during the intervening time and the node was orientated on the probe in as close to the same orientation as possible for each assessment. Spectra were then interrogated using Matlab® software on a desktop PC. Prior to interrogation a mean spectra (n=5) was created for each sample at each collection time. A mean spectra containing all the spectral information from each time point (n= 40 (time 0), n=35 (+ 10 minutes), n=35 (+30 minutes), n=40 (+60 minutes)). Statistical analysis using a paired t-test and PCA fed LDA was then performed.

5.1.2. Reproducibility Experiment 1- Results.

Histopathologically three of the nodes in this dataset were negative samples from N_0 patients, 2 were non N_0 negative nodes, one was positive for isolated tumour cells, one

for macrometastases and one contained no lymphoid material. The mean spectra for all the spectra collected from all eight samples at each separate time interval were plotted and demonstrated very few obvious differences on initial inspection (Figure 98). To statistically demonstrate this, paired t-tests were performed to compare the mean intensity of each wavenumber at time +10 minutes, +30 minutes and +60 minutes to the intensity at time 0. The null hypothesis was that there was no difference between the intensity of each wavenumber. With 6 and 7 degrees of freedom (in the 10 and 30 minute groups and 60 minute groups respectively) this would be rejected if the t value was greater than 3.14 or 3. In the 10 minute group two wavenumbers at 930 and 1648cm^{-1} recorded t values above 3.14 and in the 30minute group two different wavenumbers at 1074 and 1248cm^{-1} recorded t values above 3.14. In the 60 minute group the greatest t value that was achieved was 2.9 and therefore the null hypothesis was accepted for all wavenumbers. These results supported the conclusion that there were only very minimal changes in the spectra when recorded from the same fresh tissue sample up to 60 minutes apart. However it did not look at individual samples but instead focused on the change in time.

As the critical end point was the diagnostic output of the system further analysis was performed to determine whether the difference in time altered the diagnostic result achieved for each sample. To do this an analytical experiment was designed using the spectra collected from all the 339 lymph node samples in the series described in Chapter 4. Using PCA fed LDA and leave one node out cross validation we were able to calculate both a score for each node at the four different time intervals and a diagnostic result (Figure 99).

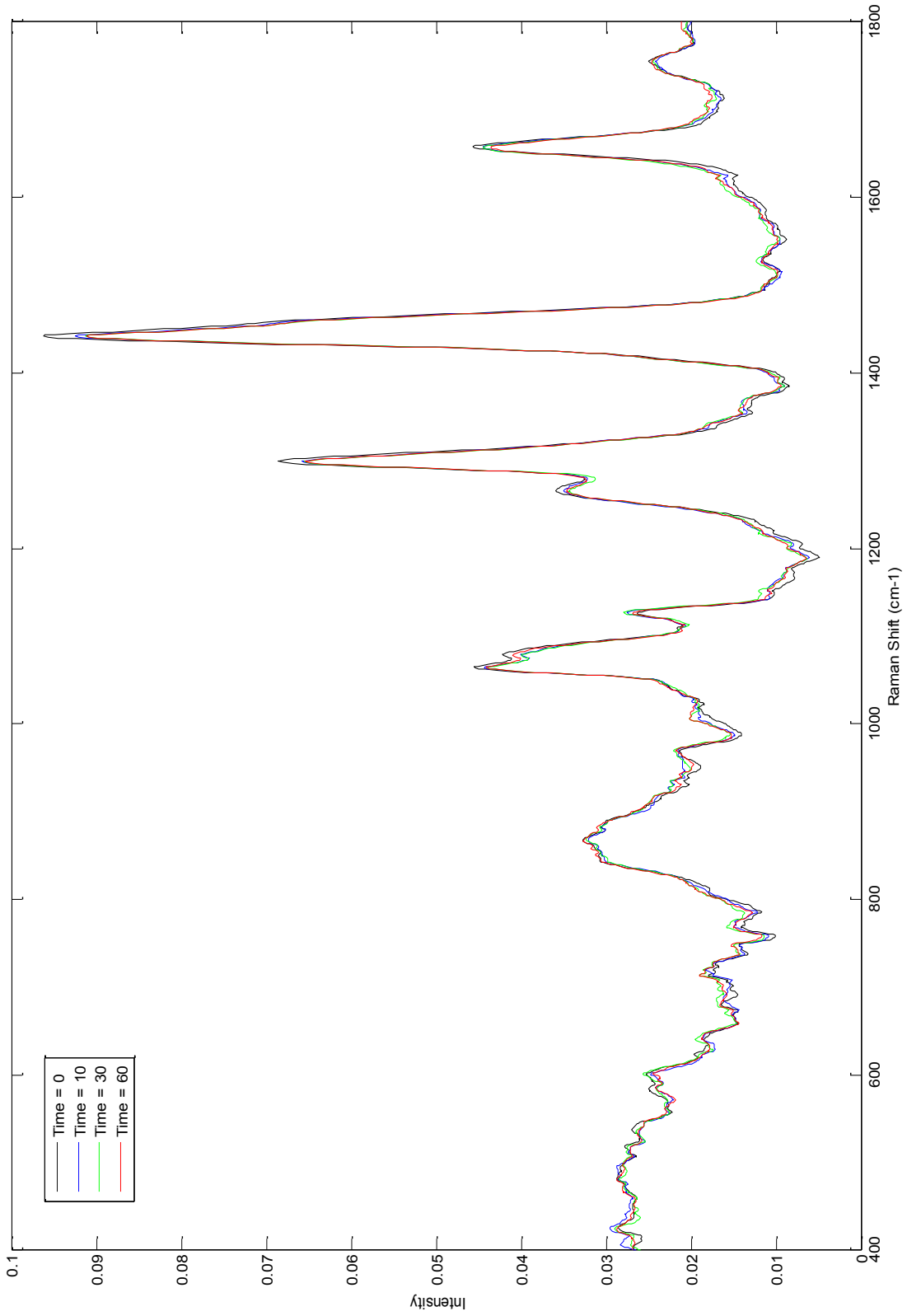

Figure 98 – Mean spectra (n=40 at time 0, n=35 at time +10, n=35 at time +30 and n=40 at time +60) from all nodes taken at different times following excision.

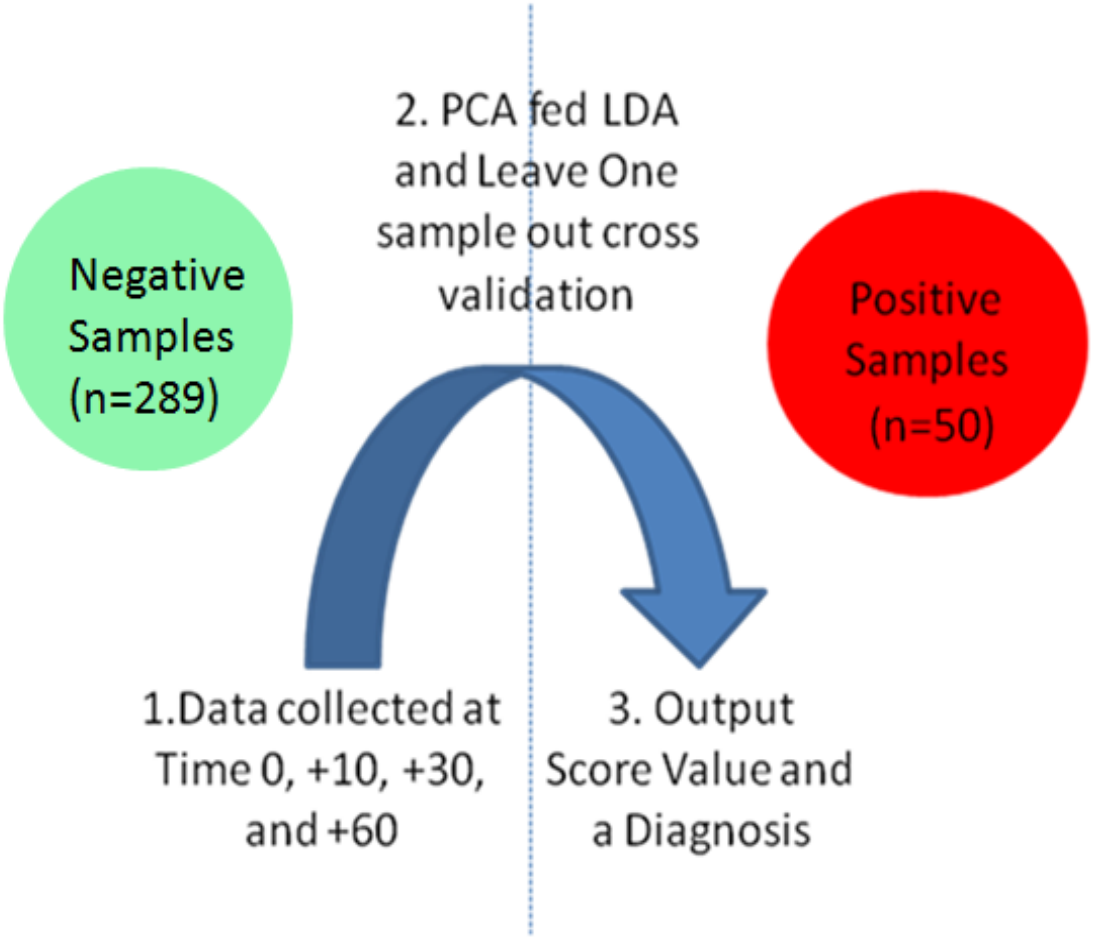

Figure 99 –Diagrammatic representation of the diagnostic assessment of data collected at different time intervals following excision.

To achieve this a dataset termed "negative" that included 289 non positive samples and a dataset termed "positive" that included 50 samples that were positive for macrometastases, micrometastases or isolated tumour cells was created . PCA fed LDA was then performed and a score was generated for each sample at each time point. A paired t-test was then used to determine the statistical significance of the differences in these scores for each sample with changing time. The null hypothesis was that there was no difference in the scores obtained over the different time ranges. With 6 and 7 degrees of freedom we were unable to reject the null hypothesis at the 99% confidence level in

any setting. There were thus no statistically significant differences in the scores recorded for each sample at the three different time points. It was interesting to note the rise in the t value as the time from the first spectral acquisition increased (Table 29). It is questionable, although this hasn't been confirmed in this study, whether beyond 60 minutes the score achieved for each sample may demonstrate significant differences. This needs to be given careful consideration as further trials and experiments are planned and set up.

The negligible affect of time, up to 60 minutes, from first spectral acquisition was further emphasised by the results achieved when projecting the data onto the LDA model (Figure 99). In all of the 8 samples the same pathological classification was made in comparison to time point 0 at time points +10 minutes, +30 minutes and +60 minutes (Table 30).

Time Point	Sample Numbers	Mean difference in sample LDA score between time 0 and time point	Standard error of the difference	t-value	p value
10	7	-0.0004	0.002	0.17	0.87
30	7	-0.003	0.003	1.0	0.3554
60	8	-0.004	0.002	1.96	0.09

Table29: Difference between the mean LDA score achieved at time 0 and at time points +10 (n=7), +30 (n=7) and +60 (n=8) minutes. Statistical significance of this difference is given by the t value and p values following a paired t-test. None of the time points have statistically significant differences but they are approaching significance at 60 minutes.

Sample	Time 0	Time 10	Time 30	Time 60
1	Neg	Neg	Neg	Neg
2	Neg	x	x	Neg
3	Neg	Neg	Neg	Neg
4	Neg	Neg	Neg	Neg
5	Neg	Neg	Neg	Neg
6	Pos	Pos	Pos	Pos
7	Neg	Neg	Neg	Neg
8	Neg	Neg	Neg	Neg

Table 30 - LDA based classification at time point 0, +10, +30 and +60 minutes. There is no difference in any of the 8 node samples at all time points (neg=negative, pos=positive).

5.1.3 Reproducibility Experiment 1- Conclusions.

As real time clinical use of Raman spectroscopy becomes closer the results of this study are pivotal. The vast majority of published Raman based studies to date are based on snap frozen samples assessed within the laboratory setting. These results support the acquisition of spectra from fresh tissue up to 60 minutes after excision. In the context of this project this time is well beyond the time available for intra-operative analysis. As has already been discussed this time period is approximately 40 minutes and thus these results support the validity of results that are achieved within this time.

5.2. Reproducibility Experiment 2 -Use of different spectrometers.

If Raman spectroscopy driven diagnostic models are to be used clinically then it is apparent that more than one spectrometer will need to be used. Indeed it may be that many spectrometers are used at different sites based on a classification model derived from one or more spectrometers. To examine the effects of using different spectrometers a MiniRam I, a similar but earlier model of the MiniRam II was obtained from Pacer UK, the UK distributor of B&W-Tek Raman spectrometers. This spectrometer was then used to acquire spectra alongside the MiniRam II during 6 days of intra-operative theatre based testing.

5.2.1. Reproducibility Experiment 2 – Methods.

To investigate the effect of using two different spectrometers an experiment protocol was set up such that each sample could be assessed using the two systems. 5 spectra were acquired from 14 node samples, from 9 different patients over 6 separate days in the series described in Chapter 4. Each sample was placed on the probe and 5 spectra were recorded using one spectrometer as described in the methods section of Chapter 4. The collection and excitation ends of the probe were then transferred to the other spectrometer and a further 5 spectra were obtained without moving or touching the node. 8 nodes were assessed first with the MiniRam I and 6 with the MiniRam II to avoid the confounding error of time. A total of 140 spectra were included in the data analysis. All data was assessed using Matlab® software. Initial interpretation of the results was made difficult as the computational method by which data was recorded and

saved by each system was slightly different and resulted in a peak shift when the raw data was plotted. Subsequently this experiment also investigated whether the correction methods that have previously been described (Chapter 4) would help overcome this.

PCA fed LDA was used to try and split the data based on the type of spectrometer used. A paired t-test was then performed and finally leave one node out cross validation testing was used to determine any differences in the classification of samples by the two systems.

5.2.2. Reproducibility Experiment 2 – Results.

Following histopathological analysis 10 of the nodes included in this dataset were negative; one was positive for isolated tumour cells, one for micrometastases and one for macrometastases. As described in Chapter 4 initial spectra correction was based on the position of the cyclohexane peaks. This helped to overcome the obvious shift that was evident in the two groups (Figure 100, 101, 102). Despite this correction the two groups could easily be differentiated by chemometric analysis. However the Mahalanobis distance, which is a measure of the variability between the two groups, fell from 4090 to 104 after this initial corrective procedure.

The second step in correcting the spectra was based on the green glass standard. The mean green glass spectra obtained from the two spectrometers were markedly different (Figure 103). This difference was corrected for all of the spectra acquired (Figure 104). When PCA fed LDA was performed on this corrected dataset the Mahalanobis distance fell further to 74.

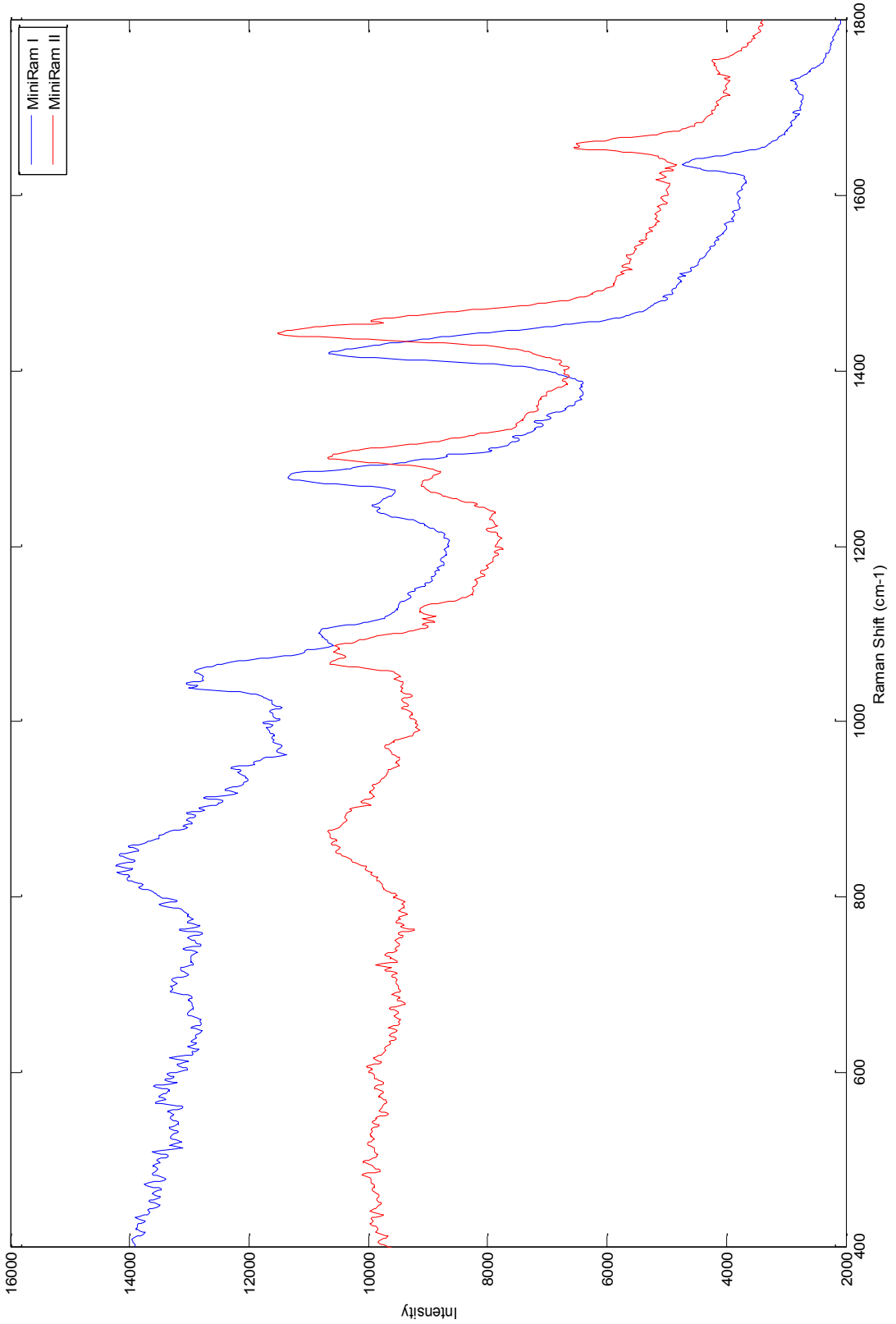

Figure 100– Mean spectra of nodal tissue collected with two different portable Raman spectroscopy devices (MiniRam I, n=70 (blue), MiniRam II, n=70(red)).

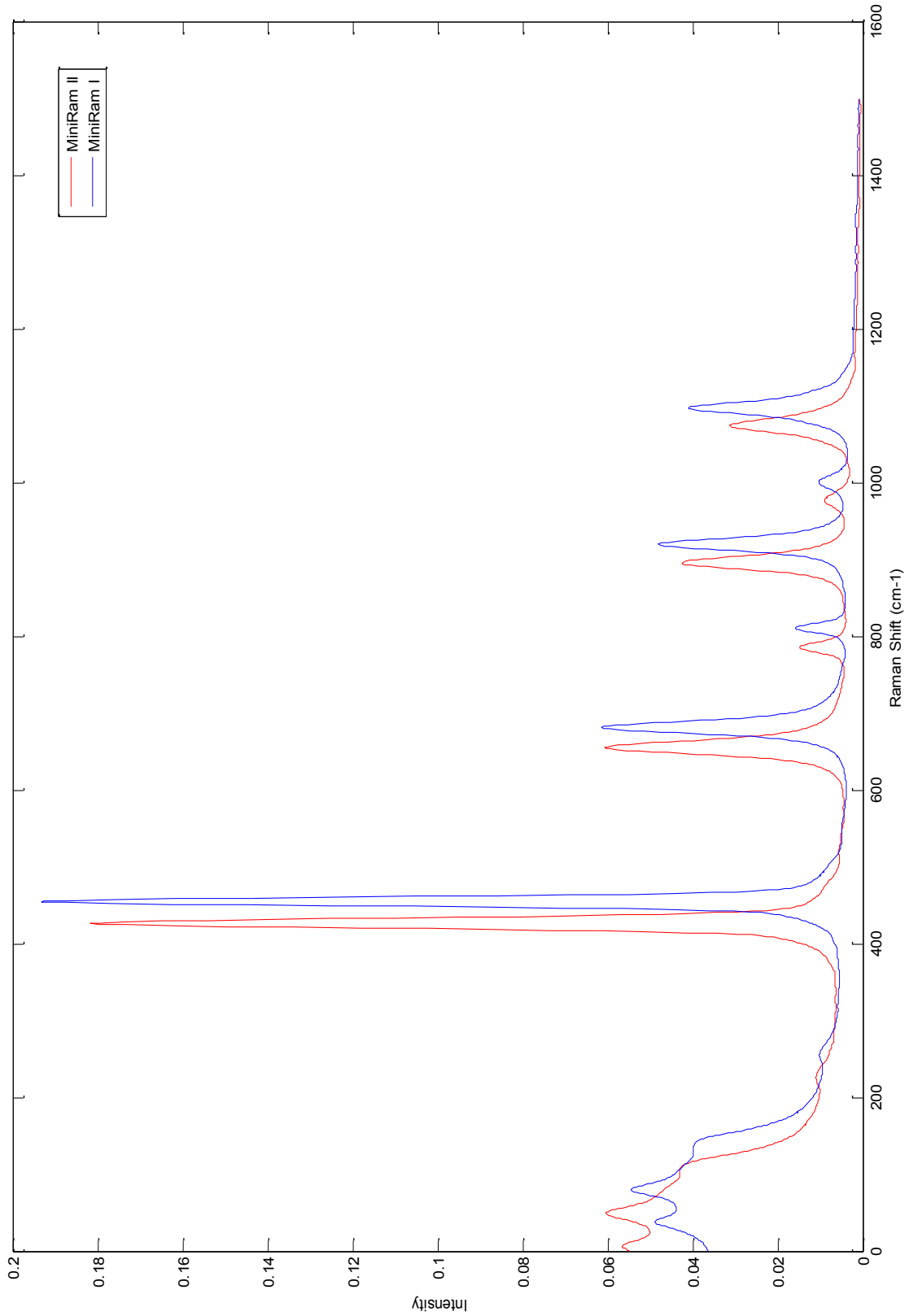

Figure 101 – Mean spectra of cyclohexane standards recorded with two different Raman spectroscopy devices (MiniRam I, n=6 (blue), MiniRam II, n=6(red)).

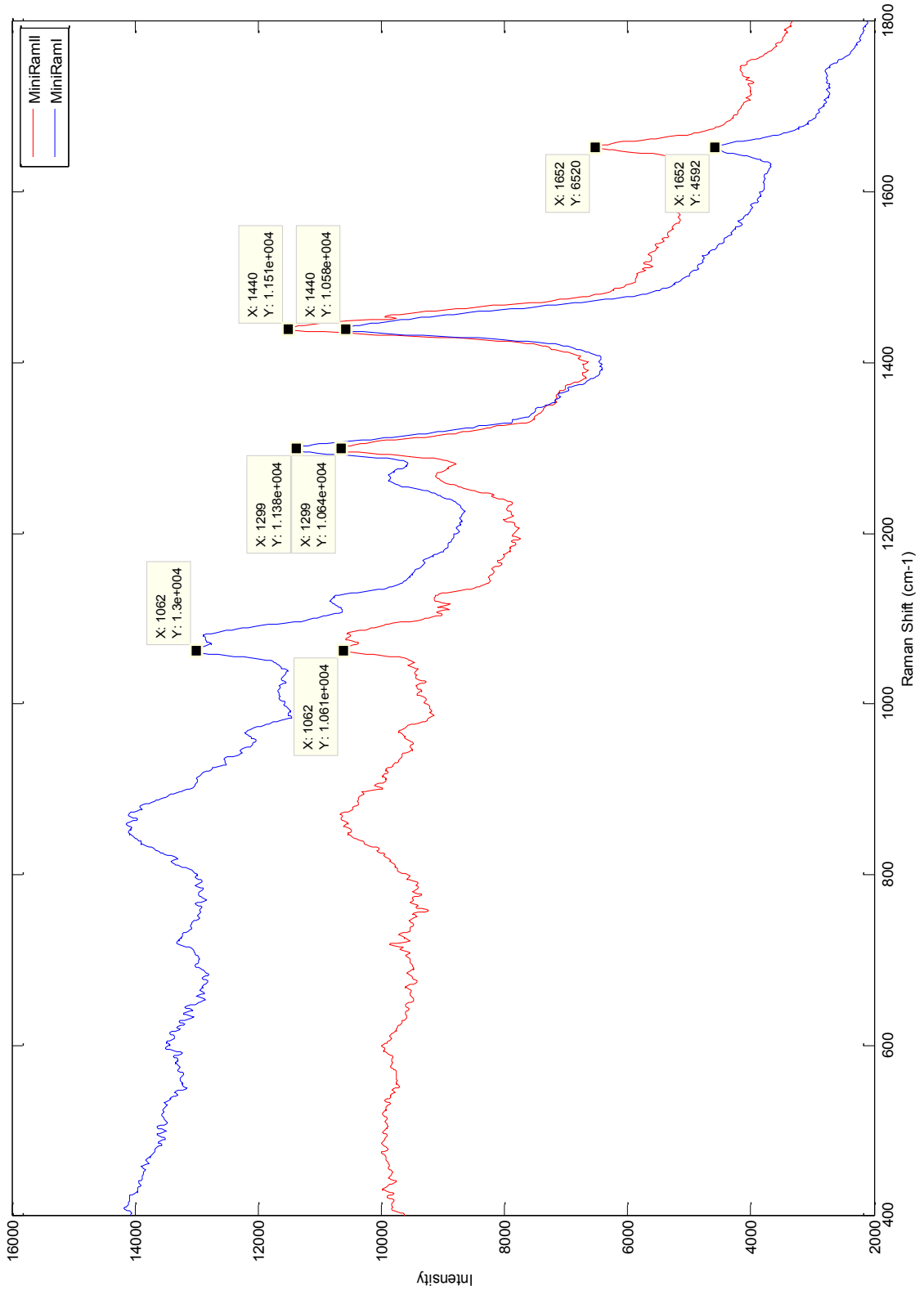

Figure 102 – Mean Spectra of nodal tissue recorded with the two different Raman spectroscopy devices after shift correction (MiniRam I, n=70 (blue), MiniRam II, n=70(red)).Labels included for clarity and to demonstrate the position of prominent peaks.

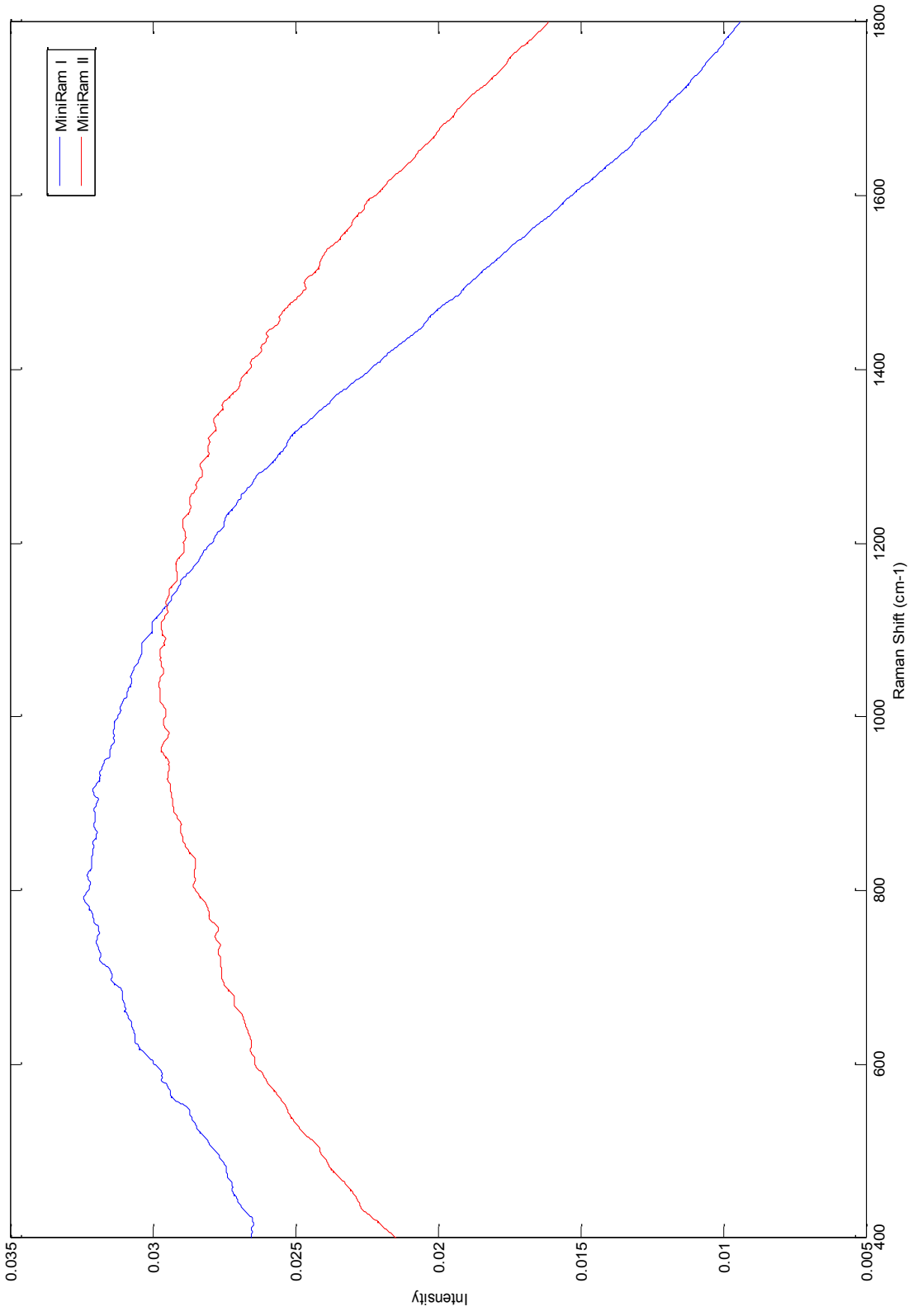

Figure 103 – Mean Spectra of green glass standards recorded with two different Raman spectroscopy devices (MiniRam I, n=6(blue), MiniRam II, n=6(red)).

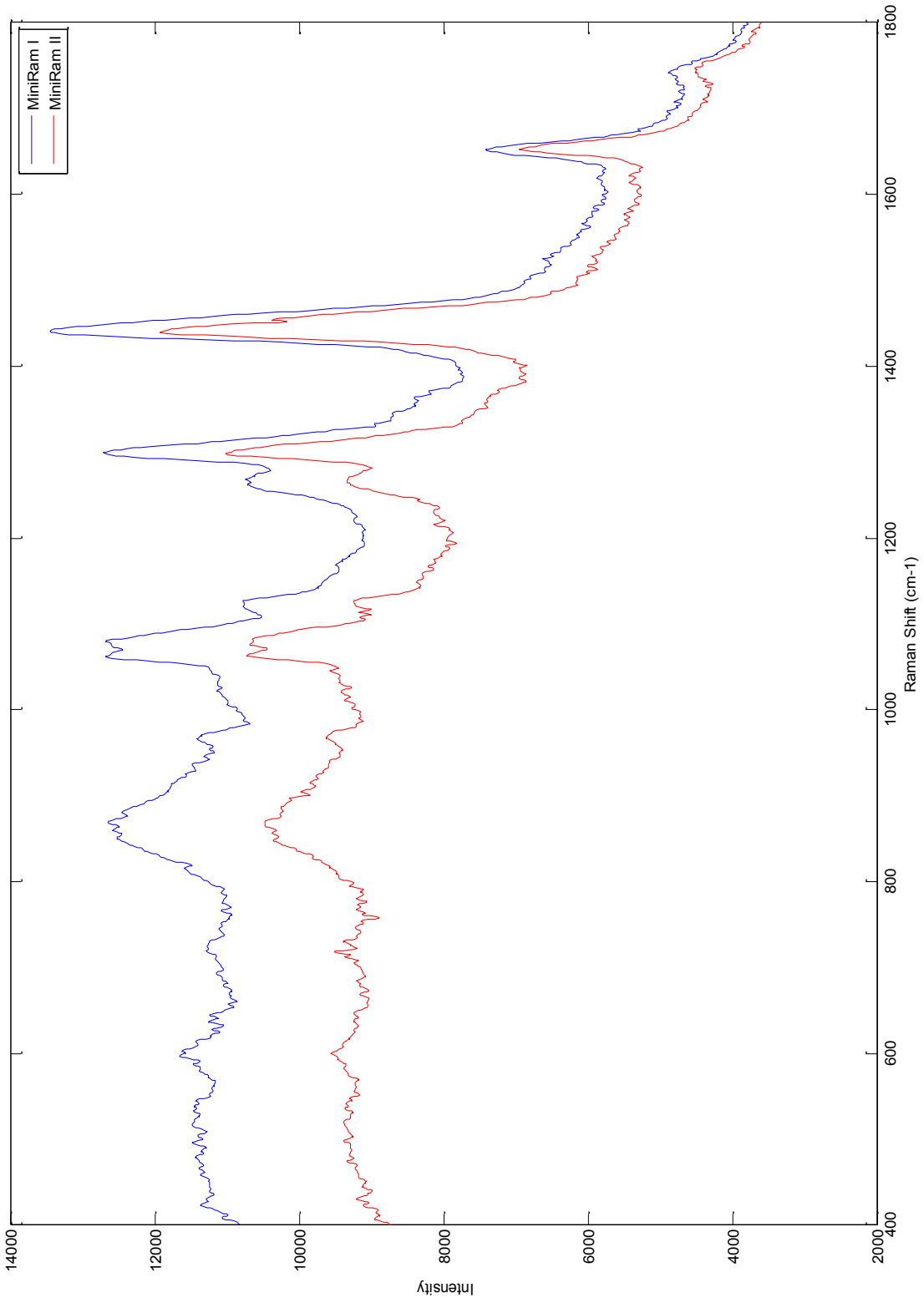

Figure 104– Mean spectra of nodal tissue collected with two different Raman spectroscopy devices after shift correction and green glass correction (MiniRam I, n=70 (blue), MiniRam II, n=70(red)).

Following the protocol in the previous chapter the next step involved baseline correction the data of the data, followed by smoothing and then normalising it. After each of these steps the Mahalanobis distance was calculated and continued to fall to 73, 64 and 26 respectively.

Following all stages of correction the mean spectra of the 14 node samples and the cyclohexane standards collected from each spectrometer were plotted (Figure 105, 106). The similarity of the two mean spectra was now more visible. This was supported by the Mahalanobis distance which had fallen from 4090 to 26. Differences still remained evident and these were highlighted when a paired t test was performed on the data.

The null hypothesis of the t-test was that there was no difference between the spectra obtained using each spectrometer following correction. With 13 degrees of freedom the null hypothesis would be rejected if the t value was greater than 2.65. The null hypothesis was rejected for 35 wavenumbers suggesting that even after correcting the data there are areas of significant difference between the spectra obtained from the two spectrometers (Figure 107).

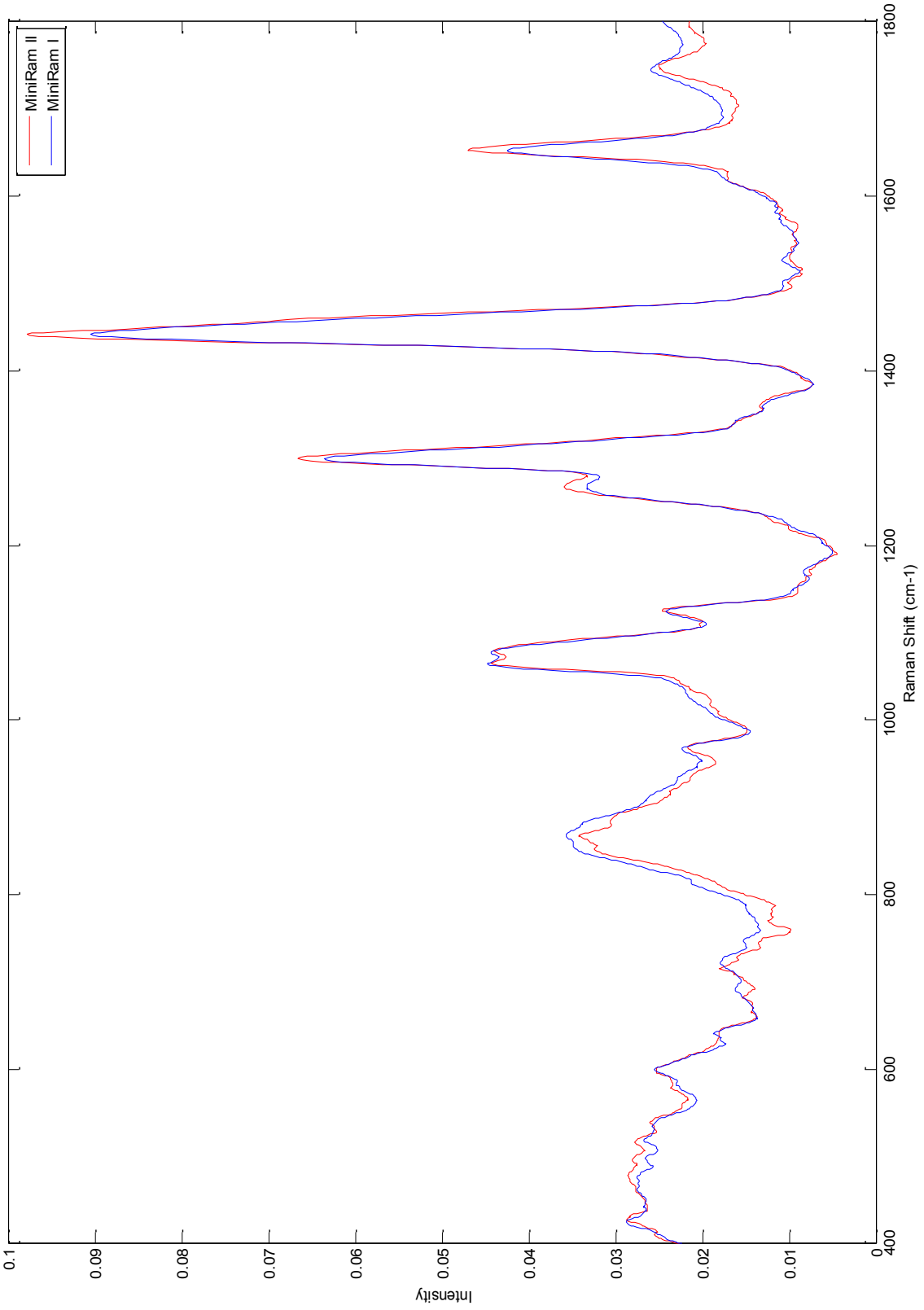

Figure 105 – Mean Spectra of nodal tissue recorded with two different Raman spectroscopy devices after correction. (MiniRam I, n=70 (blue), MiniRam II, n=70(red)).

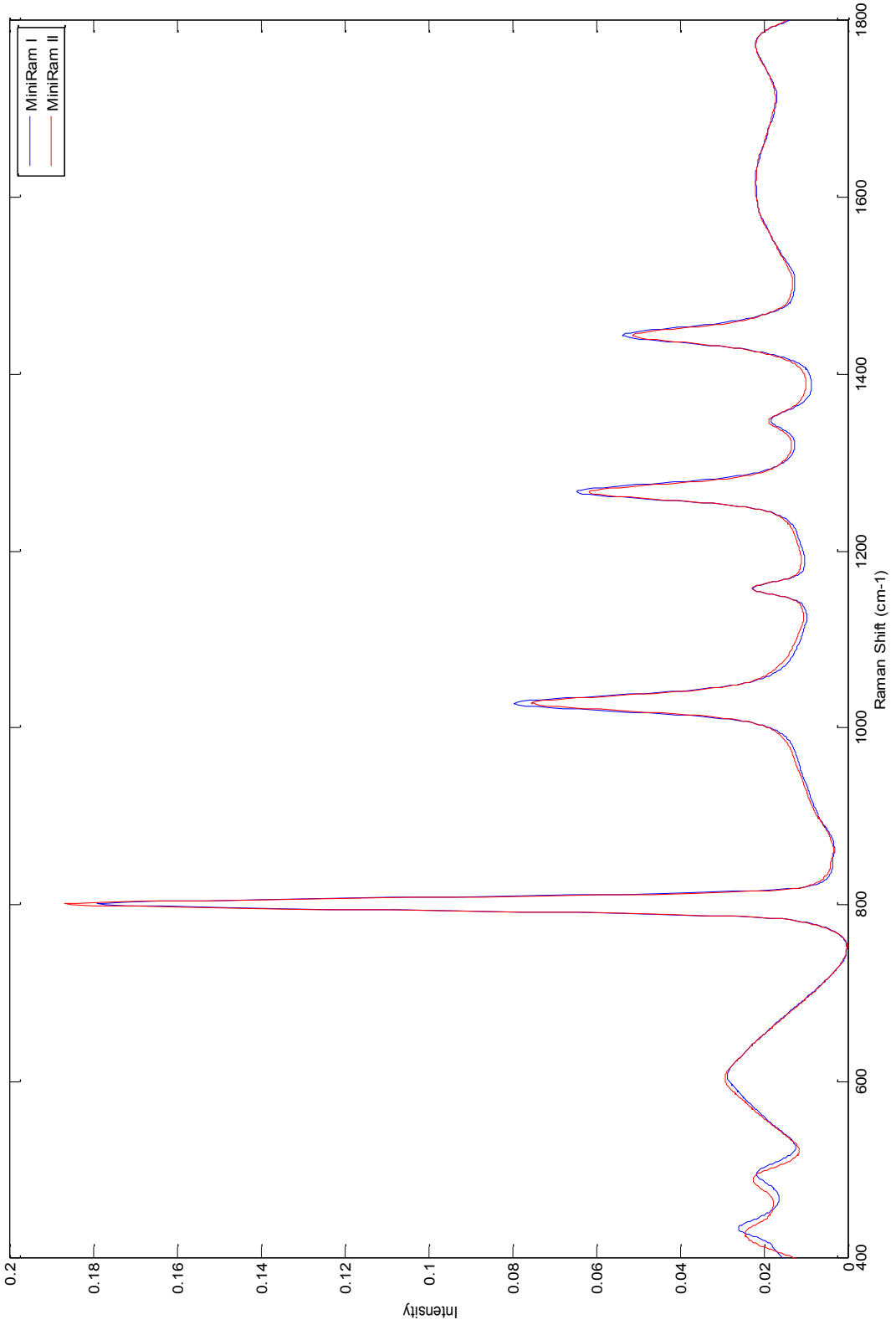

Figure 106 – Mean Spectra of cyclohexane standards recorded with the two different Raman spectroscopy devices after correction (MiniRam I, n=70 (blue), MiniRam II, n=70(red)).

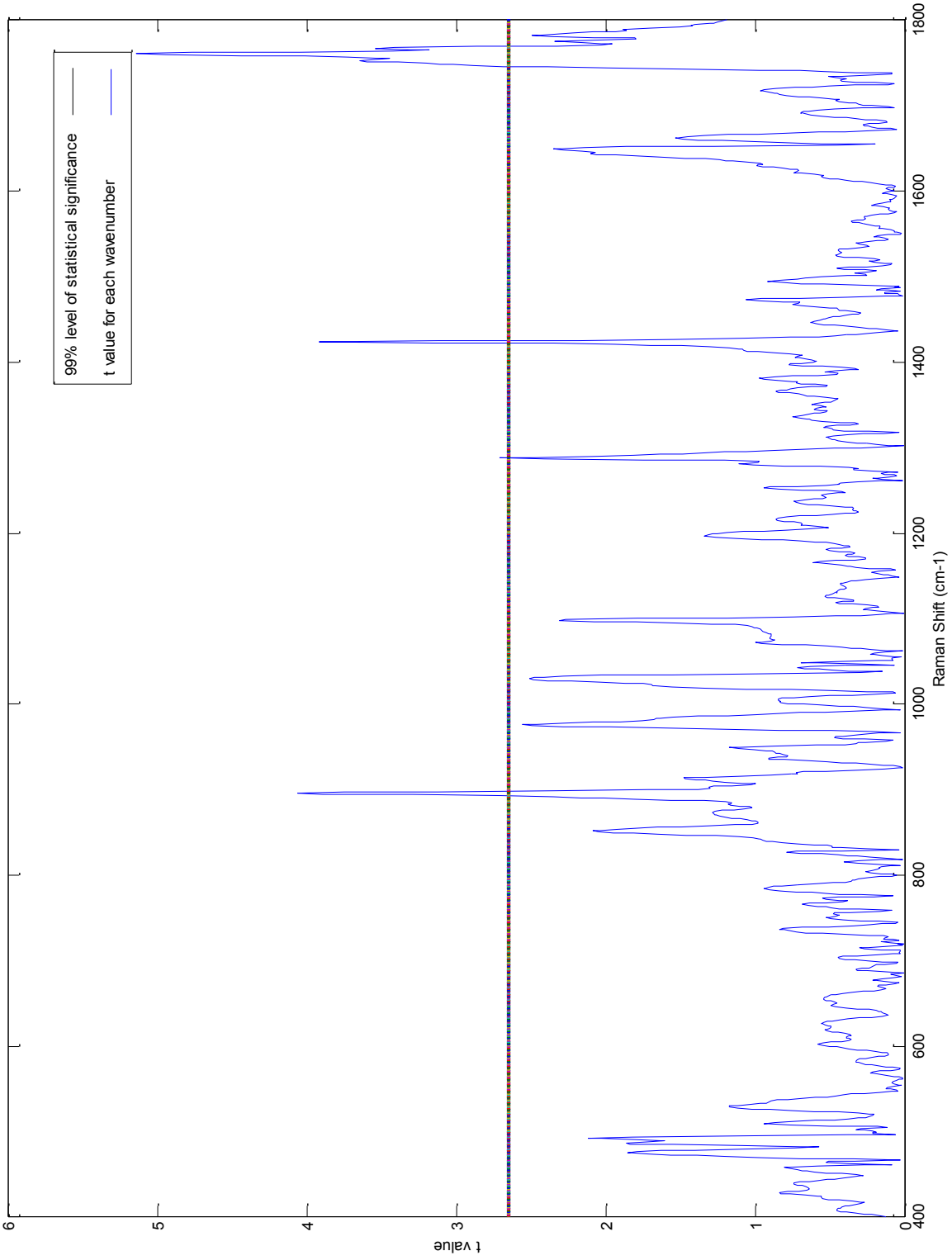

Figure 107 – Statistical significance of the residual spectral differences after correction to overcome the use of two different Raman spectrometers (x axis = Raman Shift (cm^{-1}), y axis = t value).

When these results were plotted it was clear that a significant number (24/35) of these differences occurred in the region between 1747 and 1771 cm^{-1}. As detailed in Chapter 4 there were very few significant peak differences above 1747cm^{-1}. If the dataset was cropped at 1748cm^{-1} the Mahalanobis number was further reduced to 18. Whilst recognition of the differences was important the effect on the diagnostic outcome was the key factor that the study hoped to demonstrate. Previous experiments, discussed in Chapter 4, differentiating between negative v macrometastases nodes achieved a Mahalanobis distance of 31.

Thus the differences in spectra obtained by the two spectrometers were less than the spectral differences between the two groups. It was thus felt likely that the results from either spectrometer could still be used to differentiate between the pathological groups. To test this PCA fed LDA and leave one node out cross validation was used to calculate a classification score for each sample based on the spectra collected with each spectrometer (in a similar way to the previous experiment looking at the effects of time). In the cross validation test the spectra from all the intra-operative node series (n=339) that were collected with the Mini Ram II were used. The classification scores for each sample in the series were then used to perform a paired t-test. The null hypothesis was that there was no difference between the scores achieved using the two systems. The null hypothesis would be rejected if the t value was greater than 2.65. The calculated t value was 1.1281 and thus the null hypothesis was accepted. The cross validation analysis classified each node based on the results achieved and 13/14 node samples were placed in the same pathological category. Only one sample, a node that had micrometastases on histopathology, was changed from a positive classification to a negative one.

5.2.3. Reproducibility Experiment 2 - Conclusions

Drawing conclusions from this experiment is important for the long term viability of Raman spectroscopy as a diagnostic tool. Although these results are drawn from a relatively small dataset they are one of the first that directly compare spectra acquired from human tissue in a real time clinical setting using two spectrometers. The correction protocol, described in Chapter 4, appears to give good if not perfect spectral correction. Although 35 of the wavenumbers show statistically significant differences only 10 of these were between 400- 1747cm^{-1} which equates to 0.7% of the spectra in this region. Data analysis in Chapter 4 did not highlight any significant peak differences between positive and negative nodes above 1747cm^{-1}. Importantly there was no statistical difference between the classification scores obtained for each node using either spectrometer. Only one node was re-classified using the Mini Ram I. This node was in the micrometastases group and had a classification score that placed it on the border between the positive and negative groups. These results are therefore encouraging and suggest that applying diagnostic models recorded with one spectrometer to prospective data collected from multiple spectrometers could be possible. Further testing with larger datasets and multiple spectrometers will be required prior to the clinical use of any Raman based diagnostic model.

5.3. Reproducibility Experiment 3 - Multiple Users.

One of the key elements of reproducibility is that multiple users should be able to use the equipment and still achieve the same diagnostic results. This is vital if the spectrometer is to be used in a clinical environment by multiple users often with varying levels of experience. An experiment was thus designed whereby three samples were measured using the same spectrometer by 6 individuals. 1 user had extensive experience of using the equipment, 2 had previously used the equipment on a limited basis and 3 were naïve to the system.

5.3.1. Reproducibility Experiment 3 – Methods.

In the experiment each user was given a standard instruction sheet and acquired spectra from the three samples in the same order. They were blinded to the composition of the samples they were measuring. 5 spectra were acquired from each sample and saved automatically using a standard function that was built into the spectrometer. The data was then transferred to Matlab® for further assessment. Following spectral correction (as detailed in Chapter 4), all the spectra from each sample were plotted. PCA fed LDA as outlined previously was employed to separate the 3 sample groups.

5.3.2. Reproducibility Experiment 3 – Results.

The spectra collected by each individual appeared broadly similar with only minimal differences on initial inspection of each sample group (Figure 108-110).

PCA fed LDA was then performed to test whether the spectra recorded by each individual could be used to differentiate the tissue into separate groups. A sensitivity and specificity of 100% was recorded for each of the 3 groups. As can be appreciated from reviewing the mean spectra for each sample it was much easier to differentiate the spectra from sample c from the samples a and b (Figure 108-110). There was a degree of variation in the spectra collected by each user but this was not significant enough to prevent each sample being correctly grouped using PCA fed LDA (Figure 111) (Table 31). One possible explanation for these differences was a slight difference in the position of the sample when it was placed on the probe tip. However despite this, these results demonstrate that the equipment and technique can be used to differentiate between different samples independent of who measured the sample.

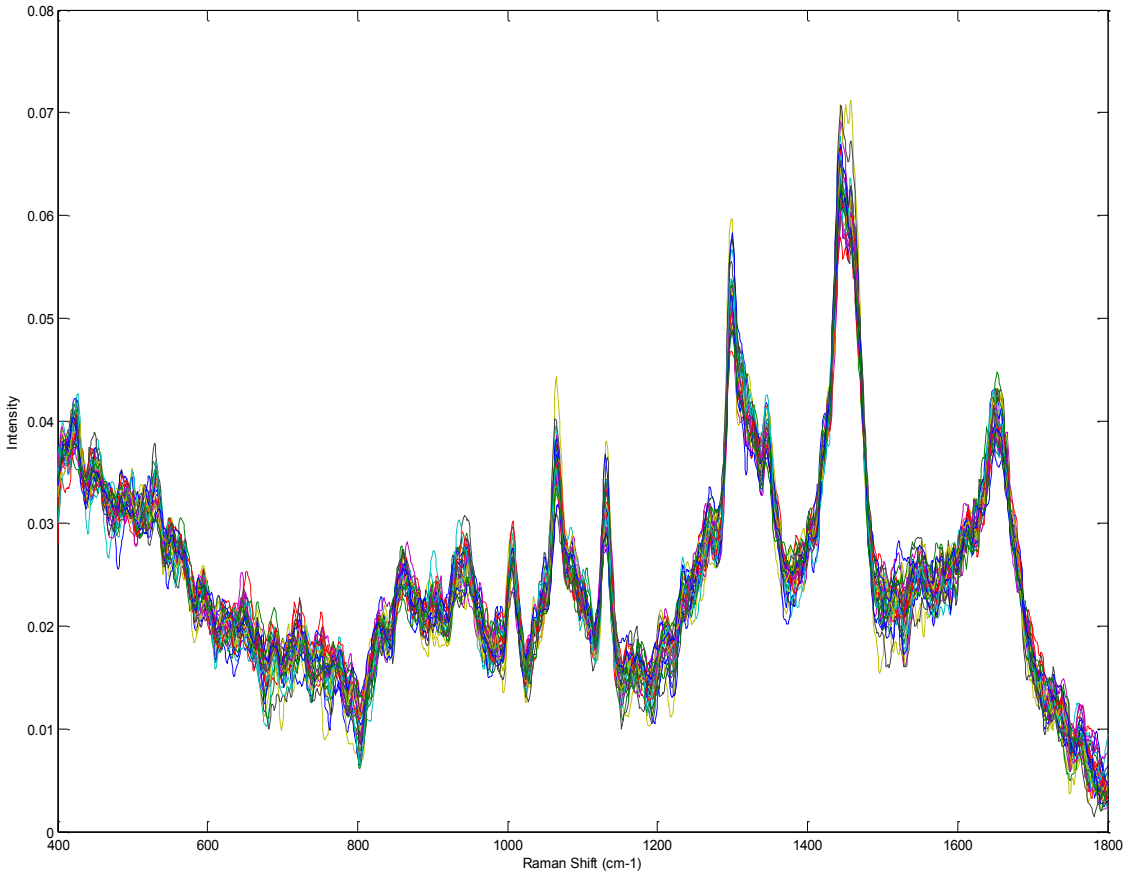

Figure 108 – All spectra collected by all 6 individual users from sample A (n=30).

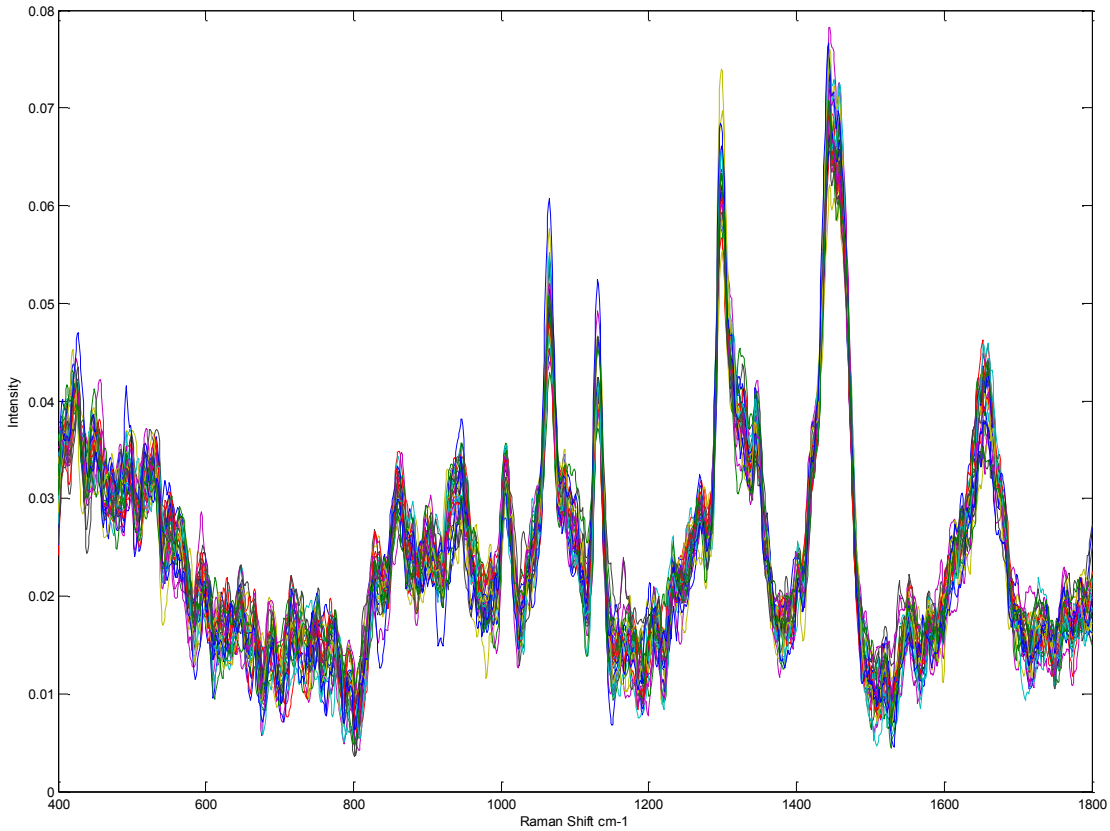

Figure 109 – Spectra collected by all 6 individual users from sample B (n=30).

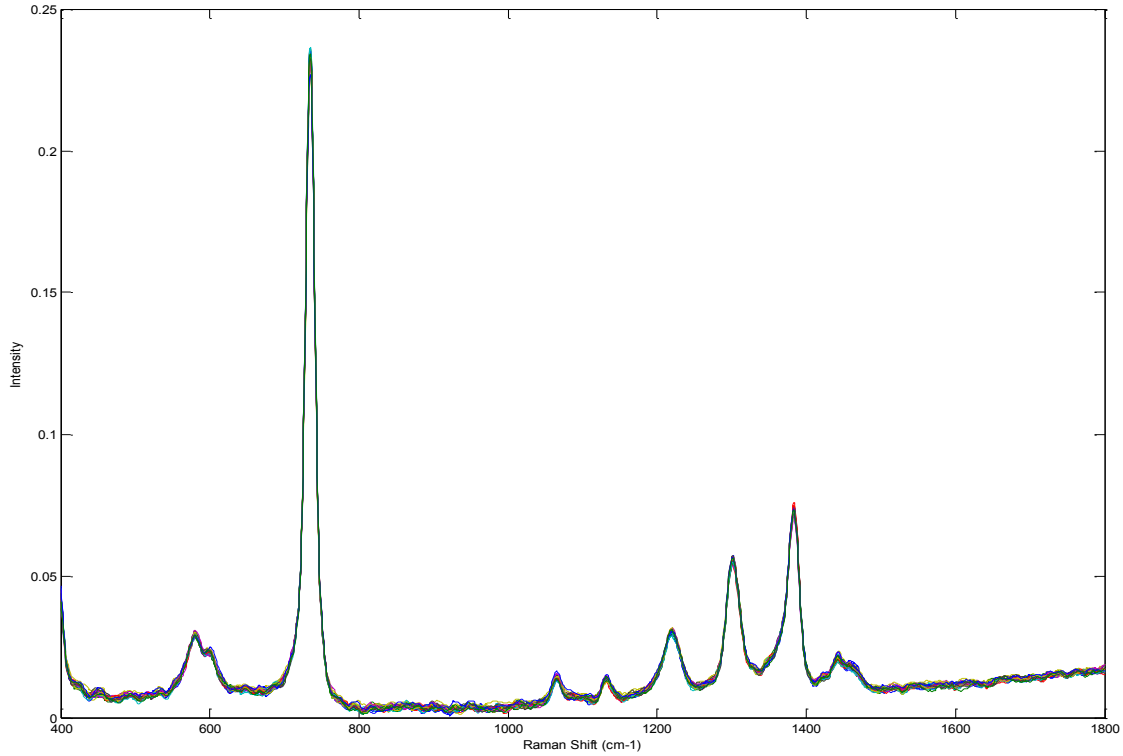

Figure 110 – Spectra collected by all 6 individual users from sample C (n=30).

	Sample A	Sample B	Sample C
Sample A	30	0	0
Sample B	0	30	0
Sample C	0	0	30

Table 31- Results demonstrating 100% sensitivity and specificity independent of the assessor

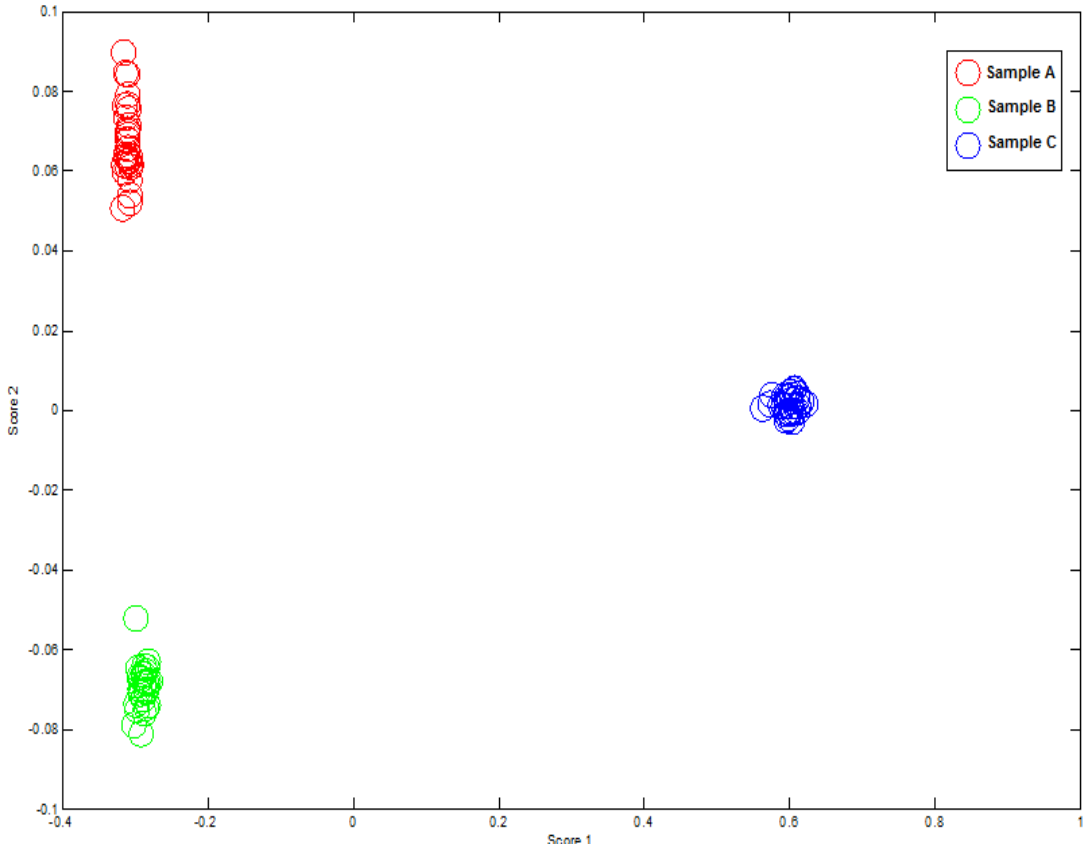

Figure 111 – Separation of the three groups based on PCA fed LDA scores for all the spectra collected by 6 different users

5.4 Reproducibility Experiment 3 – Conclusions.

The results presented in this chapter touch on what will in turn become a much wider area of research. Proving that results obtained using different spectrometers by different individuals at different times after removing the tissue from the body will be vital if this technique is to be used as part of main stream diagnostics in breast cancer.

Much more thorough testing will of course be required to satisfy the appropriate regulatory bodies than presented here. However these results for the first time start to explore these concepts and as a provisional set of results they appear very promising.

6. Discussion

Breast cancer is a disease which attracts a great deal of clinical research, of which this Raman based study, is one such example. There is a strong base of knowledge that supports the use of Raman spectroscopy as a method of differentiating between normal and malignant tissue. As systems have developed researchers have become increasingly excited about moving the research from the laboratory to the patient's bedside. This is one of the first studies to take this move. By moving to the patient the study is conducted in real time, on fresh tissue. By coupling smaller spectrometers to mathematically based diagnostic algorithms this study supports the use of Raman spectroscopy as a rapid, accurate, non destructive and potentially affordable diagnostic test.

At the start of this study there were two key questions which needed to be answered. Could a portable Raman spectrometer be used within the theatre environment and could it achieve results at differentiating between normal and metastatic nodes that were comparable to other modalities? If both were answered positively then the final question would be how can the results achieved be used to take the study forward?

6.1. Could a portable Raman spectrometer be used within theatre?

Much of the clinical Raman spectroscopy work to date has been performed within the laboratory within very stable and regulated environments. Overcoming factors

associated with both the operating theatre environment and the methods employed as part of surgical technique was thus a crucial first step in this process.

Anticipated variations in temperature have been demonstrated to have a limited effect on the spectra collected. The operating lights and ambient room lighting has been overcome with the use of light eliminator. As it turned out, because of safety precautions, this was not as vital as anticipated as all of the intra-operative work was performed within a small room adjacent to theatres. None the less this work was an important step which will allow the spectrometer to be used within theatre in the future.

One of the key concerns about any new diagnostic modality, particularly within surgical oncology, is the importance of avoiding cross contamination. The devastating effects of one patient undergoing, ultimately unnecessary, treatment based on the results of another patient must be avoided. This study utilised two different mechanisms to avoid this. The first and most important of these was ensuring that all node assessment was performed before the patient left the operating theatre. The second technique was the use of a sterile sheath. Early testing demonstrated that this had minimal effect on the spectra collected and was thus used throughout the clinical phase of this study.

The time taken to collect spectra and thus "assess" the node is not only critical to avoid clinical errors but is also important when considering the ultimate aim of guiding a clinical decision as to the need for an axillary clearance. An intra-operative test needs to provide results in a time frame that avoids any delays that would disrupt an operating list and mean that the patient is anaesthetised for a longer period of time than necessary.

Current techniques are performed on the excised node whilst the operating surgeon continues with the excision of the breast tumour. If an axillary clearance is deemed to be required then this is performed as the final part of the operation. Within this study no patient underwent further axillary surgery based on the results of either the Raman spectrometer or any other intra-operative method. Ensuring that all assessment took place before the patient left theatre, initially to prevent cross-contamination of samples, also demonstrated that the results could be delivered without undue delay if an axillary dissection was deemed necessary. It can be argued that the "assessment" carried out in this study was not complete as there was no diagnostic output, but it is anticipated that algorithms used to provide this answer will be rapid and measured in seconds.

The time frame of assessment took on further importance when the effects of time post excision of tissue were investigated. The results of the reproducibility study looking at the effects of time post excision suggest that there are no statistically significant differences up to 60 minutes after tissue removal. The trend in the t-value does however suggest that this may not be the case much beyond this time frame, and will need to be considered when planning future studies.

Introducing a new step in the management of a particular condition requires that the additional step is compatible with the established techniques. One of the concerns at the outset of the study was the effect of Patent V blue dye on the spectra obtained from the lymph nodes. Within the UK this dye is widely used to help identify the lymph node and any new test will need to be compatible with it. Although initial studies suggested that this was likely to be problematic, further studies on nodes in the Dudley series

disproved this. The identification of the principal component of blue dye and its subsequent removal from reconstituted spectra had little effect on the diagnostic potential of the results achieved. One potential problem as this project moves forward is that, although blue dye is widely used in the UK, other markers such as Indomethacin Green are used elsewhere and this will need to be accounted for.

6.2. Could a portable Raman probe achieve results at differentiating between normal and metastatic nodes that were comparable to other modalities?

In any clinically based study the "buy-in" of the clinicians whose patients you hope to recruit is vital. Before embarking on real time clinical work it was important to demonstrate to them why a diagnostic test based on Raman spectroscopy might work. This involves both a study of the previously published literature and early feasibility studies using the equipment that we had selected.

Previous work, as discussed in Chapter 2, has consistently shown, within breast tissue, that the key differences in the spectra obtained are an increased contribution of lipid in the normal tissue relative to an increased contribution of protein and DNA in the malignant tissue. These results are supported by FTIR studies in axillary, oesophageal and head and neck cancers, and by mapping Raman studies on axillary lymph nodes performed within our own unit (Smith 2005). The mapping studies and subsequent probe modelling of the data produced were carried out on tissue with a depth of several μm. To replicate this tissue depth in this study would have involved a significant preparatory step. This would have extended the time frame beyond clinical relevance

and potentially damaged tissue that remained important for the staging and thus management planning of the patients who agreed to take part in the study. A number of experiments were set up to estimate the depth from which spectral information could be collected using the MiniRam II spectrometer and probe. Whilst it is recognised that there are a number of limitations to these studies and that interpretation should therefore be performed with caution the results suggest that spectral information could be detected at depths up to 3mm. This was crucial as the vast majority of lymph nodes have been shown to be less than 9mm in diameter and metastatic deposits are initially found within the medulla of the node before spreading to the cortex. By collecting spectra from the inner surface there was confidence that spectral information particularly related to macrometastases would be detected if they were present.

Prior to commencing studies within theatre a feasibility study was performed on node samples that had been collected by collaborators at Russell's Hall Hospital, Dudley, UK. The feasibility study, discussed in Chapter 3, included 38 node samples from 17 different patients and revealed very encouraging results. A sensitivity of up to 90% and a specificity of up to 96% were achieved using unsupervised leave one node out testing. The results achieved were broadly similar even when only 5 spectra were assessed per node and enabled the "assessment" of each node to be performed in a clinically relevant time frame. There were a number of drawbacks to this study however. The samples were snap frozen, it was often difficult to determine the orientation of the node and thus definitively collect spectra from the inner half, and the "gold standard" histopathological assessment was based on a single slice with immuno-histochemistry staining. Therefore spectra may have been collected from the outer half of the node and

samples may have been mis-classified. It was however an important step in establishing the potential of the equipment we were using and it was hoped that even better results could be achieved in the real time study.

Building on both the feasibility study and the preparatory experimentation the clinically based part of this study was established. With local ethical approval a total of 66 patients undergoing 72 operative procedures were recruited and from these patients 339 samples from 176 lymph nodes were assessed. The results achieved when trying to distinguish between the two most distinct groups, the macrometastases and the N_0 patients were most promising, as discussed in Chapter 4. The unsupervised test result achieved specificity of 99.4% and a sensitivity of 93.8%, which is easily comparable if not far better than currently available intra-operative tests. Evidence that these results are based on differences in lipid, protein and DNA contributions is also consistent with previous work on breast cancer and normal breast tissue and is vital in helping explain the application of the test to clinicians. On an individual level 44/48 patients would have benefited from intraoperative testing had the results been used to guide clinical decision making. In particular 38 patients would have been spared the wait for their histopathological nodal assessment, and 6 would have avoided the need for a second operation to clear the axilla. There would have been two false positives and this will need to be addressed as the use of Raman spectroscopy moves forward. It is vital that the specificity should be maintained as close to 100% as possible, as the result of a false positive would be a recommendation for an axillary clearance that ultimately was not needed.

The subsequent inclusion of negative nodes from non-N_0 patients into the negative group had a deleterious effect on the specificity (96%) and sensitivity (84%). This is suggestive that there are some differences within nodes that although not metastatic themselves are part of a chain of nodes at least one of which is metastatic. Peak analysis demonstrated significant differences in the contribution of proteins to the spectra of non-N0 nodes. This may have affected the overall classification model and could account for the increase in both false negatives and false positives. For the individual patient involved this would not have had any deleterious effects as they would, by definition, have had another node that was positive. They would therefore already have been defined as having a positive axilla.

The effect of these non-N0 negative nodes is important in helping to design a mathematical algorithm as this project progresses forward. This data suggest that any such algorithm will need to be based on spectra from N0 patients only and not negative nodes from non-N0 patients.

In comparison to the results achieved with the macrometastases the results from the nodes with either micrometastases, 50% sensitivity, or isolated tumour cells, 40% sensitivity, were disappointing. It was interesting to note that those that were successfully identified and those that were not, appeared to be in two distinct groups based on the contribution of lipid, protein and DNA to the spectra. It could be argued therefore that within the samples which were correctly identified the foci of metastases did significantly contribute to the spectra but in the other samples it either did not at all (i.e. it was not "seen") or the greater amount of normal tissue eclipsed it. This may be a

reflection on the small size of the deposits within the tissue and the difficulty detecting them using the methodology that was employed. If it was clinically felt that the identification of micrometastases and isolated tumour cells remained important then samples used in future studies may need to be multiply sectioned before spectra were acquired to help overcome this problem. The emerging data, especially from Z-0011 suggests that this is unlikely to be the case. It is likely that patients with ITCs will continue to be classified as node negative and that those with micrometastases will increasingly not be recommended to undergo further axillary surgery. If further surgery is recommended then this should be following MDT discussion and would not, given the current evidence, be following intra-operative assessment.

In situ testing from the outer surface of the node was suggested as a possible next step forward for this project. However the results presented, a fall in sensitivity to 81% for the identification of macrometastases, do not support this. The difference can be explained by the initial presence of metastatic deposits within the medulla before spread towards the cortex occurs. Therefore by placing the probe on the outer surface, light will be scattered first by a normal cortex before it reaches a metastatic medulla. No improvements in the results for the micrometastases or isolated tumour cells were reported. Thus future testing should continue to collect spectra from the cut inner half of the node.

6.3. Future Studies

The results presented within this thesis really do open the door to real time "bed side" tissue testing using Raman spectroscopy. This technique which is quick, non destructive (thus facilitating gold standard cross checking) and affordable has many advantages over the other currently available methodologies that were outlined in Chapter 1. Before it can guide clinical management a number of future studies need to be completed.

The first and most important next step should be the production of a classification algorithm or model that can then be prospectively tested. It is envisaged that this model would be based on dataset 1 that was discussed in Chapter 4. Prospectively testing this with independent specimens could then directly compare Raman spectroscopy and its algorithmic model to the current gold standard. Particular care will be need to be paid to any false positive results as these are the cases that need to be avoided. Further sectioning of the axillary node by the pathologists may be required to ensure that the gold standard technique hasn't missed any small deposits that the Raman device is "seeing". Initially this testing would be take place at one hospital site but then latterly this could be extended to multiple units, with multiple spectrometers. The use of multiple instruments and users would build on the reproducibility experiments outline in Chapter 5. The results from these independent samples could then be added to the algorithm to further increase its size and robusticity. It is hoped that with increasing sample numbers the classification model will become more powerful resulting in further improvements in sensitivity and specificity. This work is ongoing currently and the results are awaited eagerly. It is hoped that these results will provide a catalyst for

further studies that move Raman spectroscopy away from the laboratory to the patient's bed side. Within breast cancer the demonstration that this equipment can differentiate between normal and metastatic tissue opens it up to use in the immediate assessment of core biopsy samples, within a "one-stop" breast clinic or the interrogation of margin status during a wide local excision. Outside of breast cancer the potential for Raman spectroscopy to be used in a wide range of clinical scenarios is very real. It could, for example, be used in place of frozen section analysis in parathyroid or anal surgery by giving an immediate assessment of tissue type.

6.4 Conclusions

This study has taken a very important step toward the clinical use of Raman spectroscopy to improve patient care. After many years of offering great potential its use within a real-time clinical situation has been demonstrated. At the start of Chapter 2 a table demonstrating the key features of a diagnostic tool for use in intra-operative axillary node testing was shown. The ideal technology needed to be sensitive and specific, usable within the theatre environment, fast, cost effective and non destructive. No currently available method of node assessment offers all of these features. This study has shown that Raman spectroscopy can and does meet all these criteria. Further work to develop and test a diagnostic algorithm and to enhance on the reproducibility studies described in Chapter 5 will be required, but the use of Raman spectroscopy to improve the lives of patients with breast cancer is now within touching distance.

7.Bibliography

Alfano, R. R., Das, B. B., Cleary, J., Prudente, R. and Celmer, E. J. (1991), "Light sheds light on cancer--distinguishing malignant tumors from benign tissues and tumors", *Bulletin of the New York Academy of Medicine,* vol. 67, no. 2, pp. 143-150.

Allweis, T. M., Kaufman, Z., Lelcuk, S., Pappo, I., Karni, T., Schneebaum, S., Spector, R., Schindel, A., Hershko, D., Zilberman, M., Sayfan, J., Berlin, Y., Hadary, A., Olsha, O., Paran, H., Gutman, M. and Carmon, M. (2008), "A prospective, randomized, controlled, multicenter study of a real-time, intraoperative probe for positive margin detection in breast-conserving surgery", *American Journal of Surgery,* vol. 196, no. 4, pp. 483-489.

Alvarez, S., Anorbe, E., Alcorta, P., Lopez, F., Alonso, I. and Cortes, J. (2006), "Role of sonography in the diagnosis of axillary lymph node metastases in breast cancer: a systematic review", *American Journal of Roentgenology,* vol. 186, no. 5, pp. 1342-1348

Beattie, J. R., Bell, S. E., Borgaard, C., Fearon, A. and Moss, B. W. (2006), "Prediction of adipose tissue composition using Raman spectroscopy: average properties and individual fatty acids", *Lipids,* vol. 41, no. 3, pp. 287-294.

Beattie, J. R., Bell, S. E., Borggaard, C., Fearon, A. M. and Moss, B. W. (2007), "Classification of adipose tissue species using Raman spectroscopy", *Lipids,* vol. 42, no. 7, pp. 679-685.

Benson, J. R. and Wishart, G. C. (2010), "Is intra-operative nodal assessment essential in a modern breast practice?", *European Journal of Surgical Oncology,* vol. 36, no. 12, pp. 1162-1164.

Berry, E. and Kohn, M. (2000), *Operating Room Technique,* 9th ed, Mosby, Philadelphia.

Bilimoria, K. Y., Bentrem, D. J., Hansen, N. M., Bethke, K. P., Rademaker, A. W., Ko, C. Y., Winchester, D. P. and Winchester, D. J. (2009), "Comparison of sentinel lymph node biopsy alone and completion axillary lymph node dissection for node-positive breast cancer", *Journal of Clinical Oncology,* vol. 27, no. 18, pp. 2946-2953.

Bird, B., Romeo, M., Laver, N. and Diem, M. (2009), "Spectral detection of micro-metastases in lymph node histo-pathology", *Journal of Biophotonics,* vol. 2, no. 1-2, pp. 37-46.

Bleiweiss, I. J., Nagi, C. S. and Jaffer, S. (2006), "Axillary sentinel lymph nodes can be falsely positive due to iatrogenic displacement and transport of benign epithelial cells in patients with breast carcinoma", *Journal of Clinical Oncology,* vol. 24, no. 13, pp. 2013-2018.

Blumencranz, P., Whitworth, P. W., Deck, K., Rosenberg, A., Reintgen, D., Beitsch, P., Chagpar, A., Julian, T., Saha, S., Mamounas, E., Giuliano, A. and Simmons, R. (2007), "Scientific Impact Recognition Award. Sentinel node staging for breast cancer: intraoperative molecular pathology overcomes conventional histologic sampling errors", *American Journal of Surgery,* vol. 194, no. 4, pp. 426-432.

Brock, L. (1975), "The importance of environmental conditions, especially temperature, in the operating room and intensive care ward", *British Journal of Surgery,* vol. 62, no. 4, pp. 253-258.

Burger, L. and Fitzpatrick, J. (2009), "Prevention of inadvertent perioperative hypothermia", *British Journal of Nursing,* vol. 18, no. 18, pp. 1114, 1116-9.

Burke, M. and Seeters, J. (2010) B*reast Lymph Node Assay: Headline Report.* York Health Economics Consortium and NHS Technology Adoption Centre (NTAC) Available at: www.ntac.nhs.uk [Accessed Jan 2010].

Cacaecu, T. (2008*), Spleen and Other Lymphatic Organs*, available at: http://education.vetmed.vt.edu/curriculum/vm8054/labs/Lab13/IMAGES/LYMPH%20NODE%20LOW%201.jpg [Accessed January 2010].

Cancer Research UK (2009*), TNM Breast Cancer Staging*, available at: http://www.cancerhelp.org.uk/type/breast-cancer/treatment/tnm-breast-cancer-staging [Accessed January 2010].

Cancer Research UK (2011), *Breast Cancer UK Statistics*. Available at: http://info.cancerresearchuk.org/cancerstats/types/breast/incidence (Accessed March 2011).

Carter, B. A., Jensen, R. A., Simpson, J. F. and Page, D. L. (2000), "Benign transport of breast epithelium into axillary lymph nodes after biopsy", *American Journal of Clinical Pathology,* vol. 113, no. 2, pp. 259-265.

Chao, C. (2004), "The use of frozen section and immunohistochemistry for sentinel lymph node biopsy in breast cancer", *The American Surgeon,* vol. 70, no. 5, pp. 414-419.

Chicken, D. W., Sivanadarajah, N. and Keshtgar, M. R. (2007), "Patients' view on intraoperative diagnosis of sentinel nodes in breast cancer: is it an automatic choice?", *International Journal of Surgery,* vol. 5, no. 2, pp. 76-80.

Chowdary, M. V., Kumar, K. K., Kurien, J., Mathew, S. and Krishna, C. M. (2006), "Discrimination of normal, benign, and malignant breast tissues by Raman spectroscopy", *Biopolymers,* vol. 83, no. 5, pp. 556-569.

Chowdary, M. V., Kalyan Kumar, K., Mathew, S., Rao, L., Krishna, C. M. and Kurien, J. (2009), "Biochemical correlation of Raman spectra of normal, benign and

malignant breast tissues: a spectral deconvolution study", *Biopolymers,* vol. 91, no. 7, pp. 539-546.

Cooper, K. L., Harnan, S., Meng, Y., Ward, S. E., Fitzgerald, P., Papaioannou, D., Wyld, L., Ingram, C., Wilkinson, I. D. and Lorenz, E. (2011), "Positron emission tomography (PET) for assessment of axillary lymph node status in early breast cancer: A systematic review and meta-analysis", *European Journal of Surgical Oncology* vol. 37, no. 3, pp. 187-198.

Cote,R., Giuliano,A.E., Hawes,D., Ballman,K.V., Whitworth.D., Blumencranz, P.,Reintgen,D., Morrow,M., Leitch,A.M.,Hunt,K. (2010), "ACOSOG Z0010: A multicenter prognostic study of sentinel node (SN) and bone marrow (BM) micrometastases in women with clinical T1/T2 N0 M0 breast cancer", *Journal of Clinical Oncology,* Vol. 28:18s, (suppl; abstr CRA504).

Creager, A. J. and Geisinger, K. R. (2002), "Intraoperative evaluation of sentinel lymph nodes for breast carcinoma: current methodologies", *Advances in Anatomic Pathology,* vol. 9, no. 4, pp. 233-243.

Cserni, G., Amendoeira, I., Apostolikas, N., Bellocq, J. P., Bianchi, S., Bussolati, G., Boecker, W., Borisch, B., Connolly, C. E., Decker, T., Dervan, P., Drijkoningen, M., Ellis, I. O., Elston, C. W., Eusebi, V., Faverly, D., Heikkila, P., Holland, R., Kerner, H., Kulka, J., Jacquemier, J., Lacerda, M., Martinez-Penuela, J., De Miguel, C., Peterse, J. L., Rank, F., Regitnig, P., Reiner, A., Sapino, A., Sigal-Zafrani, B., Tanous, A. M., Thorstenson, S., Zozaya, E., Wells, C. A. and European Working Group for Breast Screening Pathology (2003), "Pathological work-up of sentinel lymph nodes in breast cancer. Review of current data to be considered for the formulation of guidelines", *European Journal of Cancer ,* vol. 39, no. 12, pp. 1654-1667.

Damera, A., Evans, A. J., Cornford, E. J., Wilson, A. R., Burrell, H. C., James, J. J., Pinder, S. E., Ellis, I. O., Lee, A. H. and Macmillan, R. D. (2003), "Diagnosis of axillary nodal metastases by ultrasound-guided core biopsy in primary operable breast cancer", *British Journal of Cancer,* vol. 89, no. 7, pp. 1310-1313.

Das, K., Kendall, C., Isabelle, M., Fowler, C., Christie-Brown, J. and Stone, N. (2008), "FTIR of touch imprint cytology: A novel tissue diagnostic technique", *Journal of Photochemistry and Photobiology B: Biology,* vol. 92, no. 3, pp. 160-164.

de Boer, M., van Deurzen,C.H, van Dijck, J.A, Borm,G.F., Diest,P.J., Adang, E.M., Nortier,J.W.R,. Rutgers, E.J., Seynaeve, C., Menke-Pluymers, M., Bult, P. and Tjan-Heijnen V.C. (2009) " Micrometastases or Isolated Tumor Cells and the Outcome of Breast Cancer" *New England Journal of Medicine* vol. 361, no. 7 pp.653-663.

de Boer, M., van Dijck, J. A., Bult, P., Borm, G. F. and Tjan-Heijnen, V. C. (2010), "Breast cancer prognosis and occult lymph node metastases, isolated tumor

cells, and micrometastases", *Journal of the National Cancer Institute,* vol. 102, no. 6, pp. 410-425.

Diem, M., Chalmers, JM. and Griffiths, PR. (2008). *Vibrational spectroscopy for medical diagnosis.* 1st Edition , John Wiley and Sons 2008.

DoITPoMS, University of Cambridge, UK. *Raman Spectroscopy*. (2010) Available from: http://www.doitpoms.ac.uk/tlplib/raman/index.php [Accessed October 2010]

Early Breast Cancer Trialists' Collaborative Group (EBCTCG) (2005), "Effects of chemotherapy and hormonal therapy for early breast cancer on recurrence and 15-year survival: an overview of the randomised trials", *Lancet,* vol. 365, no. 9472, pp. 1687-1717.

Ellis, H. (2002), *Clinical Anatomy,* 10th ed, Wiley Blackwell, 2002.

Ellis, H. (2003). Anatomy of the Breast. In *Surgery- The Continuously Updated Textbook of Surgery* (CD-ROM). London, UK: The Medicine Publishing Company Ltd.

Elmore, S. A. (2006), "Histopathology of the lymph nodes", *Toxicologic Pathology,* vol. 34, no. 5, pp. 425-454.

Elston, C. W. and Ellis, I. O. (1991), "Pathological prognostic factors in breast cancer. I. The value of histological grade in breast cancer: experience from a large study with long-term follow-up", *Histopathology,* vol. 19, no. 5, pp. 403-410.

Frank, C.J., McCreery, R L., Redd, D.C, and Gansler, T.S,.(1993) "Detection of Silicone in Lymph Node Biopsy Specimens by Near-Infrared Raman Spectroscopy", *Applied Spectroscopy* Vol 47 no. 4, pp. 387-390.

Frank, C. J., McCreery, R. L. and Redd, D. C. (1995), "Raman spectroscopy of normal and diseased human breast tissues", *Analytical Chemistry,* vol. 67, no. 5, pp. 777-783.

Gelmon, K. A. (2010), "The ongoing debate about nodes", *Clinical Breast Cancer,* vol. 10, no. 4, pp. 265-266.

Giuliano, A. E., Kirgan, D. M., Guenther, J. M. and Morton, D. L. (1994), "Lymphatic mapping and sentinel lymphadenectomy for breast cancer", *Annals of Surgery,* vol. 220, no. 3, pp. 391-8; discussion 398-401.

Giuliano, A. E., McCall, L., Beitsch, P., Whitworth, P. W., Blumencranz, P., Leitch, A. M., Saha, S., Hunt, K. K., Morrow, M. and Ballman, K. (2010), "Locoregional recurrence after sentinel lymph node dissection with or without axillary dissection in patients with sentinel lymph node metastases: the American

College of Surgeons Oncology Group Z0011 randomized trial", *Annals of Surgery,* vol. 252, no. 3, pp. 426-32; discussion 432-3.

Giuliano, A. E., Hunt, K. K., Ballman, K. V., Beitsch, P. D., Whitworth, P. W., Blumencranz, P. W., Leitch, A. M., Saha, S., McCall, L. M. and Morrow, M. (2011), "Axillary dissection vs no axillary dissection in women with invasive breast cancer and sentinel node metastasis: a randomized clinical trial", *Journal of the American Medical Association,* vol. 305, no. 6, pp. 569-575.

Goyal, A. and Mansel, R. E. (2008), "Recent advances in sentinel lymph node biopsy for breast cancer", *Current Opinion in Oncology,* vol. 20, no. 6, pp. 621-626.

Haka, A. S., Shafer-Peltier, K. E., Fitzmaurice, M., Crowe, J., Dasari, R. R. and Feld, M. S. (2005), "Diagnosing breast cancer by using Raman spectroscopy", *Proceedings of the National Academy of Sciences of the United States of America,* vol. 102, no. 35, pp. 12371-12376.

Haka, A. S., Volynskaya, Z., Gardecki, J. A., Nazemi, J., Lyons, J., Hicks, D., Fitzmaurice, M., Dasari, R. R., Crowe, J. P. and Feld, M. S. (2006), "In vivo margin assessment during partial mastectomy breast surgery using raman spectroscopy", *Cancer Research,* vol. 66, no. 6, pp. 3317-3322.

Haka, A. S., Volynskaya, Z., Gardecki, J. A., Nazemi, J., Shenk, R., Wang, N., Dasari, R. R., Fitzmaurice, M. and Feld, M. S. (2009), "Diagnosing breast cancer using Raman spectroscopy: prospective analysis", *Journal of Biomedical Optics,* vol. 14, no. 5, pp. 054023.

Hejmadi, M. (2010), *An Introduction to Cancer Biology,* Verntus Publishing Available from: http://web.mef.hr/web/images/pdf/int_canc_b.pdf [Accessed April 2011]

Hirsch, J. I., Banks, W. L.,Jr, Sullivan, J. S. and Horsley, J. S.,3rd (1989), "Effect of methylene blue on estrogen-receptor activity", *Radiology,* vol. 171, no. 1, pp. 105-107.

Hollas, J. M. (2005), *Modern Spectroscopy,* 5th ed, John Wiley and Sons, London.

Horsnell, J., Smith, J., Sattlecker, M., Sammon, A., Christie-Brown, J., Kendall, C. and Stone, N. (2011) "Raman Spectroscopy, a potential new method for the intra-operative assessment of axillary lymph nodes" *The Surgeon,* doi:10.1016/j.surge.2011.02.004.

Horsnell, J., Knight, H., Court, F., Chan, C., Bristol, J. (2012) "Intra-operative Sentinel Lymph Node Assessment - How many patients will avoid a second operation?" *European Journal of Surgical Oncology,* Vol. 38, no. 5, pp 459-460.

Ioachim, H. L. and Ratech, H. (2002), *Ioachim's Lymph Node Pathology,* 3rd ed, Lippincott Williams & Wilkins, Philapdelphia, PA 19106 USA.

Isabelle,M., Stone,N., Barr,H., Vipond,M. Shepherd,N. and Rogers, K. (2008), "Lymph Node Pathology using Optical Spectroscopy in Lymph Node diagnostics" *Spectroscopy,* vol.22, no. 2-3, pp 97-104.

Johnson, K. S., Chicken, D. W., Pickard, D. C. O., Lee, A. C., Briggs, G., Falzon, M., Bigio, I. J., Keshtgar, M. R. and Bown, S. G. (2004), "Elastic scattering spectroscopy for intraoperative determination of sentinel lymph node status in the breast", *Journal of Biomedical Optics,* vol. 9, no. 6, pp. 1122-1128.

Johnstone, S. (2002), *International Handbook of Breast Cancer,* 1st ed, Euromed Communications Ltd., Haslemere.

Katzin, W. E., Centeno, J. A., Feng, L. J., Kiley, M. and Mullick, F. G. (2005), "Pathology of lymph nodes from patients with breast implants: a histologic and spectroscopic evaluation", *American Journal of Surgical Pathology,* vol. 29, no. 4, pp. 506-511.

Keller, M.D., Majumder, S. K and Mahadevan-Jansen, A. (2009) "Spatially offset Raman spectroscopy of layered soft tissues", *Optics Letters*, vol. 34 no.7, pp.926-928.

Keller, M, D., Wilson, R., Mycek, M. and Mahadevan-Jansen, A. (2010) "Monte Carlo Model of Spatially Offset Raman Spectroscopy for Breast Tumor Margin Analysis" *Applied Spectroscopy* vol. 64, no.6, pp. 607-614.

Kendall, C. (2002), A Study of Raman spectroscopy for the early detetction and classification of malignancy in oesophageal tissue (unpublished PhD. thesis), Cranfield University, UK, Cranfield, UK.

Kendall, C., Stone, N., Shepherd, N., Geboes, K., Warren, B., Bennett, R. and Barr, H. (2003), "Raman spectroscopy, a potential tool for the objective identification and classification of neoplasia in Barrett's oesophagus", *Journal of Pathology,* vol. 200, no. 5, pp. 602-609.

Kerssens, M. M., Matousek, P., Rogers, K. and Stone, N. (2010), "Towards a safe non-invasive method for evaluating the carbonate substitution levels of hydroxyapatite (HAP) in micro-calcifications found in breast tissue", *The Analyst,* vol. 135, no. 12, pp. 3156-3161.

Keshtgar, M. R. (2009), "Intra-operative assessment of sentinel nodes", in Sibbering, M. (ed.) *The Association of Breast Surgery at BASO Yearbook 2009,* ABS at BASO, London WC2A 3PE, pp. 62-65.

Keshtgar, M. R., Chicken, D. W., Austwick, M. R., Somasundaram, S. K., Mosse, C. A., Zhu, Y., Bigio, I. J. and Bown, S. G. (2010), "Optical scanning for rapid intraoperative diagnosis of sentinel node metastases in breast cancer", *British Journal of Surgery,* vol. 97, no. 8, pp. 1232-1239.

Kim, T., Giuliano, A. E. and Lyman, G. H. (2006), "Lymphatic mapping and sentinel lymph node biopsy in early-stage breast carcinoma: a meta-analysis", *Cancer,* vol. 106, no. 1, pp. 4-16.

Krag, D. N., Weaver, D. L., Alex, J. C. and Fairbank, J. T. (1993), "Surgical resection and radiolocalization of the sentinel lymph node in breast cancer using a gamma probe", *Surgical Oncology,* vol. 2, no. 6, pp. 335-9; discussion 340.

Kuby, J. (1997), *Immunology,* 3rd ed, Freeman and Company, New York.

Kurosumi, M. and Takei, H. (2007), "Significance and problems of histopathological examination and utility of real-time reverse transcriptase-polymerase chain reaction method for the detection of sentinel lymph node metastasis in breast cancer", *Breast Cancer,* vol. 14, no. 4, pp. 342-349.

Layfield, D. M., Agrawal, A., Roche, H. and Cutress, R. I. (2011), "Intraoperative assessment of sentinel lymph nodes in breast cancer", *British Journal of Surgery,* vol. 98, no. 1, pp. 4-17.

Lim, S.M. and Lam, F.L. (2005), "Laparoscopic-assisted axillary dissection in breast cancer surgery", *American Journal of Surgery,* vol.190, no.4, pp. 641-643.

Loftus P. (2010) "Doctors thought discontinued J&J cancer test was impractical." http://online.wsj.com/article/BT-CO-20100125-710277.html. T*he Wall Street Journal* 25 January 2010.

Lovat, L. B., Johnson, K., Mackenzie, G. D., Clark, B. R., Novelli, M. R., Davies, S., O'Donovan, M., Selvasekar, C., Thorpe, S. M., Pickard, D., Fitzgerald, R., Fearn, T., Bigio, I. and Bown, S. G. (2006), "Elastic scattering spectroscopy accurately detects high grade dysplasia and cancer in Barrett's oesophagus", *Gut,* vol. 55, no. 8, pp. 1078-1083.

Mangram, A. J., Horan, T. C., Pearson, M. L., Silver, L. C. and Jarvis, W. R. (1999), "Guideline for Prevention of Surgical Site Infection, 1999. Centers for Disease Control and Prevention (CDC) Hospital Infection Control Practices Advisory Committee", *American Journal of Infection Control,* vol. 27, no. 2, pp. 97-132; quiz 133-4; discussion 96.

Manoharan, R., Shafer, K., Perelman, L., Wu, J., Chen, K., Deinum, G., Fitzmaurice, M., Myles, J., Crowe, J., Dasari, R. R. and Feld, M. S. (1998), "Raman spectroscopy and fluorescence photon migration for breast cancer diagnosis and imaging", *Photochemistry and Photobiology,* vol. 67, no. 1, pp. 15-22.

Mansel, R. E., Fallowfield, L., Kissin, M., Goyal, A., Newcombe, R. G., Dixon, J. M., Yiangou, C., Horgan, K., Bundred, N., Monypenny, I., England, D., Sibbering, M., Abdullah, T. I., Barr, L., Chetty, U., Sinnett, D. H., Fleissig, A., Clarke, D. and Ell, P. J. (2006), "Randomized multicenter trial of sentinel node biopsy

versus standard axillary treatment in operable breast cancer: the ALMANAC Trial", *Journal of the National Cancer Institute,* vol. 98, no. 9, pp. 599-609.

Matern, U. and Koneczny, S. (2007), "Safety, hazards and ergonomics in the operating room", *Surgical Endoscopy,* vol. 21, no. 11, pp. 1965-1969.

Matousek, P. and Stone, N. (2007), "Prospects for the diagnosis of breast cancer by non-invasive probing of calcifications using transmission Raman spectroscopy", *Journal of Biomedical Optics,* vol. 12, no. 2, doi.10.1117/1.2718934

Molckovsky, A., Song, L. M., Shim, M. G., Marcon, N. E. and Wilson, B. C. (2003), "Diagnostic potential of near-infrared Raman spectroscopy in the colon: differentiating adenomatous from hyperplastic polyps", *Gastrointestinal Endoscopy,* vol. 57, no. 3, pp. 396-402.

Moore, K. A., A. (2005), *Essential Clinical Anatomy,* 3rd Edition ed., Lippincott Williams & Wilkins, London.

National Comprehensive Cancer Network (2012), "*Clinical Practice Guidelines in Oncology. Breast Cancer"* National Comprehensive Cancer Network Inc available at: www.nccn.org. [Accessed April 2012]

National Institute for Health and Clinical Excellence (February 2009), "Early and locally advanced breast cancer"*, Clinical Guideline 80*, National Institute for Health and Clinical Excellence, London WC1V 6NA.

NHS Breast Screening Programme (2008), *Annual Review: Saving Lives through Screening* NHSBSP, National Health Service, UK, London, UK.

NHS Cancer Screening Programmes and West Midlands Cancer Intelligence Unit (2009), *An Audit of Screen Detected Breast Cancers for the Year of Screening April 2007 to March 2008*, NHSBSP, National Health Service, UK, London, UK.

Obwegeser, R., Lorenz, K., Hohlagschwandtner, M., Czerwenka, K., Schneider, B. and Kubista, E. (2000), "Axillary lymph nodes in breast cancer: is size related to metastatic involvement?" *World Journal of Surgery,* vol. 24, no. 5, pp. 546-550.

Paik, S., Tang, G., Shak, S., Kim, C., Baker, J., Kim, W., Cronin, M., Baehner, F. L., Watson, D., Bryant, J., Costantino, J. P., Geyer, C. E.,Jr, Wickerham, D. L. and Wolmark, N. (2006), "Gene expression and benefit of chemotherapy in women with node-negative, estrogen receptor-positive breast cancer", *Journal of Clinical Oncology,* vol. 24, no. 23, pp. 3726-3734.

Patani, N., Cutuli, B. and Mokbel, K. (2008), "Current management of DCIS: a review", *Breast Cancer Research and Treatment,* vol. 111, no. 1, pp. 1-10.

Pinder, S. (2009), "Sentinel Node Biopsy Pathology", in Sibbering, M. (ed.) *The Association of Breast Surgery at BASO Yearbook 2009*, ABS at BASO, London WC2A 3PE, pp. 66-69.

Pond, C. M. and Mattacks, C. A. (2003), "The source of fatty acids incorporated into proliferating lymphoid cells in immune-stimulated lymph nodes", *British Journal of Nutrition,* vol. 89, no. 3, pp. 375-382.

Purushotham, A. D., Upponi, S., Klevesath, M. B., Bobrow, L., Millar, K., Myles, J. P. and Duffy, S. W. (2005), "Morbidity after sentinel lymph node biopsy in primary breast cancer: results from a randomized controlled trial", *Journal of Clinical Oncology,* vol. 23, no. 19, pp. 4312-4321.

Quan, M. L. and McCready, D. (2009), "The evolution of lymph node assessment in breast cancer", *Journal of Surgical Oncology,* vol. 99, no. 4, pp. 194-198.

Raftery, A. (ed.) (2000), *Applied Basic Science for Basic Surgical Training,* Illustrated Edition ed, Churchill Livingstone, London.

Redd, D. C., Feng, C., Yue, K. and Gansler, T. S. (1993), "Raman Spectroscopic Characterization of Human Breast Tissues: Implications for Breast Cancer Diagnosis", *Applied Spectroscopy,* vol. 47, no. 6, pp. 787-791.

Rhakha, E., El-Sayed, M. and Powe, D. (2008), "Invasive Lobular Carcinoma of the Breast: Response to hormonal therapy and outcome", *European Journal of Cancer*, vol.44, no.1, pp73-83.

Rosen, P. P. (2001), *Rosen's Breast Pathology,* 2nd ed, Lippincott Williams and Wilkins, Philadelphia.

Rovera, F., Frattini, F., Marelli, M., Corben, A. D., Dionigi, G., Boni, L. and Dionigi, R. (2008), "Axillary sentinel lymph node biopsy: an overview", *International Journal of Surgery,* vol. 6 Suppl 1, pp. S109-12.

Sabel, M. S. (2009), *Essentials of Breast Surgery,* 1st ed, Mosby Elsevier, Philadelphia.

Sakr, R., Barranger, E., Antoine, M., Prugnolle, H., Darai, E. and Uzan, S. (2006), "Ductal carcinoma in situ: value of sentinel lymph node biopsy", *Journal of Surgical Oncology,* vol. 94, no. 5, pp 426-430.

Sant, M., Francisci, S., Capocaccia, R., Verdecchia, A., Allemani, C., Berrino, F. and Francoisco, S. (2006) "Time trends of breast cancer survival in Europe in relation to incidence and mortality" *International Journal of Surgery* vol. 119, no.10, pp 2417-2422.

Sattlecker, M., Bessant, C., Smith, J. and Stone, N. (2010), "Investigation of support vector machines and Raman spectroscopy for lymph node diagnostics", *The Analyst,* vol. 135, no. 5, pp. 895-901.

Sibbering, M. (ed.) (2009), *The Association of Breast Surgery at BASO Yearbook 2009,* The Association of Breast Surgery at BASO, London WC2 3PE 2009.

Smith, E. and Dent, G. (2005), *Modern Raman Spectroscopy; a practical approach,* 1st ed, John Wiley and Sons, London.

Smith, J., Kendall, C., Sammon, A., Christie-Brown, J. and Stone, N. (2003), "Raman spectral mapping in the assessment of axillary lymph nodes in breast cancer", *Technology in Cancer Research & Treatment,* vol. 2, no. 4, pp. 327-332.

Smith, J. (2005), *Raman Spectroscopy in the Assessment of Axillary Lymph Nodes in Breast Cancer* (unpublished D.M. thesis), Cranfield University, UK, Cranfield, UK.

Snook, K. L., Layer, G. T., Jackson, P. A., de Vries, C. S., Shousha, S., Sinnett, H. D., Nigar, E., Singhal, H., Chia, Y., Cunnick, G. and Kissin, M. W. (2011) "Multicentre evaluation of intraoperative molecular analysis of sentinel lymph nodes in breast carcinoma" *British Journal of Surgery* ,vol. 98, no.4 527-535.

Somasundaram, S. K., Chicken, D. W. and Keshtgar, M. R. (2007), "Detection of the sentinel lymph node in breast cancer", *British Medical Bulletin,* vol. 84, pp. 117-131.

Steele, R.J., Forrest, A. P., Gibson, T., Stewart, H. J. and Chetty, U. (1985), "The efficacy of lower axillary sampling in obtaining lymph node status in breast cancer: a controlled randomized trial", *British Journal of Surgery,* vol. 72, no. 5, pp. 368-369.

Stone, N., Stavroulaki, P., Kendall, C., Birchall, M. and Barr, H. (2000), "Raman spectroscopy for early detection of laryngeal malignancy: preliminary results", *The Laryngoscope,* vol. 110, no. 10 Pt 1, pp. 1756-1763

Stone, N., Kendall, C., Smith, J., Crow, P. and Barr, H. (2004), "Raman spectroscopy for identification of epithelial cancers", *Faraday Discussions,* vol. 126, pp. 141-57; discussion 169-83.

Stropp, J., Trachta, G., Brehm, G. and Schneider, S. (2003), "A new version of AgFON substrates for high-throughput analytical SERS applications", *Journal of Raman Spectroscopy,* vol. 34, no. 1, pp. 26-32.

Suami, H., Pan, W. R., Mann, G. B. and Taylor, G. I. (2008), "The lymphatic anatomy of the breast and its implications for sentinel lymph node biopsy: a human cadaver study", *Annals of Surgical Oncology,* vol. 15, no. 3, pp. 863-871.

Tafe, L. J., Schwab, M. C., Lefferts, J. A., Wells, W. A. and Tsongalis, G. J. (2010), "A validation study of a new molecular diagnostic assay: the Dartmouth-Hitchcock Medical Center experience with the GeneSearch BLN assay in breast sentinel lymph nodes", *Experimental and Molecular Pathology,* vol. 88, no. 1, pp. 1-6.

Tamaki, Y., Akiyama, F., Iwase, T., Kaneko, T., Tsuda, H., Sato, K., Ueda, S., Mano, M., Masuda, N., Takeda, M., Tsujimoto, M., Yoshidome, K., Inaji, H., Nakajima, H., Komoike, Y., Kataoka, T. R., Nakamura, S., Suzuki, K., Tsugawa, K., Wakasa, K., Okino, T., Kato, Y., Noguchi, S. and Matsuura, N. (2009), "Molecular detection of lymph node metastases in breast cancer patients: results of a multicenter trial using the one-step nucleic acid amplification assay", *Clinical Cancer Research,* vol. 15, no. 8, pp. 2879-2884.

Tan, L. K., Giri, D., Hummer, A. J., Panageas, K. S., Brogi, E., Norton, L., Hudis, C., Borgen, P. I. and Cody, H. S.,3rd (2008), "Occult axillary node metastases in breast cancer are prognostically significant: results in 368 node-negative patients with 20-year follow-up", *Journal of Clinical Oncology,* vol. 26, no. 11, pp. 1803-1809.

Tew, K., Irwig, L., Matthews, A., Crowe, P. and Macaskill, P. (2005), "Meta-analysis of sentinel node imprint cytology in breast cancer", *British Journal of Surgery,* vol. 92, no. 9, pp. 1068-1080.

Tjan-Heijnen, V.C, Pepels, M.J., de Boer, M., Borm G.F., van Dijck, J.van Deurzen, C.H., Adang E., Menke-Pluymers M., van Diest P.J.,and Bult, P. (2009)"Impact of omission of completion axillary lymph node dissection (cALND) or axillary radiotherapy (ax RT) in breast cancer patients with micrometastases (pN1mi) or isolated tumor cells (pN0[i+]) in the sentinel lymph node (SN): Results from the MIRROR study" *Journal of Clinical Oncology ,* vol. 27, no 18s, (suppl; abstr CRA506)

Trans-Med Network. (2000*), Online Management of Breast Disease*s. Available at: www.breastdiseases.com [Accessed January 2010].

US and Finnish Food Databases (2009), "*Which oils and fats are best*?" Available from http://inhumanexperimentsblogspot.co.uk/2009/10/which-oils-and-fats-are-best-for.html [Accessed January 2011].

Veronesi, U., Zurrida, S., Mazzarol, G. and Viale, G. (2001), "Extensive frozen section examination of axillary sentinel nodes to determine selective axillary dissection", *World Journal of Surgery,* vol. 25, no. 6, pp. 806-808.

Viale, G., Dell'Orto, P., Biasi, M. O., Stufano, V., De Brito Lima, L. N., Paganelli, G., Maisonneuve, P., Vargo, J. M., Green, G., Cao, W., Swijter, A. and Mazzarol, G. (2008), "Comparative evaluation of an extensive histopathologic examination and a real-time reverse-transcription-polymerase chain reaction assay for mammaglobin and cytokeratin 19 on axillary sentinel lymph nodes of breast carcinoma patients", *Annals of Surgery,* vol. 247, no. 1, pp. 136-142.

Visser, M., Jiwa, M., Horstman, A., Brink, A. A., Pol, R. P., van Diest, P., Snijders, P. J. and Meijer, C. J. (2008), "Intra-operative rapid diagnostic method based on

CK19 mRNA expression for the detection of lymph node metastases in breast cancer", *International Journal of Cancer,* vol.122, no. 11, pp. 2562-2567.

Weaver,D., Takamaru A., Krag, M., Skelly, J., Anderson, S. Harlow,S., Julian,T., Mamounas, E., and Wolmark, N. (2011) "Effect of Occult Metastases on Survival in Node-Negative Breast Cancer" *New England Journal of Medicine*, Vol. 364 No.5 , pp. 412-421.

West Midlands Cancer Intelligence Unit (2009)*, Survival Figures for 10 years following diagnosis with breast cancer*, available at: www.wmpho.org.uk/wmciu [accessed January 2010].

Wheater, P., Burkitt, H. and Daniels, V. (1995), *Wheater's Functional Histology,* 3rd ed, Churchill Livingstone, New York.

Young, V. L. and Watson, M. E. (2006), "Prevention of perioperative hypothermia in plastic surgery", *Aesthetic Surgery Journal,* vol. 26, no. 5, pp. 551-571.

-

8. Appendices

8.1 List of Prizes

Association of Breast Surgery (ABS)

- Shortlisted for the BJS Presentation Prize, Liverpool 2012

Cranfield University

- Winner of Translational Medicine Prize, Gloucester 2011

British Association of Surgical Oncology (BASO)

- Shortlisted for Anthony Edwards Poster Prize, London 2010

South West Surgeons

- Presentation Prize for Research Paper, Bristol 2010

BUPA Foundation Research Grant

- Two year research grant awarded December 2009 for research into the use of Raman spectroscopy in breast cancer

8.2 Presentations

8.2.1 Oral Presentations

8.2.1.1 Oral Presentations - International

- J. Horsnell, C. Kallaway, C. Chan, J. Bristol, F. Court, N. Stone
  The role of Raman Spectroscopy in the intraoperative assessment of axillary lymph nodes in breast cancer
  ASGBI Liverpool May 2012

- J.Horsnell, C. Kallaway, C. Chan, J. Bristol, F. Court, N. Stone
  Real Time Assessment of Axillary Nodes Based On Molecular Differences Using Raman Spectroscopy
  EBCC Vienna, Austria 2012

- J Horsnell, N Stone
  Raman Spectroscopy- A proof of concept study to determine its efficacy in assessing axillary lymph nodes in breast cancer.
  SPEC Manchester, UK 2010

- L Orr, C Kendall, J Hutchings, M Isabelle, J Horsnell, N Stone
  Raman spectroscopy of lymph nodes in the head and neck
  SPIE San Francisco, USA 2010

8.2.1.2 Oral Presentation - National

- J. Horsnell, H. Knight, F.Court, C.Chan, J.Bristol
  Intra-operative Sentinel Lymph Node Assessment- How many patients will avoid a second operation?
  ABS Bournemouth May 2012 (shortlisted for the BJS Prize Papers)

- J. Horsnell, P. Stonelake, G. Shetty, J. Christie-Brown, C. Kendall, N. Stone
  Raman Spectroscopy a promising method of assessing axillary lymph nodes even in the presence of blue dye.
  BASO London November 2010

- J. Horsnell, P. Stonelake, G. Shetty, C. Kendall, J. Hutchings, N. Stone
  Assessment of axillary lymph nodes using Raman spectroscopy. Intraoperative use is possible.
  SARS Dublin January 2011

8.2.2 Poster Presentations

8.2.2.1 Poster Presentation - International

- J. Horsnell, P. Stonelake, G. Shetty, J. Christie-Brown, C. Kendall, J. Hutchings, N. Stone
  Raman Spectroscopy a new potential method for the assessment of axillary lymph nodes intra-operatively.
  ESSO Bordeaux , France 2010

- J. Horsnell, J. Hutchings, N Stone
  Using a hand held Raman Spectroscopy Device in an operating theatre -simple solutions to practical problems
  SPEC Manchester, UK 2010

8.2.2.2 Poster Presentation - National

- J. Horsnell, N. Stone
  Raman Spectroscopy – Could it open the door for true one stop Breast Clinics?
  SPEC Manchester, UK 2010

- J. Horsnell, H. Knight, F.Court, C.Chan, J.Bristol
  Intra-operative Sentinel Lymph Node Assessment- How many patients will avoid a second operation?
  ABS Bournemouth May 2012 (shortlisted for the BJS Prize Papers)

- J. Horsnell, C. Kallaway, C. Chan, J. Bristol, F. Court, N. Stone
  The role of Raman Spectroscopy in the intraoperative assessment of axillary lymph nodes in breast cancer
  ASGBI Liverpool May 2012

- J. Horsnell, P. Stonelake, G. Shetty, J. Christie-Brown, C. Kendall, N. Stone
  Raman Spectroscopy a promising method of assessing axillary lymph nodes even in the presence of blue dye.
  BASO London November 2010

- J. Horsnell, P. Stonelake, G. Shetty, C. Kendall, J. Hutchings, N. Stone
  Assessment of axillary lymph nodes using Raman spectroscopy. Intraoperative use is possible.
  SARS Dublin January 2011

8.3 Publications

8.3.1 Full Papers

1. J Horsnell, J. Smith, M. Sattlecker, A.Sammon, J. Christie-Brown, C.Kendall, N.Stone
   Raman Spectroscopy – A Potential New Method for the Intra-Operative Assessment of Axillary Lymph Nodes.
   Surgeon (2011), doi:10.1016/j.surge.2011.02.004

2. J. Horsnell, P. Stonelake, G. Shetty, J. Christie-Brown, C. Kendall, J. Hutchings, N. Stone
   Raman spectroscopy – A new method for the intra-operative assessment of axillary lymph nodes.
   Analyst. 2010 Dec;135(12):3042-7. Epub 2010 Nov 2.

8.3.2 Published Abstracts

1. J.Horsnell, C. Kallaway, C. Chan, J. Bristol, F. Court, N. Stone
   Real Time Assessment of Axillary Nodes Based On Molecular Differences Using Raman Spectroscopy
   European Journal of Cancer 2012, 48 (S1) Page S169

2. J Horsnell, C. Chan, J. Bristol, F. Court, N. Stone
   Real Time Intraoperative Assessment of Axillary Lymph Nodes using Raman Spectroscopy
   EJSO 2011, 37 (5) Page S6

3. J. Horsnell, P. Stonelake, G. Shetty, C. Kendall, J. Hutchings, N. Stone
   Assessment of axillary lymph nodes using Raman spectroscopy. Intraoperative Use is possible.
   Br J Surg 2011, 98 (Suppl 2): 26

4. J. Horsnell, P. Stonelake, G. Shetty, J. Christie-Brown, C. Kendall, J. Hutchings, N. Stone
   Raman Spectroscopy a new potential method for the assessment of axillary lymph nodes intra-operatively.
   EJSO 2010, 36 (9) 924-925.

5. J. Horsnell, P. Stonelake, G. Shetty, J. Christie-Brown, C. Kendall, N. Stone
   Raman Spectroscopy a promising method of assessing axillary lymph nodes even in the presence of blue dye.
   EJSO 2010, 36(11) 1112.

6. L. Orr, C. Kendall, J. Hutchings, M. Isabelle, J. Horsnell and N. Stone
   Raman spectroscopy as a tool for the identification and differentiation of neoplasias contained within lymph nodes of the head and neck
   *Head & Neck Oncology 2010, **2**(Suppl 1):O4*